層状ペロブスカイト－有機複合体の作製及びその光応答性電気伝導への応用

課題番号：10555221

平成１０～１２年度科学研究費補助金（基盤研究（Ｂ））

研究成果報告書

平成１４年３月

研究代表者　菅原　義之
（早稲田大学理工学部教授）

はしがき

研究組織

研究代表者　　菅原　義之　（早稲田大学理工学部教授）
研究分担者　　黒田　一幸　（早稲田大学理工学部教授）
研究分担者　　杉本　　渉　（信州大学繊維学部助手）

研究経費

平成１０年度　５５００　千円
平成１１年度　３６００　千円
平成１２年度　１６００　千円
計　１０７００　千円

研究期間

平成１０年度　～　平成１２年度

研究概要

１）新しいH型層状ペロブスカイトの合成

層状ペロブスカイトは既存の構造・組成にそれほど多様性がないため、新しい層状ペロブスカイトを合成するルートを開発した。Aurivillius相（$Bi_2A_{n-1}B_nO_{3n+3}$）（n=3, A=(Sr, Na), (Ca, Na), B=Nb；n=2, A=Sr, B=Ta；n=2, Aイオンなし, B=W）を酸処理し、Bi_2O_2層を選択的に溶出させると、電荷補償のために層間にプロトンが導入され、新しいH型層状ペロブスカイトが得られた。$Bi_2ANaNb_3O_{12}$（A=Sr, Ca）を塩酸で処理する事により$H_{1.8}[Bi_{0.2}A_{0.8}NaNb_3O_{10}]$を、$Bi_2SrNb_2O_9$を塩酸で処理する事により$H_{1.8}[Bi_{0.2}Sr_{0.8}Nb_2O_7]$を得た。生成物中のBiの残存は陽イオンのディスオーダーによるものであり、強誘電体で問題となっているディスオーダーを証明する結果としても重要である。また、$Bi_2W_2O_9$を塩酸で処理する事により$H_2W_2O_9$を 得た。得られた生成物はこれまでの合成手法では得られなかったものであり、本手法の有効性を示す結果である。

2） 有機誘導体型無機—有機複合体の合成

H型層状ペロブスカイト$H[LaNb_2O_7]$と各種アルコールの反応により、層表面にアルコキシル基を持つ層状ペロブスカイトを合成した。これを中間体とすることにより、直接反応しないようなバルキーなアルコールで層表面を修飾できることが明らかとなった。系中の水分に関する検討から、反応メカニズムは加水分解とアルコリシスを経ていることを明らかにした。この手法はジオールとの反応にも有効であり、エチレンジオール分子中１つのOH基だけが反応していた。また、同様に中間体を用いる手法により、末端にOH基を持つジメチルシロキサン（$HO(SiMe_2O)_nH$）が層表面を修飾することを明らかにした。この成果は層状ペロブスカイトと有機高分子の層間化合物として初めての結果である。さらに、トリフルオロ酢酸との反応により、トリフルオロアセテート基で表面を修飾することにも成功した。酢酸では層表面修飾が不可能であったことから、反応機構を推定した。

3） インターカレーション型無機—有機複合体の合成

1）で作製した新しいH型層状ペロブスカイト$H_{1.8}[Bi_{0.2}Sr_{0.8}Nb_2O_7]$と*n*-アルキルアミンとの反応により、層間でアンモニウムイオンを形成する酸塩基反応により*n*-アルキルアミンをインターカレートさせることに成功した。層間隔は炭素数の増加に伴い直線的に増加しており、層に対して約65°の角度を持つ２層構造を持つものと推定された。水素量に関しては、$[Bi_{0.2}Sr_{0.8}Nb_2O_7]$あたり1.8Hが存在するが、その中で1.0Hしか反応しなかった。この結果を層表面の構造と*n*-アルキルアミンの大きさから説明することに成功した。

4） 光照射によるフォトクロミズムの出現

2）で作製したメトキシド修飾$H[LaNb_2O_7]$に空気中で紫外光を照射したところ、青色に着色した。これを放置すると徐々に退色したが、再度紫外光を照射することにより再度着色した。電気抵抗値を２端子法で測定したところ、光照射により電気抵抗は減少し、退色に伴い徐々に増加した。これらの結果は、光誘起電子移動が起こっていることを明確に示す成果である。

研究発表

A）本研究に関する論文

1） Sugimoto, W., Shirata, M., Takemoto, M., Hayami, S., Sugahara, Y. & Kuroda, K. Synthesis and Structures of Carrier Doped Titanates with the Ruddleesden-Popper Structure $(Sr_{0.95}La_{0.05})_{n+1}Ti_nO_{3n+1-d}$ (n=1, 2). *Solid State Ionics* 108, 315-319 (1998).

2） Sugimoto, W., Shirata, M., Sugahara, Y. & Kuroda, K. New Conversion Reaction of an Aurivillius Phase into the Protonated Form of the Layered Perovskite by the Selective Leaching of the Bismuth Oxide Sheet. *J. Am. Chem. Soc.* 121, 11602-3 (1999).

3） Sugimoto, W., Ohkawa, H., Naito, M., Sugahara, Y. & Kuroda, K. Structure and Semiconducting Properties of Carrier-Doped Niobates with a Four-Layered Perovskite Structure. *J. Solid State Chem.* 148, 508-513 (1999).

4） Shirata, M., Tsunoda, Y., Sugimoto, W. & Sugahara, Y. Conversion of an Aurivillius Phase $Bi_2SrNaNb_3O_{12}$ into Its Protonated Form *via* Treatment with Various Mineral Acids. *Mater. Res. Soc. Symp. Proc.* 658, GG6.24.1-5 (2001).

5） Sugahara, Y., Tsunoda, Y., Shirata, M. & Sugimoto, W. Preparation of a Protonated Form of a Layered Perovskite by Selective Leaching of Bismuth Oxide Sheets. in *Proc. 18th Internat. Japan-Korea Seminar on Ceram.* 203-207 (Kagoshima, 2001).

6） Tsunoda, Y., Shirata, M., Sugimoto, W., Y., Liu, Z., Terasaki, O., Kuroda, K. & Sugahara, Y. Preparation and HREM Characterization of a Protonated Form of a Layered Perovskite Tantalate from an Aurivillius Phase $Bi_2SrTa_2O_9$ *via* Acid Treatment. *Inorg. Chem.* 40, 5768-71 (2001).

7） Sugimoto, W., Shirata, M., Kuroda, K. & Sugahara, Y. Conversion of Aurivillius Phases, $Bi_2ANaNb_3O_{12}$ (A=Sr or Ca), into the Protonated Forms of Layered Perovskite via Acid Treatment. *Chem. Mater.*, submitted.

8） Suzuki, H., Notsu, K., Takeda, Y., Sugimoto, W. & Sugahara, Reactions of Alkoxyl-Derivatives of a Layered Perovskite with Alcohols: Substitution Reactions on the Interlayer Surface of a Layered Perovskite. *Chem. Mater.*, submitted.

9） Tsunoda, Y., Sugimoto, W. & Sugahara, Y. Intercalation Behavior of *n*-Alkylamines into a Protonated Form of a Layered Perovskite Derived from Aurivillius Phase $Bi_2SrTa_2O_9$. *Chem. Mater.*, submitted.

10) Takeda, Y., Suzuki, H., Notsu, K., Sugimoto, W. & Sugahara, Y. Interlayer Surface Modification of a Layered Perovskite, $HLaNb_2O_7 \cdot nH_2O$ with Trifluoroacetate Groups *via* Ligand-exchange-type Reaction between *n*-Alkoxyl-derivative of $HLaNb_2O_7 \cdot nH_2O$ and Trifluoroacetic Acid. *Langmuir*, submitted.

B) 本研究に関連するもので、当該期間に発表した論文

1) Sugimoto, W., Mimuro, K., Sugahara, Y. & Kuroda, K. Synthesis and Structural Study of the KNb_4O_6-type Compound. *J. Ceram. Soc. Jpn.* 107, 318-321 (1999).
2) Sugimoto, W., Naito, M., Sugahara, Y. & Kuroda, K. Synthesis of $Na_{1-x}Ln_xNbO_3$ (Ln=La, Nd, Sm, Gd) and their structures and electrical properties. *Mater. Res. Soc. Symp. Proc.* 547, 267-272 (1999).
3) Sugimoto, W., Hirota, N., Mimuro, K., Sugahara, Y. & Kuroda, k. Synthesis of Reduced Layered Titanoniobates $KTi_{1-x}Nb_{1+x}O_5$. *Materials Letters* 39, 184-187 (1999).

C) 口頭発表

1) 白田雅史, 杉本渉, 菅原義之, 黒田一幸, Bi層状ペロブスカイトの選択的な $(Bi_2O_2)^{2+}$層の溶出により得られる新規層状ペロブスカイトの構造及びインターカレーション反応, 第11回日本セラミックス協会秋季シンポジウム, 名古屋大学, 10月 (1998).
2) 大川肇, 浜田大輔, 杉本渉, 菅原義之, 黒田一幸, $M[A_{n-1}Nb_nO_{3n+1}]$構造を持つ低酸化ニオブ酸化物の合成・構造および電気的性質, 日本MRS学術シンポジウム, かながわサイエンスパーク, 12月 (1998).
3) 杉本渉, 白田雅史, 菅原義之, 黒田一幸, $Bi_2NaANb_3O_{12}$ (A=Ca,Sr,Ba) の合成及び構造, 日本化学会(76春季年会), 神大, 3月 (1999).
4) 白田雅史, 杉本渉, 菅原義之, 黒田一幸, Bi層状ペロブスカイトの (Bi_2O_2)層のHX (X=Cl,Br,I) による選択的な溶出, 日本化学会(76春季年会), 神奈川大学,, 3月 (1999).
5) 津野田悠, 白田雅史, 杉本渉, 菅原義之, 黒田一幸, $Bi_2ATa_2O_9$ (A=Sr,Ca) の選択的な[Bi2O2]層の溶出により得られるH型層状ペロブスカイトの構造とその反応性, 日本セラミックス協会第12回秋季シンポジウム, 松江市, 10月 (1999).
6) 鈴木裕美, 杉本渉, 菅原義之, 黒田一幸, 層表面修飾した層状ペブロスカイトにおけるアルコキシル基のアルコールとのエステル交換反応, 日本セラミックス協会第12回秋季シンポジウム, 松江市, 10月 (1999).

7） 菅原義之，杉本渉，白田雅史，黒田一幸，Aurivillius構造を持つ層状ペブロスカイトの酸処理による選択的な$(Bi_2O_2)^{2+}$層の溶出と生成する新規層状ペブロスカイトのキャラクタリゼーション，無機マテリアル学会・日本無機リン化学会合同研究会，岡山大，11月 (1999).
8） Sugahara, Y., Shirata, M., Sugimoto, W. & Kuroda, K. Conversion of an Aurivillius Phase into the Protonated Form of the Layered Perovskite *via* Acid Treatment, France Japan Workshop on Nanomaterials, Tokyo Japan, August (2000).
9） 大川肇，津野田悠，杉本渉，菅原義之，$[Bi_2O_2][SrNb_2O_7]$の酸処理によるH型層状ペロブスカイトへの変換，日本セラミックス協会第13回秋季シンポジウム，北九州市，10月 (2000).
１０）津野田悠，杉本渉，菅原義之，Ta系層状ペロブスカイトから変換されたH型層状ペロブスカイトのインターカレーション反応，第39回セラミックス基礎科学討論会，津市，1月 (2001).
１１）津野田悠，杉本渉，菅原義之，$Bi_2SrTa_2O_9$の酸処理によるH型層状ペロブスカイトへの変換，第16回日本セラミックス協会関東支部研究発表会，甲府市，7月 (2000).
１２）Y. Sugahara, M. Shirata, W. Sugimoto, Novel Conversion of an Aurivillius Phase $Bi_2O_2[SrNaNb_3O_{10}]$ into the Protonated Form of the Layered Perovskite by the Selective Leaching of the Bismuth Oxide Sheet, Materials Research Society 2000 Fall Meeting, Boston, USA, November (2000).
１３）津野田悠，杉本渉，劉崢，寺崎治，菅原義之，黒田一幸，$Bi_2SrTa_2O_9$の酸処理により得られたH型層状ペロブスカイトの透過型電子顕微鏡観察，日本セラミックス協会2001年年会，早大，3月 (2001).
１４）竹田洋介，鈴木裕美，菅原義之，層表面にアルコキシル基を有する層状ペロブスカイトとトリフルオロ酢酸との反応，日本セラミックス協会2001年年会，早大，3月 (2001).

ELSEVIER

Solid State Ionics 108 (1998) 315–319

SOLID STATE IONICS

Synthesis and structures of carrier doped titanates with the Ruddlesden–Popper structure $(Sr_{0.95}La_{0.05})_{n+1}Ti_nO_{3n+1}$ ($n = 1, 2$)

Wataru Sugimoto[a], Masashi Shirata[a], Masataka Takemoto[a], Shuhei Hayami[a], Yoshiyuki Sugahara[a], Kazuyuki Kuroda[a,b,*]

[a]*Department of Applied Chemistry, School of Science and Engineering, Waseda University, Ohkubo-3, Shinjuku-ku, Tokyo 169-8555, Japan*

[b]*Kagami Memorial Laboratory for Materials Science and Technology, Waseda University, Nishiwaseda-2, Shinjuku-ku, Tokyo 169-8555, Japan*

Abstract

Carrier doping in $Sr_{n+1}Ti_nO_{3n+1}$ ($n = 1, 2$) was conducted by the substitution of La for Sr and the simultaneous introduction of oxygen vacancies. Single-phase products of $(Sr_{0.95}La_{0.05})_{n+1}Ti_nO_{3n+1-\delta}$ ($n = 1$, $\delta = 0.05$; $n = 2$, $\delta = 0.125$) were synthesized by the solid-state reaction of Sr_2TiO_4 (or $Sr_3Ti_2O_7$), La_2O_3 and Ti. When TiO_2 was used as one of the starting compounds to maintain oxygen stoichiometry, compounds with higher n were observed besides the object phases. Structural refinement by Rietveld analysis revealed that the a-axis expands while the c-axis contracts with La doping. The contraction of the c-axis is attributed to a shortened (Sr,La)–O distance, since the TiO_6 octahedra elongated in both a and c directions with doping. The change in the structure is discussed on the basis of the size of the substituting ion. The resistivity of the single-phase products was semiconducting with a very weak temperature dependence down to 80 K.

Keywords: Electrical properties; Rietveld method; Solid-state reaction; Titanates

1. Introduction

The titanium-based Ruddlesden–Popper phase $A_{n+1}Ti_nO_{3n+1}$ with $n \neq \infty$ has recently attracted attention due to its two-dimensional character. The ideal structures of the $n = 1$ and $n = 2$ compounds are shown in Fig. 1. Most studies have concentrated on the changes of the chemical and physical properties with the change of the A site ion, as the structure can be maintained for ions of various size. For example, the ionic conductivities [1–5] and ion exchange capabilities [2,3,6–11] have been studied for the $n = 1$ and $n = 3$ compounds. Such properties have been discussed based on both the difference in the A site species and the value of n. Although it has been known for nearly a quarter of a century that the reduced $n = \infty$ compound, $SrTiO_{3-\delta}$, exhibits superconductivity [12], studies on the electrical properties of the reduced $n \neq \infty$ titanates are limited. As far as we know, the study of $Ca_{n+1}Ti_nO_{3n+1-\delta}$ ($n = 2, 3$) is the only one reported in the literature [13]. By

*Corresponding author. Department of Applied Chemistry, School of Science and Engineering, Waseda University, Ohkubo-3, Shinjuku-ku, Tokyo 169-8555, Japan. E-mail: kuroda@mn.waseda.ac.jp; fax: +81 3 5286 3199.

0167-2738/98/$19.00
PII S0167-2738(98)00056-3

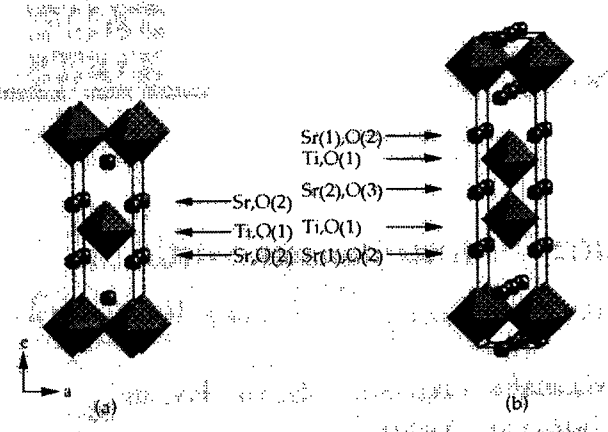

Fig. 1. The ideal crystal structure of (a) Sr_2TiO_4 and (b) $Sr_3Ti_2O_7$.

heating pellets of the insulating compounds under hydrogen atmosphere, the reduced $Ca_{n+1}Ti_nO_{3n+1-\delta}$ ($n = 2, 3, \infty$) compounds exhibit high conductivity, and the metal–nonmetal transitions have been reported in terms of the number of oxygen vacancies. On the other hand, the authors detected difficulties in the reduction of the two-dimensional compound Sr_2TiO_4 using the same method. The subject of this study is the synthesis of reduced $Sr_{n+1}Ti_nO_{3n+1-\delta}$ ($n = 1, 2$) via lanthanum substitution and the introduction of oxygen vacancies. Emphasis was placed on the change in structure by the simultaneous substitution of lanthanum for strontium and the introduction of oxygen vacancies. The electrical properties of the products were also examined.

2. Experimental

Insulating white-colored Sr_2TiO_4 ($n = 1$) and $Sr_3Ti_2O_7$ ($n = 2$) were obtained by the solid-state reaction of stoichiometric amounts of $SrCO_3$ and TiO_2 under ambient atmosphere. Polycrystalline samples with nominal composition $(Sr_{0.95}La_{0.05})_{n+1}Ti_nO_{3n+1-\delta}$ ($n = 1$, $\delta = 0$, 0.05; $n = 2$, $\delta = 0$, 0.125) were synthesized from Sr_2TiO_4 (or $Sr_3Ti_2O_7$), La_2O_3, TiO_2 and Ti according to the equations

$$0.95Sr_2TiO_4 + 0.05La_2O_3 + 0.025TiO_2 + 0.025Ti \rightarrow Sr_{1.9}La_{0.1}TiO_4 \quad (n = 1, \delta = 0), \tag{1}$$

$$0.95Sr_3Ti_2O_7 + 0.075La_2O_3 + 0.0625TiO_2 + 0.0375Ti \rightarrow Sr_{2.85}La_{0.15}Ti_2O_7 \quad (n = 2, \delta = 0), \tag{2}$$

$$0.95Sr_2TiO_4 + 0.05La_2O_3 + 0.025Ti \rightarrow Sr_{1.9}La_{0.1}TiO_{3.95} \quad (n = 1, \delta = 0.05), \tag{3}$$

$$0.95Sr_3Ti_2O_7 + 0.075La_2O_3 + 0.0375Ti \rightarrow Sr_{2.85}La_{0.15}Ti_2O_{6.875} \quad (n = 2, \delta = 0.125). \tag{4}$$

La_2O_3 was prefired at 1000°C for 1 h and all the other oxides were dried for at least 1 day at 100°C before grinding. After thorough grinding, the reagents were pressed and placed in an alumina boat surrounded by powder having the same composition in order to prevent contamination. The reactor tube was evacuated to $\sim 8.5 \times 10^{-3}$ Pa before argon purging and Ti powder was placed in the reactor tube as an oxygen getter in order to minimize oxidation during synthesis. The reagents were fired for 10–70 h at temperatures ranging from 1000 to 1250°C depending on the composition.

Crystalline phases were identified using a Mac Science MXP^3 diffractometer (monochromated Cu K_α radiation). Crystallographic data were obtained by the Rietveld analysis program RIETAN-97 [14,15]. Resistivity data were collected from 80 to 280 K using a standard d.c. four-probe method.

3. Results and discussions

3.1. Phase formation

The obtained reduced samples were light grey in color. Samples with stoichiometric oxygen content ($\delta = 0$) according to Eqs. (1) and (2) were synthesized under various firing conditions. Although slight changes in the lattice parameters were observed, the formation of higher-n members of the homologous series besides the object phase was observed along with considerable peak broadening of the object phase. On the other hand, when oxygen vacancy was induced according to Eqs. (3) and (4), peak broadening and the formation of higher-n members of the homologous series were substantially suppressed. A single phase was obtained for a

sample with nominal composition $Sr_{1.9}La_{0.1}TiO_{3.95}$ by the following firing sequence: (a) 10 h at 1000°C, (b) 30 h at 1100°C, (c) 10 h at 1150°C, and (e) 10 h at 1200°C (with intermittent regrinding every 10 h). Without this multi-process sequence, formation of the $n=2$ phase was observed. Contrary to the $n=1$ compound, when a similar multi-process sequence was adopted for the synthesis of nominal composition $Sr_{2.85}La_{0.15}Ti_2O_{6.875}$, the $n=\infty$ phase formed at 1100°C. However, a single phase was obtained for the sample fired for 10 h at 1250°C. Repeated firing resulted in broader and weaker diffraction peaks.

3.2. Structural characterization

Rietveld refinement was conducted based on the space group I4/mmm (No. 139). First, the refinement was conducted based on random substitution of lanthanum, and also random oxygen vacancies. The reliability factors R_{wp} were ~10%, indicating reasonable fits. Next, the oxygen vacancies and lanthanum ions were distributed at specific sites. The oxygen vacancy distribution at O(1) for both $Sr_{1.9}La_{0.1}TiO_{3.95}$ and $Sr_{2.85}La_{0.15}Ti_2O_{6.875}$ was the only one resulting in a lower reliability factor. A similar tendency has been reported for $Ca_3Ti_2O_{7-\delta}$. Although discussion of the distribution of oxygen vacancies from powder patterns should be handled with care, the results imply that the oxygen vacancies have a tendency to distribute in the *ab* planes of the perovskite block regardless of the n value. The substitution of lanthanum at specific sites for $Sr_{2.85}La_{0.15}Ti_2O_{6.875}$ resulted in higher reliability factors than for random distribution. Therefore, the refinement was conducted based on the random distribution of lanthanum at each strontium site. The output from the Rietveld analysis of the diffraction data for $Sr_{1.9}La_{0.1}TiO_{3.95}$ and $Sr_{2.85}La_{0.15}Ti_2O_{6.875}$ is shown in Fig. 2. The obtained crystallographic data are given in Tables 1 and 2. For both compounds, expansion of the a-axis and contraction of the c-axis was observed, resulting in an overall decrease in c/a. Selected bond distances are listed in Tables 3 and 4. For the $n=1$ compound, all the M–O distances in the perovskite block increased with doping. This is not unexpected, as the average ionic radius [16] of the B site ion increases by 1.3 pm (20% Ti^{3+} substitution), whereas the average

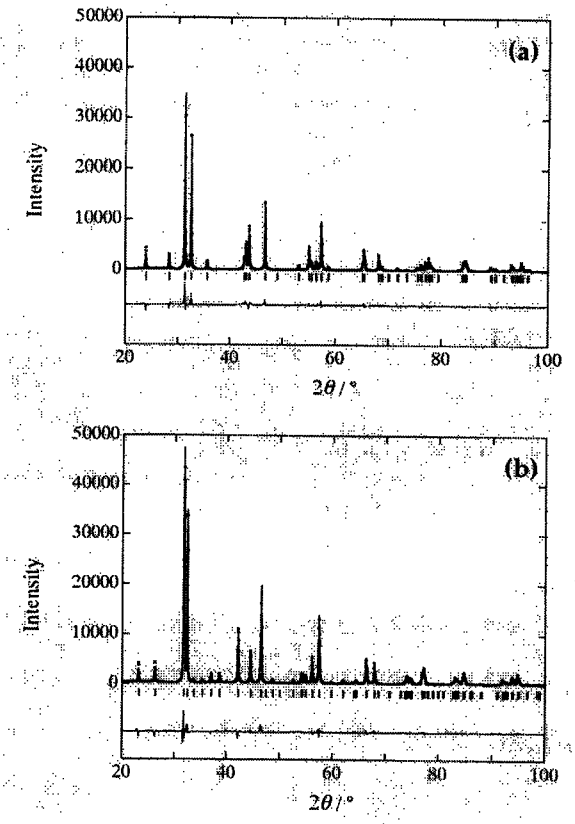

Fig. 2. XRD pattern fittings for (a) $Sr_{1.9}La_{0.1}TiO_{3.95}$ and (b) $Sr_{2.85}La_{0.15}Ti_2O_{6.875}$. The observed (solid) and calculated (dots) patterns are shown at the top. The vertical lines in the middle represent the positions of the possible Bragg reflections. The lower curves are the difference between the observed and calculated intensities.

ionic radius of the A site ion decreases only by 0.47 pm (5% La^{3+} substitution). The NaCl block, on the other hand, exhibited a contraction along the c-axis; the (Sr,La)–O(2) distance decreased along the c-axis. For the $n=2$ compound, the Ti–O(1) distance along the a-axis and the Ti–O(2) distance towards the apical oxygen increased with doping, while the Ti–O(3) distance remained unchanged. The (Sr,La)(1)–O(2) distance in the NaCl block along the c-axis decreased, similar to the $n=1$ compound. Hence, judging from the changes in the M–O distances observed for the $n=1$ and $n=2$ compounds, the increase in the a-axis is attributed to the increase in the volume of the perovskite block,

Table 1
Crystallographic data for $Sr_{1.9}La_{0.1}TiO_{3.95}$ (SG I4/mmm; No. 139)

Atom	Position	x	y	z	B (nm^2)	g
(Sr,La)	4e	0	0	0.3538(4) [0.3542(3)]	0.003(1) [0.005(1)]	1
Ti	2a	0	0	0	0.003 [0.003(2)]	1
O(1)	4c	0	0.5	0	0.005(7) [0.004(5)]	0.975 [1]
O(2)	4e	0	0	0.160(2) [0.157(1)]	0.007(7) [0.004(4)]	1 [1]
Lattice parameters (nm)	a=0.3890(1) [0.38859(6)]	c=1.2585(3) [1.2597(2)]				
R_{wp}=0.1145 [0.0944]	R_I=0.0389 [0.0266]	R_p=0.0878 [0.0652]	R_e=0.0402 [0.0501]	R_F=0.0190 [0.0188]		

Numbers in brackets are data for Sr_2TiO_4.
Number in parentheses represent the estimated standard deviation.
Values without standard deviation are constrained.

Table 2
Crystallographic data for $Sr_{2.85}La_{0.15}Ti_2O_{6.875}$ (SG I4/mmm; No. 139)

Atom	Position	x	y	z	B (nm^2)	g
(Sr,La)(1)	4e	0	0	0.1852(3) [0.1849(2)]	0.007(1) [0.004(1)]	1
(Sr,La)(2)	2b	0	0	0.5	0.006(2) [0.004(1)]	1
Ti	4e	0	0	0.0982(4) [0.0980(5)]	0.01 [0.001(1)]	1
O(1)	8g	0	0.5	0.094(1) [0.0957(9)]	0.007(6) [0.004(3)]	0.96875 [1]
O(2)	4e	0	0	0.195(2) [0.193(1)]	0.01(1) [0.008(7)]	1 [1]
O(3)	2a	0	0	0	0.01(1) [0.002(9)]	1 [1]
Lattice parameters (nm)	a=0.3903(1) [0.39007(6)]	c=2.0341(6) [2.0356(3)]				
R_{wp}=0.101 [0.0867]	R_I=0.0323 [0.0229]	R_p=0.0755 [0.0750]	R_e=0.0318 [0.0336]	R_F=0.0252 [0.0159]		

Numbers in brackets are data for $Sr_3Ti_2O_7$.
Number in parentheses represent the estimated standard deviation.
Values without standard deviation are constrained.

while the decrease in the c-axis is attributed to the contraction of the NaCl block.

3.3. Electrical properties

The temperature dependence of the resistivity for the $n=1$ and $n=2$ compounds is shown in Fig. 3. Although reduced calcium titanates were reported to show metallic behavior at high temperature [13], the reduced strontium titanates were semiconducting with very weak temperature dependence. The temperature dependence was slightly weaker for the $n=2$ compound, showing intermediate behavior between the $n=\infty$ (metallic) and $n=1$ (semiconducting) compounds. The effect of oxygen vacancy distribution within the conducting route may be

Table 3
Selected bond distances (nm) for $Sr_{1.9}La_{0.1}TiO_{3.95}$ and Sr_2TiO_4

	$Sr_{1.9}La_{0.1}TiO_{3.95}$	Sr_2TiO_4
(Sr,La)–O(1)	0.2677(3)	0.2673(2)
(Sr,La)–O(2)	0.2756(2)	0.2751(1)
(Sr,La)–O(2)*	0.243(3)	0.247(2)
Ti–O(1)	0.19452(6)	0.19429(3)
Ti–O(2)	0.201(3)	0.198(2)

*(Sr,La)–O distance along the *c*-axis direction in the NaCl block.

Table 4
Selected bond distances (nm) for $Sr_{2.85}La_{0.15}Ti_2O_{6.875}$ and $Sr_3Ti_2O_7$

	$Sr_{2.85}La_{0.15}Ti_2O_{6.875}$	$Sr_3Ti_2O_7$
(Sr,La)(1)–O(2)	0.2767(3)	0.2763(1)
(Sr,La)(1)–O(2)*	0.243(4)	0.248(2)
(Sr,La)(1)–O(3)	0.268(2)	0.266(1)
(Sr,La)(2)–O(1)	0.274(2)	0.275(1)
(Sr,La)(2)–O(3)	0.27602(9)	0.27593(5)
Ti–O(1)	0.1953(1)	0.19510(6)
Ti–O(2)	0.197(5)	0.193(3)
Ti–O(3)	0.199(1)	0.199(1)

*(Sr,La)–O distance along the *c*-axis direction in the NaCl block.

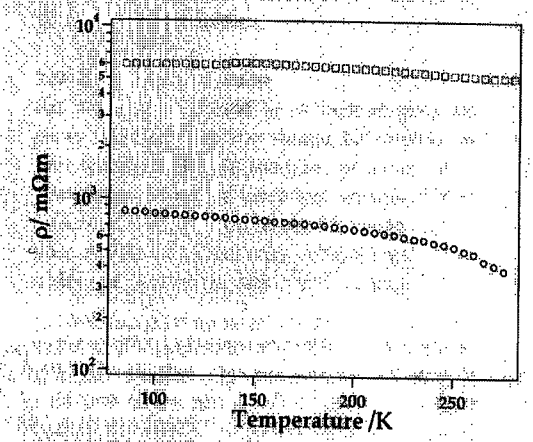

Fig. 3. The temperature dependence of resistivity for $Sr_{1.9}La_{0.1}TiO_{3.95}$ (circles) and $Sr_{2.85}La_{0.15}Ti_2O_{6.875}$ (squares).

neglected as the cause for the lack of metallic behavior, since the calcium titanates exhibited higher conductivity with an increase in oxygen vacancies. One possibility for the difference may be the weaker overlap of the d-orbitals due to the longer *a*-axis for the strontium titanates (0.3903(1) nm for $Sr_{2.85}La_{0.15}Ti_2O_{6.875}$; nominal titanium valence 3.8+; compared to 0.38321(2) nm for $Ca_3Ti_2O_{6.893}$; nominal titanium valence 3.89+).

Acknowledgements

One of the authors (Y.S.) thanks the Advanced Research Center for Science and Engineering, Waseda University, for financial support. This work was financially supported, in part, by a Grant-in-Aid for JSPS Fellows (No. 5727) from the Ministry of Education, Science, Sports, and Culture.

References

[1] K. Toda, K. Kameo, M. Fujimoto, M. Sato, J. Ceram. Soc. Jpn. 102 (1994) 737.
[2] K. Toda, S. Kurita, M. Sato, Solid State Ionics 81 (1995) 267.
[3] K. Toda, Y. Kameo, S. Kurita, M. Sato, J. Alloys Comp. 234 (1996) 19.
[4] K. Toda, J. Watanabe, M. Sato, Solid State Ionics 90 (1996) 15.
[5] S. Byeon, K. Park, M. Itoh, J. Solid State Chem. 121 (1996) 430.
[6] J. Gopalakrishnan, V. Bhat, Inorg. Chem. 26 (1987) 4299.
[7] M. Richard, L. Brohan, M. Tournoux, J. Solid State Chem. 112 (1994) 345.
[8] M. Richard, G. Goglio, L. Brohan, Mater. Res. Bull. 30 (1995) 925.
[9] S. Byeon, J. Yoon, S. Lee, J. Solid State Chem. 127 (1996) 119.
[10] K. Toda, J. Watanabe, M. Sato, Mater. Res. Bull. 31 (1996) 1427.
[11] K. Toda, S. Kurita, M. Sato, J. Ceram. Soc. Jpn. 104 (1996) 140.
[12] J.F. Schooley, W.R. Hosler, Phys. Rev. Lett. 12 (1964) 474.
[13] I. Kim, M. Itoh, T. Nakamura, J. Solid State Chem. 101 (1992) 77.
[14] F. Izumi, in: R.A. Young (Ed.), The Rietveld Method, Oxford University Press, Oxford, 1993, p. 236.
[15] Y.I. Kim, F. Izumi, J. Ceram. Soc. Jpn. 102 (1994) 401.
[16] R.D. Shannon, Acta Crystallogr. A 32 (1976) 751.

New Conversion Reaction of an Aurivillius Phase into the Protonated Form of the Layered Perovskite by the Selective Leaching of the Bismuth Oxide Sheet

Wataru Sugimoto,[†,§] Masashi Shirata,[†]
Yoshiyuki Sugahara,*[,†] and Kazuyuki Kuroda[†,‡]

Department of Applied Chemistry
School of Science and Engineering, Waseda University
Ohkubo-3, Shinjuku-ku, Tokyo 169-8555, Japan
Kagami Memorial Laboratory for Materials Science and Technology, Waseda University, Nishiwaseda-2
Shinjuku-ku, Tokyo 169-0051, Japan

Received August 2, 1999

Oxides with the general formula $M[A_{n-1}B_nO_{3n+1}]$ and $M_2[A_{n-1}B_nO_{3n+1}]$ (M = Rb, K, etc., A = Na, Ca, La, etc., B=Ti, Nb and Ta) represent a class of perovskite-related oxides with layered structures, where $[A_{n-1}B_nO_{3n+1}]$ denotes a negatively charged perovskite-like slab with thickness of n, and M is an ion-exchangeable monovalent-interlayer cation.[1,2] The monovalent-interlayer cation is readily exchanged with protons ($M^+ \rightarrow H^+$) by ion-exchange reactions with acidic solutions, resulting in their corresponding protonated forms, $H[A_{n-1}B_nO_{3n+1}]$ and $H_2[A_{n-1}B_nO_{3n+1}]$.[3−6] These protonated forms have attracted increased attention, as they exhibit various properties and can be utilized as hosts for various functional materials.[7] Because the synthesis of $M[A_{n-1}B_nO_{3n+1}]$ and $M_2[A_{n-1}B_nO_{3n+1}]$ has been limited to those with B = Ti, Nb, and Ta, the B-site cations of the corresponding protonated forms have been restricted to these elements.

The Aurivillius phases, $Bi_2O_2[A_{n-1}B_nO_{3n+1}]$, are a series of perovskite-related oxides possessing layered structures, where $[A_{n-1}B_nO_{3n+1}]$ denotes the perovskite-like slab.[8] The perovskite-like slab in $Bi_2O_2[A_{n-1}B_nO_{3n+1}]$ is structurally analogous to that in the layered perovskites with ion-exchange capability (Figure 1). The perovskite-like slab in the layered perovskites with ion-exchange capability is relatively stable in acidic solutions, since the protonated forms were obtained by acid treatment.[2−5] By analogy, the perovskite-like slab in $Bi_2O_2[A_{n-1}B_nO_{3n+1}]$ is also presumed to be stable in acidic solutions. On the other hand, bismuth oxosalts (which possesses a structure similar to the bismuth oxide sheet in $Bi_2O_2[A_{n-1}B_nO_{3n+1}]$[8c]) and bismuth oxide are soluble in acidic solutions.[9] Such a large difference in acid resistance between the perovskite-like slab and the bismuth oxide sheet may lead to a selective leaching of the bismuth oxide sheet by acid treatment.

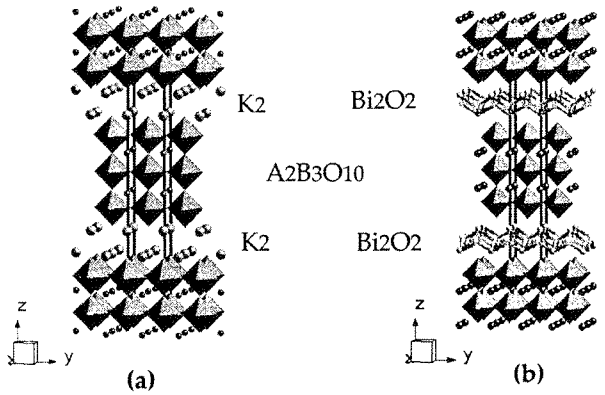

Figure 1. The schematic structures of $n = 3$ layered perovskites (a) $K_2[A_2B_3O_{10}]$ and (b) $Bi_2O_2[A_2B_3O_{10}]$.

We report in this communication a new conversion reaction for preparing a protonated form of a layered perovskite by hydrochloric acid treatment of an Aurivillius phase $Bi_2O_2[SrNaNb_3O_{10}]$. The present reaction involves not only the selective leaching of the bismuth oxide sheet, but also the introduction of protons for charge compensation to maintain the layered perovskite-like structure. As numerous Aurivillius phase compounds have been reported with combinations of various elements and n values (A = Na, Ca, Bi, etc.; B = W, Nb, Ti, etc.; $1 \leq n \leq 8$),[10] the present conversion reaction opens the possibility to achieve protonated forms of layered perovskites with an extensive range of compositions.

The synthesis[11] of polycrystalline $Bi_2O_2[SrNaNb_3O_{10}]$ (BSNN) was conducted by a procedure similar to those of $Bi_2O_2[Bi_{0.5}Na_{1.5}Nb_3O_{10}]$[12] and $Bi_2O_2[CaNaNb_3O_{10}]$.[13] The acid-treated product (HSNN) was prepared by stirring 1 g of BSNN in 200 mL of 6 M HCl at room temperature for 72 h. After the reaction, the centrifuged and washed HSNN was dried under ambient conditions.

The lattice parameters of BSNN (tetragonal; S.G. *I4/mmm*, $Z = 2$; $a = 0.39007(1)$ nm, $c = 3.2926(1)$ nm) refined by Rietveld analysis[14] of the XRD pattern (Figure 2a) were comparable to those of structurally related compounds, i.e. $Bi_2O_2[Bi_{0.5}Na_{1.5}Nb_3O_{10}]$[12] and $Bi_2O_2[CaNaNb_3O_{10}]$.[13] The XRD pattern for HSNN (Figure 2b) was successfully indexed based on a tetragonal cell with $a = 0.390 \pm 0.001$ nm and $c = 1.43 \pm 0.02$ nm.[15] The (00*l*) diffraction peaks of BSNN disappeared after the acid treatment, and new (00*l*) diffraction peaks appeared at higher 2θ angles. On the other hand, the diffraction peaks characteristic of the perovskite sublattice (110) and (200) were observed at the same 2θ angles. The (*hk*0) peaks revealed the retention of the structure along the *ab* plane, while the presence of the (00*l*) peaks at higher 2θ angles indicated the contraction of the basal spacing. The broadness of the (*hkl*) ($l \neq 0$) peaks compared to the (*hk*0)

† School of Science and Engineering.
‡ Kagami Memorial Laboratory for Materials Science and Technology.
§ Current address: Department of Fine Materials Engineering, Faculty of Textile Science and Technology, Shinshu University, 3-15-1 Tokida, Ueda, 386-8567, Japan.

(1) Jacobson, A. J. *Chemical Physics of Intercalation II*; P. Brenier: New York, 1993; pp 117−139.
(2) Dion, M.; Ganne, M.; Tournoux, M. *Mater. Res. Bull.* **1981**, *16*, 1429.
(3) Jacobson, A. J.; Johnson, J. W.; Lewandowski, J. T. *Inorg. Chem.* **1985**, *24*, 3727.
(4) Dion, M.; Ganne, M.; Tournoux, M. *Rev. Chim. Miner.* **1986**, *23*, 61.
(5) Gopalakrishnan, J.; Bhat, V. *Inorg. Chem.* **1987**, *26*, 4299.
(6) Ollivier, P. J.; Mallouk, T. E. *Chem. Mater.* **1998**, *10*. 2585.
(7) For example, see: (a) Jacobson, A. J.; Johnson, J. W.; Lewandowski, J. T. *Mater. Res. Bull.* **1987**, *22*, 45. (b) Subramanian, M. A.; Gopalakrishnan, J.; Sleight, A. W. *Mater. Res. Bull.* **1988**, *23*, 837. (c) Matsuda, T.; Miyamae, N.; Takeuchi, M. *Bull. Chem. Soc. Jpn.* **1993**, *66*, 1551. (d) Takahashi, S.; Nakato, T.; Hayashi, S.; Sugahara, Y.; Kuroda, K. *Inorg. Chem.* **1995**, *34*, 5065. (e) Ebina, Y.; Tanaka, A.; Kondo, J. N.; Domen, K. *Chem. Mater.* **1996**, *8*, 2534.
(8) (a) Aurivillius, B. *Ark. Kemi* **1949**, *1*, 463. (b) Aurivillius, B. *Ark. Kemi* **1949**, *1*, 499. (c) Aurivillius, B. *Ark. Kemi* **1950**, *2*, 519.
(9) (a) *Gmelins Handbuch der Anorganischen Chemie: Bismuth*; Springer-Verlag: Berlin, 1964. (b) *A Dictionary of Chemical Solubilities: Inorganic*; Comey, A. M., Hahn, D. A., Eds.; The Macmillan Company: New York, 1921; pp 93−94.
(10) For example, see: (a) Subbarao, E. C. *J. Am. Ceram. Soc.* **1962**, *45*, 166. (b) Subbarao, E. C. *J. Phys. Chem. Solids* **1962**, *23*, 665. (c) Wolfe, R. W.; Newnham, R. E. *J. Electrochem. Soc.* **1969**, *116*, 832. (d) Subbarao, E. C. *Ferroelectrics* **1973**, *5*, 267. (e) Kikuchi, T.; Watanabe, A.; Uchida, K. *Mater. Res. Bull.* **1977**, *12*, 299.
(11) A stoichiometric mixture of $Bi_2O_2[SrNb_2O_7]$ and $NaNbO_3$ was fired at 1100 °C for 3 h twice to obtain the single-phase product.
(12) Kikuchi, T. *Mater. Res. Bull.* **1979**, *14*, 1561.
(13) Muramatsu, K.; Shimazu, M.; Tanaka, J.; Horiuchi, S. *J. Solid State Chem.* **1981**, *36*, 179.
(14) (a) Izumi, F. In *The Rietveld Method*; Young, R. A., Ed.; Oxford University Press: Oxford, 1993; pp 236−253. (b) Kim, Y. I.; Izumi, F. *J. Ceram. Soc. Jpn.* **1994**, *102*, 401.
(15) The lattice parameters were refined by the nonlinear least-squares method.

10.1021/ja9927265 CCC: $18.00
Published on Web 11/25/1999

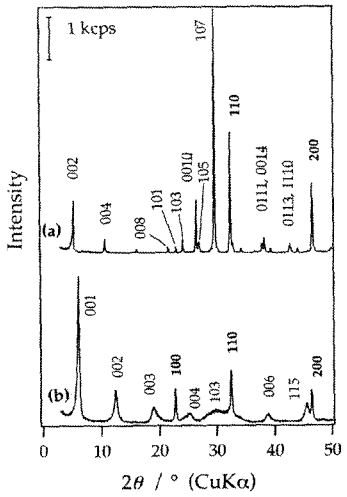

Figure 2. The XRD patterns (a) before and (b) after the acid treatment of $Bi_2O_2[SrNaNb_3O_{10}]$.

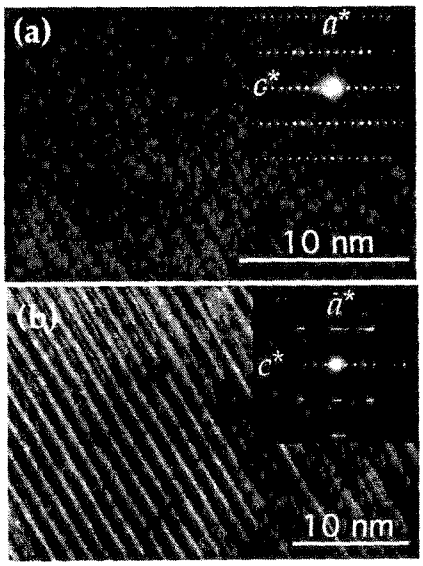

Figure 3. TEM lattice images along the [010] zone (a) before and (b) after the acid treatment of $Bi_2O_2[SrNaNb_3O_{10}]$. The corresponding ED patterns are shown in the insets.

peaks indicated stacking disorder. The appearance of the (100) diffraction peak showed that the doubling of the *c* axis observed in BSNN does not occur in HSNN.[16] The lattice parameter of HSNN was comparable to the values of protonated forms of layered perovskite with $n = 3$ obtained by conventional ion-exchange reactions, i.e. $HCa_2Nb_3O_{10}$ ($a = 0.3849$ nm and $c = 1.437$ nm)[3] and $H_2La_2Ti_3O_{10}$ ($a = 0.382$ nm and $c = 2.766$ nm (the *c* axis is doubled due to the displacement of the perovskite-like slabs)).[5]

Transmission electron micrographs (TEM) and the corresponding electron diffraction (ED) patterns along the [010] zone of BSNN and HSNN are shown in Figure 3. Alternating rows of dark and light contrast were observed for both BSNN and HSNN, in accordance with the retention of the layered structure observed by XRD. The periodicities between the alternating rows were 1.6 and 1.4 nm before and after the acid treatment, in agreement with the *c* axis (half the *c* axis in the case of BSNN) obtained from XRD.

Scanning electron microscopic observations showed no distinct difference in the size (~5 μm) or morphology of the particles before and after the acid treatment. Furthermore, ED studies of numerous HSNN particles showed no ring pattern, indicating that all the particles were crystalline solids. Consequently, the simultaneous dissolution of both the bismuth oxide sheet and the perovskite-like slab and the possibility of amorphization as a result of the acid treatment can be disregarded.

Inductively coupled plasma emission spectroscopy (ICP) revealed the composition ratios of metals were Bi:Sr:Na:Nb = 2.00:1.00:1.02:3 for BSNN and Bi:Sr:Na:Nb = 0.21:0.80:0.95:3 for HSNN, indicating the selective leaching of Bi and the partial loss of Sr from BSNN. As the composition analysis results were the same even after acid treatment for a month, partially undissolved Bi cannot be due to incomplete reaction. These results, combined with the fact that (Bi+Sr):Nb = 1.01:3, suggest that partial disordering of cations (Bi ⇄ Sr) is present in the parent compound BSNN, similar to that reported for $Bi_2O_2[ANb_2O_7]$ (A = Ca, Sr, Ba, and Pb).[17]

Thermogravimetric analysis of HSNN dried at 120 °C revealed 2.7 mass % loss which started from 160 °C, agreeing with the proton content according to the overall reaction

$$Bi_{1.8}Sr_{0.2}O_2[Bi_{0.2}Sr_{0.8}NaNb_3O_{10}] \xrightarrow{HCl} H_{1.8}[Bi_{0.21}Sr_{0.80}Na_{0.95}Nb_3O_{10}]$$

Notice that the proton content is equivalent to the formal charge of the perovskite-like slab. The overall reaction can thus be regarded as the replacement of the positively charged bismuth-oxide sheet (containing Sr) with protons so as to compensate for the negatively charged perovskite-like slab ($\{[Bi_{1.8}Sr_{0.2}O_2]^{1.8+}\}_x \rightarrow 1.8xH^+$).

The intercalation of butylamine (C4A) and octylamine (C8A) was performed as alkylamines are known to be intercalated into the interlayer space of protonated forms of layered niobates.[1,18] The *c* axis increased when HSNN was reacted with C4A (1.41 → 2.46 nm) and C8A (1.41 → 3.33 nm), while the *a* axis was the same as that of HSNN ($a = 0.390$ nm). These values are comparable to those of related intercalation compounds, C4A−$H[Ca_2Nb_3O_{10}]$ and C8A−$H[Ca_2Nb_3O_{10}]$.[3,7a] Chemical analysis revealed 0.9 mol of C4A and 1.0 mol of C8A per unit of $[Bi_{0.21}Sr_{0.80}Na_{0.95}Nb_3O_{10}]$ were intercalated. These results show the formation of C4A- and C8A-HSNN intercalation compounds, which strongly supports the layered structure of HSNN. Although fractional amounts of alkylamine intercalated into layered oxides are not uncommon,[19] unoptimized intercalation conditions may also be a reason for the partial intercalation. The capability of HSNN to accommodate alkylamines, in contrast to $H_2La_2Ti_3O_{10}$,[20] suggests a notable difference in the reactivity of the protons attached to NbO_6 and TiO_6 octahedra.[20]

Acknowledgment. This work was financially supported in part by the Grant-in-Aid for Scientific Research (No. 10555221) from the Ministry of Education, Science, Sports, and Culture, Japan.

JA9927265

(16) The lack of *c* axis doubling implies that no displacement of the perovskite-like slabs is involved, unlike BSNN where the perovskite-like slabs are displaced by 1/2 along the diagonal direction of the two *a* axes.

(17) (a) Srikanth, V.; Idink, H.; White, W. B.; Subbarao, E. C.; Rajagopal, H.; Sequeira, A. *Acta Crystallogr.* **1996**, *B52*, 432. (b) Blake, S. M.; Falconer, M. J.; McCreedy, M.; Lightfoot, P. *J. Mater. Chem.* **1997**, *7*, 1609. (c) Ismunandar; Hunter, B. A.; Kennedy, B. J. *Solid State Ionics* **1998**, *112*, 281.

(18) Mallouk, T. E.; Kim, H.-N.; Ollivier, P. J.; Keller, S. W. *Comprehensive Supramolecular Chemistry*; Alberti, G., Bein, T., Eds.; Elsevier Science, Oxford, UK, 1996; Vol. 7, pp 189−218.

(19) For example, see: (a) Clément, P.; Marchand, R. *C. R. Acad. Sci. Paris II* **1983**, *296*, 1161. (b) Mohan Ram R. A.; Clearfield, A. *J. Solid State Chem.* **1991**, *94*, 45.

(20) Gopalakrishnan, J.; Uma, S.; Bhat, V. *Chem. Mater.* **1993**, *5*, 132.

Conversion of an Aurivillius Phase $Bi_2SrNaNb_3O_{12}$ into Its Protonated Form *via* Treatment with Various Mineral Acids

Masashi Shirata, Yu Tsunoda, Wataru Sugimoto,[1] and Yoshiyuki Sugahara
Department of Applied Chemistry, School of Science and Engineering, Waseda University, Shinjuku-ku, Tokyo 169-8555 JAPAN
[1]Department of Fine Materials Engineering, Faculty of Textile Science and Technology, Shinshu University, Ueda, Nagano, 386-8567 JAPAN

ABSTRACT

A protonated form of a layered perovskite was prepared from an Aurivillius phase $Bi_2SrNaNb_3O_{12}$ *via* acid treatments, and the effect of the type of mineral acids was investigated. The treatment with HX (X = Cl, Br, I) resulted in the formation of a protonated form $H_{1.8}[Sr_{0.8}Bi_{0.2}NaNb_3O_{10}]$, while no reactions were observed for HNO_3 and H_2SO_4 under the present experimental conditions. All the products obtained by HX-treatments exhibited layered structures and the structures of the perovskite-like slabs were preserved.

INTRODUCTION

Layered perovskites possess two-dimensional perovskite-like slabs in their structures. Among them, ion-exchangeable layered perovskites consist of perovskite-like slabs ($[A_{n-1}B_nO_{3n+1}]$; A = Sr, Ca, *etc.*, B = Ti, Nb, Ta) and monovalent exchangeable interlayer cations (M; M = Na, K, Rb, *etc.*) [1]. There have been two homologous series reported, that are called Dion-Jacobson phases ($M[A_{n-1}B_nO_{3n+1}]$) [2,3] and Ruddlesden-Popper phases ($M_2[A_{n-1}B_nO_{3n+1}]$) [4-6]. When these layered perovskites were treated with mineral acids, they were converted into corresponding protonated forms ($H[A_{n-1}B_nO_{3n+1}]$ and $H_2[A_{n-1}B_nO_{3n+1}]$) [3,6-8]. These protonated forms exhibit interesting properties including photocatalytic behavior [9], proton conduction [10], and intercalation of organic amines [11]. These protonated forms can also be utilized as precursors for oxide syntheses [12].

Aurivillius phases ($Bi_2A_{n-1}B_nO_{3n+3}$ or alternately expressed as $Bi_2O_2[A_{n-1}B_nO_{3n+1}]$) are known to exhibit excellent dielectric properties. In terms of structures, they consist of perovskite-like slabs ($[A_{n-1}B_nO_{3n+1}]$) and Bi_2O_2 layers, and it should be noted that the structures of perovskite-like slabs in the Aurivillius phases are identical with those in the aforementioned ion-exchangeable layered perovskites [13]. Suzuki *et al.* [14] reported the acid treatment of a $Bi_2SrTa_2O_9$ single crystal, and observed drastic variation in X-ray diffraction patterns; they ascribed this observation to the structural change in the perovskite-like slabs. We have recently reported that HCl-treatment of another Aurivillius phase, $Bi_2SrNaNb_3O_{12}$, led to the selective leaching of the Bi_2O_2 layers and the introduction of protons for charge compensation to form a corresponding protonated form [15]. Since no structural change in the perovskite-like slabs occurred, this reaction is considered to be the conversion of the Aurivillius phase into a protonated form of a Ruddlesden-Popper phase (though the layer charge is slightly reduced from 2- per $[A_{n-1}B_nO_{3n+1}]$, the general value for the Ruddlesden-Popper phases, to ~1.8- per $[A_{n-1}B_nO_{3n+1}]$ because of the disorder between Bi and Sr). Very recently, Gopalakrishnan *et al.* [16] reported a reverse reaction of the aforementioned reaction, namely the conversion of a

Ruddlesden-Popper phase into an Aurivillius phase through a metathesis reaction using BiOCl. Thus, the Ruddlesden-Popper phases and the Aurivillius phases are actually interconvertible.

Here, we report the effect of the type of mineral acids used on the conversion of $Bi_2SrNaNb_3O_{12}$. As acids, hydrochloric acid (HCl), hydrobromic acid (HBr), hydroiodic acid (HI), nitric acid (HNO_3), and sulfuric acid (H_2SO_4) were used. The products were analyzed by X-ray diffraction (XRD), transmission electron microscopy (TEM), compositional analysis, and scanning electron microscopy (SEM).

EXPERIMENTAL

$Bi_2SrNaNb_3O_{12}$ (BSNN) was prepared by the heat treatment of a stoichiometric mixture of $Bi_2SrNb_2O_9$ [17] and $NaNbO_3$ at 1100 °C for 6 h with intermediate grinding. The metal ratio of BSNN (Bi:Sr:Na:Nb = 2.00:1.00:1.02:3) was consistent with the nominal one. The XRD pattern of BSNN can be indexed based on a tetragonal cell. The lattice parameters refined with the Rietveld program RIETAN [18,19] and in the space group *I4/mmm* were a = 0.39007(1) and c = 3.2926(1) nm.

About 1 g of BSNN was dispersed in 200 mL of 6 M HX (X = Cl, Br, I), 6 M HNO_3, or 3 M H_2SO_4 at room temperature for 72 h. The resulting product was washed with water, and dried at 120 °C.

XRD patterns were obtained using a Rigaku RINT-2500 diffractometer using monochromated CuKα radiation. Compositions of metals were determined by inductively-coupled plasma emission spectrometry (ICP; Nippon Jarrell Ash, ICAP 575 MARK II) after dissolving samples using a mixture of HNO_3, HF, and HCl. The amounts of protons were determined from mass losses above 160 °C by using thermogravimetry (TG; MacScience, TG-DTA 2000S) operated in air. Morphology of samples was studied by scanning electron microscopy (Hitachi, S-2500). Transmission electron microscopy was performed using Hitachi H-8100A.

RESULTS AND DISCUSSION

Figure 1 shows XRD patterns of the starting material BSNN and the products of BSNN treated with various acids. When BSNN is treated with HX (X = Cl, Br, I), the XRD patterns drastically change. The (002) peak, that corresponds to the thickness of one perovskite-like slab and one Bi_2O_2 layer in BSNN, shifts to higher angles after the HX-treatment. Correspondingly, its higher orders clearly shift to higher angles, indicating the presence of layered structures possessing smaller repeating distances in the HX-treated products. On the contrary, no shifts were observed for (*hk*0) peaks (typically (110) and (200) in Figure 1), suggesting the preservation of the perovskite-like slabs after the HX-treatments. It should also be noted that these three XRD patterns were very similar, indicating similar reactivity irrespective of the type of the X^- anion. The peaks of the products treated with HX were successfully indexed based on a tetragonal cell. The lattice parameters of the product treated with HCl are a = 0.391±0.002 and c = 1.39±0.02 nm. The a parameter of the HCl-treated product is essentially identical with that of BSNN, while the c parameter is smaller than that of BSNN, consistent with the aforementioned observations.

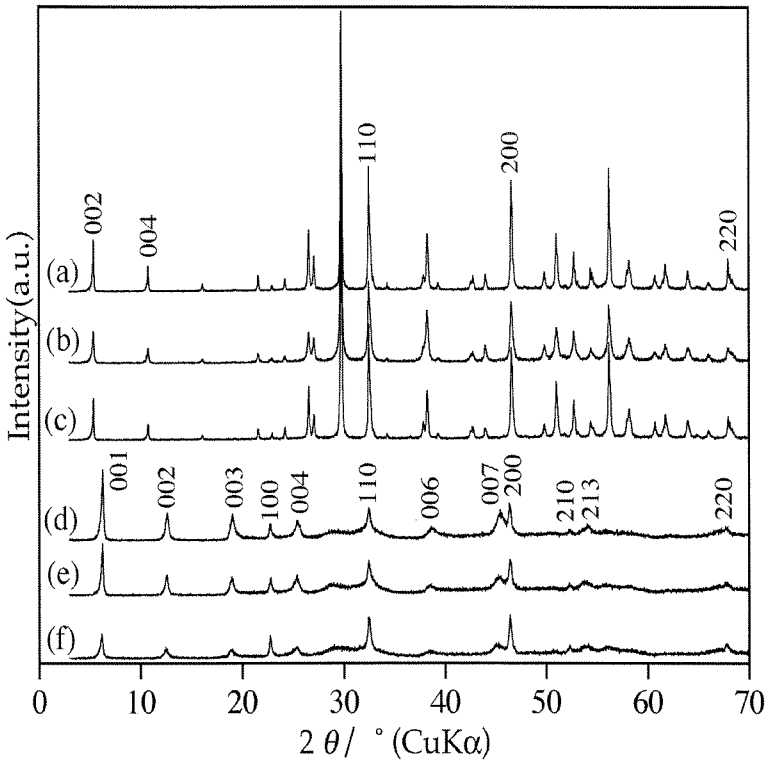

Figure 1. *XRD patterns of (a) BSNN, (b) BSNN treated with HNO_3, (c) BSNN treated with H_2SO_4, (d) BSNN treated with HCl, (e) BSNN treated with HBr, and (f) BSNN treated with HI.*

The XRD patterns of BSNN treated with HNO_3 and H_2SO_4 are completely different from those of BSNN treated with HX, and are essentially identical with that of BSNN. Thus, under the present experimental conditions, the reactions of BSNN with acids take place only when HX (X = Cl, Br, I) is used even with the same proton concentration; halide ions seem to play an important role in this conversion reaction.

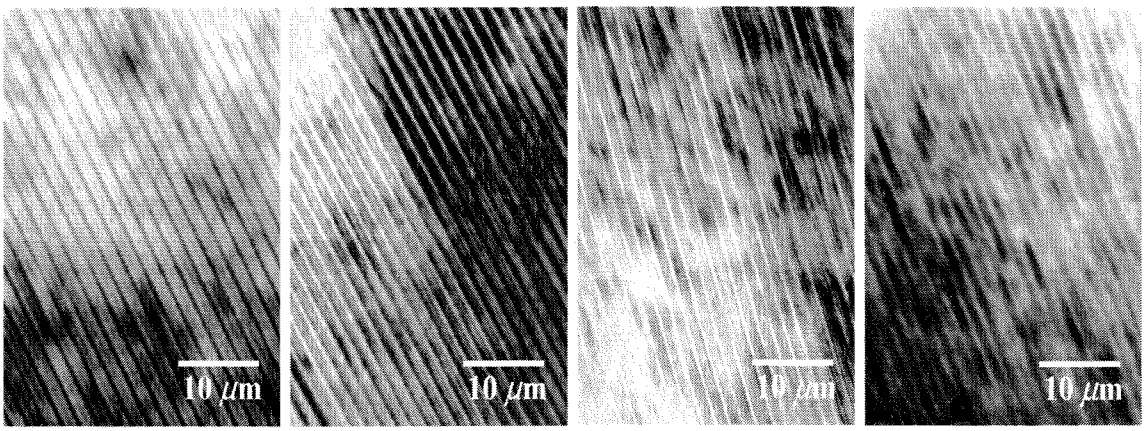

Figure 2. *TEM images of (a) BSNN, (b) BSNN treated with HCl, (c) BSNN treated with HBr, and (d) BSNN treated with HI.*

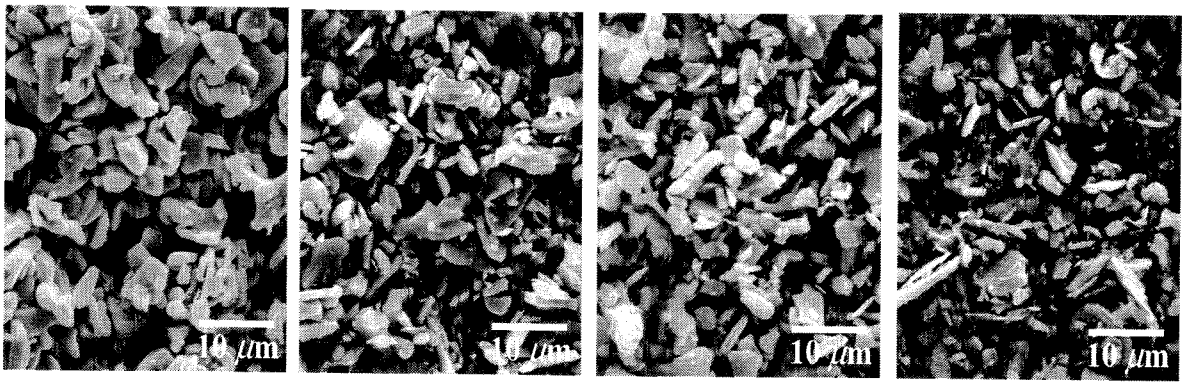

(a) (b) (c) (d)

Figure 3. *Scanning electron micrographs of (a) BSNN, (b) BSNN treated with HCl, (c) BSNN treated with HBr, and (d) BSNN treated with HI.*

The presence of layered structures in the products treated with HX is clearly shown by TEM images. Figure 2 demonstrates the TEM images along the [010] zone. Alternating lines with dark and light contrasts are observed for BSNN and all the products treated with HX, consistent with the layered structures. The repeating distance of the dark and light rows in BSNN is about 1.6 nm (~c/2), and decreases to about 1.4 nm for all the products treated with HX, consistent with the XRD observations (c = 1.39±0.02 nm for the product treated with HCl).

In order to investigate the structures of the products treated with HX, their morphology was investigated with SEM (Figure 3). All the HX-treated products exhibit a morphology that is very similar to that of BSNN. Thus, dissolution of BSNN and subsequent crystallization are very unlikely as a mechanism of the present reactions with HX.

The variation in the compositions is demonstrated in Table I. The drastic decreases in Bi contents (from 2.0 to ~0.2) are clearly shown for all the HX-treated products. On the other hand, slight losses of Sr (~0.2 Sr per 3 Nb) are always detected for the HX-treated products. We ascribe these observations to the selective leaching of the Bi_2O_2 layers containing Sr due to cation disorder ($Bi_{1.8}Sr_{0.2}O_2$) [15,20]. For charge compensation, 1.8 H^+ are introduced per 3 Nb. Thus, the overall reaction can be written as follows:

$$(Bi_{1.8}Sr_{0.2}O_2)[Sr_{0.8}Bi_{0.2}NaNb_3O_{10}] \xrightarrow{HX} H_{1.8}[Sr_{0.8}Bi_{0.2}NaNb_3O_{10}]$$

Table I. *Variation in compositions of BSNN after the treatment with HX (X = Cl, Br, I) (in molar ratio)*

	BSNN	HX-treated		
		HCl	HBr	HI
Bi	2.0	0.21	0.25	0.23
Sr	1.0	0.80	0.77	0.78
Na	1.0	1.0	1.0	1.0
Nb*	3	3	3	3
H	-	1.8	1.8	1.8

*set to be three

For dissolution of metal oxides, the effects of anions have been reported. Based on a surface complexation model [21], anions can influence the rate of dissolution *via* the formation of surface complexes, inductive effects, and thermodynamic changes in solubility. Some of these factors may play a role in the significant effect of anions observed in the present study.

CONCLUSIONS

We have demonstrated that the type of anion in the mineral acids exhibited a significant effect on the conversion of the Aurivillius phase $Bi_2SrNaNb_3O_{12}$ into its protonated form. HX (X = Cl, Br, I) was effective for this conversion, while HNO_3 and H_2SO_4 did not lead to successful conversion under the present experimental conditions. These observations imply that halide ions play an important role in the conversion reaction.

ACKNOWLEDGMENTS

The authors would like to thank Prof. Kazuyuki Kuroda (Department of Applied Chemistry, Waseda University) for valuable discussion and Mr. Minekazu Fujiwara (Material Characterization Central Laboratory, Waseda University) for his assistance in TEM observation. This work was financially supported partly by the Grant-in-Aid for Scientific Research (No. 10555221) from the Ministry of Education, Science, Sports, and Culture, Japan.

REFERENCES

1. J. Gopalakrishnan, *Rev. Solid State Sci.* **1**, 515 (1988).
2. M. Dion, M. Ganne and M. Tournoux, *Mater. Res. Bull.* **16**, 1429 (1981).
3. A. J. Jacobson, J. W. Johnson and J. T. Lewandowski, *Inorg. Chem.* **24**, 3727 (1985).
4. S. N. Ruddlesden and P. Popper, *Acta Crystllogr.* **10**, 538 (1957).
5. S. N. Ruddlesden and P. Popper, *Acta Crystllogr.* **11**, 54 (1958).
6. J. Gopalakrishnan, V. Bhat and B. Raveau, *Mater. Res. Bull.* **22**, 413 (1987).
7. M. Dion, M. Ganne and M. Tournoux, *Rev. Chim. Miner.* **23**, 61 (1986).
8. A. J. Jacobson, J. T. Lewandowski and J. W. Johnson, *J. Less-Common Met.* **116**, 137 (1986).
9. Y. Ebina, A. Tanaka, J. N. Kondo and K. Domen, *Chem. Mater.* **8**, 2534 (1996).
10. M. A. Subramanian, J. Gopalakrishnan and A. W. Sleight, *Mater. Res. Bull.* **23**, 837 (1988).
11. A. J. Jacobson, J. W. Johnson and J. T. Lewandowski, *Mater. Res. Bull.* **22**, 45 (1987).
12. P. J. Olivier and T. E. Mallouk, *Chem. Mater.* **10**, 2585 (1998).
13. C. N. R. Rao and B. Raveau, *Transition Metal Oxide, 2nd edition*, (Wiley-VCH, 1998) pp.74-75.
14. M. Suzuki, N. Nagasawa, A. Machida and T. Ami, *Jpn. J. Appl. Phys.* **35**, L564 (1996).
15. W. Sugimoto, M. Shirata, Y. Sugahara and K. Kuroda, *J. Am. Chem. Soc.* **121**, 11601 (1999).
16. J. Gopalakrishnan, T. Sivakumar, K. Ramesha, V. Thangadurai and G N. Subbanna, *J. Am. Chem. Soc.* **122**, 6237 (2000).
17. Ismunandar and B. J. Kennedy, *J. Solid State Chem.* **126**, 135 (1996).
18. F. Izumi, Rietveld Analysis Programs RIETAN and PREMOS and Special Applications,

Rietveld Analysis, ed. R. A. Young, (Oxford University Press, 1993) pp.236-253.
19. Y. I. Kim and F. Izumi, *J. Ceram. Soc. Jpn.* **102**, 401 (1994).
20. S. M. Blake, M. J. Falconer, M. McCreedy and P. Lightfoot, *J. Mater. Chem.* **7**, 1609 (1997).
21. M. A. Bleza, P. J. Morando and A. E. Regazzoni, *Chemical Dissolution of Metal Oxides*, (CRC Press, 1994) pp.172-177.

Journal of Solid State Chemistry 148, 508–512 (1999)
Article ID jssc.1999.8488, available online at http://www.idealibrary.com on IDEAL®

Synthesis and Structures of Reduced Niobates with Four Perovskite-like Layers and Their Semiconducting Properties

W. Sugimoto,*,[1] H. Ohkawa,* M. Naito,* Y. Sugahara,*,[2] and K. Kuroda*,†

*Department of Applied Chemistry, School of Science and Engineering, Waseda University, Ohkubo-3, Shinjuku-ku, Tokyo 169-8555, Japan; and
†Kagami Memorial Laboratory for Materials Science and Technology, Waseda University, Nishiwaseda-2, Shinjuku-ku, Tokyo 169-0051, Japan

Received March 29, 1999; in revised form July 27, 1999; accepted August 27, 1999

Carriers were successfully doped into $RbCa_2NaNb_4O_{13}$ by the substitution of Sr^{2+} for Na^+, yielding electroconducting niobates with a layered structure consisting of four perovskite-like layers. Single-phase products of polycrystalline $RbCa_2Na_{1-x}Sr_xNb_4O_{13}$ ($x = 0.2$ and 0.4) were synthesized by the solid-state reaction of $RbCa_2Nb_3O_{10}$, $Sr_5Nb_4O_{15}$, Nb_2O_5, and Nb metal. The solid solutions were indexed based on a tetragonal structure, corresponding to the end-member $RbCa_2NaNb_4O_{13}$. With the increase in the amount of strontium substitution, an expansion of the c-axis was observed while the a-axis was essentially constant. The products showed semiconducting properties.

Key Words: **niobate; solid-state reaction; layered perovskite; reduced oxidation state; Rietveld analysis; electrical conduction.**

1. INTRODUCTION

A large class of transition metal oxides possess structures consisting of two-dimensionally stacked perovskite-like slabs: $A_{n+1}B_nO_{3n+1}$ (1), $Bi_2A_{n-1}B_nO_{3n+3}$ (2), and $MA_{n-1}B_nO_{3n+1}$ are well-known examples (3, 4). These structures are ideal for relating the thickness of the perovskite-like slabs n with the properties. For example, the change in the electrical properties of $(La, Sr)_{n+1}Mn_nO_{3n+1}$ ($n = 1$, 2, 3, and ∞) (5), $Sr_{n+1}V_nO_{3n+1}$ ($n = 1$, 2, and ∞) (6, 7), $La_{n+1}Ni_nO_{3n+1}$ ($n = 1$, 2, 3, and ∞) (8), and $(Sr_{0.95}, La_{0.05})_{n+1}Ti_nO_{3n+1-\delta}$ ($n = 1$ and 2) (9) has been discussed based on the difference in the thickness of the perovskite-like slabs.

Recently, the incorporation of conducting electrons into niobates with a layered-perovskite structure, $M[A_{n-1}Nb_nO_{3n+1}]$, has drawn attention. The structure of $M[A_{n-1}Nb_nO_{3n+1}]$ consists of n perovskite-like layers with a monovalent cation M occupying the interlayer space. The reduced niobates for the $n = 2$ and 3 compounds have been synthesized by chemical or electrochemical intercalation of excess ions (H^+, Li^+, and Rb^+) into the interlayer (9–17) and by cation substitution by solid-state reaction (18, 19). Most of the early studies have emphasized the structural characterization of the reduced products.

The electrical properties of carrier-doped $n = 2$ and 3 members have been reported recently. We have reported the synthesis and electrical properties of the $n = 3$ member $KCa_{2-x}Ln_xNb_3O_{10}$ (Ln = La, Ce, Nd, Sm, and Gd) (18, 19). The observed ($\log \rho$) $\propto T$ dependence was interpreted based on a model assuming tunneling conduction through vibrating barriers, and the structure–property relation was established (18, 19). Recently, it has been reported that the $n = 3$ member $Li_xKCa_2Nb_3O_{10}$ shows a superconducting transition below 6 K (15–17), whereas the $n = 2$ member $Li_xKLaNb_2O_7$ shows no superconducting transition down to 0.5 K (15). This suggests that the thickness of the perovskite-like slabs influences the superconducting properties in $M[A_{n-1}Nb_nO_{3n+1}]$.

The synthesis and structural characterization of the $n = 4$ member, $RbCa_2NaNb_4O_{13}$, have been reported (4, 20). The schematic structure of $RbCa_2NaNb_4O_{13}$ is shown in Fig. 1. In light of the variation in the electrical properties as a function of n in the two-dimensional perovskites reported so far, the electrical properties of higher n members of $M[A_{n-1}Nb_nO_{3n+1}]$ are of interest. Here, we report the doping of carriers into the $n = 4$ member of the layered perovskite $RbCa_2NaNb_4O_{13}$ by the substitution of Sr^{2+} for Na^+ and their structures and electrical properties.

2. EXPERIMENTAL

$RbCa_2Nb_3O_{10}$, $Sr_5Nb_4O_{15}$, and $NaNbO_3$ were prepared by the solid-state reactions of appropriate amounts of Rb_2CO_3, $CaCO_3$, $SrCO_3$, Na_2CO_3, and Nb_2O_5 under ambient atmosphere. A 50% excess amount of Rb_2CO_3 was used in the case of $RbCa_2Nb_3O_{10}$. The product was washed

[1] Current address: Department of Fine Materials Engineering, Faculty of Textile Science and Technology, Shinshu University, 3-15-1 Tokida, Ueda 386-8567, Japan.
[2] To whom correspondence should be addressed. E-mail: ys6546@mn.waseda.ac.jp.

0022-4596/99 $30.00

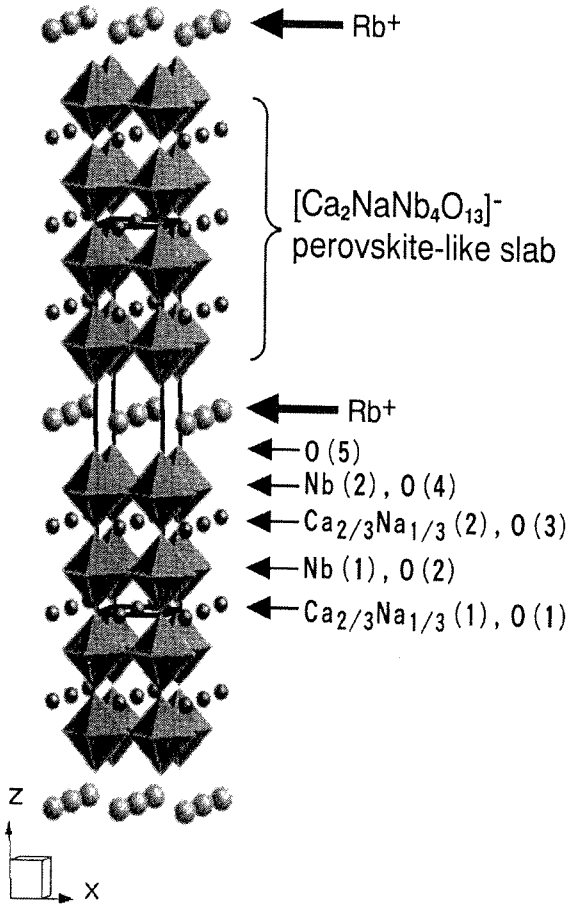

FIG. 1. Schematic crystal structure of $RbCa_2NaNb_4O_{13}$.

with deionized water after completion of the reaction. X-ray diffraction (XRD) (Mac Science MXP^3 diffractometer with monochromated Cu$K\alpha$ radiation) of the above oxides indicated single-phase formation, and inductively coupled plasma emission spectroscopy (ICP) (Nippon Jarrell Ash, ICAP575 Markll) showed that the cation ratios were consistent with the nominal ones.

Polycrystalline samples with nominal compositions of $RbCa_2Na_{1-x}Sr_xNb_4O_{13}$ ($x = 0.2$, 0.4, and 0.5) were synthesized from $RbCa_2Nb_3O_{10}$, $NaNbO_3$, $Sr_5Nb_4O_{15}$, and Nb according to the following equation:

$$RbCa_2Nb_3O_{10} + (1-x)NaNbO_3 + (0.2x)Sr_5Nb_4O_{15} + (0.2x)Nb \rightarrow RbCa_2Na_{1-x}Sr_xNb_4O_{13}. \quad [1]$$

All of the starting oxides were dried for at least 1 day at 100°C before use. The end-member $RbCa_2NaNb_4O_{13}$ was synthesized by the solid-state reactions of $RbCa_2Nb_3O_{10}$ and $NaNbO_3$ at 1200°C for 3 h in air (20). After thorough grinding, the reagents were pressed and placed in an alumina boat surrounded by powders having the same composition to prevent contamination. The reactor tube was evacuated to $\sim 8.5 \times 10^{-3}$ Pa before argon purging and Ti powder was placed in the reactor tube as an oxygen getter to minimize oxidation during the synthesis. The reagents were fired at 1200°C for several hours, with intermittent grinding after every 3 h of firing. The firing sequence was repeated twice.

The morphology of the products was studied with a scanning electron microscope (SEM) (Hitachi, S-2500). Crystalline phases were identified by XRD. Structural parameters were determined by the Rietveld analysis program RIETAN (21, 22). The cation ratios were determined by ICP analysis. For the ICP measurements, the samples were decomposed in a mixture of HF, HCl, and HNO_3 by heating at 200°C for at least 3 h. Resistivity data were collected from 80 to 280 K using a standard dc four-probe method.

3. RESULTS AND DISCUSSION

Table 1 summarizes the compositional analysis results of the products obtained as single phases. The cation ratios were in agreement with the nominal composition for all x. Thus, the discussion herein is based on the assumption that the substitution of Sr^{2+} for Na^+ produces an equimolar amount of Nb^{4+} during the synthesis.

The XRD patterns of the products are shown in Fig. 2. Preferred orientation was observed along the [00l] plane, consistent with the plate-like morphology of the samples observed in the scanning electron micrographs. The XRD

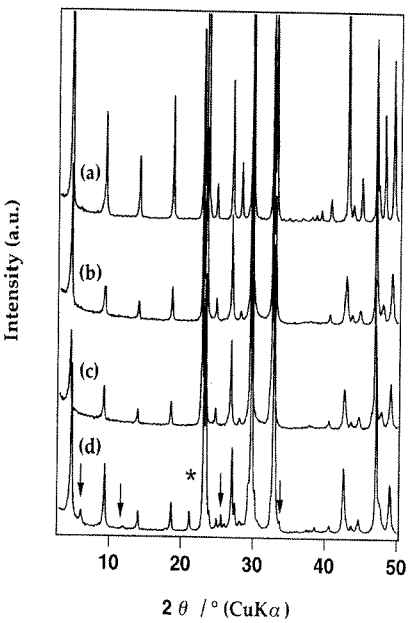

FIG. 2. XRD patterns of $RbCa_2Na_{1-x}Sr_xNb_4O_{13}$ with (a) $x = 0$, (b) $x = 0.2$, (c) $x = 0.4$, and (d) $x = 0.5$. Arrows in (d) represent peaks due to the $n = 3$ compound. The peak with an asterisk in (d) is an unidentified peak.

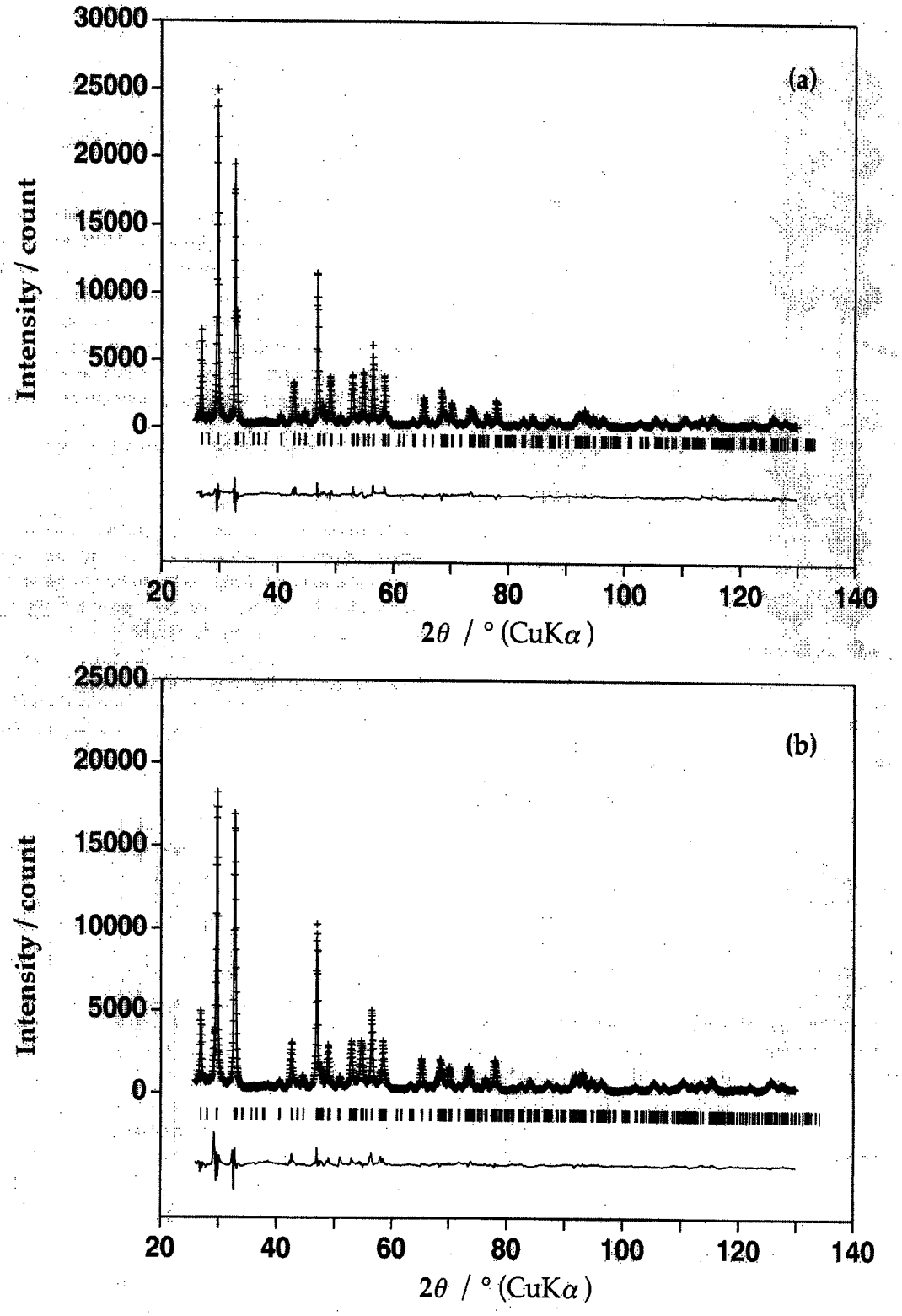

FIG. 3. XRD pattern fittings for (a) $RbCa_2Na_{0.8}Sr_{0.2}Nb_4O_{13}$ and (b) $RbCa_2Na_{0.6}Sr_{0.4}Nb_4O_{13}$. The observed (crosses) and calculated (solid line) patterns are shown in the top traces. The vertical lines in the middle represent the positions of the possible Bragg reflections. The lower curves are the difference between the observed and calculated intensities.

TABLE 1
Composition of the Products

x	Composition[a,b]
0	$Rb_{1.00}Ca_{2.06}Na_{1.06}Nb_4O_{13}$
0.2	$Rb_{1.00}Ca_{2.00}Na_{0.80}Sr_{0.21}Nb_4O_{13}$
0.4	$Rb_{1.04}Ca_{2.07}Na_{0.61}Sr_{0.40}Nb_4O_{13}$

[a] Compositions were normalized by setting the amount of niobium to 4.
[b] Amount of oxygen was set to 13.

pattern for $x = 0$ was indexed based on a primitive-tetragonal cell, in agreement with a previous report (20). Single-phase $RbCa_2Na_{1-x}Sr_xNb_4O_{13}$ was obtained for $x = 0.2$ and 0.4 with repeated firings. No extra reflections for $x = 0.2$ and 0.4 were evident in the XRD patterns when compared to that of $x = 0$, and all the diffraction peaks were indexed based on a primitive-tetragonal cell. When $x = 0.5$, an unidentified peak at $2\theta = 21.16°$ and weak diffraction peaks due to $RbCa_2Nb_3O_{10}$ were observed besides the intended phase. A single phase for $x = 0.5$ could not be obtained even with repeated firings or firing at higher temperature. Thus, the solubility limit is between $x = 0.4$ and 0.5 under the present synthetic conditions.

The structure of the $x = 0$ compound was refined by Rietveld analysis assuming a random distribution of Ca and Na at the A site (20). The crystallographic data corresponded to those of a previous report (20). Since the indexing of the XRD patterns for $x = 0.2$ and 0.4 indicated the preservation of the symmetry with substitution. Rietveld analysis for these compounds was conducted with the same space group as that for $x = 0$. A random distribution of the A-site cations (Ca, Na, and Sr) was also assumed. The outputs from the Rietveld refinement are shown in Fig. 3, and the crystallographic data are given in Table 2. The a-axis was

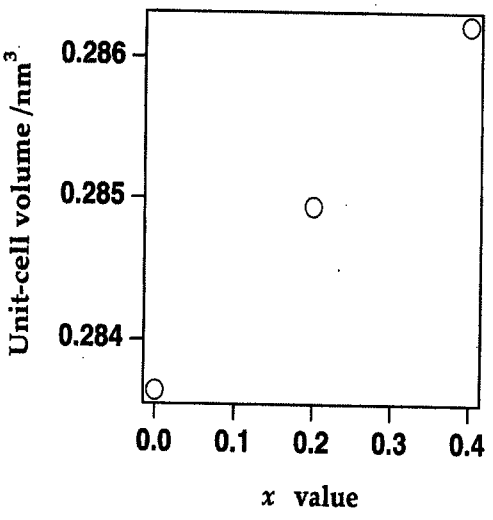

FIG. 4. Evolution of the unit-cell volume as a function of x.

TABLE 2
Crystallographic data for $RbCa_2NaNb_4O_{13}$, $RbCa_2Na_{0.8}Sr_{0.2}Nb_4O_{13}$, and $RbCa_2Na_{0.6}Sr_{0.4}Nb_4O_{13}$[a]

Sample	Atom	Position	x	y	z	B (nm^2)[c]
$RbCa_2NaNb_4O_{13}$	Rb	1*d*	0.5	0.5	0.5	0.028(3)
	A(1)[b]	1*c*	0.5	0.5	0	0.010(2)
$a = 0.38727(1)$ nm	*A*(2)[b]	2*h*	0.5	0.5	0.2240(7)	0.010
$c = 1.89116(6)$ nm	Nb(1)	2*g*	0	0	0.1057(2)	0.0028(9)
	Nb(2)	2*g*	0	0	0.3293(2)	0.0028
$R_{wp} = 0.1299$	O(1)	1*a*	0	0	0	0.036(4)
$R_p = 0.0969$	O(2)	4*i*	0	0.5	0.101(1)	0.036
$R_e = 0.0340$	O(3)	2*g*	0	0	0.205(2)	0.036
$R_I = 0.0349$	O(4)	4*i*	0	0	0.309(1)	0.036
$R_F = 0.0217$	O(5)	2*g*	0	0	0.420(2)	0.036
$RbCa_2Na_{0.8}Sr_{0.2}Nb_4O_{13}$	Rb	1*d*	0.5	0.5	0.5	0.048(4)
	A(1)[b]	1*c*	0.5	0.5	0	0.012(1)
$a = 0.38716(1)$ nm	*A*(2)[b]	2*h*	0.5	0.5	0.2248(7)	0.010
$c = 1.90092(8)$ nm	Nb(1)	2*g*	0	0	0.1054(3)	0.0030(8)
	Nb(2)	2*g*	0	0	0.3289(3)	0.0030
$R_{wp} = 0.0990$	O(1)	1*a*	0	0	0	0.037(3)
$R_p = 0.0769$	O(2)	4*i*	0	0.5	0.104(2)	0.037
$R_e = 0.0355$	O(3)	2*g*	0	0	0.214(2)	0.037
$R_I = 0.0339$	O(4)	4*i*	0	0	0.308(1)	0.037
$R_F = 0.0221$	O(5)	2*g*	0	0	0.416(2)	0.037
$RbCa_2Na_{0.6}Sr_{0.4}Nb_4O_{13}$	Rb	1*d*	0.5	0.5	0.5	0.044(5)
	A(1)[b]	1*c*	0.5	0.5	0	0.008(2)
$a = 0.38704(3)$ nm	*A*(2)[b]	2*h*	0.5	0.5	0.2236(9)	0.008
$c = 1.9107(1)$ nm	Nb(1)	2*g*	0	0	0.1056(5)	0.006(10)
	Nb(2)	2*g*	0	0	0.3285(4)	0.006
$R_{wp} = 0.1216$	O(1)	1*a*	0	0	0	0.034(5)
$R_p = 0.0881$	O(2)	4*i*	0	0.5	0.101(3)	0.034
$R_e = 0.0359$	O(3)	2*g*	0	0	0.215(3)	0.034
$R_I = 0.0426$	O(4)	4*i*	0	0	0.309(2)	0.034
$R_F = 0.0243$	O(5)	2*g*	0	0	0.421(3)	0.034

[a] Space group *P4/mmm*; No. 123. 2θ step size = 0.04, total number of reflections = ca. 400, number of profile points = 2601. Number in parentheses represents estimated standard deviation. Values without standard deviation were constrained. The occupation factor was set to unity for all positions.
[b] The cation ratios in *A*(1) and *A*(2) were confined to Ca:Na = 2/3:1/3 for $RbCa_2NaNb_4O_{13}$, Ca:Na:Sr = 2/3:4/15:1/15 for $RbCa_2Na_{0.8}Sr_{0.2}Nb_4O_{13}$, and Ca:Na:Sr = 2/3:3/15:2/15 for $RbCa_2Na_{0.6}Sr_{0.4}Nb_4O_{13}$.
[c] The istropic atomic displacement parameters for the same cation species were constrained to be equal.

essentially unchanged, while the c-axis increased linearly, resulting in an overall increase in the unit-cell volume (Fig. 4). The increase is attributed to the larger ionic radii of Sr^{2+} (0.144 nm) and Nb^{4+} (0.068 nm) compared to Na^+ (0.139 nm) and Nb^{5+} (0.064 nm) (23).

Calculation of the bond distances showed that the Nb–O bond extending toward the interlayer had the shortest distance (Nb(2)–O(5) = 0.177(6) nm). The longest Nb–O bond was Nb(2)–O(3) = 0.216(7) nm. The inner two perovskite-like slabs are closer to an ideal octahedron than the outer ones, as was the case for $x = 0$ (20). No drastic change in the

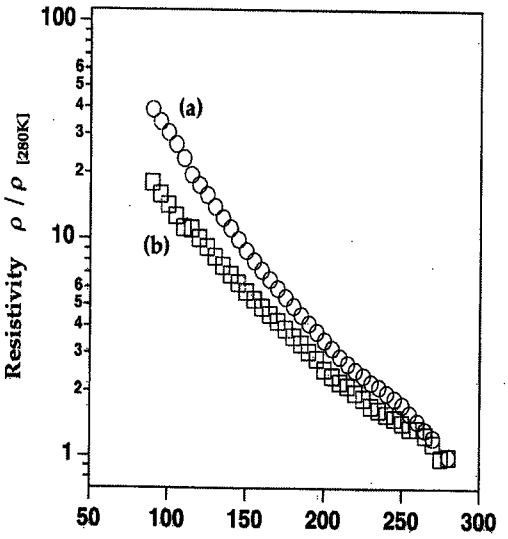

FIG. 5. Temperature dependence of the normalized resistivity for (a) $RbCa_2Na_{0.8}Sr_{0.2}Nb_4O_{13}$ and (b) $RbCa_2Na_{0.6}Sr_{0.4}Nb_4O_{13}$.

crystallographic environments of the inner and outer two perovskite-like slabs upon doping was apparent.

The temperature dependence of the normalized resistivity on a logarithmic scale is shown in Fig. 5. The samples showed semiconducting behavior, with typical resistivity at room temperature in the order of 10^1–10^2 Ω m. The resistivity for $RbCa_2Na_{0.6}Sr_{0.4}Nb_4O_{13}$ was slightly less temperature-dependent than that of $RbCa_2Na_{0.8}Sr_{0.2}Nb_4O_{13}$. Since a linear relation could not be obtained in the (log ρ) vs T^{-1} plot in the temperature region $80 \leq T \leq 280$, the thermally activated electron-hopping conduction mechanism could not be applied. In the case of $Na_{1-x}Sr_xNbO_3$ ($0.2 \leq x \leq 0.4$) (24) and $KCa_{2-x}La_xNb_3O_{10}$ ($0.1 \leq x \leq 0.3$) (18), a linear (log ρ) $\propto T$ relation was observed in the temperature region $80 \leq T \leq 280$. The electrical properties in these compounds were interpreted based on the tunneling conduction of small polarons through vibrating barriers (25). The general shape of the (log ρ) vs T plot (Fig. 5) suggests that the resistivity behavior of $RbCa_2Na_{1-x}Sr_xNb_4O_{13}$ may also be explained by the tunneling conduction of small polarons through vibrating barriers (25). However, since the linearity was not preserved throughout the whole temperature region studied ($80 \leq T \leq 280$), other conduction mechanisms should also contribute to the electrical properties. A deviation from the apparent (log ρ) $\propto T$ behavior was also observed for $Na_{1-x}Sr_xNbO_3$ ($x = 0.10$ and 0.15) when the Sr content was small (24).

4. CONCLUSIONS

Polycrystalline samples of reduced niobates possessing a four-layered perovskite structure, $RbCa_2Na_{1-x}Sr_xNb_4O_{13}$ ($x = 0.2$ and 0.4), were synthesized and their structures and electrical properties were studied. The tetragonal structure of the end member $RbCa_2NaNb_4O_{13}$ was retained with the substitution. The a-axis was essentially constant, while the c-axis increased linearly with an increase in x. Semiconducting properties were obtained for both $x = 0.2$ and $x = 0.4$.

ACKNOWLEDGMENTS

Y.S. thanks the Advanced Research Center for Science and Engineering at Waseda University for financial support as Individual Research. This work was financially supported in part by a Grant-in-Aid for JSPS Fellows (5727) from the Ministry of Education, Science, Sports, and Culture, Japan.

REFERENCES

1. (a) S. N. Ruddlesden and P. Popper, *Acta Crystallogr.* **10**, 538 (1957). (b) S. N. Ruddlesden and P. Popper, *Acta Crystallogr.* **11**, 54 (1958).
2. (a) B. Aurivillius, *Ark. Kemi.* **1**, 463 (1949). (b) B. Aurivillius, *Ark. Kemi.* **1**, 499 (1949). (c) B. Aurivillius, *Ark. Kemi.* **2**, 519 (1950).
3. M. Dion, M. Ganne, and M. Tournoux, *Mater. Res. Bull.* **16**, 1429 (1981).
4. M. Dion, M. Ganne, and M. Tournoux, *Rev. Chim. Miner.* **23**, 61 (1986).
5. R. A. Mohan Ram, P. Ganguly, and C. N. R. Rao, *J. Solid State Chem.* **70**, 82 (1987).
6. A. Nozaki, H. Yoshikawa, T. Wada, H. Yamauchi, and S. Tanaka, *Phys. Rev. B* **43**, 181 (1991).
7. M. Itoh, M. Shikano, H. Kawaji, and T. Nakamura, *Solid State Commun.* **80**, 545 (1991).
8. R. A. Mohan Ram, L. Ganapathi, P. Ganguly, and C. N. R. Rao, *J. Solid State Chem.* **63**, 139 (1986).
9. R. Jones and W. R. McKinnon, *Solid State Ionics* **45**, 173 (1991).
10. P. Gomez-Romero, M. R. Palacin, N. Casan, and A. Fuertes, *Solid State Ionics* **63–65**, 424 (1993).
11. M. Sato, T. Jin, and H. Ueda, *Chem. Lett.* **1994**, 161 (1994).
12. A. R. Armstrong and P. A. Anderson, *Inorg. Chem.* **33**, 4366 (1994).
13. M. R. Palacin, M. Lira, J. L. Garcia, M. T. Caldes, N. Casan-Pastor, A. Fuertes, and P. Gomez-Romero, *Mater. Res. Bull.* **31**, 217 (1996).
14. C. Bohnke, O. Bohnke, and J. L. Fourquet, *J. Electrochem. Soc.* **144**, 1151 (1997).
15. Y. Takano, S. Takayanagi, S. Ogawa, T. Yamadaya, and N. Mori, *Solid State Commun.* **103**, 215 (1997).
16. H. Fukuoka, T. Isami, and S. Yamanaka, *Chem. Lett.* **1997**, 703 (1997).
17. Y. Takano, H. Taketomi, H. Tsurumi, T. Yamadaya, and N. Mori, *Physica B* **237–238**, 68 (1997).
18. D. Hamada, M. Machida, Y. Sugahara, and K. Kuroda, *J. Mater. Chem.* **6**, 69 (1996).
19. D. Hamada, W. Sugimoto, Y. Sugahara, and K. Kuroda, *J. Ceram. Soc. Jpn.* **105**, 284 (1997).
20. M. Sato, Y. Kono, and T. Jin, *J. Ceram. Soc. Jpn.* **101**, 980 (1993).
21. F. Izumi, *in* "The Rietveld Method," p. 236. Oxford Univ. Press, London, 1993.
22. Y. I. Kim and F. Izumi, *J. Ceram. Soc. Jpn.* **102**, 401 (1994).
23. R. D. Shannon, *Acta Crystallogr., Sect. A* **32**, 751 (1976).
24. B. Ellis, J. P. Doumerc, P. Dordor, M. Pouchard, and P. Hagenmuller, *Solid State Commun.* **51**, 913 (1984).
25. C. M. Hurd, *J. Phys. C* **18**, 6487 (1985).

Preparation of a Protonated Form of a Layered Perovskite by Selective Leaching of Bismuth Oxide Sheets

Yoshiyuki Sugahara, Yu Tsunoda, Masashi Shirata, and Wataru Sugimoto*
Department of Applied Chemistry, School of Science and Engineering,
Waseda University
*Department of Fine Materials Engineering,
Faculty of Textile Science and Technology, Shinshu University

Abstract

$Bi_2SrTa_2O_9$ was treated with 3 M HCl, and a resultant product was structurally and compositionally characterized. Acid-treated $Bi_2SrTa_2O_9$ exhibited a tetragonal symmetry with $a = 0.391 \pm 0.004$ and $c = 0.98 \pm 0.01$ nm. After the acid treatment, the structure of perovskite-like slabs was preserved, while the repeating distance (perpendicular to the perovskite-like slabs) decreased from that of $Bi_2SrTa_2O_9$ ($c/2 = 1.253$ nm). The compositional analyses revealed that the acid-treated product corresponded to $H_{1.8}[Sr_{0.8}Bi_{0.2}Ta_2O_7]$. These observations indicate that bismuth oxide sheets in $Bi_2SrTa_2O_9$ were selectively leached to form a protonated form of a layered perovskite. The presence of Bi in the perovskite-like slabs should be ascribed to the cation disorder between Sr and Bi. The morphology did not change after the acid treatment, supporting the aforementioned reaction mechanism.

Introduction

It is well known that some layered compounds undergo topotactic reactions such as intercalation reactions and ion-exchange ones, and clays, layered polysilicates, and layered transition metal oxides were typical host oxides [1]. Since the structures of layers in the starting compounds are preserved, only the axis perpendicular to layers (in many cases *c*-axis) is generally changed. Ion-exchangeable layered perovskites consist of perovskite-like slabs and interlayer cations. Two homologous series called Dion-Jacobson phases ($M[A_{n-1}B_nO_{3n+1}]$) and Ruddlesden-Popper phases ($M_2[A_{n-1}B_nO_{3n+1}]$) are known so far, and both of them are reported to exhibit ion-exchange and intercalation capability [2,3]. Interlayer cations can be replaced with other monovalent and divalent cations by ion-exchange reactions [4,5]. Similarly, the replacement with proton can be achieved by acid treatments [4,6]. The protonated forms undergo intercalation reactions with *n*-alkylamines by acid-base mechanism [2,3].

Aurivillius phases ($Bi_2A_{n-1}B_nO_{3n+3}$ or alternatively expressed as $(Bi_2O_2)[A_{n-1}B_nO_{3n+1}]$) consist of bismuth oxide sheets and perovskite-like slabs [7]. Since the structures of the perovskite-like slabs in the Aurivillius phases are identical with those of the ion-exchangeable layered perovskites, it appears to be possible to convert the Aurivillius phases into protonated forms of layered perovskites by the replacement of the bismuth oxide sheets with proton. In the

previous work [8], we have demonstrated that the acid treatment of $Bi_2SrNaNb_3O_{12}$ resulted in the selective leaching of bismuth oxide sheets and corresponding introduction of proton for charge compensation of negatively charged perovskite-like slabs. Though this reaction was irreversible, the structure of the perovskite-like slabs was preserved. The compositional analysis revealed that a part of Bi (11 %) was present in the perovskite-like slabs because of cation disorder.

Here, we report the conversion of $Bi_2SrTa_2O_9$ into a protonated form of a layered perovskite by HCl treatment. Suzuki *et al.* [9] reported the structural change of $Bi_2SrTa_2O_9$ upon the acid treatment, and they ascribed the variation in X-ray diffraction (XRD) patterns to the structural change in perovskite-like slabs. We performed structural and compositional analyses of the acid-treated $Bi_2SrTa_2O_9$, and revealed that the bismuth oxide sheets in $Bi_2SrTa_2O_9$ were selectively leached by the acid treatment.

Experimental procedures

$Bi_2SrTa_2O_9$ was prepared from a stoichiometric mixture of Bi_2O_3, $SrCO_3$, and Ta_2O_5 through solid-state reaction. The calcination schedule was based on the previous report for $Bi_2SrNb_2O_9$ [10]. Typically, 1 g of $Bi_2SrTa_2O_9$ was dispersed in 200 mL of 3 M HCl for 72 h at ambient temperature. Then the crude product was washed with water, and dried at 120.C for 24 h.

XRD patterns were obtained with a Rigaku RINT-2500 diffractometer using monochromated CuK_α radiation. Rietveld analysis was performed by using the program RIETAN [11]. Electron diffraction (ED) patterns were obtained by using a transmission electron microscope Hitachi H-8100A operated at 200 kV. The compositions of metals were determined by inductively-coupled plasma emission spectrometry (ICP; Nippon Jarrell Ash ICAP-575 II) after dissolution by heating samples in a mixture of HCl, HNO_3, and HF at 200.C at least for 2 h. The amount of proton in acid-treated $Bi_2SrTa_2O_9$ was determined by thermogravimetry (TG) using a MacScience TG-DTA2000S (heating rate: 10.C/min). The morphology was studied with a scanning electron microscope (HITACHI, S-2500).

Results and Discussion

Figure 1 shows XRD patterns of $Bi_2SrTa_2O_9$ and its acid-treated product. The lattice parameters of $Bi_2SrTa_2O_9$ were refined based on the reported space group $A2_1am$ (with a orthorhombic cell) and were determined to be a = 0.5520, b = 0.5521, and c = 2.505 nm [12]. The a and b parameters were consistent with $\sqrt{2}a_p$ (a_p is the lattice parameter of cubic perovskite oxides, and is around 0.39 nm). Since the c parameter is doubled, the thickness for one perovskite-like slab and one bismuth oxide sheet should be $c/2$ (= 1.253 nm).

The XRD pattern of acid-treated $Bi_2SrTa_2O_9$ consists of broad peaks, which can be indexed with a tetragonal cell. Lattice parameters are calculated to be $a = 0.391 \pm 0.004$ and $c = 0.98 \pm 0.01$ nm. It should be noted that the a parameter corresponds to a_p. Since ($hk0$) peaks of

$Bi_2SrTa_2O_9$ [the (200) and (020) peaks (overlapped) and the (220) one in Fig. 1] are present at the same positions after the acid treatment, the preservation of the perovskite-like slabs is suggested. The change in the lattice parameters for perovskite-like slabs (the *a* and *b* parameters for $Bi_2SrTa_2O_9$ and the *a* parameter for acid-treated $Bi_2SrTa_2O_9$) should be ascribed to the difference in the symmetry of unit cells ([110] direction of acid-treated $Bi_2SrTa_2O_9$ corresponds to [100] direction of $Bi_2SrTa_2O_9$). The *c* parameter of acid-treated $Bi_2SrTa_2O_9$ is not doubled, which is consistent with the appearance of a (100) peak. Thus, the repeating distance along the *c* axis contracted from 1.253 to 0.98 nm after the acid treatment.

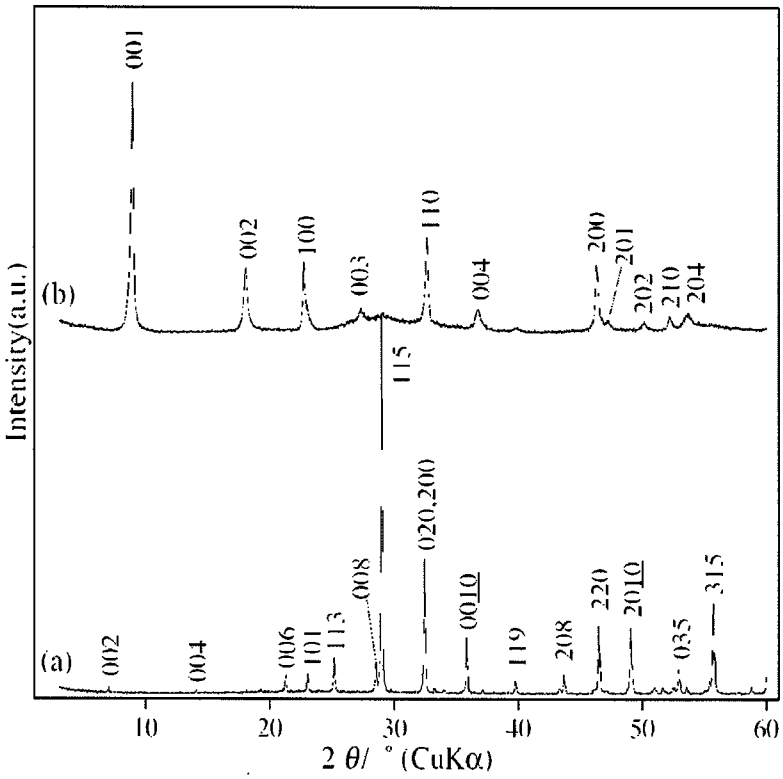

Figure 1 *XRD patterns of (a) $Bi_2SrTa_2O_9$ and (b) its acid-treated product.*

The preservation of the perovskite-like slabs during the acid treatment is further demonstrated by the ED analysis. Figure 2 demonstrates the ED pattern of $Bi_2SrTa_2O_9$ and that of acid-treated $Bi_2SrTa_2O_9$ along the [001] zone. Since the *a* and *b* parameters of $Bi_2SrTa_2O_9$ are very close, we interpret the pattern of $Bi_2SrTa_2O_9$ with a pseudo-tetragonal symmetry ($a_{tetra} = a/\sqrt{2}$) These patterns are very similar, indicating that the structure of the perovskite-like slabs in $Bi_2SrTa_2O_9$ is essentially unchanged during the acid treatment.

Table 1 summarizes the ICP and TG results of $Bi_2SrTa_2O_9$ and acid-treated $Bi_2SrTa_2O_9$. The Bi/Ta ratio decreases from 2.0 to 0.19 by the acid-treatment. The Sr/Ta ratio also decreases to some extent (0.98→0.79). These observations indicate that the bismuth oxide sheets containing Sr (present because of cation disorder) are selectively leached. The layer charge is calculated to be 1.8- ($[Sr_{0.8}Bi_{0.2}Ta_2O_7]^{1.8-}$), which is well consistent with the amount of proton (1.8 per $[Sr_{0.8}Bi_{0.2}Ta_2O_7]$).

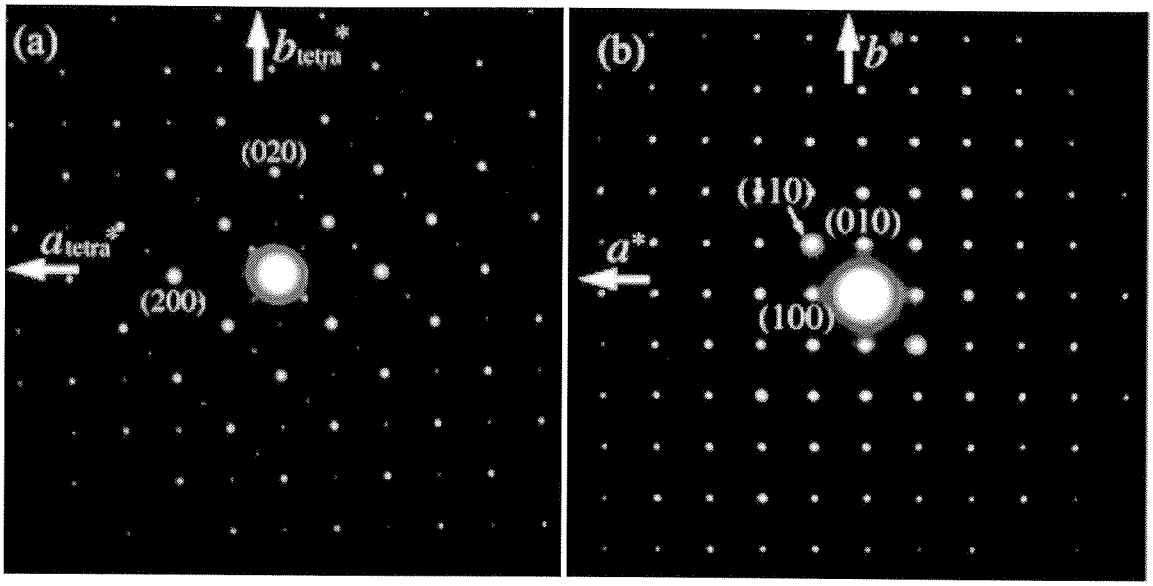

Figure 2 *ED patterns of (a) $Bi_2SrTa_2O_9$ and (b) its acid-treated product.*

Table 1 *Composition of $Bi_2SrTa_2O_9$ before and after the acid treatment (in molar ratio).*

	Bi	Sr	Ta*	H**
Before the Acid Treatment	2.0	0.98	*2*	—
After the Acid Treatment	0.19	0.79	*2*	1.8

*Set to be 2. **Determined by TG.

Scanning electron micrographs of $Bi_2SrTa_2O_9$ and acid-treated $Bi_2SrTa_2O_9$ are shown in Fig. 3. No obvious morphological change is evident. Thus, it is very unlikely that the reaction mechanism of this conversion is dissolution-recrystallization-type, supporting the selective leaching mechanism.

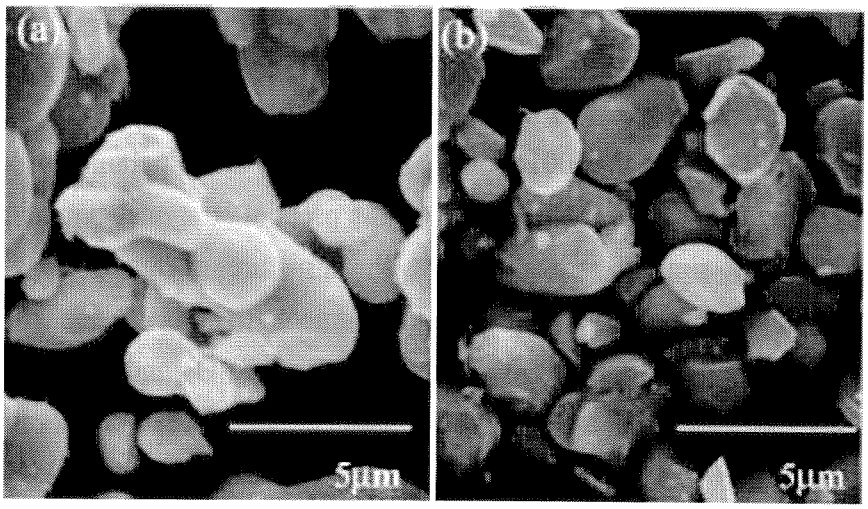

Figure 3 *Scanning electron micrographs of (a) $Bi_2SrTa_2O_9$ and (b) its acid-treated product.*

Conclusions

We have demonstrated that the bismuth oxide sheets in the Aurivillius phase, $Bi_2SrTa_2O_9$, were selectively leached by the HCl treatment to form the protonated form of the ion-exchangeable layered perovskite, $H_{1.8}[Sr_{0.8}Bi_{0.2}Ta_2O_7]$. Since the B-site ions in the conventional ion-exchangeable layered perovskites (the Dion-Jacobson and Ruddlesden-Popper phases) are very limited, this conversion method from the Aurivillius phases can provide a variety of layered perovskites, which cannot be prepared by the solid-state reactions.

Acknowledgements

The authors thank Prof. Kazuyuki Kuroda (Department of Applied Chemistry, Waseda University) for valuable discussion. This work was financially supported in part by the Grant-in-Aid for Scientific Research (No. 10555221) from the Ministry of Education, Science, Sports, and Culture, Japan.

References

[1] "*Intercalation Chemistry*", M. S. Whittingham and A. J. Jacobson eds., Academic Press, New York, 1982.

[2] J. Gopalakrishnan, *Rev. Solid State Sci.*, **1**, 515 (1988).

[3] R. E. Schaak and T. E. Mallouk, *Chem. Mater.*, **12**, 3427 (2000).

[4] J. Gopalakrishnan and V. Bhat, *Inorg. Chem.*, **26**, 4299 (1987).

[5] T. Matsuda, T. Fujita, N. Miyamae, M. Takeuchi, and I. Kunou, *J. Mater. Chem.*, **4**, 955 (1994).

[6] A. J. Jacobson, J. T. Lewandowski, and J. W. Johnson, *J. Less-Common Met.*, **116**, 137 (1986).

[7] B. Frit and J. P. Mercurio, *J. Alloys Compd.*, **188**, 27 (1992).

[8] W. Sugimoto, M. Shirata, Y. Sugahara, and K. Kuroda, *J. Am. Chem. Soc.*, **121**, 11601 (1999).

[9] M. Suzuki, N. Nagasawa, A. Machida, and T. Ami, *Jpn. J. Appl. Phys.*, **35**, L564 (1996).

[10] Ismunandar, B. J. Kennedy, Gunawan, and Marsongkohadi, *J. Solid State Chem.*, **126**, 135 (1996).

[11] F. Izumi, in *Rietveld Analysis* , R. A. Young ed., Oxford University Press, Oxford, 1993, pp 236-253.

[12] A. D. Rae, J. G. Thompson, and R. L. Withers, *Acta Crystallogr.*, **B48,** 418 (1992).

Preparation and HREM Characterization of a Protonated Form of a Layered Perovskite Tantalate from an Aurivillius Phase $Bi_2SrTa_2O_9$ via Acid Treatment

Yu Tsunoda, Masashi Shirata, Wataru Sugimoto, Zheng Liu, Osamu Terasaki, Kazuyuki Kuroda, and Yoshiyuki Sugahara

Department of Applied Chemistry, School of Science and Engineering, Waseda University, Shinjuku-ku, Tokyo 169-8555, Japan, Department of Fine Materials Engineering, Faculty of Textile Science and Technology, Shinshu University, Ueda, Nagano 386-8567, Japan, CREST, JST, Tohoku University, Aoba-ku, Sendai, Miyagi 980-8578, Japan, Department of Physics, Graduate School of Science and CIR, Tohoku University, Aoba-ku, Sendai, Miyagi 980-8578, Japan, and Kagami Memorial Laboratory for Materials Science and Technology, Waseda University, Nishiwaseda-2, Shinjuku-ku, Tokyo 169-0051, Japan

Inorganic Chemistry®

Reprinted from
Volume 40, Number 23, Pages 5768–5771

Here, we report the conversion of another Aurivillius phase, $Bi_2SrTa_2O_9$, into a protonated form of a layered perovskite via acid treatment. The acid treatment of single-crystal $Bi_2SrTa_2O_9$ was previously reported,[13] but the variation in the XRD patterns was interpreted as a structural change of the perovskite-like slabs in $Bi_2SrTa_2O_9$ during the acid treatment. In the present study, $Bi_2SrTa_2O_9$ powder was treated with 3 M hydrochloric acid, and the resultant product was fully characterized. Furthermore, we discuss the structure of the acid-treated product on the basis of transmission electron microscopy observation.

Experimental Section

Preparation of $Bi_2SrTa_2O_9$. $Bi_2SrTa_2O_9$ was prepared from a stoichiometric mixture of Bi_2O_3, $SrCO_3$, and Ta_2O_5 by solid-state reactions. The heating schedule is based on the preparative method used for $Bi_2SrNb_2O_9$: the starting compounds were thoroughly ground and heated at 900 °C for 15 h, 1000 °C for 15 h, and 1200 °C for 24 h with intermittent grinding.[14]

Acid Treatment of $Bi_2SrTa_2O_9$. About 1 g of $Bi_2SrTa_2O_9$ was dispersed in 200 mL of 3 M hydrochloric acid for 72 h. The acid-treated product was centrifuged, washed with water, and air-dried. The air-dried product was further heated at 120 °C under ambient atmosphere.

Analyses. The amounts of metals were determined by inductively coupled plasma emission spectrometry (ICP: Nippon Jarrell Ash, ICAP575 MarkII) after the samples were dissolved by heating in a mixture of HCl, HNO_3, and HF at 200 °C for at least 2 h. The amount of hydrogen was determined by thermogravimetry (TG: MacScience, TG-DTA2000S, 10 °C/min). X-ray diffraction (XRD) patterns were obtained by using a Rigaku RINT-2500 diffractometer (monochromated Cu Kα radiation). A Rietveld analysis of $Bi_2SrTa_2O_9$ was performed by using the program RIETAN.[15] Lattice parameters of the acid-treated product were refined by the nonlinear least-squares method. Electron diffraction (ED) patterns and high-resolution electron microscopy (HREM) images were obtained using a transmission electron microscope (TEM: JEOL JEM-4000EX) operated at 400 kV. Morphology was studied by scanning electron microscopy (SEM: Hitachi S-5000).

Results and Discussion

Acid Treatment of $Bi_2SrTa_2O_9$. Scanning electron micrographs of $Bi_2SrTa_2O_9$ and its acid-treated product are shown in Figure 1. Both $Bi_2SrTa_2O_9$ and the acid-treated product consist of particles with diameters of 1−5 μm, and no notable change in particle shape is observed, indicating that the dissolution of $Bi_2SrTa_2O_9$ and subsequent precipitation are very unlikely.

XRD patterns of $Bi_2SrTa_2O_9$ and its acid-treated product are shown in Figure 2. The XRD pattern of $Bi_2SrTa_2O_9$ (Figure 2a) can be indexed on the basis of an orthorhombic cell (a = 0.5520(4) nm, b = 0.5521(4) nm, c = 2.505(2) nm), consistent with a previous report (a = 0.5525(4) nm, b = 0.5526(6) nm, c = 2.508(5) nm; space group, $A2_1am$).[16] The a and b parameters correspond to $\sqrt{2}a_p$ (a_p is the lattice parameter of the cubic perovskite oxides and is ca. 0.39 nm). It is also noted that two perovskite-like slabs are present in the unit cell, which is shown by a doubled c parameter of $Bi_2SrTa_2O_9$ ($c/2$ = 1.25 nm). The crude acid-treated product showed broad peaks, which can be indexed on the basis of a tetragonal cell. After heating at 120 °C, we found that the XRD peaks became sharper, and the acid-treated product heated at 120 °C also exhibits tetragonal symmetry (Figure 2b). The lattice parameters of the acid-treated product heated at 120 °C are a = 0.391 ± 0.004 nm and c = 0.98 ± 0.01 nm. It should be noted that the lattice parameter a of the acid-treated product heated at 120 °C is in good agreement with the a_p value.

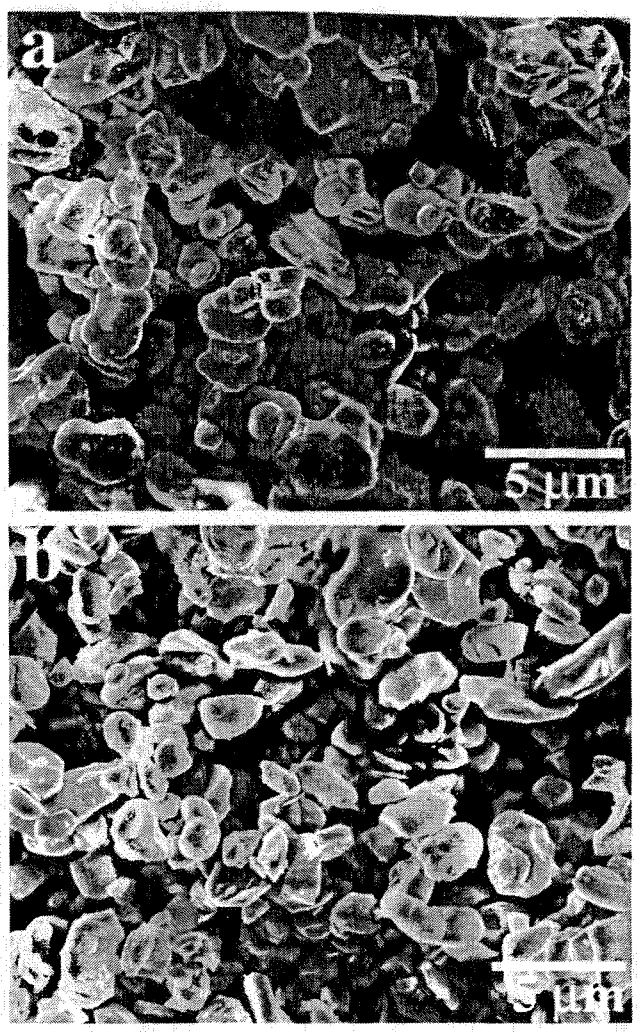

Figure 1. Scanning electron micrographs of (a) $Bi_2SrTa_2O_9$ and (b) acid-treated $Bi_2SrTa_2O_9$.

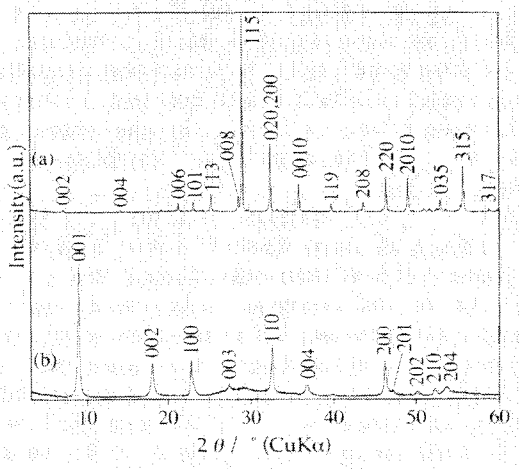

Figure 2. XRD patterns of (a) $Bi_2SrTa_2O_9$ and (b) acid-treated $Bi_2SrTa_2O_9$.

Figure 3a shows the ED pattern of the acid-treated product along the [001] zone and the corresponding HREM image of the acid-treated product. The ED pattern can be indexed on the

(13) Suzuki, M.; Nagasawa, N.; Machida, A.; Ami, T. *Jpn. J. Appl. Phys.* **1996**, *35*, L564.
(14) Ismunandar; Kennedy, B. J.; Gunawan; Marsongkohadi *J. Solid State Chem.* **1996**, *126*, 135−141.
(15) (a) Izumi, F. In *Rietveld Analysis*; Young, R. A., Ed.; Oxford University Press: Oxford, 1993; pp 236−253. (b) Kim, Y. I.; Izumi, F. *J. Ceram. Soc. Jpn.* **1994**, *102*, 401.
(16) Rae, A. D.; Thompson, J. G.; Withers, R. L. *Acta Crystallogr.* **1992**, *B48*, 418.

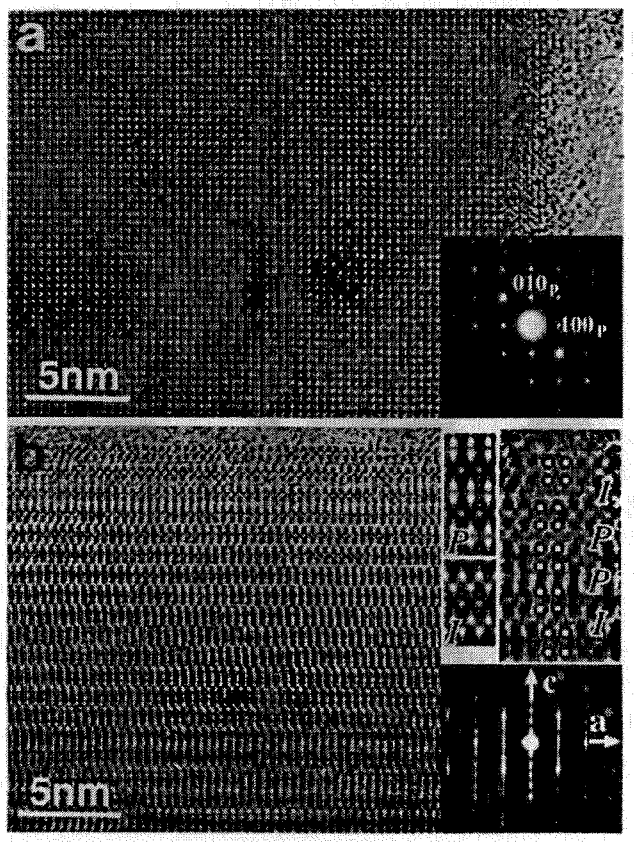

Figure 3. HREM images of acid-treated $Bi_2SrTa_2O_9$ along (a) [001] and (b) [010]. Corresponding ED patterns are given in the insets. In panel b, two simulated images for *P*- and *I*-type cells (middle) and an enlarged, simulated image (right) are also presented.

basis of a tetragonal cell, consistent with the XRD results. The HREM image exhibits a regular dot array, which is identical to [100] images of cubic perovskite oxides. The ED pattern along the [010] zone and the corresponding HREM image of the acid-treated product are shown in Figure 3b. The HREM image can be explained on the basis of a lamellar structure. These observations clearly indicate that the structure of the perovskite-like slabs is retained after the acid treatment. We emphasize that all the examined particles of the acid-treated product (several hundreds) were crystalline on the basis of the ED analysis.

A Bi:Sr:Ta metal composition ratio of 2.0:0.98:2.0 was found for $Bi_2SrTa_2O_9$ by ICP, consistent with the nominally indicated ratio. The composition of metals was drastically changed to 0.19:0.79:2.0 after the acid treatment. Taking the ED and HREM results into account, we ascribe the loss of the large portion of bismuth to the selective leaching of the bismuth oxide sheets in $Bi_2SrTa_2O_9$. The remaining bismuth (Bi:Ta = 0.19:2) and the loss of a corresponding amount of strontium (Sr:Ta = 0.19:2) should be ascribed to cation disorder (B ↔ Sr), which was observed in our previous study on $Bi_2SrNaNb_3O_{12}$[10] and structural analyses of other Aurivillius phases.[17,18] Hence, the composition of the perovskite-like slabs in $Bi_2SrTa_2O_9$ and its acid-treated product should be $Sr_{0.8}Bi_{0.2}Ta_2O_7$.

The amount of hydrogen in the acid-treated product was determined by TG (Figure 4). The acid-treated product heated at 120 °C exhibits a mass loss (2.7 wt %) starting at ~180 °C. The mass loss, ascribed to dehydration, corresponds to 1.8 H

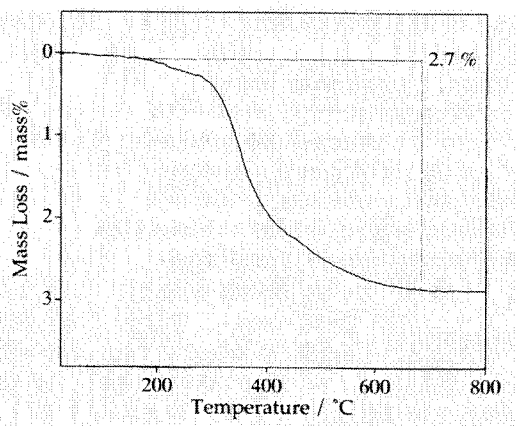

Figure 4. TG curve of acid-treated $Bi_2SrTa_2O_9$ heated at 120 °C.

per $Sr_{0.8}Bi_{0.2}Ta_2O_7$. Since the layer charge of the perovskite-like slab is −1.8 due to cation disorder ($[Sr_{0.8}Bi_{0.2}Ta_2O_7]^{1.8-}$), the amount of hydrogen is in good agreement with the following overall reaction:

$$(Bi_{1.8}Sr_{0.2}O_2)[Sr_{0.8}Bi_{0.2}Ta_2O_7] \xrightarrow{H^+} H_{1.8}[Sr_{0.8}Bi_{0.2}Ta_2O_7]$$

Suzuki et al.[13] reported the acid treatment of a $Bi_2SrTa_2O_9$ single crystal. In the XRD pattern of the acid-treated $Bi_2SrTa_2O_9$, a series of peaks assignable to a 00*l* reflection was observed, and the position of the low-angle peak (d = 0.9807 nm) is close to the c parameter in the present study. Thus, the reported structural change of the $Bi_2SrTa_2O_9$ single crystal appears to be identical to that observed in the present reaction.

Structure of $H_{1.8}[Sr_{0.8}Bi_{0.2}Ta_2O_7]$. Stacking sequences of the perovskite-like slabs in the layered perovskites depend on both compositions of the perovskite-like slabs and interlayer cations.[19,20] In a simple stacking sequence, an adjacent perovskite-like slab is located exactly above the other perovskite-like slab without displacement. It is also possible that an adjacent perovskite-like slab is stacked with displacement. For protonated forms of the layered perovskites, two types of stacking sequences of the perovskite-like slabs were reported: the simple stacking sequence without displacement[2,6,8,19,21,22] and the stacking sequence with a displacement by $(a + b)/2$.[4,9a,23,24] The unit cells of protonated phases possessing the simple stacking sequences contain only one perovskite-like slab, and the space group reported so far is *P*4/*m* for $H[LaNb_2O_7]$.[19] On the contrary, the relative displacement by $(a + b)/2$ leads to a doubling of c parameters, and the structures of $H_2[SrNb_2O_7]$ and $H_2[SrTa_2O_7]$ (heated at 300 °C) were reported to possess *I*-type tetragonal cells.[9a] These previous reports suggest that either a unit cell with a simple stacking of the perovskite-like slabs (most likely a tetragonal *P*-type cell) or a unit cell with a stacking of the perovskite-like slabs with a displacement by $(a + b)/2$ (a tetragonal *I*-type cell) appears to be adopted for $H_{1.8}[Sr_{0.8}Bi_{0.2}Ta_2O_7]$. The presence of the (100) peak in both the XRD and ED patterns (the (100) peak does not appear for tetragonal *I*-type

(17) Blake, S. M.; Falconer, M. J.; McCreedy, M.; Lightfoot, P. *J. Mater. Chem.* **1997**, *7*, 1609.
(18) Ismunandar; Kennedy, B. J. *J. Mater. Chem.* **1999**, *9*, 541.
(19) Sato, M.; Abo, J.; Jin, T.; Ohta, M. *J. Alloys Compd.* **1993**, *192*, 81.
(20) Toda, K.; Teranishi, T.; Ye, Z.-G.; Sato, M.; Hinatsu, Y. *Mater. Res. Bull.* **1999**, *34*, 971.
(21) Gopalakrishnan, J.; Bhat, V.; Raveau, B. *Mater. Res. Bull.* **1987**, *22*, 413.
(22) Palacín, M. R.; Lira, M.; García, J. L.; Caldés, M. T.; Casañ-Pastor, N.; Fuertes, A.; Gómez-Romero, P. *Mater. Res. Bull.* **1996**, *31*, 217.
(23) Richard, M.; Brohan, L.; Tournoux, M. *J. Solid State Chem.* **1994**, *112*, 345.
(24) Schaak, R. E.; Mallouk, T. E. *J. Solid State Chem.* **2000**, *155*, 46–54.

cells) and the lack of doubling of the c parameter (0.98 ± 0.01 nm) suggest that the structure of $H_{1.8}[Sr_{0.8}Bi_{0.2}Ta_2O_7]$ possesses a P-type cell as an average structure.

Closer inspection of the structure of $H_{1.8}[Sr_{0.8}Bi_{0.2}Ta_2O_7]$ by HREM provides further information on the stacking sequence. The HREM image along the [010] shows the presence of two types of stacking sequences (Figure 3b). To interpret this image, we simulated HREM images of $H_{1.8}[Sr_{0.8}Bi_{0.2}Ta_2O_7]$ for both P-type (no displacement) and I-type (relative displacement by $(a + b)/2$) cells. In simulated images, black dots are assigned to TaO_6 octahedrons, and the displacement in the I-type cell is clearly demonstrated. The comparison of these two images with an enlarged image of $H_{1.8}[Sr_{0.8}Bi_{0.2}Ta_2O_7]$ indicates that the two observed types of stacking sequences correspond to P- and I-type cells. Obvious streaks along c^* in the corresponding ED pattern (taken with the [010] incidence) are consistent with this stacking disorder.

Conclusions

$Bi_2SrTa_2O_9$ was converted into $H_{1.8}[Sr_{0.8}Bi_{0.2}Ta_2O_7]$ via acid treatment. HREM observations and diffraction results (XRD and ED) of $H_{1.8}[Sr_{0.8}Bi_{0.2}Ta_2O_7]$ clearly revealed that $H_{1.8}[Sr_{0.8}Bi_{0.2}Ta_2O_7]$ retained the structure of the perovskite-like slabs in $Bi_2SrTa_2O_9$. Since no morphological change occurred during the acid treatment, the conversion reaction proceeded via the selective leaching of the bismuth oxide sheets in $Bi_2SrTa_2O_9$. HREM observations further demonstrated that two types of stacking sequences (P- and I-type) were present in $H_{1.8}[Sr_{0.8}Bi_{0.2}Ta_2O_7]$. The present reaction is the second successful conversion of the Aurivillius phase into the protonated form of the layered perovskite, and the present results strongly suggest that this type of conversion reaction can be applicable to various Aurivillius phases. Very recently, the conversion of a Ruddlesden–Popper phase ($K_2[La_2Ti_3O_{10}]$) into an Aurivillius phase ($Bi_2La_2Ti_3O_{12}$) was reported and corresponds to the reverse reaction of our conversions.[25] Hence, the Ruddlesden–Popper phases and the Aurivillius phases are likely to be interconvertible using newly discovered reactions.

Acknowledgment. This work was financially supported in part by a Grant-in-Aid for Scientific Research (Grant 10555221) from the Ministry of Education, Science, Sports, and Culture of Japan.

IC010266M

(25) Gopalakrishnan, J.; Sivakumar, T.; Ramesha, K.; Thangadurai, V.; Subbanna, G. N. *J. Am. Chem. Soc.* **2000**, *122*, 6237.

Conversion of Aurivillius Phases, $Bi_2ANaNb_3O_{12}$ (A=Sr or Ca), into the Protonated Forms of Layered Perovskite via Acid Treatment

Wataru Sugimoto,[†,§] Masashi Shirata,[†] Kazuyuki Kuroda[†,‡] and Yoshiyuki Sugahara,[*,†]

Department of Applied Chemistry, School of Science and Engineering, Waseda University, Ohkubo-3, Shinjuku-ku, Tokyo 169-8555 JAPAN
Kagami Memorial Laboratory for Materials Science and Technology, Waseda University, Nishiwaseda-2, Shinjuku-ku, Tokyo 169-0051 JAPAN

Protonated forms of layered perovskites were derived from Aurivillius phases, $Bi_2ANaNb_3O_{12}$ (A=Sr or Ca), by the substitution of bismuth oxide sheets with protons via acid treatment. The conversion into the protonated forms was achieved easily using 6 M HCl at room temperature. Preservation of the layered structure of the host Aurivillius phases and contraction in the *c* axis were confirmed by X-ray and electron diffraction analysis as well as by transmission electron microscopy. The compositions of the resulting products were determined to be $H_{1.8}[A_{0.8}Bi_{0.2}NaNb_3O_{10}]$ (A=Sr or Ca) by inductively-coupled plasma emission spectroscopy and thermogravimetry. The acid-treated product $H_{1.8}[Sr_{0.8}Bi_{0.2}NaNb_3O_{10}]$ was capable of accommodating *n*-alkylamines in the interlayer space, which is in good agreement with the proposed layered structure.

Introduction

Extensive research has recently been devoted to layered perovskites possessing ion-exchange capabilities. These compounds are expressed by the general formula $M_2[A_{n-1}B_nO_{3n+1}]$ (the so-called Ruddlesden-Popper phases[1]) or $M[A_{n-1}B_nO_{3n+1}]$ (the so-called Dion-Jacobson phases[2]), where M is an alkali-metal ion, A is an alkaline-earth or rare-earth metal ion, and B is a transition-metal ion. $[A_{n-1}B_nO_{3n+1}]$ denotes the perovskite-like slabs derived by termination of the three-dimensional ABO_3 perovskite structure along the (100) axis, which are interleaved with alkali metal ions giving a characteristic layered structure. Typical three-layered structures are shown schematically in Scheme 1.

Scheme 1

One of the unique characteristics of these oxides is that the interlayer alkali metal ions can be exchanged with other monovalent or divalent cations. For example, reactions of $M_2[A_{n-1}B_nO_{3n+1}]$ and $M[A_{n-1}B_nO_{3n+1}]$ with aqueous acids lead to their corresponding protonated forms $H_2[A_{n-1}B_nO_{3n+1}]$ and $H[A_{n-1}B_nO_{3n+1}]$ via a proton-exchange reaction ($M^+ \rightarrow H^+$).[2-4] These protonated forms of layered perovskites have drawn considerable interest across a wide range of chemistry fields, since they exhibit numerous properties,[5] examples of which includes ion-exchange capability,[6] Brønsted acidity,[2a,2c,6a,7-10] proton conduction[11] and photochemical properties.[12] Various functional materials have also been derived from these protonated forms of layered perovskites, including intercalation compounds,[2b,2c,6a,7-9] alkoxyl derivatives,[13,14] porous materials,[12b,15] metastable three-dimensional perovskites,[4,16] and layer-by-layer assembly of exfoliated layered perovskites.[17]

The Aurivillius phases ($Bi_2A_{n-1}B_nO_{3n+3}$ or alternatively expressed as $Bi_2O_2[A_{n-1}B_nO_{3n+1}]$)[18] are also members of the layered perovskites, and extensive research has been devoted to their synthesis as well as the characterization of their ferroelectric property.[19] As shown in Scheme 1, the Aurivillius, Ruddlesden-Popper and Dion-Jacobson phases all possess analogous perovskite-like slabs, $[A_{n-1}B_nO_{3n+1}]$. The

major difference between the Aurivillius phases and the ion-exchangeable layered perovskites (Ruddlesden-Popper and Dion-Jacobson phases) is that the perovskite-like slabs are interleaved with bismuth oxide sheets in the former case and with alkali-metal ions in the latter. Despite this structural similarity, the conversion of Aurivillius phases into related layered perovskites or *vice versa* has not been considered until recently.

We recently reported on the conversion of an Aurivillius phase, $Bi_2SrNaNb_3O_{12}$, to a protonated form of a layered perovskite by acid treatment.[20,21] The reaction involves a selective leaching of the bismuth oxide sheets with simultaneous proton incorporation into the interlayer space formed between the perovskite-like slabs. The incorporation of protons allows the preservation of charge neutrality and the two-dimensional characteristic of the layered perovskite structure. The resulting product is therefore similar to the protonated forms of layered perovskites obtained by the conventional proton-exchange reaction ($M^+ \rightarrow H^+$) for the Ruddlesden-Popper and the Dion-Jacobson phases. Acid treatment of an n=2 member Aurivillius phase, $Bi_2SrTa_2O_9$, was conducted earlier by Suzuki *et al.*[22] They reported that an anisotropic structural modification occurred, but attributed the modification to the decomposition of the perovskite-like slabs. We have shown that acid treatment of $Bi_2SrTa_2O_9$ leads to $H_{1.8}[Sr_{0.8}Bi_{0.2}TaO_7]$ via selective leaching of the bismuth oxide sheets.[23] Another interesting reaction concerning the Aurivillius phases was recently reported by Gopalakrishnan *et al.*[24] Ruddlesden-Popper phases were converted into Aurivillius phases through metathesis reactions:

$$K_2[A_{n-1}B_nO_{3n+1}] \xrightarrow[800\text{-}900\ ^\circ C]{BiOCl} Bi_2O_2[A_{n-1}B_nO_{3n+1}] + 2\ KCl \qquad [1]$$

The two correlated conversion reactions based on the Aurivillius phases establish a new general relationship between the Aurivillius phases and the ion-exchangeable layered perovskites.

Here, we report the details of the conversion of two n=3 members of the Aurivillius phases, $Bi_2SrNaNb_3O_{12}$ and $Bi_2CaNaNb_3O_{12}$, into their corresponding

protonated forms of layered perovskites. The reaction of $Bi_2SrNaNb_3O_{12}$ was reported in brief earlier.[20,21] The structures and compositions of the protonated forms as well as the mechanism of the conversion reaction will be compared and discussed with conventional proton-exchange reactions.

Experimental Section

Synthesis of $Bi_2ANaNb_3O_{12}$ (A=Sr or Ca). Polycrystalline $Bi_2SrNaNb_3O_{12}$ (BSNN) was prepared following a procedure similar to that employed for $Bi_{2.5}Na_{1.5}Nb_3O_{12}$[25] and $Bi_2CaNaNb_3O_{12}$.[26] BSNN was prepared by a solid-state reaction of a 1:1 mixture of $Bi_2SrNb_2O_9$ and $NaNbO_3$ at 1100°C for 3 h. The calcination procedure was repeated after grinding to ensure a complete reaction. $Bi_2SrNb_2O_9$ was prepared in accordance with the procedures in a previous report.[27] $NaNbO_3$ was prepared from Na_2CO_3 and Nb_2O_5 by firing at 1000°C for 1 h in air. The purity of $Bi_2SrNb_2O_9$ and $NaNbO_3$ was confirmed by powder X-ray diffraction (XRD, Mac Science MXP^3 diffractometer with monochromated Cu Kα radiation) and inductively-coupled plasma emission (ICP) spectrometry (Nippon Jarrell Ash, ICAP 575 MARK II). Polycrystalline $Bi_2CaNaNb_3O_{12}$ (BCNN) was prepared similarly by the solid-state reaction of a 1:1 mixture of $Bi_2CaNb_2O_9$ and $NaNbO_3$.

The composition ratios of metals determined by ICP for BSNN and BCNN were consistent with the nominal ratios within the range of experimental error (see Table 1 in Results and Discussion). The XRD pattern of BSNN was successfully indexed based on a tetragonal cell. Structural refinement of BSNN was performed by the Rietveld analysis program RIETAN[28] using the space group *I4/mmm*. The final refined lattice parameters were a=0.39007(1) and c=3.2926(1) nm (Supplementary Information available). The XRD pattern of BCNN was indexed based on an orthorhombic cell. Structural refinement was performed using the space group *B2cb*. The final refined lattice parameters were a=0.54836(3), b=0.54585(4) and c=3.2731(1) nm

(Supplementary Information available).

Acid Treatment of $Bi_2ANaNb_3O_{12}$ (A=Sr or Ca). Typically, 1 g of BSNN or BCNN was treated with 200 cm^3 of 6 M HCl (M=mol dm^{-3}) at room temperature for 72 h to obtain acid-treated BSNN and BCNN. Acid treatment was conducted with various acid concentrations and reaction periods. The results for the acid-treated products presented throughout this paper are for the products treated with 6 M HCl for 72 h unless otherwise stated. The acid-treated products were collected either by filtration or centrifugation. After washing with de-ionized H_2O, the products were dried at room temperature or 120°C.

Reaction of the Acid-treated Product with Alkylamines. The product obtained by acid treatment of BSNN with 6 M HCl for 72 h was reacted with *n*-butylamine (C4A) or *n*-octylamine (C8A) in a 50 % alkylamine/heptane mixture under reflux conditions. The products were washed with excess heptane and dried at room temperature.

Analyses. The XRD patterns of the acid-treated products were collected with a Mac Science MXP^3 diffractometer. The lattice parameters of the acid-treated products were refined by the non-linear least-squares method. The cation ratios of the products were determined by ICP. The products were dissolved with a mixture of conc. HNO_3 (5 cm^3), HF (5 cm^3) and conc. HCl (10 cm^3) for the ICP measurements. After approximately 30 mg of the products had been dissolved by heating in the mixed acid, the resultant solution was further diluted with 6 M HCl. Thermogravimetry (TG, Mac Science, TG-DTA 2000S) was performed under a constant flow of dry air with a heating rate of 10°C min^{-1}. The structural characterization of the amine-treated products was conducted by XRD (Mac Science $M03XHF^{22}$ diffractometer) with Ni filtered Fe Kα radiation. The morphology of the products was studied with a scanning electron microscope (HITACHI, S-2500). Transmission electron microscopy (TEM, Hitachi H-8100A) was conducted at 200 kV.

Results and Discussion

Structural Evaluation by Diffraction Techniques. Figure 1 compares the XRD patterns of BSNN and BSNN treated with 6 M HCl for 72 h after drying at room temperature. After acid treatment, new diffraction peaks that could be indexed as a series of (00*l*) reflections were observed. In contrast to the appearance of new (00*l*) peaks, the positions of the (*hk*0) peaks were unchanged. The broadness of the (*hkl*) ($l \neq 0$) peaks compared to the (*hk*0) peaks suggests that stacking disorders are present in acid-treated BSNN. The (*hkl*) ($l \neq 0$) peaks of acid-treated BSNN sharpen slightly and shift to higher diffraction angles after drying at 120°C.

Figure 1

ED analysis was conducted for BSNN and acid-treated BSNN in order to obtain further details concerning the structural changes. The ED patterns of BSNN and acid-treated BSNN were both indexed based on a tetragonal cell. Typical ED patterns along the [001] and [010] zones are shown in Fig. 2. The ED pattern along the [001] zone for acid-treated BSNN was essentially identical to that of BSNN and could be indexed based on a tetragonal cell with $a \sim 0.39$ nm, which indicates that no structural change occurred along the *a* axes. On the other hand, the ED patterns along the [010] zone revealed a contraction in the *c*-axis after acid treatment. In view of the facts that the (00*l*) planes are characteristic of a layered structure and that the (*hk*0) planes are characteristic of the perovskite-like slabs, it is concluded that acid treatment of BSNN leads to a structural transformation only along the *c* axis, while the perovskite-like structure is preserved along the *ab* plane, in correspondence to the XRD results.

Figure 2

Electron Microscopy Studies. Typical SEM images of BSNN and acid-treated BSNN are shown in Fig. 3. The size and plate-like morphology are preserved after acid treatment, showing that the acid-treated product is not obtained by a dissolution-redeposition process. It is notable that the ED patterns along the [001] zone (Fig. 2) were easily observable, while those along the [010] zone were much more difficult to

observe. Such tendencies are due to the preferential cleavage plane along the *c* axis of the plate-like morphology of the samples. Furthermore, characterization of numerous particles along the [001] zone revealed strong and well-resolved diffraction spots for the acid-treated product, indicating that no amorphous depositions were produced during acid treatment. The streaks along c^* suggest the presence of stacking disorders, which is consistent with the XRD results.

Figure 3

Typical [010] TEM images for BSNN and acid-treated BSNN are shown in Fig. 4. Rows of dark and light contrast were observed at a periodicity of 1.6 nm for BSNN, which corresponds to *c*/2 of the unit-cell. After acid treatment, the periodicity of the rows of dark and light contrasts decreased to 1.4 nm, which is consistent with the basal spacing observed by XRD and ED.

Figure 4

Compositional Evaluation. The cation ratios of BSNN treated with 6 M HCl for various treatment periods are summarized in Table 1. A dramatic decrease in the Bi/Nb ratio was observed upon acid treatment. In contrast, the Na/Nb ratio remained at unity regardless of the treatment conditions. A slight decrease in the Sr/Nb ratio upon acid treatment was also detected. These results indicate a selective leaching of Bi from BSNN. The composition of acid-treated BSNN was unchanged for treatments longer than 12 h, indicating that steady state was apparently obtained after 12 h of treatment. Even when extensive treatment lasting up to a month was conducted, a small amount of bismuth, coupled with a decrease in strontium content, was always detected. The progressive change in cation ratios as a function of treatment time was in good agreement with the structural transformation obtained by XRD (Supplementary Information available).

Table 1

Compositional analysis of a supernatant solution was also conducted. The amount of Nb in the supernatant solution was <0.1 mass% of the initial mass of Nb used for the reaction (~0.07 mg of Nb detected from an initial ~353 mg of Nb in 1000 mg

BSNN). Since the results of the diffraction and microscopy analyses indicated that no amorphous materials were produced as a result of acid treatment, the cation ratios obtained by ICP can be taken as the composition of the perovskite-like slabs in acid-treated BSNN.

Acid Treatment of BCNN. Acid treatment of $Bi_2CaNaNb_3O_{12}$, the Ca analogue of BSNN, was also conducted. Figure 5 compares the XRD patterns of BCNN and BCNN treated with 6 M HCl for 72 h and dried at 120°C. The structural transformation observed after acid treatment of BCNN was similar to that observed after acid treatment of BSNN; new diffraction peaks that could be indexed as a series of (00*l*) reflections were observed, while the positions of the (*hk*0) peaks were unchanged. The cation ratios of acid-treated BCNN are summarized in Table 1. The changes in the cation ratios after acid treatment indicate a selective leaching of Bi from BCNN. Partial loss of Ca and a small amount of undissolved Bi was also detected, similar to the observation for acid treatment of BSNN.

Figure 5

Reactions during Acid Treatment of BSNN and BCNN. Figure 6 shows the TG curves of $H_{1.8}[Bi_{0.2}Sr_{0.8}NaNb_3O_{10}]$ and $H_{1.8}[Bi_{0.2}Ca_{0.8}NaNb_3O_{10}]$, the products obtained by treatment of BSNN and BCNN with 6 M HCl for 72 h. The samples were dried at 120°C in order to avoid the influence of adsorbed and/or interlayer water. The shape of the TG curves closely resembles those of protonated forms of layered perovskites obtained by conventional ion-exchange reactions with similar composition, such as $HCa_2Nb_3O_{10}$,[7c,8,11c] $H_2La_2Ti_3O_{10}$,[11e] and $H_2Sr_{1.5}Nb_3O_{10}$.[4b] The observed mass loss of 2.7 mass% between ~160 and ~550°C can be attributed to dehydroxylation, which is in excellent agreement with the anticipated mass loss of 2.8 mass% according to the equation:

$$H_{1.8}[Bi_{0.2}Sr_{0.8}NaNb_3O_{10}] \xrightarrow{\Delta} Bi_{0.2}Sr_{0.8}NaNb_3O_{9.1} + 0.9\ H_2O \qquad [2].$$

Accordingly, the observed mass loss of 3.1 mass% between ~130 and ~550°C corresponds to the anticipated mass loss of 3.0 mass% according to the equation:

$$H_{1.8}[Bi_{0.2}Ca_{0.8}NaNb_3O_{10}] \xrightarrow{\Delta} Bi_{0.2}Ca_{0.8}NaNb_3O_{9.1} + 0.9\ H_2O \qquad [3].$$

Figure 6

The slight amount of residual bismuth and strontium (or calcium) in $H_{1.8}[Bi_{0.2}Sr_{0.8}NaNb_3O_{10}]$ (or $H_{1.8}[Bi_{0.2}Ca_{0.8}NaNb_3O_{10}]$) can be understood based on the partial occupancy of Bi in the A site of the perovskite-like slabs of the host compounds, BSNN and BCNN. Partial disordering of Bi in the bismuth oxide sheets and the A-site cation in the perovskite-like slabs (Bi↔A) has been reported for n=2 members of Aurivillius phases $Bi_2AB_2O_9$ (A=Ca, Sr, Ba, Pb, B=Nb, Ta).[29] It therefore seems natural to assume that similar disordering also exists in BSNN and BCNN. It is worth noting that this process can provide quantitative information for the cation disorders in the Aurivillius phases. Since the type of A-site cation in the Aurivillius phases affects their ferroelectric properties,[30] this process appears to be a valuable approach to the structural characterization of the Aurivillius phases.

Assuming that the residual bismuth is due to a disorder of cations, the overall reaction could be expressed as follows:

$$(Bi_{1.8}A_{0.2}O_{2.0})^{1.8+}[Bi_{0.2}A_{0.8}NaNb_3O_{10}]^{1.8-} \xrightarrow{\text{aq. HCl}}$$

$$H^+_{1.8}\,[Bi_{0.2}A_{0.8}NaNb_3O_{10}]^{1.8-}\cdot nH_2O \text{ (A=Sr or Ca)} \qquad [4]$$

where n denotes interlayer and/or surface adsorbed water (typically n=0.4 for an air-dried sample).[31]

Accordingly, the overall reaction can be regarded as the replacement of the positively-charged bismuth-oxide sheets (containing Sr or Ca) with protons to compensate for the negatively-charged perovskite-like slabs ($\{(Bi_{1.8}A_{0.2}O_2)^{1.8+}\}_x \rightarrow 1.8xH^+$, where A=Sr or Ca). The reaction is schematically shown in Scheme 2. This should be compared with the proton-exchange reaction ($M^+ \rightarrow H^+$) in ion-exchangeable layered perovskites.

Scheme 2

Mechanism of Selective Leaching. Protonated-layered perovskites which possess perovskite-like slab compositions similar to $H_{1.8}[Bi_{0.2}Sr_{0.8}NaNb_3O_{10}]$ and $H_{1.8}[Bi_{0.2}Ca_{0.8}NaNb_3O_{10}]$ have been reported; for example, $H[BiNb_2O_7]$, $H[A_2Nb_3O_{10}]$ (A=Sr or Ca), $H_2[A_{1.5}Nb_3O_{10}]$ (A=Sr or Ca), and $H[Ca_2NaNb_4O_{13}]$.[2b,4b,9,12e] These

were obtained by ion-exchange reactions using concentrated acids at 60°C for a few days. These conditions are similar to or more severe than the conditions applied in this study. These previous results, combined with the fact that the process in this study involves no dissolution of Nb (as shown by the ICP results of the supernatant solution), show the relatively high stability of the Nb-based perovskite-like slabs in Aurivillius phases towards acid treatment under the present experimental conditions. The bismuth-oxide sheets in the Aurivillius phases on the other hand are isostructural to those in the Sillen phase BiOCl, which is also a lamellar oxide.[32] BiOCl is known to be soluble in acidic solutions.[33] The selective leaching of the bismuth-oxide sheets can be therefore understood based on differences in the stabilities of the perovskite-like slabs and the bismuth-oxide sheets in acidic solutions.

The use of high acid concentrations such as 6 M HCl is not necessarily a prerequisite for complete conversion. Identical ICP results (Table 1) and XRD results (not shown) can be achieved under milder conditions, such as, by using 3 M HCl for 72 h. Even with 1 M HCl, a slight decrease in the Bi/Nb ratio was detected after treatment for 72 h, suggesting that the conversion reaction may progress at lower acid concentrations with extended treatment.

Structural Consideration of the Acid-treated Products. Since the characteristic two-dimensional structures of BSNN and BCNN were preserved in the acid-treated products, the structures of $H_{1.8}[Bi_{0.2}Sr_{0.8}NaNb_3O_{10}]$ and $H_{1.8}[Bi_{0.2}Ca_{0.8}NaNb_3O_{10}]$ should be closely related to those of the host compounds. Initially, indexing of the XRD pattern of $H_{1.8}[Bi_{0.2}Sr_{0.8}NaNb_3O_{10}]$ (dried at 120°C) was attempted using a tetragonal cell with body-centered symmetry (*I*4/*mmm*) and a~0.39, c~2.86 nm. Although most of the peaks could be indexed, the sharp diffraction peak at 2θ~22.7° (d~0.39 nm) could not be indexed reliably as the (103) peak ($2\theta_{(obs)}$~22.7°; $2\theta_{(cal)}$~24.7°). Moreover, we could not find any evidence for c-axis doubling in either the XRD or the ED patterns. The most reliable indexing of the XRD pattern for acid-treated BSNN was based on a primitive tetragonal symmetry with no c-axis doubling. In this case, the sharp diffraction peak at 2θ~22.7° could be reliably indexed as the (100) diffraction peak

($2\theta_{(obs)}$~22.7°; $2\theta_{(cal)}$~22.7°). The refined lattice parameters for $H_{1.8}[Bi_{0.2}Sr_{0.8}NaNb_3O_{10}]$ (dried at 120°C) were a=0.391±0.002 and c=1.39±0.02 nm.[34] Likewise, the XRD pattern for $H_{1.8}[Bi_{0.2}Ca_{0.8}NaNb_3O_{10}]$ (120°C dried) was indexed based on a primitive tetragonal symmetry with no c-axis doubling; the refined lattice parameters were a=0.390±0.003 and c=1.41±0.01 nm.

$H_2La_2Ti_3O_{10}$ obtained by ion-exchange of the Ruddlesden-Popper phase $K_2La_2Ti_3O_{10}$ was reported to possess a structure with a relative displacement of the perovskite-like slabs by $(a+b)/2$, leading to a doubled c axis.[4] Although the host compounds, BSNN and BCNN, possess structures with a doubled c axis, no doubling of the c axis was observed in the acid-treated products. Both the XRD [broadness of the (hkl) peaks] and ED (streaks along c^*) results for acid-treated BSNN indicate the presence of stacking disorders, which should complicate the accurate determination of the cell symmetry and stacking sequence of the perovskite-like slabs by the powder XRD patterns. In fact, HREM observations of $H_{1.8}[Sr_{0.8}Bi_{0.2}Ta_2O_7]$ derived by a "bismuth oxide sheet to proton substitution" reaction of an n=2 member of the Aurivillius phase, $Bi_2SrTa_2O_9$, indicated the existence of two types of perovskite-like slab stacking: a stacking sequence with no displacement of the perovskite-like slabs (P-type) and a stacking sequence with relative displacement by $(a+b)/2$ (I-type).[23] On the contrary, the XRD pattern of $H_{1.8}[Sr_{0.8}Bi_{0.2}Ta_2O_7]$ was indexed based on a structure without displacement of the perovskite-like slabs. These observations indicate the presence of more than one local interlayer environment that cannot be detected by XRD in acid-treated BSNN. The indexing for $H_{1.8}[Bi_{0.2}Sr_{0.8}NaNb_3O_{10}]$ and $H_{1.8}[Bi_{0.2}Ca_{0.8}NaNb_3O_{10}]$ based on a primitive cell without c axis doubling consequently represents only the "average structure", disregarding the local stacking sequence of the perovskite-like slabs.

Intercalation Chemistry of $H_{1.8}[Bi_{0.2}Sr_{0.8}NaNb_3O_{10}]$. Since protonated forms of layered niobates are known to accommodate alkylamines,[5,9a,35] reaction of alkylamines with $H_{1.8}[Bi_{0.2}Sr_{0.8}NaNb_3O_{10}]$ was conducted. After the reaction of $H_{1.8}[Bi_{0.2}Sr_{0.8}NaNb_3O_{10}]$ with alkylamines, all of the (00l) diffraction peaks were shifted

to higher diffraction angles, while the (*hk*0) diffraction peaks were observed at the same diffraction angles, indicating intercalation of alkylamines into the interlayer space of $H_{1.8}[Bi_{0.2}Sr_{0.8}NaNb_3O_{10}]$ (Fig. 7). The lattice parameters of C4A- and C8A-intercalated $H_{1.8}[Bi_{0.2}Sr_{0.8}NaNb_3O_{10}]$ were in good agreement with C4A- and C8A-intercalated $HCa_2Nb_3O_{10}$,[2b,6a] as summarized in Table 2. Chemical analysis revealed that 0.9 moles of C4A (C, 8.0 mass %; H, 1.9 mass %; N, 1.7 mass %) and 1.0 mole of C8A (C, 14.7 mass %; H, 3.1 mass %; N, 2.0 mass %) per $[Bi_{0.21}Sr_{0.80}Na_{0.95}Nb_3O_{10}]$ were intercalated. To the best of our knowledge, this is the first evidence of intercalation of alkylamines into layered perovskites where the perovskite-like slabs possess a charge higher than one.[36]

Figure 7

Table 2

Conclusions

We have developed a novel method for obtaining protonated forms of layered perovskites derived from the Aurivillius phases. The structural and compositional analyses revealed that $H_{1.8}[Bi_{0.2}Sr_{0.8}Na_{1.0}Nb_3O_{10}]$ and $H_{1.8}[Bi_{0.2}Ca_{0.8}Na_{1.0}Nb_3O_{10}]$ were derived through acid treatment of $Bi_2SrNaNb_3O_{12}$ and $Bi_2CaNaNb_3O_{12}$, respectively. The bismuth oxide sheet to proton substitution reaction of the Aurivillius phases involves selective leaching of the bismuth oxide sheets accompanied by the introduction of interlayer protons ($\{(Bi_{1.8}A_{0.2}O_2)^{1.8+}\}_x \rightarrow 1.8xH^+$), a reaction resembling the conventional proton-exchange reaction ($M^+ \rightarrow H^+$). The small amount of residual Bi in the acid-treated product was suggested to result from the partial occupancy of Bi in the A site of the perovskite-like slabs in the Aurivillius phases, *i.e.* $Bi_{1.8}A_{0.2}O_2[Bi_{0.2}A_{0.8}NaNb_3O_{10}]$ (A=Sr or Ca). The increase in basal spacing upon reaction of $H_{1.8}[Bi_{0.21}Sr_{0.80}Na_{0.95}Nb_3O_{10}]$ with *n*-alkylamines provides evidence for the preservation of the characteristic layered structure.

We propose that the Aurivillius phases can be considered as a new homologous

series of oxides for preparing protonated forms of layered-perovskite related oxides. Numerous Aurivillius phases have been reported with combinations of various elements and n values (A=Na, Ca, Bi, etc.; B=Nb, Ti, etc.; $1 \leq n \leq 8$).[18,19] The findings of Pb-substituted Aurivillius phases has given rise to an even larger numbers of new Aurivillius phases with varying perovskite-like slab charge density.[37] The novel method of converting Aurivillius phases into the protonated forms of the layered perovskites opens up the possibility of obtaining an extensive range of new compounds.

Acknowledgments. The authors thank Mr. Minekazu Fujiwara at the Materials Characterization Central Laboratory Waseda University for the TEM observations. Experimental assistance by Mr. Yu Tsunoda and Ms. Fumi Nakasone is also acknowledged. This work was financially supported in part by the Grant-in-Aid for Scientific Research (No. 10555221) from the Ministry of Education, Science, Sports, and Culture, Japan.

Supporting Information Available. The output from the Rietveld analysis, the crystallographic data obtained for $Bi_2SrNaNb_3O_{12}$ and $Bi_2CaNaNb_3O_{12}$, and the stacked plot for the variation in the XRD pattern as a function of reaction time are available free of charge on the Internet at http://pubs.acs.org.

References

*) Corresponding author. E-mail: ys6546@waseda.ac.jp

†) School of Science and Engineering

‡) Kagami Memorial Laboratory for Materials Science and Technology

§ Current address: Department of Fine Materials Engineering, Faculty of Textile Science and Technology, Shinshu University, Tokida 3-15-1, Ueda, Nagano, 386-8567 JAPAN

(1) (a) Ruddlesden, S.N.; Popper, P. *Acta Cryst.* **1957**, *10*, 538.

(b) Ruddlesden, S.N.; Popper, P. *Acta Cryst.* **1958**, *11*, 54.

(2) (a) Dion, M.; Ganne, M.; Tournoux, M. *Mater. Res. Bull.* **1981**, *16*, 1429.

(b) Jacobson, A.J.; Johnson, J.W.; Lewandowski, J.T. *Inorg. Chem.* **1985**, *24*, 3727.

(c) Dion, M.; Gannet, M.; Tournoux, M. *Rev. Chim. Miner.* **1986**, *23*, 61.

(3) Gopalakrishnan, J.; Bhat, V. *Inorg. Chem.* **1987**, *26*, 4299.

(4) (a) Ollivier, P. J.; Mallouk, T. E. *Chem. Mater.* **1998**, *10*, 2585.

(b) Bhuvanesh, N.S.P.; Crosnier-Lopez, M-P.; Duroy, H.; Fourquet, J-L. *J. Mater. Chem.* **2000**, *10*, 1685.

(5) Jacobson, A.J. *Chemical Physics of Intercalation II*; P. Brenier: New York, 1993; pp 117.

(6) For example, see: (a) Jacobson, A.J.; Johnson, J.W.; Lewandowski, J.T. *Mater. Res. Bull.* **1987**, *22*, 45.

(b) Matsuda, T.; Miyamae, N.; Takeuchi, M. *Bull. Chem. Soc. Jpn.* **1993**, *66*, 1551.

(7) (a) Gopalakrishnan, J.; Bhat, V.; Raveau, B. *Mater. Res. Bull.* **1987**, *22*, 413.
(b) Uma, S.; Raju, A.R.; Gopalakrishnan, J. *J. Mater. Chem.* **1993**, *3*, 709.
(c) Gopalakrishnan, J.; Uma, S.; Bhat, V. *Chem. Mater.* **1993**, *5*, 132.
(d) Uma ,A.; Gopalakrishnan, J. *J. Solid State Chem.* **1993**, *102*, 332.
(e) Uma, A.; Gopalakrishnan, J. *Chem. Mater.* **1994**, *6*, 907.

(8) Mohan Ram, R.A.; Clearfield, R.A. *J. Solid State Chem.* **1991**, *94*, 45.

(9) Nakato, T.; Nakade, M.; Kuroda, K.; Kato, C. *Studies Surf. Sci. Catal.* **1994**, *90*, 285.

(10) Matsuda, T.; Fujita, T.; Miyamae, M.; Takeuchi, M.; Kanda, K. *Bull. Chem. Soc. Jpn.* **1993**, *66*, 1548.

(11) (a) Subramanian, M.A.; Gopalakrishnan, J.; Sleight, A.W. *Mater. Res. Bull.* **1988**, *23*, 837.

(b) Mangamma, G.; Bhat, V.; Gopalakrishnan, J.; Bhat, S.V. *Solid State Ionics* **1992**, *58*, 303.

(c) Sato, M.; Jin, T.; Uematsu, K. *J. Solid State Chem.* **1993**, *102*, 557.

(d) Sato, M.; Abo, J.; Jin, T.; Ohta, M. *J. Alloys and Comp.* **1993**, *192*, 81.

(e) Thangadurai, V.; Shukla, A.K.; Gopalakrishnan, J. *Solid State Ionics* **1994**, *73*, 9.

(12) (a) Yoshimura, J.; Ebina, Y.; Kondo, J.; Domen, K.; Tanaka, K. *J. Phys. Chem.* **1993**, *97*, 1970.

(b) Ebina, Y.; Tanaka, A.; Kondo, J.N.; Domen, K. *Chem. Mater.* **1996**, *8*, 2534.

(c) Takata, T.; Furumi, Y.; Shinohara, K.; Tanaka, A.; Hara, M.; Kondo, J. N.; Domen, K. *Chem. Mater.* **1997**, *9*, 1063.

(d) Takata, T.; Shinohara, K.; Tanaka, A.; Hara, M.; Kondo, J.N.; Domen, K. *J. Photochem. Photobiol.* **1997**, *106*, 45.

(e) Nakato, T.; Ito, K.; Kuroda, K.; Kato, C. *Microporous Mater.* **1993**, *1*, 283.

(13) Matsuda, T.; Miyamae, N.; Takeuchi, M. *Bull. Chem. Soc. Jpn.* **1993**, *66*, 1551.

(14) Takahashi, S.; Nakato, T., Hayashi, S.; Sugahara, Y; Kuroda, K. *Inorg. Chem.* **1995**, *34*, 5065.

(15) Matsuda, T.; Udagawa, M.; Kunou, I. *J. Catal.* **1997**, *168*, 26.

(16) (a) Richard, M.; Brohan, L.; Tournoux, M. *J. Solid State Chem.* **1994**, *112*, 345.

(b) Gondrand, M.; Joubert, J.-C. *Rev. Chim. Miner.* **1987**, *24*, 33.

(c) Byeon, S.-H.; Yoon, J.-J.; Lee, S.-O. *J. Solid State Chem.* **1997**, *130*, 119.

(d) Schaak, R.E; Mallouk, T.E. *J. Am. Chem. Soc.* **2000**, *122*, 2798.

(17) (a) Schaak, R.E; Mallouk, T.E. *Chem. Mater.* **2000**, *12*, 2513.

(b) Schaak, R.E; Mallouk T.E. *Chem Mater.* **2000**, *12*, 3427.

(18) (a) Aurivillius, B. *Ark. Kemi* **1949**, *1*, 463.

(b) Aurivillius, B. *Ark. Kemi* **1949**, *1*, 499.

(c) Aurivillius, B. *Ark. Kemi* **1950**, *2*, 519.

(19) For example, see: (a) Subbarao, E.C. *J. Am. Ceram. Soc.* **1962**, *45*, 166.

(b) Subbarao, E.C. *J. Phys. Chem. Solids* **1962**, *23*, 665.

(c) Wolfe, R.W.; Newnham, R.E. *J. Electrochem. Soc.* **1969**, *116*, 832.

(d) Subbarao, E.C. *Ferroelectrics* **1973**, *5*, 267.

(e) Kikuchi, T.; Watanabe, A.; Uchida, K. *Mater. Res. Bull.* **1977**, *12*, 299.

(20) Sugimoto, W.; Shirata, M.; Sugahara, Y.; Kuroda, K. *J. Am. Chem. Soc.* **1999**, *121*, 11602.

(21) Shirata, M.; Tsunoda, Y.; Sugimoto, W.; Sugahara, Y. *Mat. Res. Soc. Symp. Proc.*, "Solid-State Chemistry of Inorganic Materials" Ed. M.J. Geselbracht, J.E. Greedan, D.C. Johnson, M.A. Subramanian, **2001**, *658*, GG6.24.1.

(22) Suzuki, M.; Nagasawa, N.; Machida, A.; Ami, T. *Jpn. J. Appl. Phys.* **1996**, *35*, L565.

(23) Tsunoda, Y.; Shirata, M.; Sugimoto, W.; Liu, Z.; Terasaki, O.; Sugahara, Y.; Kuroda, K. *Inorg. Chem.* **2001**,*40*, 5768.

(24) Gopalakrishnan, J.; Sivakuma, T.; Ramesha, K.; Thangadurai, V.; Subbanna, G.N. *J. Am. Chem. Soc.* **2000**, *122*, 6237.

(25) Kikuchi, T. *Mater. Res. Bull.* **1979**, *14*, 1561.

(26) Muramatsu, K.; Shimazu, M.; Tanaka, J.; Horiuchi, S. *J. Solid State Chem.* **1981**, *36*, 179.

(27) Ismundar; Kennedy, B.J.; Gunawan; Marsongkohadi *J. Solid State Chem.* **1996**, *126*, 135.

(28) (a) Izumi, F. *The Rietveld Method*; R.A. Young Ed.; Oxford University Press: Oxford, 1993; pp.236-253.

(b) Kim, Y.I.; Izumi, F. *J. Ceram. Soc. Japan* **1994**, *102*, 401.

(29) (a) Srikanth, V.; Idink, H.; White, W.B.; Subbarao, E.C.; Rajagopal, H.; Sequeira, A. *Acta Crystallogr.* **1996**, *B52*, 432.

(b) Blake, S.M.; Falconer, M.J.; McCreedy, M.; Lightfoot, P. *J. Mater. Chem.* **1997**, *7*, 1609.

(c) Ismundar; Hunter, B.A.; Kennedy, B.J. *Solid State Ionics* **1998**, *112*, 281.

(d) Ismundar; Kennedy, B.J. *J. Mater. Chem.* **1999**, *9*, 541.

(e) Macquart R.; Kennedy, B.J.; Shirakawa Y. *J. Solid State Chem.* **2001**, *160*,

Figure captions

Scheme 1. The schematic structures of n=3 layered perovskites. (a) Ruddlesden-Popper phases $K_2[A_2B_3O_{10}]$, (b) Dion-Jacobson phases $Rb[A_2B_3O_{10}]$, and (c) Aurivillius phases $Bi_2O_2[A_2B_3O_{10}]$. The octahedrons represent the BO_6 units, and the black balls represent the 12-coordinated A site cations in the perovskite-like slabs. The gray balls represent the interlayer K ions in (a) and the Rb ions in (b). The gray and white balls in (c) represent the bismuth and oxygen ions in the bismuth oxide sheets, respectively.

Scheme 2. Schematic representation of the conversion of the Aurivillius phases $Bi_2ANaNb_3O_{12}$ (A=Sr or Ca) to the corresponding protonated forms of layered perovskite $H_{1.8}Bi_{0.2}A_{0.8}NaNb_3O_{10}$ (A=Sr or Ca) by the bismuth oxide sheet to proton substitution reaction.

Figure 1. XRD patterns of (a) BSNN, (b) the room temperature-dried product of BSNN treated with 6 M HCl for 72 h, and (c) the 120°C-dried product of BSNN treated with 6 M HCl for 72 h.

Figure 2. ED patterns along the [001] and [010] zones of (a) BSNN and (b) acid-treated BSNN obtained by 72-h treatment with 6 M HCl.

Figure 3. SEM images of (a) BSNN and (b) acid-treated BSNN obtained by 72-h treatment with 6 M HCl.

Figure 4. TEM images along the [010] zone of (a) BSNN and (b) acid-treated BSNN obtained by 72-h treatment with 6 M HCl.

Figure 5. XRD patterns of (a) BCNN and (b) acid-treated BSNN obtained by 72-h treatment with 6 M HCl, followed by drying at 120°C.

Figure 6. TG curves of the products obtained by acid treatment of (a) BSNN and (b) BCNN with 6 M HCl for 72 h, followed by drying at 120°C.

Figure7. XRD patterns of (a) $H_{1.8}[Bi_{0.2}Sr_{0.8}Na_{1.0}Nb_3O_{10}]$, (b) C4A-$H_{1.8}[Bi_{0.2}Sr_{0.8}Na_{1.0}Nb_3O_{10}]$, and (c) C8A-$H_{1.8}[Bi_{0.2}Sr_{0.8}Na_{1.0}Nb_3O_{10}]$.

Table 1. The cation ratios of the products.

Host compound	Treatment time / h	Acid	Molar ratio				
			Bi	Sr	Ca	Na	Nb[a]
BSNN	0	—	2.00	1.00	—	1.02	3
BSNN	1	6 M HCl	1.55	0.94	—	0.99	3
BSNN	12	6 M HCl	0.27	0.75	—	1.00	3
BSNN	24	6 M HCl	0.29	0.79	—	0.99	3
BSNN	72	6 M HCl	0.21	0.80	—	1.00	3
BSNN	720	6 M HCl	0.19	0.74	—	0.95	3
BSNN	72	3 M HCl	0.22	0.76	—	0.99	3
BSNN	72	1 M HCl	1.83	0.96	—	1.04	3
BCNN	0	—	1.96	—	1.03	1.04	3
BCNN	72	6 M HCl	0.19	—	0.82	0.99	3

[a] Set to 3.

Table 2. Lattice parameters of the host Aurivillius phases and the corresponding protonated forms and intercalation compounds.[a]

Composition	*a* / nm	*c* / nm	reference
$Bi_2SrNaNb_3O_{12}$	0.39007(1)	1.6463(1)[e]	this work
$Bi_2CaNaNb_3O_{12}$	0.38686(3)[d]	1.6365(1)[e]	this work
$H_{1.8}[Bi_{0.2}Sr_{0.8}Na_{1.0}Nb_3O_{10}]\cdot nH_2O$[b]	0.390(1)	1.43(2)	[20]
$H_{1.8}[Bi_{0.2}Sr_{0.8}Na_{1.0}Nb_3O_{10}]$[c]	0.391(2)	1.39(2)	this work
$H_{1.8}[Bi_{0.2}Ca_{0.8}Na_{1.0}Nb_3O_{10}]$[c]	0.390(3)	1.41(1)	this work
C4A-$H_{1.8}[Bi_{0.2}Sr_{0.8}Na_{1.0}Nb_3O_{10}]$	0.390	2.43	this work
C8A-$H_{1.8}[Bi_{0.2}Sr_{0.8}Na_{1.0}Nb_3O_{10}]$	0.390	3.26	this work
C4A-$H[Ca_2Nb_3O_{10}]$	0.3855	2.4952	[6a]
C8A-$H[Ca_2Nb_3O_{10}]$	0.3854	3.1514	[6a]

[a] The lattice parameters of the host Aurivillius phases were refined by Rietveld analysis. The lattice parameters of the protonated forms were refined by the non-linear least-squares method. The *a* and *c* lattice parameters of the intercalation compounds were calculated from the (100) and (001) diffraction peaks, respectively.

[b] Dried at room temperature.

[c] Dried at 120°C.

[d] For the sake of comparison, the lattice parameter was reduced to $a_p=(a+b)/\sqrt{2}$ due to the difference in structure.

[e] For the sake of comparison, the lattice parameter was reduced to $c/2$ due to the difference in structure.

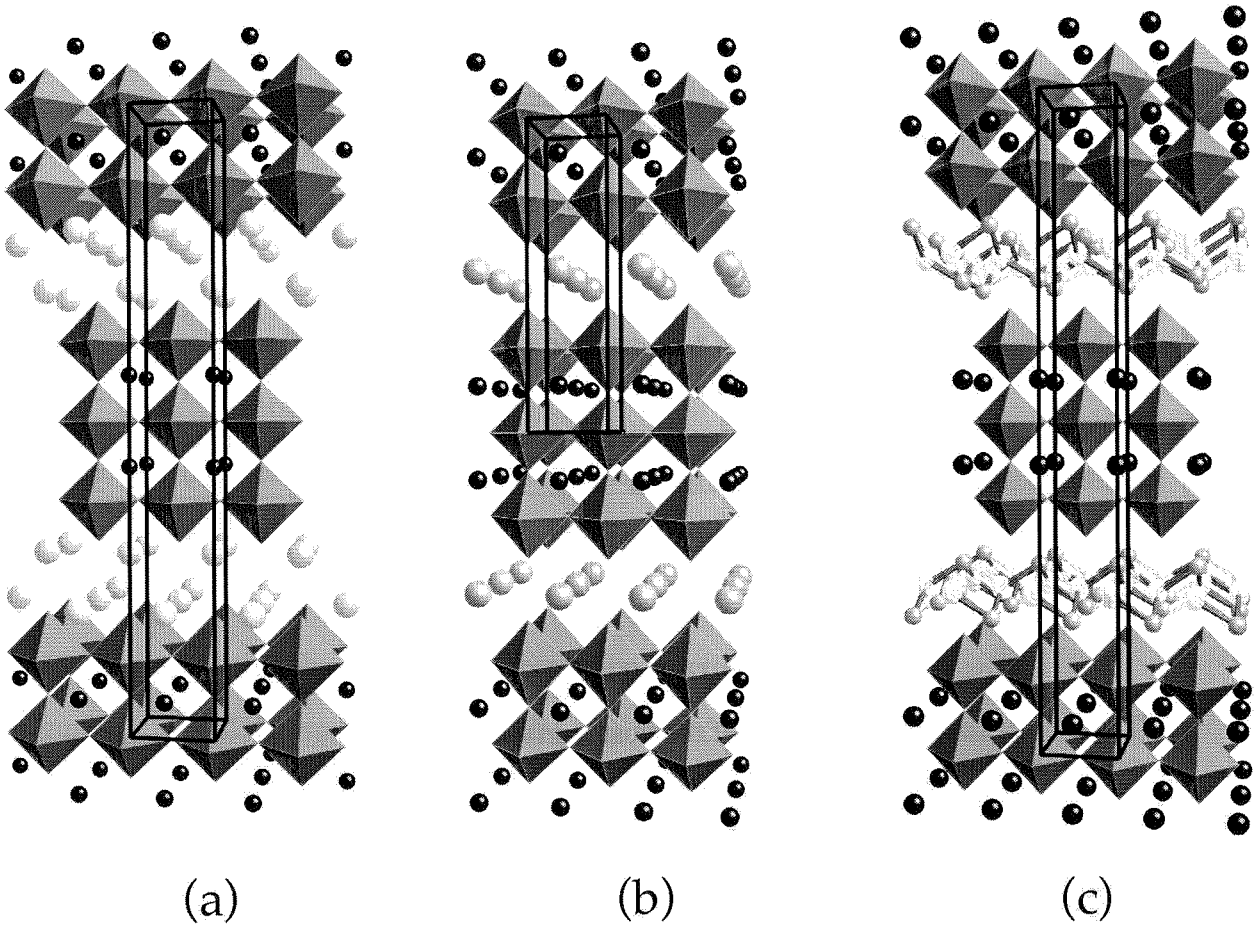

Scheme 1. The schematic structures of n=3 layered perovskites. (a) Ruddlesden-Popper phases $K_2[A_2B_3O_{10}]$, (b) Dion-Jacobson phases $Rb[A_2B_3O_{10}]$, and (c) Aurivillius phases $Bi_2O_2[A_2B_3O_{10}]$. The octahedrons represent the BO_6 units, and the black balls represent the 12-coordinated A site cations in the perovskite-like slabs. The gray balls represent the interlayer K ions in (a) and the Rb ions in (b). The gray and white balls in (c) represent the bismuth and oxygen ions in the bismuth oxide sheets, respectively.

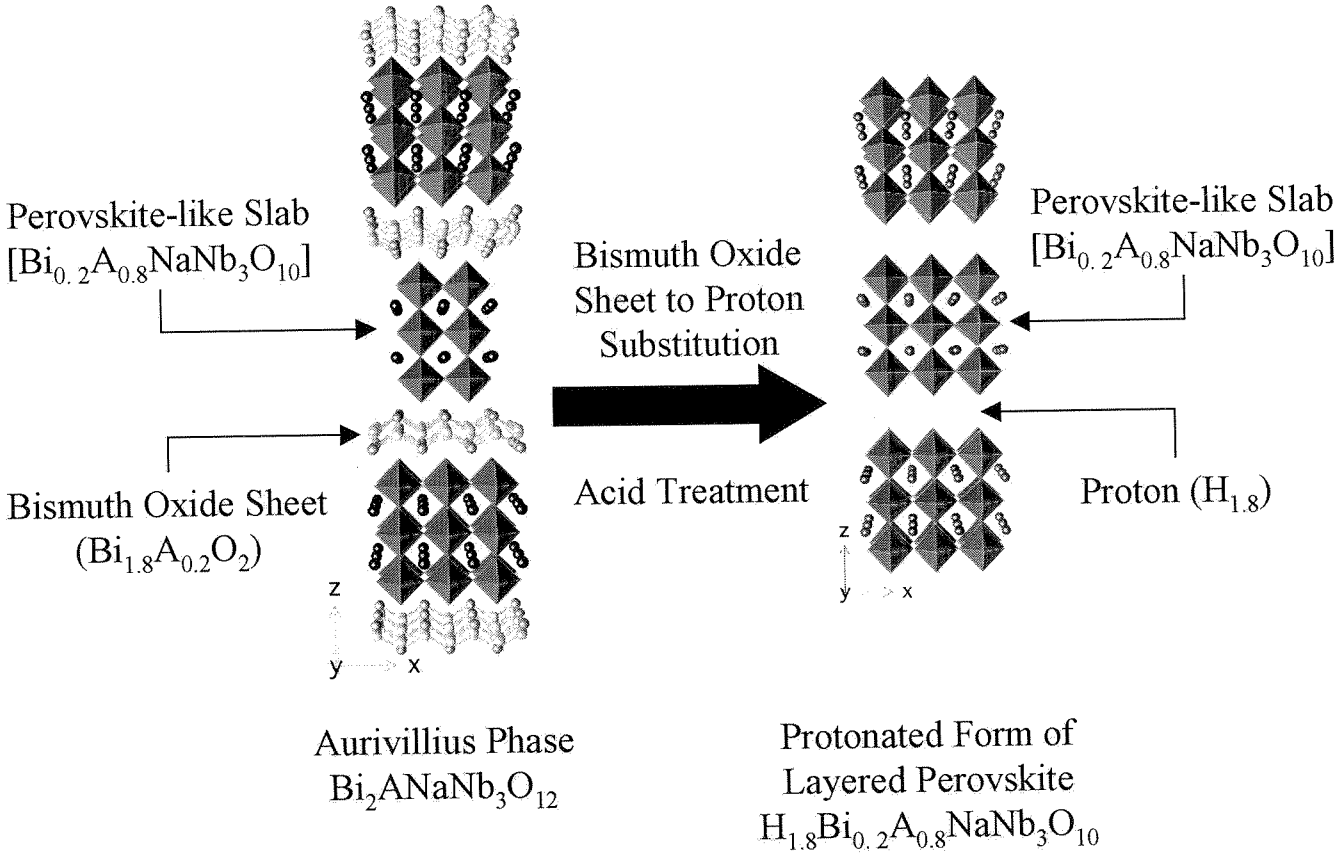

Scheme 2. Schematic representation of the conversion of the Aurivillius phases $Bi_2ANaNb_3O_{12}$ (A=Sr or Ca) to the corresponding protonated forms of layered perovskite $H_{1.8}Bi_{0.2}A_{0.8}NaNb_3O_{10}$ (A=Sr or Ca) by the bismuth oxide sheet to proton substitution reaction.

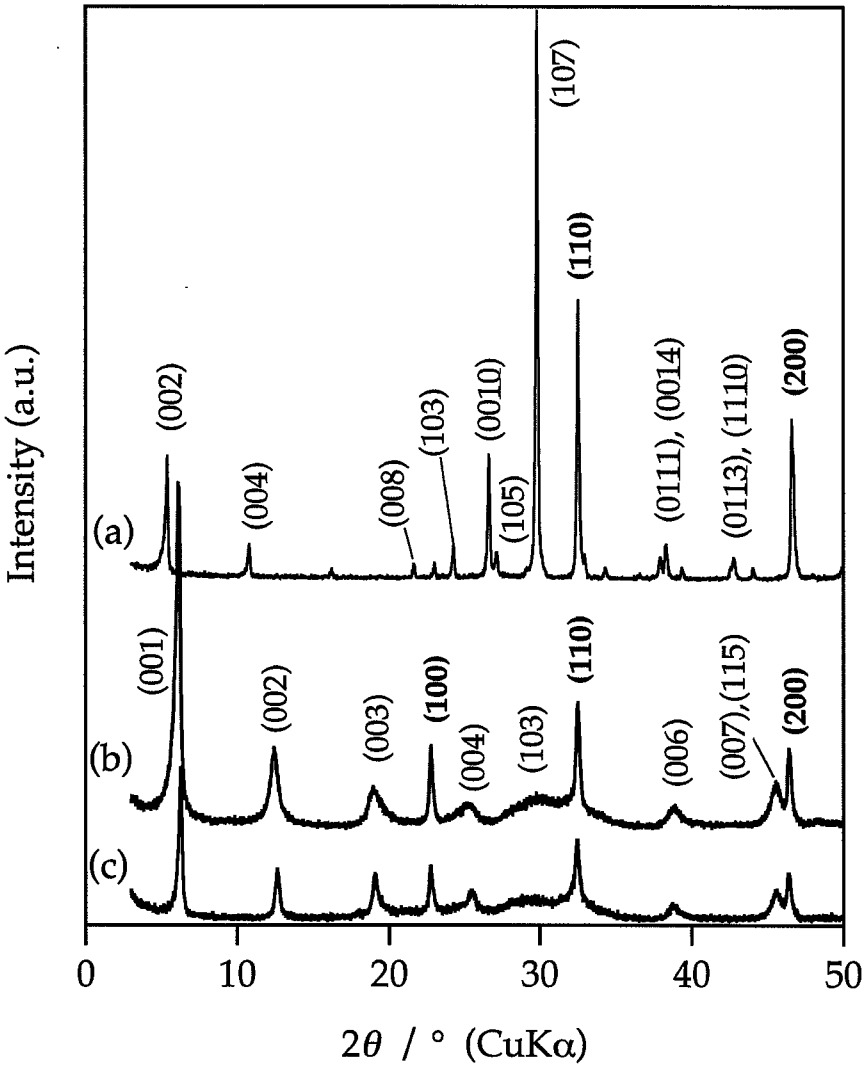

Figure 1. XRD patterns of (a) BSNN, (b) the room temperature-dried product of BSNN treated with 6 M HCl for 72 h, and (c) the 120°C-dried product of BSNN treated with 6 M HCl for 72 h.

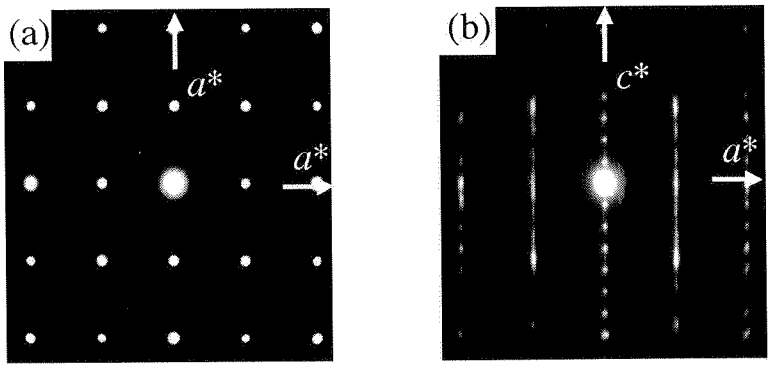

Figure 2. ED patterns along the [001] and [010] zones of (a) BSNN and (b) acid-treated BSNN obtained by 72-h treatment with 6 M HCl.

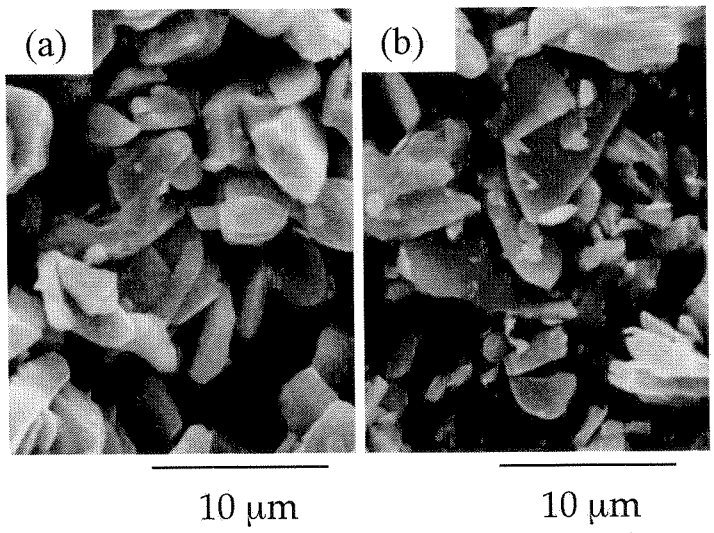

Figure 3. SEM images of (a) BSNN and (b) acid-treated BSNN obtained by 72-h treatment with 6 M HCl.

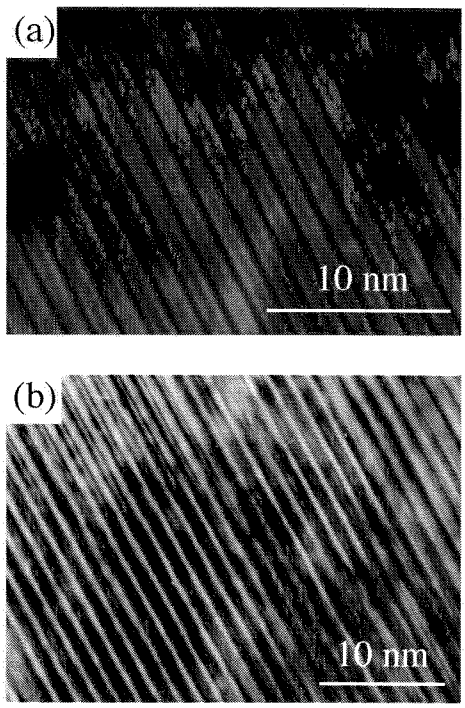

Figure 4. TEM images along the [010] zone of (a) BSNN and (b) acid-treated BSNN obtained by 72-h treatment with 6 M HCl.

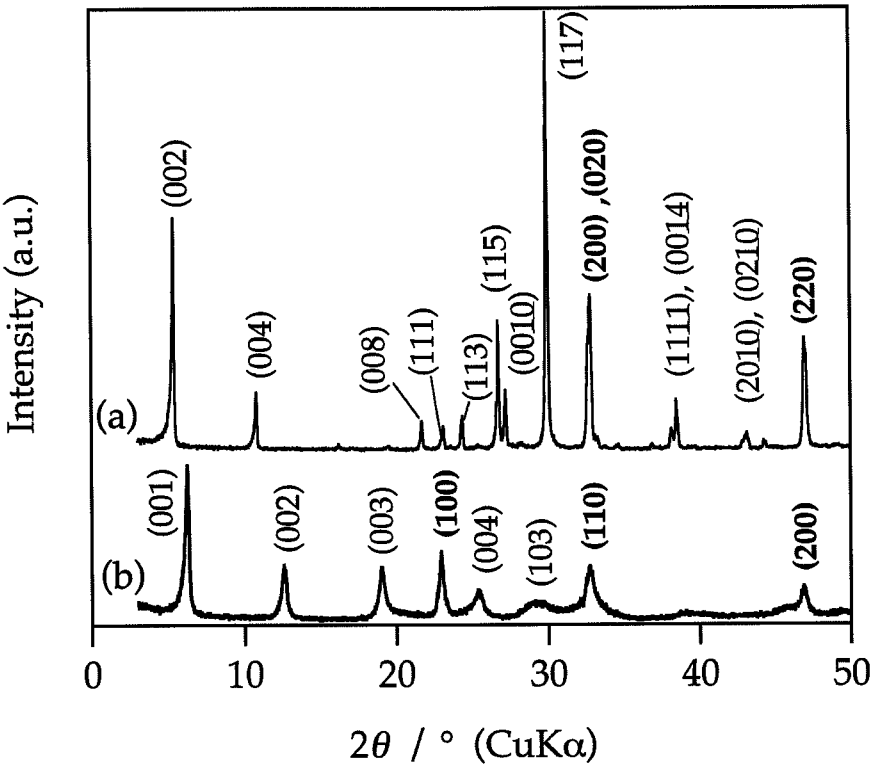

Figure 5. XRD patterns of (a) BCNN and (b) acid-treated BSNN obtained by 72-h treatment with 6 M HCl, followed by drying at 120°C.

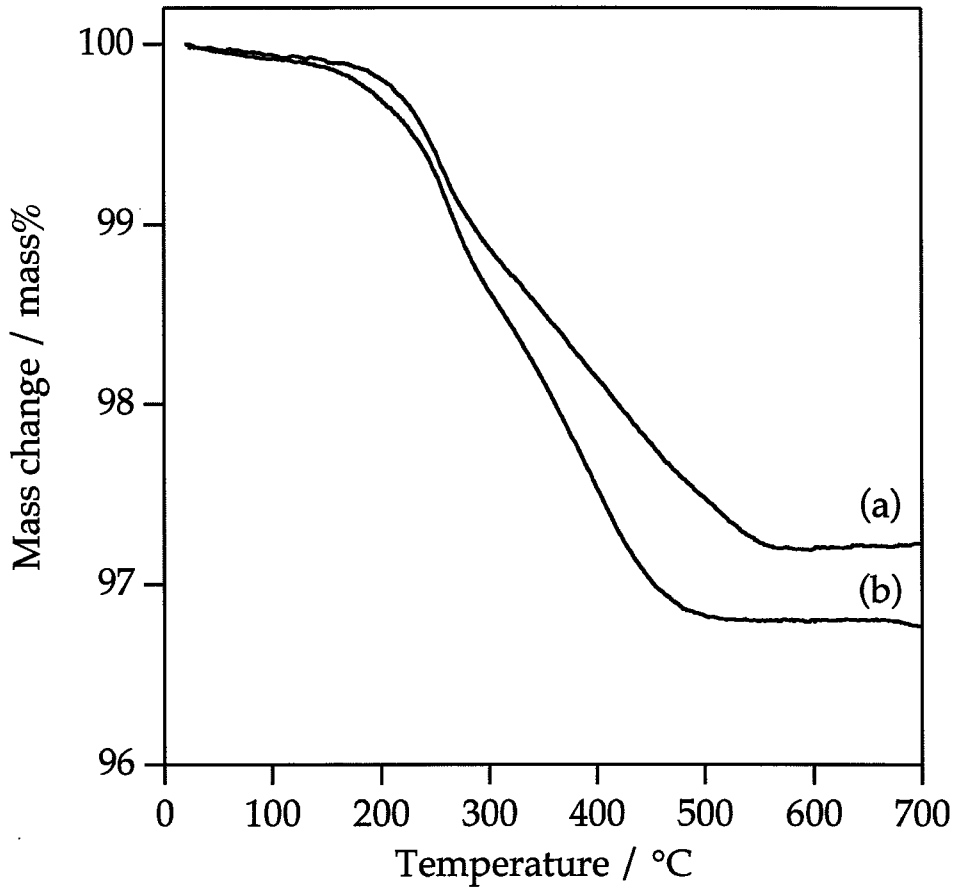

Figure 6. TG curves of the products obtained by acid treatment of (a) BSNN and (b) BCNN with 6 M HCl for 72 h, followed by drying at 120°C.

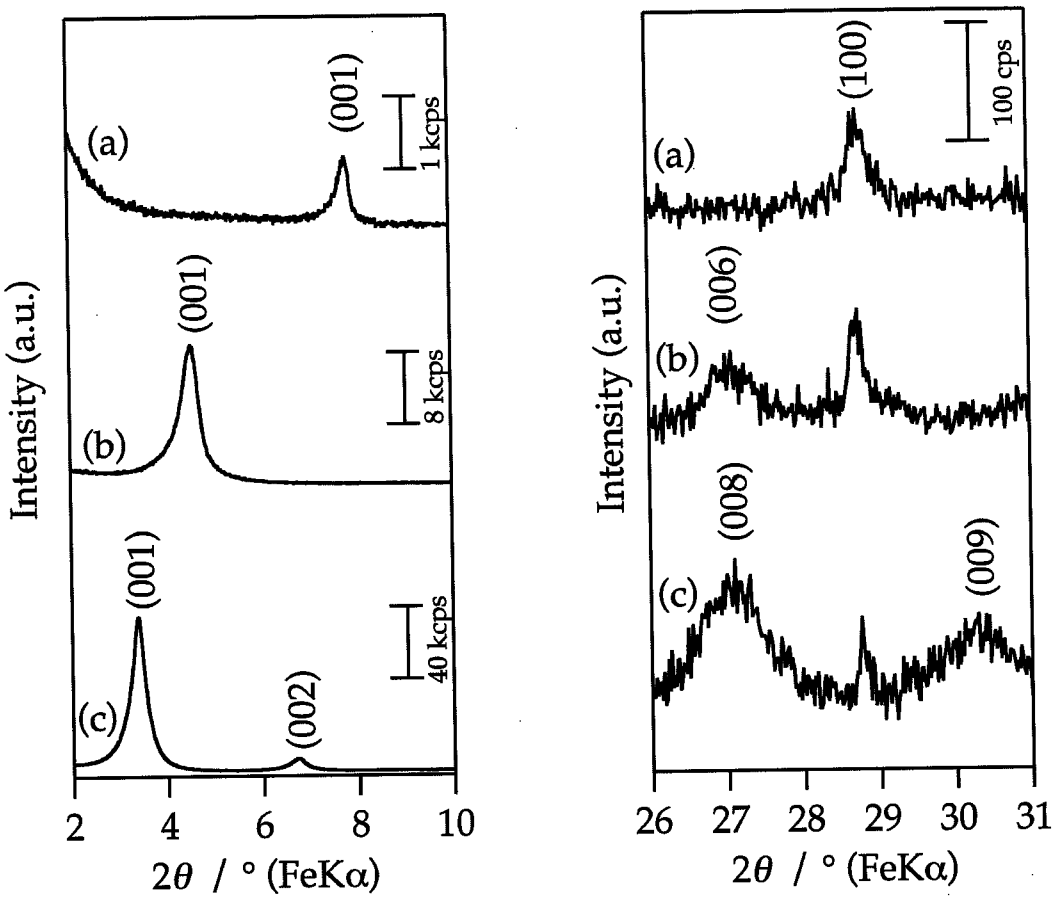

Figure7. XRD patterns of (a) $H_{1.8}[Bi_{0.2}Sr_{0.8}Na_{1.0}Nb_3O_{10}]$, (b) C4A-$H_{1.8}[Bi_{0.2}Sr_{0.8}Na_{1.0}Nb_3O_{10}]$, and (c) C8A-$H_{1.8}[Bi_{0.2}Sr_{0.8}Na_{1.0}Nb_3O_{10}]$.

Reactions of Alkoxyl-Derivatives of a Layered Perovskite with Alcohols: Substitution Reactions on the Interlayer Surface of a Layered Perovskite

Hiromi Suzuki, Kazuya Notsu, Yosuke Takeda, Wataru Sugimoto,† and Yoshiyuki Sugahara*

Department of Applied Chemistry, School of Science and Engineering, Waseda University, Shinjuku-ku, Tokyo 169-8555 JAPAN

† Current Address: Department of Fine Materials Engineering, Faculty of Textile Science and Technology, Shinshu University, Ueda, Nagano, 386-8567 JAPAN

Abstract

Organic derivatives of a layered perovskite compound, $HLaNb_2O_7 \cdot xH_2O$ (HLN), with interlayer surfaces possessing *n*-alkoxyl groups (*n*-decoxyl and *n*-propoxyl) have been allowed to react with various alcohols and a diol (ethylene glycol) to form new organic derivatives *via* substitution reactions. The reaction of a *n*-propoxyl derivative of HLN with *n*-decanol leads to the formation of *n*-decoxyl groups bound to the interlayer surface of the perovskite-like $[LaNb_2O_7]$ slab. In a similar fashion, the reaction of an *n*-decoxyl derivative of HLN with *sec*-propanol results in the formation of a *sec*-propoxyl derivative. The reaction of the *n*-decoxyl derivative of HLN with *tert*-butanol also proceeds, though the reaction is not completed even after 14 d. After the reaction of the *n*-decoxyl derivative of HLN with ethylene glycol, only one of the two hydroxyl groups in ethylene glycol is reacted, and $-OCH_2CH_2OH$ groups are present on the interlayer surface. Water is required for proceeding the substitution reaction between the *n*-propoxyl derivative of HLN and *n*-decanol, and the reaction mechanism involving hydrolysis of the alkoxyl groups on the interlayer surface and subsequent esterification is proposed.

Keywords: layered perovskite, Dion-Jacobson phase, alcohol-exchange, surface modification, intercalation, hydrolysis, esterification

Introduction

Inorganic-organic hybrids have attracted increasing attention as a new class of materials. Various inorganic layered compounds can accommodate organic ions and molecules in the interlayer space to form intercalation compounds, where inorganic sheets and layers of the organic molecules or ions are interstratified at a molecular level.[1-4] Intercalation compounds are generally prepared *via* ion-exchange reactions and/or adsorption based on interactions with interlayer cations or surfaces. In addition, grafting reactions (alternatively called substitution reactions) of some layered compounds can be utilized to form two-dimensional inorganic-organic hybrids, where organic groups are covalently bound to the surfaces of inorganic layers. For example, layered polysilicates (such as magadiite and kenyaite) can be modified *via* the reaction of their interlayer surfaces, where silanol (SiOH) groups are located, with silylation agents (such as chlorosilanes and alkoxysilanes)[5,6] and alcohols.[7] Similar reactions involving AlOH groups were reported for kaolinite recently.[8,9] FeOCl can also react with various compounds including amines and alcohols.[2,10] Another typical example is zirconium phosphate, which reacts with phosphoric ester ions.[11,12]

Ion-exchangeable layered perovskites ($M_m[A_{n-1}B_nO_{3n+1}]$; M=Rb, K, *etc.*, A=Sr, Ca, La, *etc.*, B=Ti, Nb, Ta, m=1 or 2) consist of perovskite-like slabs (n: thickness of the perovskite-like slab) and interlayer cations, and various cations including proton, alkali-earth metal ions, and divalent cations are successfully intercalated.[13,14] Some of their protonated forms accommodate alkylamines, and intercalated alkylamines form alkylammonium ions in the interlayer space *via* acid-base reactions.[15-23] It is also possible to replace protons with organic cations *via* ion-exchange reactions.[24,25] We have demonstrated that the reaction of a protonated form of a Dion-Jacobson phase (ion-exchangeable layered perovskite with m=1, $HLaNb_2O_7 \cdot xH_2O$) with n-alcohols did not result in simple intercalation,[26] but led to the formation of n-alkoxyl-derivatives, whose interlayer surfaces were covered with alkoxyl groups.[27]

Metal alkoxide chemistry has been investigated for decades, since metal alkoxides are attractive precursors for metal oxides *via* sol-gel process.[28] Among their reactions,

those with alcohols have been studied extensively, since such reactions are utilizable for preparing metal alkoxides possessing various alkoxyl groups;[29]

$$M(OR)_y + z\ R'OH \rightleftharpoons M(OR')_z(OR)_{y-z} + z\ ROH$$

These reactions are called alcohol-exchange (or alcohol-interchange) reactions or alcoholysis reactions, and niobium alkoxides were reported to undergo these reactions.[30-33]

Here, we report substitution reactions of alkoxyl derivatives of the protonated form of the Dion-Jacobson-type layered niobate ($HLaNb_2O_7 \cdot xH_2O$; HLN) with alcohols (*n*-decanol, *sec*-propanol, and *tert*-butanol) and ethylene glycol. The overall reaction resembles the alcohol-exchange reactions of the metal alkoxides. Reaction products were analyzed by X-ray diffraction (XRD), solid-state nuclear magnetic resonance spectroscopy (NMR), differential thermal analysis (DTA), and compositional analyses. The reaction mechanism is discussed by focusing on the role of water in the reaction process.

Experimental

Preparation of $RbLaNb_2O_7$. $RbLaNb_2O_7$ was prepared from a mixture of Rb_2CO_3, La_2O_3, and Nb_2O_5 by calcining at 1100°C for 48 h with intermediate grinding after 24 h.[17] La_2O_3 was calcined at 1100°C for 1 h before use for dehydration. Excess Rb_2CO_3 (30% as Rb) was added to compensate the loss of Rb during calcination. The crude product was washed with distilled water and dried at 120°C. All the X-ray diffraction (XRD) peaks of the washed product can be assigned to $RbLaNb_2O_7$. Inductively-coupled plasma emission spectrometry (ICP) showed that the cation ratio of the washed product corresponded to $RbLaNb_2O_7$. All of these analytical results indicated the successful formation of $RbLaNb_2O_7$.

Preparation of $HLaNb_2O_7 \cdot xH_2O$ (HLN). A protonated form ($HLaNb_2O_7 \cdot xH_2O$; HLN) was prepared by the treatment of $RbLaNb_2O_7$ with 6 M HNO_3 at 60°C for 72 h. The product was centrifuged and washed with distilled water. The product was then dried at ambient temperature, and further drying at 120°C led to the

formation of a single-phase anhydrous phase ($HLaNb_2O_7$). The XRD pattern of the product dried at 120°C showed a tetragonal structure with a = 0.389 nm and c = 1.05 nm, consistent with the previous work (a = 0.394 nm and c = 1.095 nm).[17] ICP analysis revealed that 100 % of Rb were leached during the acid-treatment.

Modification of HLN with *n*-propanol. HLN was modified with *n*-propanol based on the previous report.[27] Typically 2 g of HLN, 35 ml of *n*-propanol, and 5 ml of distilled water were allowed to react in a sealed glass ampoule at 80°C for 3 d. The resultant product was centrifuged and air-dried to obtain a white powder. XRD analysis revealed the increase in the basal spacing to 1.53 nm. The solid-state ^{13}C CP/MAS NMR revealed the presence of three carbon environments (12, 26, 80 ppm) assignable to *n*-propyl groups. A DTA curve of the product exhibited exothermic peaks at >300°C. All of these analytical results indicated the formation of an *n*-propoxyl derivative of HLN (*n*-propoxyl-HLN).

Reaction of *n*-propoxyl-HLN with *n*-decanol. Typically, 2 g of *n*-propoxyl-HLN was reacted with 40 ml of *n*-decanol in a sealed glass ampoule at 80°C for 7 d. After centrifugation, the crude product was washed with acetone and dried at ambient temperature to obtain a white powder. To investigate the effect of water, the reaction was also conducted with a small amount of water; about 0.2 g of *n*-propoxyl-HLN was reacted with 39 ml of *n*-decanol and 1 ml of distilled water (corresponding to 3 mass % of water) in a sealed glass ampoule at 80°C for 1 or 7 d. The same reaction was also conducted under dry conditions; *n*-propoxyl-HLN (0.2 g) previously dried under reduced pressure and decanol (40 mL) distilled over CaH_2 under nitrogen atmosphere were utilized, and they were sealed in a glass ampoule under nitrogen atmosphere.

Reactions with other alcohols. Typically, 1.5 g of the reaction product between *n*-decanol and *n*-propoxyl-HLN was reacted with 30 ml of *sec*-propanol, *tert*-butanol, or ethylene glycol (EG) in a sealed glass ampoule at 80°C for 7 d (*sec*-propanol and EG) or 14 d (*tert*-butanol). After the centrifugation, the crude product was washed with acetone and dried at ambient temperature to obtain a white powder. The reaction

product with EG was further dried at 200°C. The reactions with *sec*-propanol were also conducted using HLN and the *n*-propoxyl-HLN as intermediates in a similar fashion.

Deintercalation reactions of the reaction product between *n*-decanol and *n*-propoxyl-HLN. About 0.1 g of the reaction product between *n*-decanol and *n*-propoxyl-HLN was hydrolyzed with 2 mL of distilled water, 3 M HNO_3, or 3 M KOH for 24 h with stirring. The resultant hydrolyzed product was centrifuged and air-dried. In order to identify organic species formed *via* hydrolysis, the reaction product between *n*-decanol and *n*-propoxyl-HLN was hydrolyzed with an excess of 3 M KOH (prepared using D_2O) for 24 h. Organic species were extracted from 3 M KOH using deuterated benzene (C_6D_6). Similarly, the reaction product between *n*-decanol and *n*-propoxyl-HLN was dispersed in an excess of C_6D_6 overnight. The hydrolysis of the reaction product between EG and *n*-propoxyl-HLN was performed with 3 M KOH (prepared using D_2O) in a similar fashion.

Deintercalation reactions at high temperature. The hydrolysis behavior at 80°C was investigated as follows. About 0.2 g of *n*-propoxyl-HLN or the reaction product between *n*-decanol and *n*-propoxyl-HLN was reacted with 40 mL of distilled water in a sealed glass ampoule at 80°C for 4 d. After centrifugation, the crude product was washed with acetone and dried at ambient temperature. The same reaction was also conducted by using a mixture of 39 mL of 2-pentanone and 1 mL of distilled water. The amounts of distilled water corresponded to 3 mass % of the total liquid (2-pentanone and water).

Analyses. XRD patterns of the products were obtained with a Mac Science $M0^3XHF^{22}$ diffractometer (Mn-filtered Fe $K\alpha$ radiation). Solid-state ^{13}C NMR spectra were recorded on a JEOL NM-GSX400 spectrometer with cross polarization and magic angle spinning techniques (CP/MAS) at 100.40 MHz. Contact time was 2 ms and pulse delay was 5 s. Chemical shifts were all reported with respect to external TMS. Liquid-state ^1H (270.17 MHz) and ^{13}C (61.94 MHz) NMR was performed with a JEOL NM-EX270 spectrometer. Chemical shifts were reported using internal 2,2'-dimethyl-2-silapentane-5-sulfonate (DSS) for aqueous solutions. DTA curves were obtained with

MacScience TG-DTA2000S. The heating rate was 10°C/min and α-Al_2O_3 was utilized as a standard. The amounts of metals were determined by ICP using Nippon Jarrell Ash, ICAP575 Mark II. The amounts of carbon were determined by internal service at Waseda University Materials Characterization Center. The compounds released during the reactions were identified by gas chromatography-mass spectrometry (GC-MS) using a Hewlett-Packard H.P. 5971A instrument.

Results and Discussion

Reaction of the *n*-propoxyl-HLN with *n*-decanol. Figure 1 shows XRD patterns of *n*-propoxyl-HLN and its reaction product with *n*-decanol. The basal spacing calculated from the low-angle XRD peak increases from 1.53 nm to 2.73 nm after the reaction with *n*-decanol. On the contrary, the XRD peak at $2\theta = 28.8°$, the (100) peak of HLN, is present after the reaction with *n*-decanol, indicating the preservation of the structure of the perovskite-like slabs. Takahashi *et al.* prepared an *n*-decoxyl derivative of HLN by the direct reaction between HLN and *n*-decanol, and observed a similar basal spacing.[27]

Figure 1

The DTA curves of *n*-propoxyl-HLN and its reaction product with *n*-decanol are demonstrated in Fig. 2. The DTA curve of *n*-propoxyl-HLN exhibits two exothermic peaks at 342 and 415°C. After the reaction with *n*-decanol, the first peak becomes sharper and shifts to lower temperature (321°C), and the second peak becomes weaker.

Figure 2

Solid-state ^{13}C NMR spectra of *n*-propoxyl-HLN and its reaction product with *n*-decanol are shown in Fig. 3. After the reaction with *n*-decanol, the three signals assignable to *n*-propyl groups disappear and new signals appear at 15, 24, 28, 33 (with a shoulder at lower frequency), and 80 ppm. All of these new signals can be ascribed to *n*-decyl groups. Thus, *n*-propyl groups are removed and *n*-decyl groups are introduced in the reaction product with *n*-decanol.

Figure 3

The amount of *n*-decyl groups is estimated from the carbon content by assuming that all the carbon atoms are present as the decyl groups (Table 1). The estimated value is 0.87 group per [$LaNb_2O_7$] unit. This value is close to the number of propoxyl groups in starting *n*-propoxyl-HLN (0.85).

Table 1

The supernatant liquid was separated after the reaction, and analyzed with GC-MS. In addition to *n*-decanol, *n*-propanol was clearly detected, indicating that *n*-propoxyl groups were released as *n*-propanol molecules.

Deintercalation of the reaction product between *n*-decanol and *n*-propoxyl-HLN. After the C_6D_6 treatment of the reaction product between *n*-decanol and *n*-propoxyl-HLN, no organic species was extracted. Hence, the reaction product between *n*-decanol and *n*-propoxyl-HLN was treated with an excess of water (distilled water, 3 M HNO_3, or 3 M KOH) to remove the guest species from the interlayer space *via* hydrolysis. When distilled water was utilized, the XRD pattern was unchanged, indicating no reaction. A similar result was obtained for the treatment with 3 M HNO_3. On the contrary, the basal spacing decreases to 1.28 nm [close to that of HLN (1.22 nm; hydrated phase)[17]] after the treatment with 3 M KOH (Fig. 1). A DTA curve of the KOH-treated product showed a mass loss up to 100°C (with an endothermic peak), and no exothermic peak was detected. These observations indicate the successful removal of the organic component from the interlayer space after the KOH treatment.

After the hydrolysis with 3 M KOH, organic compounds in 3 M KOH were extracted using C_6D_6, and *n*-decanol was clearly identified by ^1H and ^{13}C NMR. As water-soluble species, only a trace of *n*-propanol was detected by ^1H and ^{13}C NMR.

Guest Species in the reaction product between *n*-decanol and *n*-propoxyl-HLN. The *n*-decyl groups can be present as *n*-decanol intercalated in the interlayer space or *n*-decoxyl groups bound to the surface of the perovskite-like slabs. The removal of *n*-decoxyl groups from the interlayer space should involve hydrolytic bond cleavage, while *n*-decanol intercalated as a molecule is expected to be easily removed by dispersing intercalation compounds in organic solvents. Since no organic

compound was extracted from the reaction product using C_6D_6, the presence of *n*-decanol as an intercalated molecule is very unlikely; the presence of *n*-decoxyl groups is strongly suggested. The presence of *n*-decoxyl groups appears to be further supported by a large downfield shift of its α-carbon signal from the signal position observed for the liquid-state ^{13}C NMR (62.7 ppm), since the methoxyl group signal of a methoxyl derivative of HLN was observed at 69 ppm,[27] which is shifted from the liquid-state ^{13}C NMR signal of methanol (49.3 ppm).[34] A similar large downfield shift of the α-carbon signal was observed for *n*-propoxyl-HLN (63.4 --> 80 ppm). These observations indicate that the product is an *n*-decoxyl derivative of HLN. The *n*-decoxyl derivative of HLN, hereafter labeled as *n*-decoxyl-HLN, was further utilized as an intermediate of the syntheses described below.

Reactions of *n*-decoxyl-HLN with *sec*-propanol and *tert*-butanol. The reactions of *n*-decoxyl-HLN with bulky alcohols have been examined. After the reactions with *sec*-propanol and *tert*-butanol, the basal spacing decreases to 1.54 and 2.00 nm, respectively (Fig. 1). The preservation of the (100) peak position ($2\theta = 28.8°$) indicates that the structure of the perovskite-like slabs is retained after the reactions.

DTA curves of the reaction products with *sec*-propanol and *tert*-butanol exhibit exothermic peaks (Fig. 2); a peak starting from ~270 °C for the product with *sec*-propanol and a peak starting from ~ 190 °C for the product with *tert*-butanol. It should be noted that the DTA curve profiles are changed from that of *n*-decoxyl-HLN after the reactions.

Solid-state ^{13}C CP/MAS NMR spectra of the products treated with *sec*-propanol and *tert*-butanol are shown in Fig. 3. In the spectrum of the product with *sec*-propanol, the signals due to decyl groups disappear, and two signals which can be assigned to *sec*-propyl groups are detected at 27 and 84 ppm. The α-carbon signal (at 84 ppm) shifts considerably from that of *sec*-propanol (63.4 ppm), and similar downfield shifts were observed for methoxyl-HLN[27] and *n*-alkoxyl-HLN (as described above). Thus, it is concluded that *n*-decoxyl groups are exchanged with *sec*-propoxyl groups. Similarly, signals due to *tert*-butyl groups are detected at 26 and 93 ppm in the spectrum

of the product treated with *tert*-butanol. The α-carbon signal (at 93 ppm) also exhibits a considerable downfield shift from that of *tert*-butanol (68.7 ppm), suggesting that organic species are present as *tert*-butoxyl groups. In the spectrum, however, the signals assignable to *n*-decyl groups (marked with asterisks) are also present. Thus, the reaction with *sec*-propanol is essentially completed, while that with bulkier *tert*-butanol is not completed even after 14 d under the present experimental conditions. Based on these observations, we conclude that the bulkiness of the reacting alcohol affects this type of reactions.

The amount of alkoxyl groups is estimated for the product treated with *sec*-propanol, and is determined to be 1.0 per [$LaNb_2O_7$] unit (Table 1). This is slightly larger than that of starting *n*-decoxyl-HLN, but does not exceed the amount of proton in HLN (1.0 per [$LaNb_2O_7$] unit).

Reactions of *n*-decoxyl-HLN with ethylene glycol (EG). The XRD patterns of a reaction product between EG and *n*-decoxyl-HLN are demonstrated in Fig. 1. After the reaction, the basal spacing decreases from that of *n*-decoxyl-HLN (2.73 nm) to 1.58 nm. The basal spacing further decreases to 1.46 nm upon drying at 200°C.

A DTA curve of the air-dried product with EG exhibits an exothermic peak at ~300°C (Fig. 2). It should be noted that the profile of the DTA curve is changed from that of *n*-decoxyl-HLN.

The solid-state ^{13}C CP/MAS NMR spectrum of the product heated at 200 °C exhibits two signals at 64 and 77 ppm (Fig. 3). It is clearly shown that the *n*-decyl groups are removed during the reaction. The guest species were extracted *via* hydrolysis using 3 M KOH, and EG was clearly identified by both ^1H and ^{13}C NMR.

Since the ^{13}C NMR signals of α-carbon atoms in NbOR groups show downfield shifts from those of corresponding alcohols in this study, the 77-ppm signal, which shifts from the chemical shift of liquid EG (63.8 ppm), can be ascribed to the α-carbon (Nb-OCH_2CH_2O-). On the contrary, the solid-state ^{13}C NMR analysis of several organic derivatives of layered compounds prepared by the reactions with EG were reported near that of EG; the derivatives of magadiite,[35] kaolinite,[36,37] and boehmite[38]

exhibited ^{13}C NMR signals in the range of 62-65 ppm. This discrepancy appears to be ascribed to the effect of metal atoms to which alkoxyl groups are bound; actually methoxyl groups in the methoxyl derivative of HLN showed a ^{13}C NMR signal at 69 ppm,[27] while that in the methoxyl derivative of kaolinite showed a signal at 51.1 ppm;[39] Consequently, the 64-ppm signal is ascribed to the carbon atoms attached to hydroxyl groups (Nb-OCH_2CH_2OH).

The amount of C_2H_4 groups is estimated from the carbon content (Table 1). The amount is 0.93 group per [$LaNb_2O_7$] unit, and is close to that of *n*-decoxyl-HLN. Since 0.5 EG per [$LaNb_2O_7$] unit is required by assuming both of the hydroxyl groups in EG molecule are reacted, this value indicates that only one of the two hydroxyl groups in EG molecule is reacted. Similar grafting styles of EG were reported for other derivatives of layered materials.[36,38]

Reaction Processes. To investigate the effect of the intermediates, a direct reaction between HLN and *sec*-propanol was attempted, and no reaction was observed; intermediates should be utilized for the reaction with *sec*-propanol. Furthermore, when *n*-propoxyl-HLN was utilized as an intermediate instead of *n*-decoxyl-HLN, no reaction was observed with *sec*-propanol, indicating that an intermediate with appropriate alkoxyl groups should be selected.

In terms of an NbO_6 octahedron, the present results can be summarized in the following "alcohol-exchange" type equation as an overall reaction;

$$(RO)NbO_5 + R'OH \longrightarrow (R'O)NbO_5 + ROH.$$

Two reaction mechanisms appear to be possible for the observations. One possible mechanism is the nucleophilic attack of alcohol molecules to the $(RO)NbO_5$ site and subsequent release of ROH, which is similar to those for alcohol-exchange reactions of metal alkoxides.[29] The other one is a two-step process, which consists of hydrolysis of the $(RO)NbO_5$ site by water (present in the system as an impurity and produced by water-generating esterification of an unmodified site [$(HO)NbO_5$]) and subsequent esterification of the $(HO)NbO_5$ site with alcohol.

In order to explore the reaction mechanism, the role of water is investigated (Fig.

4). During the reaction of *n*-propoxyl-HLN with *n*-decanol containing 3 mass % of distilled water, the peak due to *n*-propoxyl-HLN (1.53 nm) disappears within 1 d, and the peak due to *n*-decoxyl-HLN (2.73-2.74 nm) develops after 7 d. It should also be noted that the protonated form (HLN) is not detected in the XRD patterns. On the contrary, the reaction of *n*-propoxyl-HLN with *distilled n*-decanol under dry conditions did not lead to the appearance of new peaks, and only the peak due to *n*-propoxyl-HLN is observed at d=1.54 nm even after 7 d. Thus, it is likely that the reaction proceeded *via* a hydrolysis-esterification mechanism.

Figure 4

The hydrolysis behavior was further monitored by heating *n*-decoxyl-HLN or *n*-propoxyl-HLN in distilled water or 2-pentanone containing 3 % of distilled water. As a solvent 2-pentanone was selected, because it dissolves water and bears no hydroxyl groups. When *n*-propoxyl-HLN was heated in distilled water, partial hydrolysis was observed, as shown by the presence of two XRD peaks corresponding to *n*-propoxyl-HLN (1.53 nm) and anhydrous HLN (1.07 nm). On the contrary, *n*-decoxyl-HLN was not hydrolyzed after 4 d. Thus, without base catalysis, the hydrolysis of the *n*-decoxyl groups was very slow even at 80°C, consistent with the hydrolysis behavior at ambient temperature (described in "deintercalation of the reaction product between *n*-decanol and *n*-propoxyl-HLN" section). Since the interlayer space of *n*-decoxyl-HLN is more hydrophobic than that of *n*-propoxyl-HLN, partial hydrolysis occurred only for *n*-propoxyl-HLN. When the water-containing 2-pentanone was utilized, both *n*-propoxyl-HLN and *n*-decoxyl-HLN were hydrolyzed. Interestingly, an opposite tendency was observed; the hydrolysis proceeded to a large extent for *n*-decoxyl-HLN, while the degree of hydrolysis for *n*-propoxyl-HLN was very low. Thus, it is likely that the *n*-alkoxyl groups in the intermediates (*n*-decoxyl-HLN and *n*-propoxyl-HLN) were hydrolyzed by a small amount of water in organic solvents that can dissolve water, such as alcohols and diols.

Based on these observations, the reaction mechanism is proposed as shown in Scheme 1. Initially, the $(RO)NbO_5$ site is hydrolyzed to form the $(HO)NbO_5$ site. The

(HO)NbO_5 site then undergoes the esterification reaction with a reactant alcohol (R'OH) (or ethylene glycol) to form a new modified site, (R'O)NbO_5. For the unmodified (HO)NbO_5 site, which is present initially in the intermediate, the esterification can occur directly, and generated water further reacts with an (RO)NbO_5 site. Since the direct reaction between HLN and *sec*-propanol did not proceed, it is reasonable to assume that the esterification reaction proceeds before collapse of the layers by complete hydrolysis of the *n*-alkoxyl groups in the same interlayer space; the unhydrolyzed site, (RO)NbO_5, expands the interlayer space to make the intercalation of the reactant alcohol or diol molecules possible. The advantage of *n*-decoxyl-HLN over *n*-propoxyl-HLN as an intermediate appears to be ascribed to faster hydrolysis of *n*-decoxyl groups in organic solvents and/or a larger interlayer distance.

Scheme 1

Conclusions

We have demonstrated that the alkoxyl groups bound to the surface of the [$LaNb_2O_7$] slab can be substituted with other alkoxyl groups and HOC_2H_4O groups by heating in the corresponding alcohols (*n*-decanol, *sec*-propanol, *tert*-butanol) and the diol (EG). The reactions are affected by both the kind of *n*-alkoxyl groups in the intermediates and the bulkiness of reactant alcohols. The advantage of this type of reactions is clearly demonstrated by the unsuccessful direct reaction between HLN and *sec*-propanol. Water, which is present as impurity and produced *in situ* by esterification of unmodified site, plays an important role, and the reaction mechanism *via* the hydrolysis of the alkoxyl groups on the surface of the perovskite-like slabs and subsequent esterification is proposed. The present results provide new methodology for modifying the interlayer surface of layered perovskites, and appear to be useful for designing their interlayer spaces *via* chemical modifications.

Acknowledgment. The authors gratefully thank Prof. Kazuyuki Kuroda, Department of Applied Chemistry, Waseda University, for valuable discussion. Experimental assistance by Yohei Kobahashi is also acknowledged. This work was financially supported in part by the Grant-in-Aid for Scientific Research (No. 10555221) from the Ministry of Education, Science, Sports, and Culture, Japan.

References

1) Whittingham, M. S.; Jacobson, A. J. *Intercalation Chemistry*; Academic Press: New York, 1982.

2) Jacobson, A. J. *Intercalation Reactions of Layered Compounds*; Cheetham, A. K. and Day, P., Ed.; Clarendon Press: Oxford, 1992, pp 182.

3) O'Hare, D. *Inorganic Intercalation Compounds*; 2nd edition ed.; Bruce, D. W. and O'Hare, D., Ed.; John Wiley & Sons: Chichester, 1996, pp 171.

4) Ogawa, M.; Kuroda, K. *Bull. Chem. Soc. Jpn.* **1997**, *70*, 2593.

5) Ruiz-Hitzky, E.; Rojo, J. M. *Nature* **1980**, *287*, 28.

6) Ogawa, M.; Okutomo, S.; Kuroda, K. *J. Am. Chem. Soc.* **1998**, *120*, 7361.

7) Mitamura, Y.; Komori, Y.; Hayashi, S.; Sugahara, Y.; Kuroda, K. *Chem. Mater.* **2001**, *13*, 3747.

8) Mercier, L.; Facey, G. A.; Detellier, C. *J. Chem. Soc. Chem. Commun.* **1994**, *1994*, 2111.

9) Komori, Y.; Enoto, H.; Takenawa, R.; Hayashi, S.; Sugahara, Y.; Kuroda, K. *Langmuir* **2000**, *16*, 5506.

10) Kikkawa, S.; Kanamaru, F.; Koizumi, M. *Inorg. Chem.* **1976**, *15*, 2195.

11) Yamanaka, S.; Hattori, M. *Chem. Lett.* **1979**, *1979*, 1073.

12) Alberti, G.; Vivani, R.; Marmottini, F. *J. Porous Mater.* **1998**, *5*, 205.

13) Gopalakrishnan, J. *Rev. Solid State Sci.* **1988**, *1*, 515.

14) Mahler, C. H.; Cushing, B. L.; Lalena, J. N.; Wiley, J. B. *Mater. Res. Bull.* **1998**, *33*, 1581.

15) Jacobson, A. J.; Johnson, J. W.; Lewandowski, J. T. *Inorg. Chem.* **1985**, *24*, 3727.

16) Gopalakrishnan, J.; Bhat, V. *Inorg. Chem.* **1987**, *26*, 4299.

17) Gopalakrishnan, J.; Bhat, V.; Raveau, B. *Mater. Res. Bull.* **1987**, *22*, 413.

18) Jacobson, A. J.; Johnson, J. W.; Lewandowski, J. T. *Mater. Res. Bull.* **1987**, *22*, 45.

19) Mohan-Ram, R. A.; Clearfield, A. *J. Solid State Chem.* **1991**, *94*, 45.

20) Gopalakrishnan, J.; Uma, S.; Bhat, V. *Chem. Mater.* **1993**, *5*, 132.

21) Uma, S.; Raju, A. R.; Gopalakrishnan, J. *J. Mater. Chem.* **1993**, *3*, 709.

22) Nakato, T.; Nakade, M.; Kuroda, K.; Kato, C. *Studies Surf. Sci. Catal.* **1994**, *90*, 285.

23) Zhong, Z.; Ding, W.; Hou, W.; Chen, Y.; Chen, X.; Zhu, Y.; Min, N. *Chem. Mater.* **2001**, *13*, 538.

24) Schaak, R. E.; Mallouk, T. E. *Chem. Mater.* **2000**, *12*, 3427.

25) Han, Y.-S.; Park, I.; Choi, J.-H. *J. Mater. Chem.* **2001**, *11*, 1277.

26) Matsuda, T.; Miyamae, N.; Takeuchi, M. *Bull. Chem. Soc. Jpn.* **1993**, *66*, 1551.

27) Takahashi, S.; Nakato, T.; Hayashi, S.; Sugahara, Y.; Kuroda, K. *Inorg. Chem.* **1995**, *34*, 5065.

28) Brinker, C. J.; Scherer, G. W. *Sol-Gel Science. The Physics and Chemistry of Sol-Gel Processing*; Academic Press: Boston, 1990.

29) Bradley, D. C.; Mehrotra, R. C.; Gaur, D. P. *Metal Alkoxides*; Academic Press: London, 1978.

30) Bradley, D. C.; Chakravarti, B. N.; Wardlaw, W. *J. Chem. Soc.* **1956**, *1956*, 4439.

31) Bradley, D. C.; Chakravarti, B. N.; Chatterjee, A. K.; Wardlaw, W.; Whitley, A. *J. Chem. Soc.* **1958**, *1958*, 99.

32) Mehrotra, R. C.; Kapoor, P. N. *J. Less-Comm. Met.* **1965**, *8*, 419.

33) Kapoor, R. N.; Prakash, S.; Kapoor, P. N. *Z. Anorg. Allg. Chim.* **1967**, *351*, 219.

34) Anderson, M. W.; Klinowski, K. *J. Am. Chem. Soc.* **1990**, *112*, 10.

35) Tunney, J. J.; Detellier, C. *J. Chem. Soc., Chem. Comm.* **1994**, *1994*, 2111.

36) Tunney, J. J.; Detellier, C. *Chem. Mater.* **1993**, *5*, 747.

37) Tunney, J. J.; Detellier, C. *Clays Clay Miner.* **1994**, *42*, 552.

38) Inoue, M.; Kominami, H.; Kondo, Y.; Inui, T. *Chem. Mater.* **1997**, *9*, 1614.

39) Tunney, J. J.; Detellier, C. *J. Mater. Chem.* **1996**, *6*, 1679.

Figure Captions

Figure 1. XRD patterns of (a) $HLaNb_2O_7$ (anhydrous HLN), (b) *n*-propoxyl derivative of HLN (*n*-propoxyl-HLN), (c) *n*-propoxyl-of HLN after the treatment with *n*-decanol (*n*-decoxyl-HLN), (d) *n*-decoxyl-HLN hydrolyzed with 3 M KOH, (e) *n*-decoxyl-HLN treated with *sec*-propanol, (f) *n*-decoxyl-HLN treated with *tert*-butanol, (g) *n*-decoxyl-HLN treated with ethylene glycol (EG), and (h) (g) heated at 200 °C.

Figure 2. DTA curves of (a) $HLaNb_2O_7$ (anhydrous HLN), (b) *n*-propoxyl derivative of HLN (*n*-propoxyl-HLN), (c) *n*-propoxyl-of HLN after the treatment with *n*-decanol (*n*-decoxyl-HLN), (d) *n*-decoxyl-HLN treated with *sec*-propanol, (e) *n*-decoxyl-HLN treated with *tert*-butanol, and (f) *n*-decoxyl-HLN treated with ethylene glycol (EG).

Figure 3. Solid-state ^{13}C CP/MAS NMR spectra of (a) *n*-propoxyl derivative of HLN (*n*-propoxyl-HLN), (b) *n*-propoxyl-HLN after the treatment with *n*-decanol (*n*-decoxyl-HLN), (c) *n*-decoxyl-HLN treated with *sec*-propanol, (d) *n*-decoxyl-HLN treated with *tert*-butanol, and (e) *n*-decoxyl-HLN treated with ethylene glycol (EG).

Figure 4. XRD patterns of (a) *n*-propoxyl-HLN after the treatment with *n*-decanol containing 3 mass % of distilled water for 1 d, (b) *n*-propoxyl-HLN after the treatment with *n*-decanol containing 3 mass % of distilled water for 7 d, (c) *n*-propoxyl-HLN after the treatment with distilled *n*-decanol for 1 d, (d) *n*-propoxyl-HLN after the treatment with distilled *n*-decanol for 7 d.

Scheme 1 Proposed reaction mechanism.

Table 1. Amounts of alkloxyl groups bound to HLN after the treatments with alcohols

Alcohol	Amout of Groups per [$LaNb_2O_7$]
n-propanol*	0.85
n-decanol**	0.87
sec-propanol***	1.0
ethylene glycol***	0.93

*Prepared by the direct reaction with HLN (*n*-propoxyl-HLN).
**Prepared by the reaction with *n*-propoxyl-HLN (*n*-decoxyl-HLN).
***Prepared by the reaction with *n*-decoxyl-HLN.

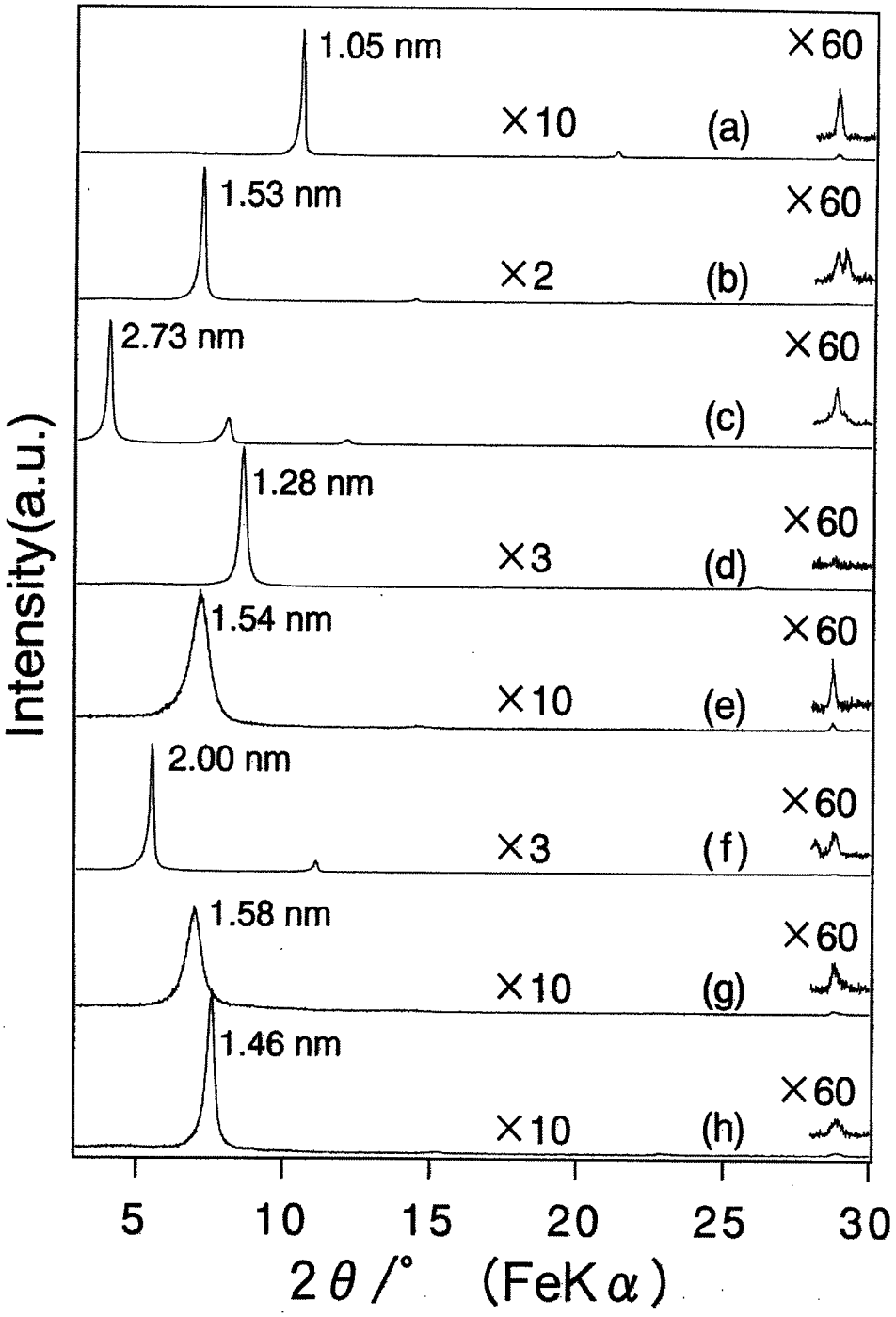

Figure 1. XRD patterns of (a) $HLaNb_2O_7$ (anhydrous HLN), (b) n-propoxyl derivative of HLN (n-propoxyl-HLN), (c) n-propoxyl derivative of HLN after the treatment with n-decanol (n-decoxyl-HLN), (d) n-decoxyl-HLN hydrolyzed with 3 M KOH, (e) n-decoxyl-HLN treated with sec-propanol, (f) n-decoxyl-HLN treated with tert-butanol, (g) n-decoxyl-HLN treated with ethylene glycol (EG), and (h) (g) heated at 200 °C.

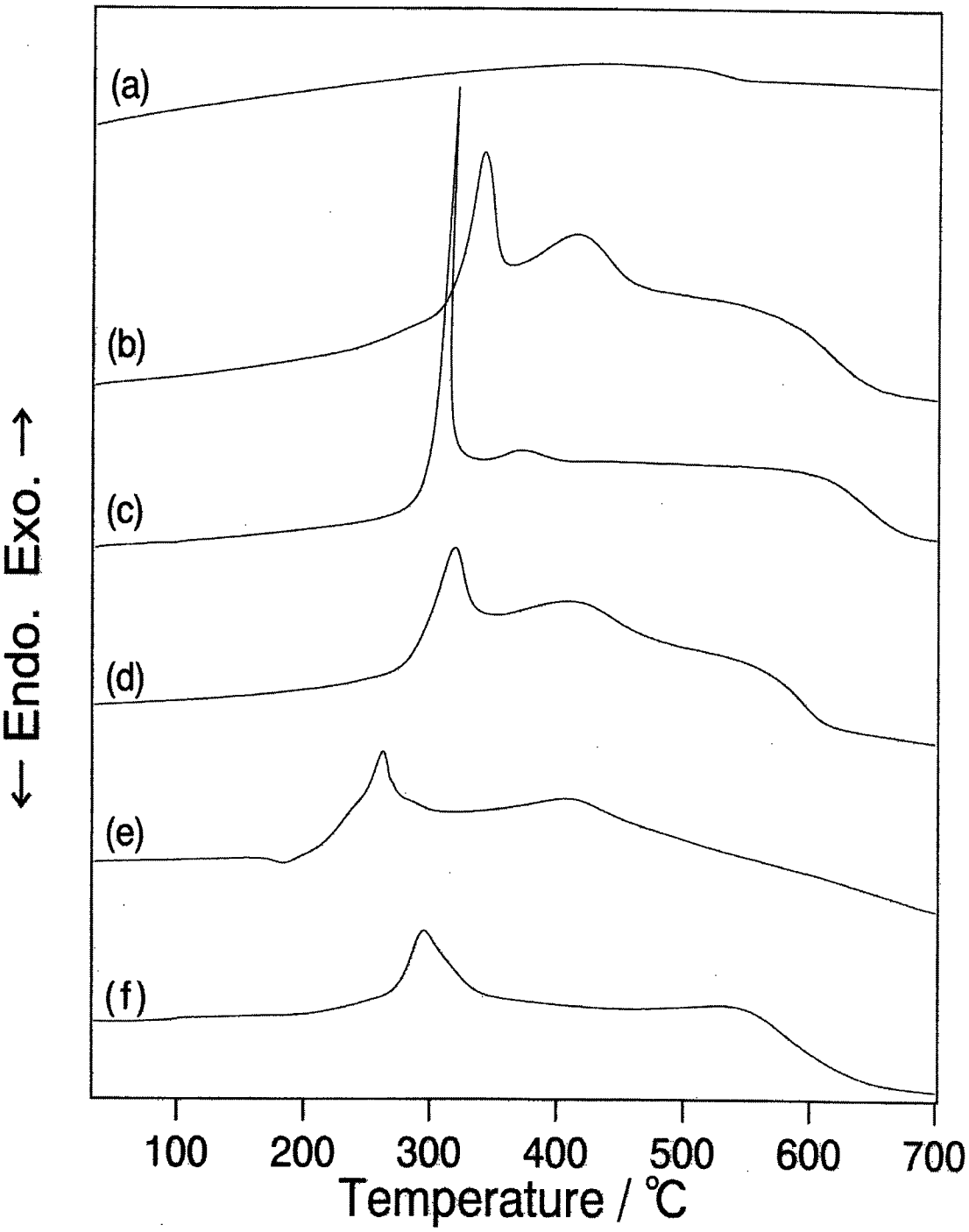

Figure 2. DTA curves of (a) $HLaNb_2O_7$ (anhydrous HLN), (b) n-propoxyl derivative of HLN (n-propoxyl-HLN), (c) n-propoxyl derivative of HLN after the treatment with n-decanol (n-decoxyl-HLN), (d) n-decoxyl-HLN treated with sec-propanol, (e) n-decoxyl-HLN treated with tert-butanol, and (f) n-decoxyl-HLN treated with ethylene glycol (EG).

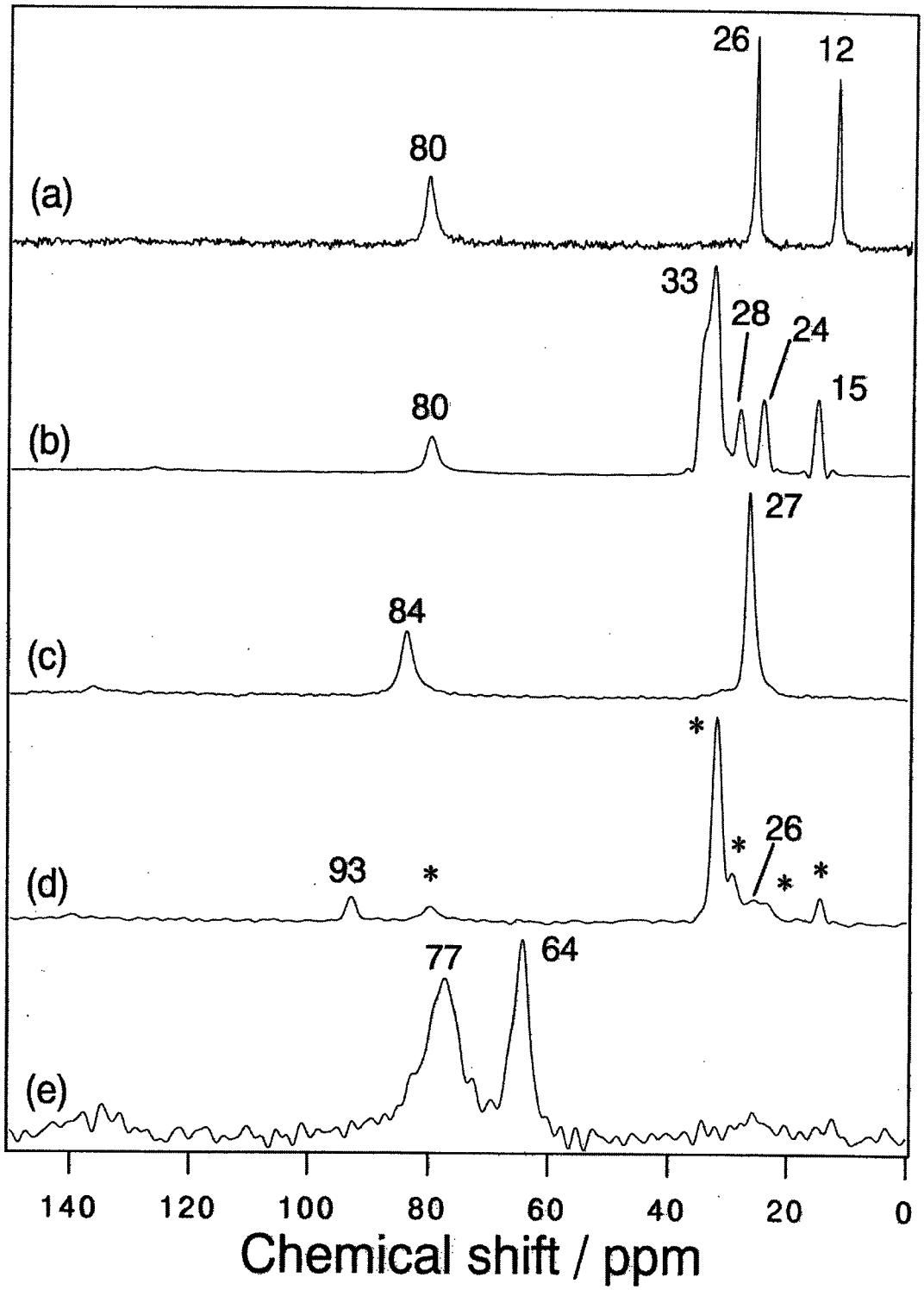

Figure 3. Solid-state ^{13}C CP/MAS NMR spectra of (a) n-propoxyl derivative of HLN (n-propoxyl-HLN), (b) n-propoxyl derivative of HLN after the treatment with n-decanol (n-decoxyl-HLN), (c) n-decoxyl-HLN treated with sec-propanol, (d) n-decoxyl-HLN treated with tert-butanol, and (e) n-decoxyl-HLN treated with ethylene glycol (EG).

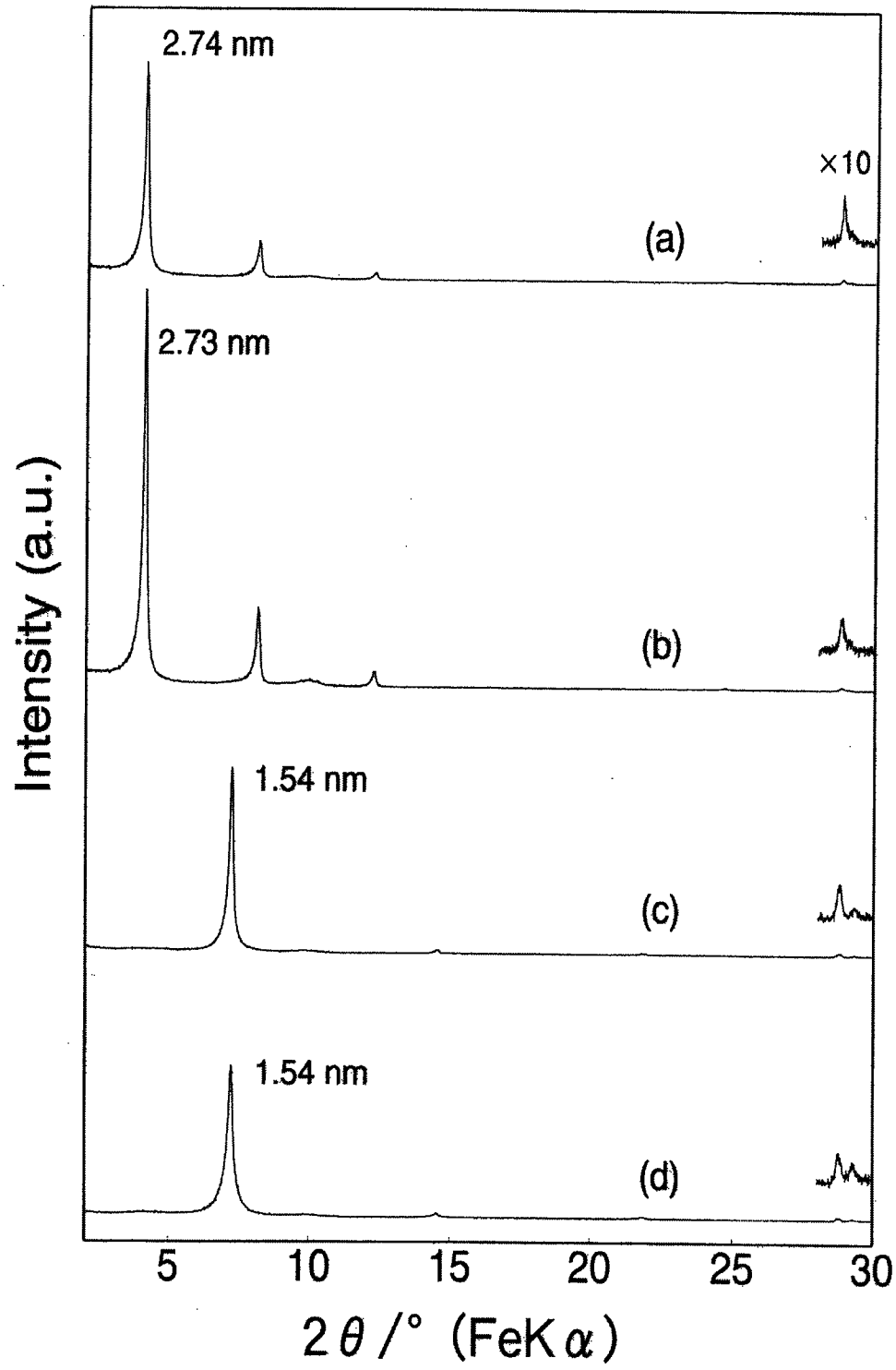

Figure 4. XRD patterns of (a) n-propoxyl-HLN after the treatment with n-decanol containing 3 mass % of distilled water for 1 d,
(b) n-propoxyl-HLN after the treatment with n-decanol containing 3 mass % of distilled water for 7 d,
(c) n-propoxyl-HLN after the treatment with distilled n-decanol for 1 d,
(d) n-propoxyl-HLN after the treatment with distilled n-decanol for 7 d.

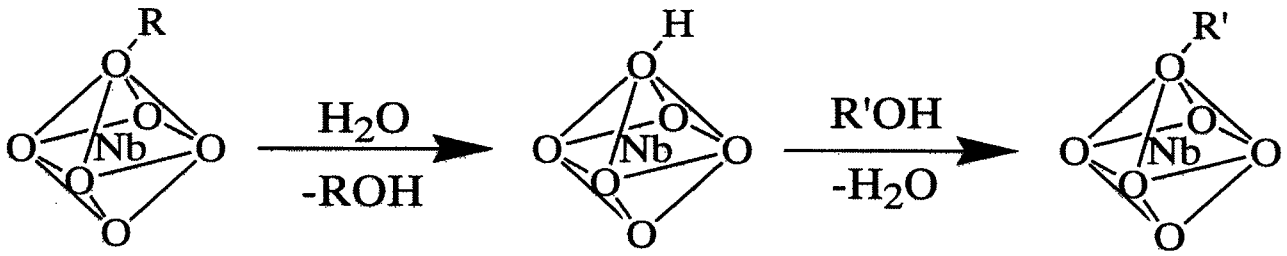

Scheme 1 Proposed reaction mechanism.

Interlayer Surface Modification of a Layered Perovskite, $HLaNb_2O_7 \cdot nH_2O$ with Trifluoroacetate Groups *via* Ligand-exchange-type Reaction between *n*-Alkoxyl-derivative of $HLaNb_2O_7 \cdot nH_2O$ and Trifluoroacetic Acid

Yosuke Takeda, Hiromi Suzuki, Kazuya Notsu, Wataru Sugimoto,§
and Yoshiyuki Sugahara*

Department of Applied Chemistry, School of Science and Engineering,
Waseda University, Shinjuku-ku, Tokyo 169-8555 JAPAN
§Current Address: Department of Fine Materials Engineering, Faculty of Textile Science and Technology, Shinshu University, Ueda, Nagano, 386-8567 JAPAN

Abstract:

Trifluoroacetate groups (CF_3COO; TFA) have been successfully bound to the interlayer surface of a protonated Dion-Jacobson-type layered perovskite, $HLaNb_2O_7 \cdot nH_2O$ (HLN), *via* the reaction between its *n*-propoxyl derivative and trifluoroacetic acid (CF_3COOH; TFAH). The basal spacing increases to ~1.8 nm upon the treatment with TFAH, and varies because of water adsorption in the interlayer space. The high stability of the guest species upon dispersing in organic solvents and the change in IR profile from that of TFAH indicate that the guest species are the TFA groups bound to the surface of perovskite-like slabs of HLN. The TFA groups possess a bilayer arrangement, and an unidentate type of coordination is assumed based on structural consideration. After the treatment of an *n*-decoxyl derivative of HLN with acetic acid, the acetate groups bound to the interlayer surface do not form, and most of the *n*-decoxyl groups are removed. We interpret this observation based on the instability of the acetate groups; the acetate groups are once bound to the surface of the perovskite-like slabs and are then hydrolyzed. On the contrary, the TFA groups are stable against hydrolysis, consistent with water-adsorption property of the TFAH-treated product.

Introduction

It is well known that some layered compounds can accommodate organic ions and molecules in the interlayer space to form intercalation compounds.[1,2] The interactions between organic guests and inorganic hosts range from week ones, such as hydrogen bonding and ion-dipole interactions, to strong ionic bonds. If layered inorganic compounds possess reactive groups on the interlayer surface, it is also possible to bind organic groups *via* covalent bonds through grafting reactions. Typical examples of host compounds are layered polysilicates (magadiite, illerite, kenyaite), where silanol groups (SiOH) are present on the interlayer surface; the silanol groups can react with silylation reagents, such as cholorosilanes and alkoxysilanes to form new siloxane bonds and alcohols to produce alkoxide groups bound directly to silicate layers.[3-5] Other typical examples are kaolinite[6] and FeOCl,[7] where OH groups and OCl groups undergo grafting reactions, respectively.

Ion-exchangeable layered perovskites ($M_xA_{n-1}B_nO_{3n+1}$, ; M=Rb, K, *etc.*, A=Sr, Ca, La, *etc.*, B=Ti, Nb, Ta; x=1: Dion-Jacobson phases, x=2: Ruddlesden-Popper phases) consist of perovskite-like slabs ($[A_{n-1}B_nO_{3n+1}]$, n represents its thickness) and exchangeable cations.[8] They can be easily converted into their protonated forms by acid treatments.[9-15] One of the protonated forms of the layered perovskites, $HLaNb_2O_7 \cdot nH_2O$ (HLN), reacted with *n*-alcohols to form *n*-alkoxyl groups bound on the perovskite-like slabs *via* esterification.[16] Recently, we have reported that these alkoxyl derivatives of HLN reacted with other alcohols to form new alkoxyl groups on the interlayer surface.[17] In terms of an NbO_6 octahedron, this reaction can be expressed as follows;

$$(RO)NbO_5 + R'OH \longrightarrow (R'O)NbO_5 + ROH.$$

It should be noted that this reaction is very similar to alcohol-exchange reactions of metal alkoxides,[18] though the reactions proceed *via* a hydrolysis-esterification mechanism. [17] On the other hand, it is also known that metal alkoxides react with carboxylic acids *via* ligand-exchange reactions; [18]

$$M(OR)_x + yR'COOH \longrightarrow (RO)_{x-y}M(R'COO)_y + y\,ROH.$$

In terms of niobium alkoxides, this type of reaction with acetic acid was reported.[19] Thus, it is expected that *n*-alkoxyl derivatives of HLN can react with carboxylic acids to undergo ligand-exchange-type reactions.

Here we report the reaction between an *n*-propoxyl-derivative of HLN and trifluoroacetic acid (CF_3COOH; TFAH). The structural and spectroscopic characterization is presented to identify guest species and to discuss the structure of the interlayer space. We also report the reaction of *n*-alkoxyl-derivatives of HLN with acetic acid (CH_3COOH; AcOH). The reaction mechanisms are discussed for the reactions with these two carboxylic acids.

Experimental

Preparation of *n*-Propoxyl-derivative of HLN. The preparation of $RbLaNb_2O_7$ and its conversion into $HLaNb_2O_7 \cdot H_2O$ (HLN) were described elsewhere.[17] HLN possessed a tetragonal cell with $a = 0.389$ nm and $c = 1.22$ nm, and drying of HLN at 120°C led to the formation of its anhydrous form ($HLaNb_2O_7$: $a = 0.388$ nm and $c = 1.05$ nm).[12] The composition of metals in HLN was determined by inductively coupled plasma emission spectrometry (ICP, Nippon Jarrell Ash, ICAP-575MK-II) after the dissolution of HLN in a mixture of HNO_3, H_2SO_4, and HF at 200°C for 2 h, and was well consistent with its formula. The amount of hydrogen in dried HLN was determined to be 0.97 per [$LaNb_2O_7$] by thermogravimetry (TG).

The *n*-propoxyl derivative of HLN (*n*-propoxyl-HLN) was prepared by refluxing HLN in an excess of *n*-propanol containing 10 mass % of water for 3 d. The product was centrifuged, washed with acetone, and air-dried. The basal spacing increased to 1.54 nm, consistent with the pervious report. [17] The solid-state ^{13}C NMR revealed the presence of signals at 13, 26, and 81 ppm. The downfield shift of α-carbon signal (81 ppm) from that of *n*-propanol (63.6 ppm) indicated the formation of *n*-propoxyl groups, which were covalently bound to the perovskite-like slabs. [17] The *n*-decoxyl derivative of HLN (*n*-decoxyl-HLN) was prepared by heating a mixture

of about 1 g of *n*-propoxyl HLN and 40 mL of *n*-decanol at 80°C for 7 d in a sealed glass ampoule, as described elsewhere.

Reaction of *n*- Alkoxyl-HLN with Trifluoloacetic Acid or Acetic Acid. Typically 0.5 g of *n*-propoxyl-HLN and 25 g of trifluoloacetic acid (CF_3COOH; TFAH) were sealed in a glass ampoule, and heated at 70°C for 7 d. The product was centrifuged, and dried at 80°C under reduced pressure. The supernatant liquid separated by centrifugation was characterized by ^{13}C NMR. For the reaction with acetic acid (CH_3COOH; AcOH), *n*-propoxyl-HLN and *n*-decoxyl-HLN were used as intermediates. A direct reaction between HLN and TFAH (containing 10 mass % of H_2O) was performed in a similar fashion.

Deintercalation of *n*-Propoxyl-HLN Treated with TFAH. *N*-propoxyl-HLN treated with TFAH was dispersed in an excess of water, benzene, or hexane for 1 d. Then, the solid was removed by centrifugation, and the supernatant liquid was characterized by ^{19}F NMR.

Analyses. XRD patterns were obtained with a MacScience M03XHF[22] diffractometer (Mn filtered Fe K_α radiation). TG-differential thermal analysis (DTA) curves were recorded simultaneously on a MacScience TG-DTA 2000S instrument under dry air flow. The heating rate is 10°C/min, and α-Al_2O_3 was used as a DTA standard. Solid-state ^{13}C MAS NMR spectra were obtained with a JEOL CMX-400 at 100.54 MHz. A 90° pulse was used and repetition time was 30 s. IR spectra were recorded on a Perkin Elmer Spectrum One spectrometer with KBr or Nujol mull technique. Samples were prepared under nitrogen atmosphere if nujol technique was employed. Liquid-state NMR was performed with a JEOL NM-EX270 at 67.94 (^{13}C) and 254.05 (^{19}F) MHz. Water adsorption measurements were performed with a Nippon Bell Belsorp 18 instrument operated at ambient temperature. The samples were heated at 80°C for 5 h before the measurements.

Results

A direct reaction between HLN and TFAH did not led to any change in a XRD pattern, indicating no reactions. Thus, we used *n*-propoxyl-HLN as an intermediate. The XRD pattern of the reaction product between *n*-propoxyl-HLN and TFAH is demonstrated in Figure 1 along with those of HLN and *n*-propoxyl-HLN. The low-angle peak of *n*-propoxyl-HLN becomes broad and shifts to a lower angle. A typical *d* value of the low-angle peak was 1.83 nm, but varied to some extent (*vide infra*). The (100) peak of HLN at $2\theta = 28.8°$ does not shift after the reaction, indicating that the structure of the perovskite-like slabs is preserved during the reaction with TFAH. Thus, the reaction with TFAH changes the interlayer distance without affecting the structure of the perovskite-like slabs. Hereafter, we interpret the low-angle peaks as the peaks expressing basal spacings.

Figure 1

The basal spacing varied in the range from ~1.7 nm to ~1.9 nm among the reaction products. For example, when the basal spacing of a dried TFAH-treated product was measured twice with an interval of 15 min, the basal spacing increased from 1.75 nm to 1.92 nm. A probable reason for the variation in basal spacing is demonstrated by the water adsorption measurements (Fig. 2). Compared with HLN and *n*-propoxyl-HLN, the reaction product adsorbed a much larger amount of water. Thus, the variation in the basal spacing of the reaction product should be ascribed to the intercalation of water. The observations on HLN and *n*-propoxyl-HLN are reasonable; the interlayer space of *n*-propoxyl-HLN should be relatively hydrophobic and only a limited amount of water can be present in the interlayer space of HLN.[12]

Figure 2

The ^{13}C MAS NMR spectra of *n*-propoxyl-HLN and its reaction product with TFAH are shown in Fig. 3. The signals of the *n*-propoxyl groups at 13, 26, and 81 ppm disappear, and new signals appear at 116 and 164 ppm, which are consistent with chemical shifts for TFAH (114.0 and 160.2 ppm) as well as those for the TFA groups bound to titanium in complexes (114.23-115.41, 160.06-163.66).[20]

Figure 3

The IR spectrum of the reaction product between *n*-propoxyl-HLN and TFAH (spectrum with the KBr technique; Fig. 4b) exhibits no $\nu_{(CH)}$ and $\delta_{(CH)}$ bands that are clearly detected in the spectrum of the *n*-propoxyl- HLN (Fig. 4a; $\nu_{(CH)}$, 2853, 2875, 2920, 2937, 2965, and 2973 cm^{-1}; $\delta_{(CH)}$ 1457 cm^{-1}), consistent with the loss of the *n*-propoxyl groups shown by ^{13}C MAS NMR results.[21-23] Instead, new bands appear at 1000-1200 (br), 1450, 1667, and 3000-3500 (br) cm^{-1} (Fig. 4b). The broad band at 3000-3500 cm^{-1} should be ascribed to a $\nu_{(OH)}$ band of adsorbed water, since this band disappears in the spectrum of the dried product measured with the nujol technique to prevent the exposure to air (Fig. 4c). The new band at 1000-1200 cm^{-1} can be assigned to $\nu_{(CF)}$ mode.[21-23] The bands at 1450 and 1667 cm^{-1} are shifted considerably from those of TFAH ($\nu_{(CO)}$, 1463 cm^{-1}; $\nu_{(C=O)}$, 1784 cm^{-1}; Fig. 4d). It should be noted that the band at 1667 cm^{-1} can be overlapped with the $\delta_{(OH)}$ band of water in the spectrum with the KBr technique, so that the precise band position is determined in the spectrum with the Nujol-mull technique to be 1664 cm^{-1} (Fig. 4c).

Figure 4

The DTA curves of *n*-propoxyl-HLN and its reaction product with TFAH are exhibited in Fig. 5. The profile drastically changes after the reaction with TFAH; the exothermic peak of *n*-propoxyl-HLN shifts to lower temperature (~240°C), being consistent with spectroscopic results showing the variation in organic components.

Figure 5

The released species after the treatment of *n*-propoxyl-HLN with TFAH was identified by liquid-state ^{13}C NMR. Signals at 10.1 (s), 22.3 (s), 72.0 (s), 115.3 (q) and 163.4 (q) ppm were observed, and were ascribed to CF_3COOPr^n, that should form *via* esterification between TFAH and Pr^nOH.

The stability of the reaction product between *n*-propoxyl-HLN and TFAH is demonstrated by dispersing in an absolute amount of a solvent. If the reaction product is dispersed in benzene or hexane, the basal spacing is similar to that before the extraction, indicating no deintercalation reaction. On the contrary, the basal spacing

decreases to 1.23 nm, when the reaction product is treated with water. The basal spacing of 1.23 nm is consistent with that of HLN (hydrated phase). IR analysis of the residue revealed that no organic species was present in the residue, and correspondingly TFAH was clearly identified in a supernatant liquid by ^{19}F NMR.

The reactions with AcOH (CH_3COOH) were conducted using two intermediates. When *n*-propoxyl-HLN was treated with AcOH, no reaction was observed under the present experimental conditions. On the other hand, the reaction of *n*-decoxyl-HLN with AcOH led to the decrease in the basal spacing (2.73 → 1.14 nm). IR analysis exhibited that no AcOH molecules or AcO groups (CH_3COO) were present in the product treated with AcOH. The amount of carbon considerably decreased; based on the TG curve, remaining *n*-decoxyl groups were estimated to be 0.07 groups per [$LaNb_2O_7$], which was significantly lower than that of *n*-decoxyl-HLN (0.71).

Discussion

Identification of Guest Species in the TFAH-treated Product. The presence of TFAH (CF_3COOH) or its related species in the interlayer space is indicated by the fact that TFAH is identified after the deintercalation by water. The stability of the guest species in the organic solvents (hexane and benzene) indicates that the guest spices are strongly bound in the interlayer space (Fig. 1). This is supported by the relatively-high decomposition temperature without thermal deintercalation (Fig. 5). Furthermore, the IR profile of the reaction product between *n*-propoxyl-HLN and TFAH in the range from ~1400 to ~1700 cm^{-1} is very different from that of the TFAH molecule (Fig. 4). Thus, the presence of TFAH molecules in the interlayer space is very unlikely, and we conclude that the TFA groups (CF_3COO) are directly bound to the perovskite-like slabs to form CF_3COO-Nb bonds. On the basis of this interpretation, the IR bands at 1450 and 1664 cm^{-1} can be assigned to the $\nu_{s(COO)}$ and $\nu_{as(COO)}$ modes of the TFA groups (*vide infra*).[24]

Structure of TFAH-treated Product. The TFA groups should be present on the interlayer surface, as indicated by the increase in the basal spacing. Thus, the apical

oxygen atoms in the NbO_6 octahedra actually form CF_3COO groups. The basal spacing of the dried TFAH-treated product is around 1.7 nm, while that of anhydrous HLN is 1.05 nm; gallery height is thus ~ 0.7 nm. Since the maximum size of the TFA group is ~ 0.37 nm, the TFA groups appear to form bilayer arrangement in the interlayer space. The intercalation of water into the interlayer space of the TFAH-treated product upon exposure to air is ascribed to the presence of hydrophilic COO groups and the relatively high stability of the TFA groups against hydrolysis (*vide infra*).

Three types of coordination are known for carboxylate groups [including TFA and AcO groups (CH_3COO)]; unidentate-type, bidentate-type, and bridging-type. [24] In the perovskite-like slabs of HLN, Nb atom is coordinated by six oxygen atoms. Thus, bidentate state of the TFA groups is very unlikely because seven-coordinated Nb atom should be present. Bridging state is also unlikely because of the relatively long Nb-Nb distance (the shortest distance corresponds to the *a* parameter of HLN; 0.389 nm) and the requirement of seven-coordinated Nb atoms caused by additional coordination of the C=O group to the neighboring Nb atom; thus only unidentate-type coordination is probable.

The coordination type is frequently discussed on the basis of IR spectra. [24] In terms of TFA groups and the AcO groups in complexes, a separation between a $\nu_{s(COO)}$ band and a $\nu_{as(COO)}$ band ($\Delta\nu$) is indicative of the type of coordination. If the observed $\Delta\nu$ is much larger than those of ionic compounds, the type of coordination is unidentate. If the observed $\Delta\nu$ is much smaller than those of ionic compounds, bidentate or bridging type is indicated. In the present results, the observed $\Delta\nu$ is 214 cm^{-1}, which is slightly larger than that of the TFA groups in ionic NH_4(TFA) (202 cm^{-1}); the observed $\Delta\nu$ does not support the presence of unidentate TFA groups. A recent papers on the AcO groups on the surface of MgO, however, claimed the exception; though $\Delta\nu$ values are ~120-130 cm^{-1} and those of ionic compounds are in the range of 140-160 cm^{-1}, the IR measurement with polarized light evidenced the presence of unidentate AcO groups.[25] Thus, it is probable that the unidentate TFA groups on

the surface of the perovskite-like slabs show smaller $\Delta\nu$ values than those in complexes (264-372 cm^{-1}).[26]

Reaction Mechanism. The release of *n*-propanol (detected as CF_3COOPr^n) indicates that the overall reaction (in terms of an NbO_6 octahedron) should be expressed as follows;

$$(Pr^nO)NbO_5 + CF_3COOH \text{ ----› } (CF_3COO)NbO_5 + Pr^nOH.$$

In the presence of an excess of TFAH, the reaction is considered to be initiated by the protonation of an NbO_6 octahedron. Only an apical oxygen atom forming the $NbOPr^n$ group can accept proton in a $(Pr^nO)NbO_5$ site, since the other oxygen atoms are involved in forming corner-sharing NbO_6 network. If TFA anion subsequently attacks to the protonated $(Pr^nO)NbO_5$ site [$(Pr^n(H)O)NbO_5$], a $(CF_3COO)NbO_5$ site should be directly formed with a release of ROH (Scheme 1, path a). In addition, since water should be present as an impurity or form *in situ* by the reaction between TFAH and *n*-propanol, another pathway involving hydrolysis can be possible (Scheme 1, path b). The hydrolysis of the $(Pr^nO)NbO_5$ site gives a $(HO)NbO_5$ site, which can be further protonated. A subsequent attack by the TFA anion leads to the formation of the $(CF_3COO)NbO_5$ site. The hydrolysis of the $(Pr^nO)NbO_5$ site did not proceed at room temperature even under acidic conditions, but it proceeded to some extent at high temperature without catalysts.[17] Furthermore, the presence of organic solvents that dissolve water promoted hydrolysis. Thus, the second path is also probable in the present system. The reaction between the protonated $(HO)NbO_5$ site [$(H_2O)NbO_5$] and the TFA anion should also be considered for an unmodified $(HO)NbO_5$ site, which is initially present.

Scheme 1

In spite of successful modification using TFAH, the reactions of *n*-alkoxyl derivatives with AcOH (CH_3COOH) give different results. AcOH does not react with *n*-propoxyl-HLN, and the reaction between AcOH and *n*-decoxyl-HLN leads only to the loss of the *n*-decoxyl groups. Since TFAH is much stronger acid than AcOH (AcOH, pK_a=4.75; TFAH, pK_a=0.23), the presence of a much smaller amount of

protons may explain the lack of reaction between *n*-propoxyl-HLN and AcOH. On the other hand, the loss of the *n*-decoxyl groups instead of CH_3COO-Nb (AcO-Nb) formation upon AcOH treatment appears to be ascribed to the difference in hydrolysis behavior. It is likely that the hydrolysis under acidic conditions is initiated by the protonation at a carbonyl oxygen atom. Then the subsequent attack of water and the migration of H^+ cause the release of R'COOH and H_3O^+ to give the $(HO)NbO_5$ site (Scheme 2). Since the hydrolysis behavior of esters generally depends on the steric factor, the bulkiness of the CF_3 groups is expected to reduce the hydrolysis rate with the presence of limited amount of water. Thus, CF_3COONb groups are clearly detected in the final product. On the contrary, the hydrolysis of the CH_3COONb groups is more facile because of the size of the CH_3 groups. Thus, the CH_3COONb groups once form through the path shown in Scheme 1, and are subsequently hydrolyzed to give the $(HO)NbO_5$ site. This is consistent with the uptake of water by the TFAH-treated product without collapsing *via* hydrolysis.

Scheme 2

Conclusions

We have demonstrated that the surface of perovskite-like slabs of HLN ($HLaNb_2O_7 \cdot nH_2O$) can be modified with the TFA (CF_3COO) groups *via* the treatment of *n*-propoxyl-HLN with TFAH (CF_3COOH). The stability of the guest species and IR profile analysis indicate that the TFA groups are covalently attached to niobium. The TFA groups form bilayers in the interlayer space, and the type of coordination appears to be unidentate. The reaction could proceed *via* 1) the direct reaction of the TFA groups with a protonated $(Pr^nO)NbO_5$ site and/or 2) the hydrolysis of the $(Pr^nO)NbO_5$ site and subsequent attack of the protonated $(Pr^nO)NbO_5$ site by the TFA ions. The reaction between *n*-decoxyl-HLN and AcOH (CH_3COOH) results in the loss of the *n*-decoxyl groups only. The unsuccessful modification using AcOH is ascribed to the instability of the CH_3COO-Nb groups against hydrolysis; the CH_3COO-Nb groups once form, and are subsequently hydrolyzed. The stability of

the TFA groups against hydrolysis is consistent with water-absorbing property of the TFA-treated product. The present results provide an additional method for the modification of the interlayer surface of layered perovskites to design the interlayer space with various functional groups.

Acknowledgments. The authors gratefully thank Prof. Kazuyuki Kuroda, Department of Applied Chemistry, Waseda University, for valuable discussion. This work was financially supported in part by the Grant-in-Aid for Scientific Research (No. 10555221) from the Ministry of Education, Science, Sports, and Culture, Japan.

Refernces

(1) Jacobson, A. J. In *Solid State Chemistry: Compounds*; Cheetham, A. K., Day, P., Eds.; Clarendon Press: Oxford, 1992, pp 182-233.

(2) O'Hare, D. In *Inorganic Materials*; 2nd edition ed.; Bruce, D. W., O'Hare, D., Eds.; John Wiley & Sons: Chichester, 1996, pp 171-254.

(3) Ruiz-Hitzky, E.; Rojo, J. M. *Nature* **1980**, *287*, 28.

(4) Ogawa, M.; Okutomo, S.; Kuroda, K. *J. Am. Chem. Soc.* **1998**, *120*, 7361.

(5) Mitamura, Y.; Komori, Y.; Hayashi, S.; Sugahara, Y.; Kuroda, K. *Chem. Mater.* **2001**, *13*, 3747.

(6) Tunney, J. J.; Detellier, C. *Chem. Mater.* **1993**, *5*, 747.

(7) Kikkawa, S.; Kanamaru, F.; Koizumi, M. *Inorg. Chem.* **1976**, *15*, 2195.

(8) Gopalakrishnan, J. *Rev. Solid State Sci.* **1988**, *1*, 515.

(9) Jacobson, A. J.; Johnson, J. W.; Lewandowski, J. T. *Inorg. Chem.* **1985**, *24*, 3727.

(10) Jacobson, A. J.; Lewandowski, J. T.; Johnson, J. W. *J. Less-Common Met.* **1986**, *116*, 137.

(11) Gopalakrishnan, J.; Bhat, V. *Inorg. Chem.* **1987**, *26*, 4299.

(12) Gopalakrishnan, J.; Bhat, V.; Raveau, B. *Mater. Res. Bull.* **1987**, *22*, 413.

(13) Richard, M.; Brohan, L.; Tournoux, M. *J. Solid State Chem.* **1994**, *112*, 345.

(14) Byeon, S.-H.; Yoon, J.-J.; Lee, S.-O. *J. Solid State Chem.* **1996**, *127*, 119.

(15) Schaak, R. E.; Mallouk, T. E. *J. Solid State Chem.* **2000**, *155*, 46.

(16) Takahashi, S.; Nakato, T.; Hayashi, S.; Sugahara, Y.; Kuroda, K. *Inorg. Chem.* **1995**, *34*, 5065.

(17) Suzuki, H.; Notsu, K.; Takeda, Y.; Sugimoto, W.; Sugahara, Y. *Chem. Mater.* submitted.

(18) Bradley, D. C.; Mehrotra, R. C.; Gaur, D. P. *Metal Alkoxides*; Academic Press: London, 1978.

(19) Griesmar, P.; Papin, G.; Sahchez, C.; Livage, J. *Chem. Mater* **1991**, *3*, 335-339.

(20) Gibson, D. H.; Ding, Y.; Miller, R. L.; Sleadd, D. A.; Mashuta, M. S.; Richardson, J. F. *Polyhedron* **1999**, *18*, 1189.

(21) Redington, R. L.; Lin, K. C. *Spectrochim. Acta* **1971**, *27A*, 2445.

(22) Fuson, N.; Josien, M.-L.; Johns, E. A. *J. Chem. Phys.* **1952**, *20*, 1627.

(23) Erin, A. V.; Prozorovskaya, Z. N.; Yaroslavtsev, A. B. *Russ. J. Inorg. Chem.* **1993**, *38*, 618.

(24) Deacon, G. B.; Phillips, R. J. *Coord. Chem. Rev.* **1980**, *33*, 227.

(25) Xu, C.; Koel, B. E. *J. Chem. Phys* **1995**, *102*, 8158.

(26) Pei, Z.-F.; Ponec, V. *Appl. Surf. Sci.* **1996**, *103*, 171.

Figure Captions

Figure 1 XRD patterns of (a) $HLaNb_2O_7$ (anhydrous HLN), (b) *n*-propoxyl-HLN, and (c) the reaction product between *n*-propoxyl-HLN and TFAH.

Figure 2 Water-adsorption isotherms of $HLaNb_2O_7$ (anhydrous HLN; ○), (b) *n*-propoxyl-HLN (△), and (c) the reaction product between *n*-propoxyl-HLN and TFAH (□).

Figure 3 Solid-state MAS ^{13}C NMR of (a) *n*-propoxyl-HLN and (b) the reaction product between *n*-propoxyl-HLN and TFAH. A peak with asterisk is ascribed to materials in the probe.

Figure 4 IR spectra of (a) *n*-propoxyl-HLN, (b) the reaction product between *n*-propoxyl-HLN and TFAH (KBr method), (c) the reaction product between *n*-propoxyl-HLN and TFAH (Nujol-mull method), and (d) TFAH.

Figure 5 DTA curves of (a) $HLaNb_2O_7$ (anhydrous HLN), (b) *n*-propoxyl-HLN, and (c) the reaction product between *n*-propoxyl-HLN and TFAH.

Scheme 1 Proposed reaction mechanism for the reaction between *n*-propoxyl-HLN and TFAH.

Scheme 2 Proposed reaction mechanism for the hydrolysis of RCOO-Nb groups.

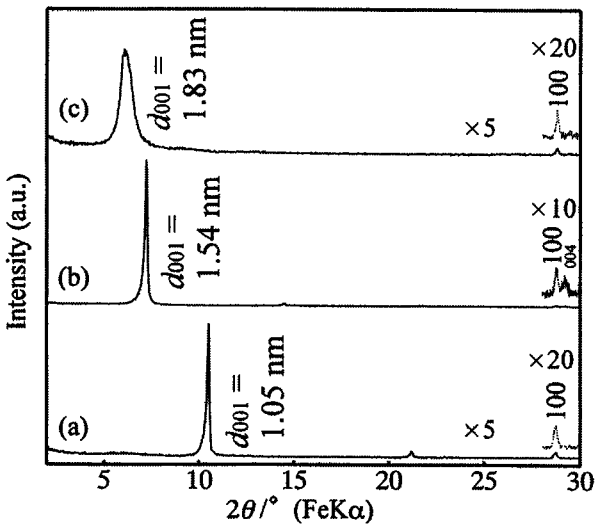

Figure 1 XRD patterns of (a) $HLaNb_2O_7$ (anhydrous HLN), (b) n-propoxyl-HLN, and (c) the reaction product between n-propoxyl-HLN and TFAH.

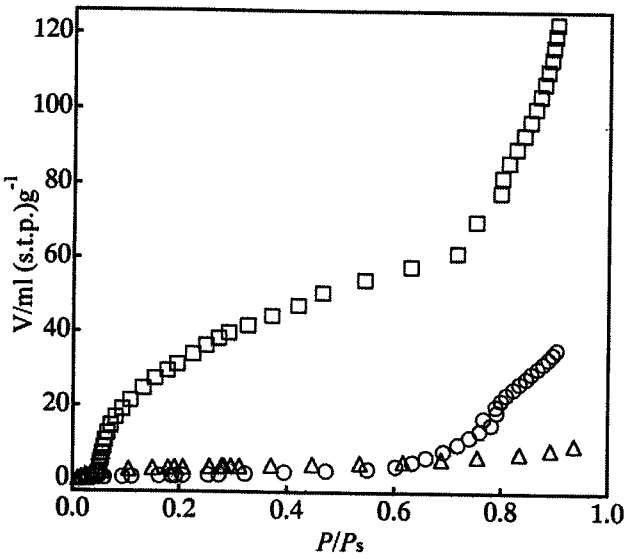

Figure 2 Water-adsorption isotherms of $HLaNb_2O_7$ (anhydrous HLN;○), (b) n-propoxyl-HLN (△Z14), and
(c) the reaction product between n-propoxyl-HLN and TFAH (□).

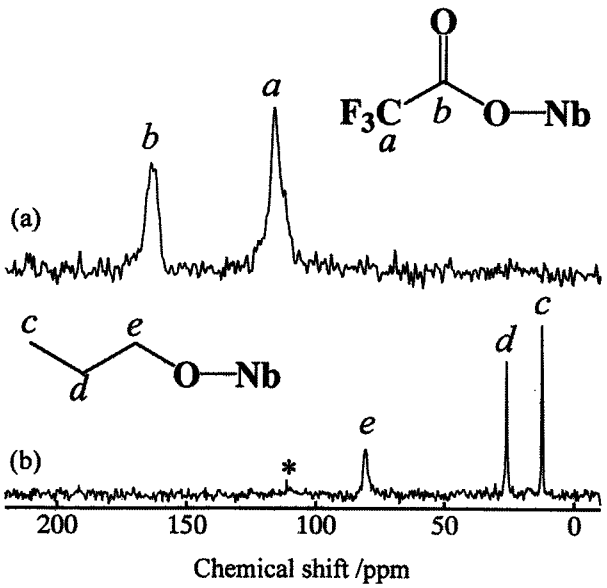

Figure 3 Solid-state MAS ^{13}C NMR of (a) n-propoxyl-HLN and (b) the reaction product between n-propoxyl-HLN and TFAH. A peak with asterisk is ascribed to materials in the probe.

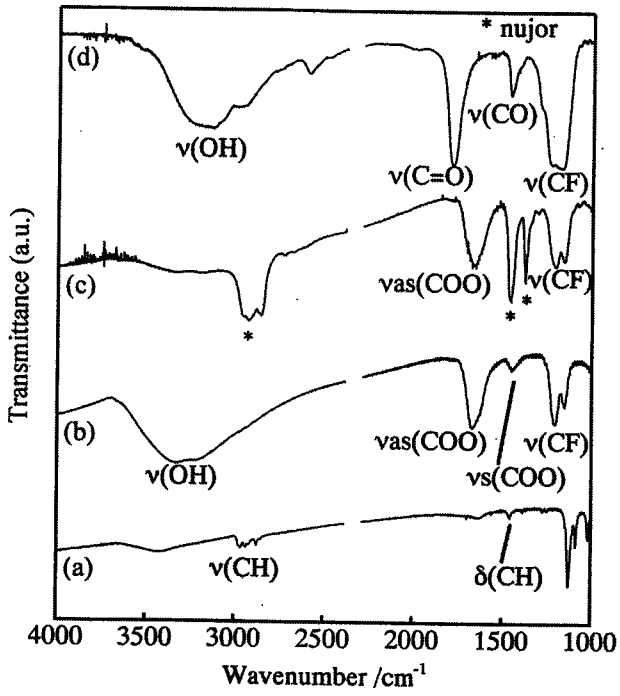

Figure 4 IR spectra of (a) n-propoxyl-HLN,
(b) the reaction product between n-propoxyl-HLN and TFAH (KBr method),
(c) the reaction product between n-propoxyl-HLN and TFAH (Nujol-mull method),
and (d) TFAH.

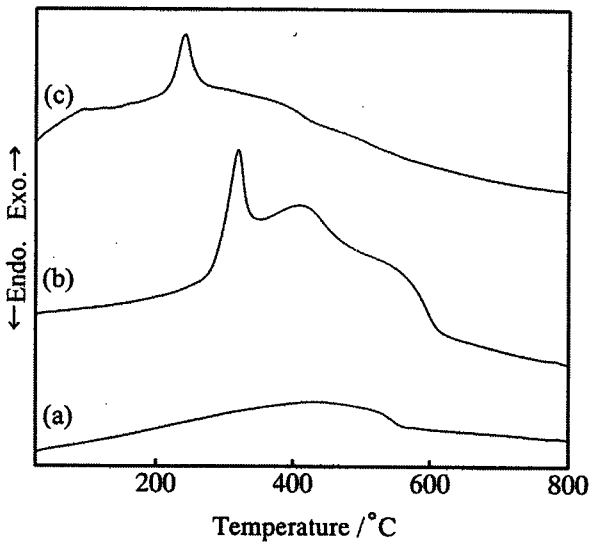

Figure 5 DTA curves of (a) $HLaNb_2O_7$ (anhydrous HLN),
(b) n-propoxyl-HLN, and
(c) the reaction product between n-propoxyl-HLN and TFAH.

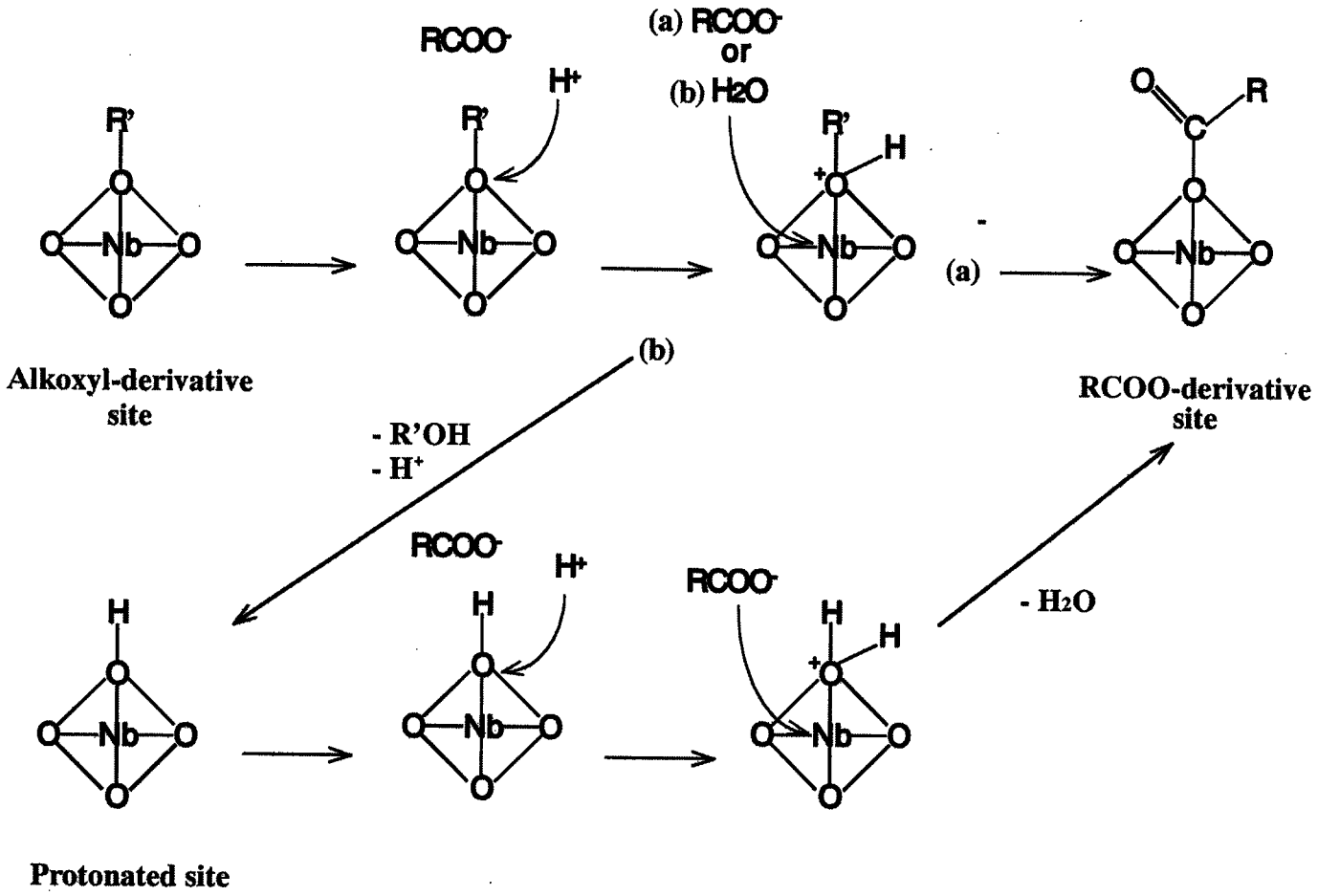

Scheme 1 Proposed reaction mechanism for the reaction between *n*-propoxyl-HLN and TFAH.

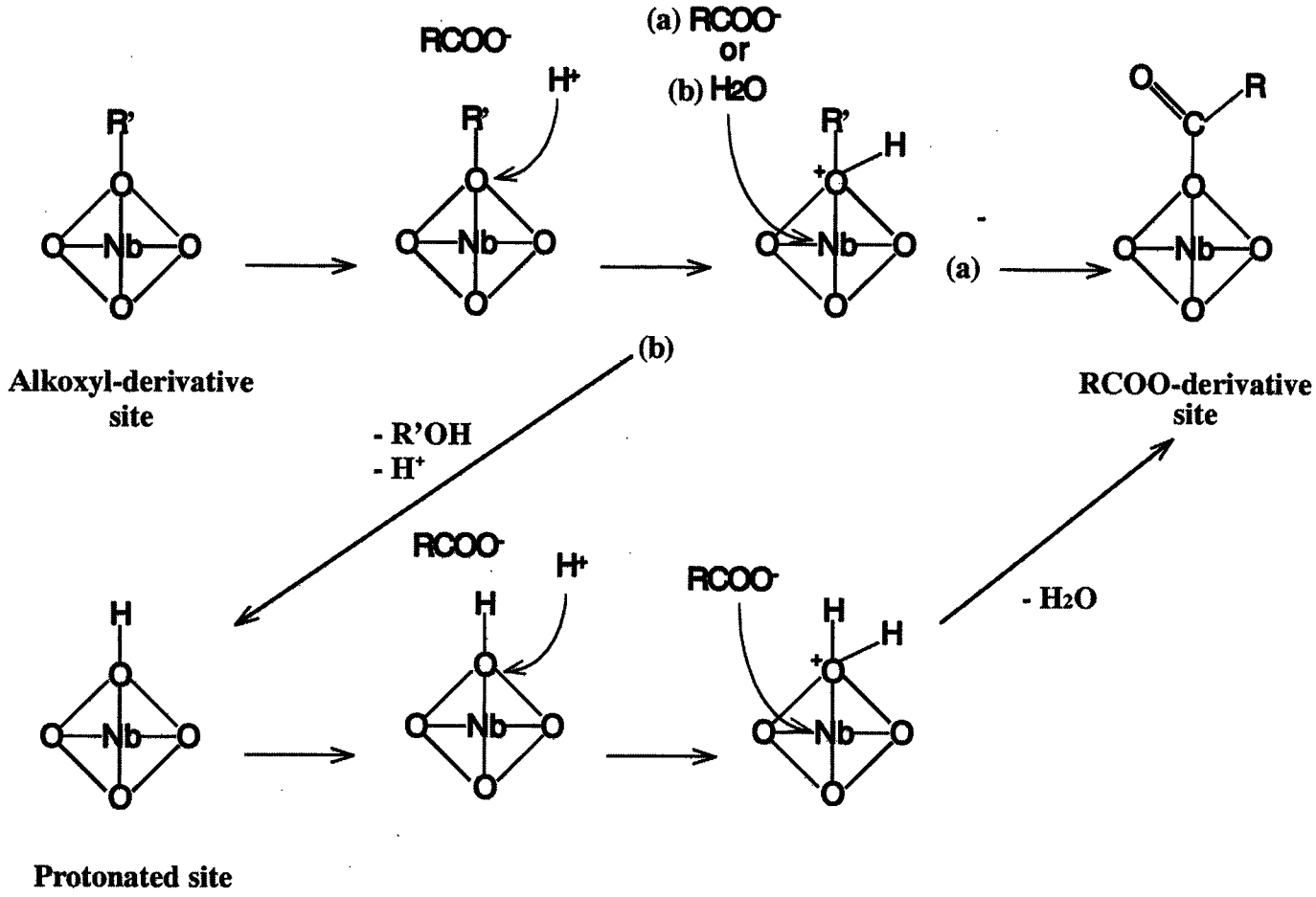

Scheme 1 Proposed reaction mechanism for the reaction between *n*-propoxyl-HLN and TFAH.

Intercalation Behavior of *n*-Alkylamines into a Protonated Form of a Layered Perovskite Derived from Aurivillius Phase $Bi_2SrTa_2O_9$

Yu Tsunoda, Wataru Sugimoto,† and Yoshiyuki Sugahara*

Department of Applied Chemistry, School of Science and Engineering, Waseda University, Shinjuku-ku, Tokyo 169-8555 JAPAN
†Current Address: Department of Fine Materials Engineering, Faculty of Textile Science and Technology, Shinshu University, Ueda, Nagano, 386-8567 JAPAN

Abstract:

Intercalation behavior of *n*-alkylamines into a protonated form of a layered perovskite $H_{1.8}[Sr_{0.8}Bi_{0.2}Ta_2O_7]$ derived from an Aurivillius phase, $Bi_2SrTa_2O_9$, has been investigated. $H_{1.8}[Sr_{0.8}Bi_{0.2}Ta_2O_7]$ can accommodate *n*-alkylamines ($C_mH_{m+1}NH_2$; m=4, 8, 12, 18) to form intercalation compounds *via* an acid-base mechanism. The basal spacing increases to 2.12 (m=4), 2.88 (m=8), 3.99 (m=12), and 5.22 (m=18) nm. On the contrary, $H_{1.8}[Sr_{0.8}Bi_{0.2}Ta_2O_7]$ does not form any intercalation compound with pyridine, which is a weak base, indicating that the protons in $H_{1.8}[Sr_{0.8}Bi_{0.2}Ta_2O_7]$ are weakly acidic. The IR spectra of the intercalation compounds with *n*-alkylamines (m=12 and 18) clearly show that *n*-alkyl chains possess an all-trans conformation. A linear relationship is observed between the basal spacing and the number of carbon atoms in *n*-alkyl chains, and this corresponds to a bilayer arrangement of the *n*-alkyl chains with a tilt angle of 65°. In spite of the relatively high proton content (1.8 H^+ per $[Sr_{0.8}Bi_{0.2}Ta_2O_7]$), only 0.9-1.0 mol of *n*-alkylamines per $[Sr_{0.8}Bi_{0.2}Ta_2O_7]$ is intercalated. This observation can be reasonably interpreted based on the surface geometry of the perovskite-like slab and the size of *n*-alkylamines.

Keywords: intercalation, layered perovskite, Aurivillius phases, protonated form, acid-base reaction, *n*-alkylamine

Introduction

It is well known that various layered compounds accommodate organic ions and molecules to form intercalation compounds.[1-3] The reaction mechanisms include ion-exchange, ion-dipole interaction, hydrogen-bonding, redox reactions, and acid-base reactions. The acid-base reactions are involved in intercalation chemistry for protonated forms of various layered transition metal oxides,[4] such as layered titanates,[5] titanoniobate,[6,7] and niobates.[8]

Ion-exchangeable layered perovskites consist of perovskite-like slabs terminated along the <100> plane of 3D perovskites and interlayer cations. These are classified into two groups, Dion-Jacobson phases ($M[A_{n-1}B_nO_{3n+1}]$) and Ruddlesden-Popper phases ($M_2[A_{n-1}B_nO_{3n+1}]$).[9-12] Both of these phases can be converted into their protonated forms ($H[A_{n-1}B_nO_{3n+1}]$ and $H_2[A_{n-1}B_nO_{3n+1}]$) by acid treatment.[10,13-18] The protonated forms of the Dion-Jacobson phases can accommodate *n*-alkylamine in their interlayer spaces *via* the acid-base mechanism.[10,14,15,19-24] On the contrary, a protonated form of a Ruddlesden-Popper phase, $H_2La_2Ti_3O_{10}$, did not accommodate *n*-alkylamines.[22] This difference was ascribed to the displacement in layer stacking by $(a+b)/2$ in $H_2La_2Ti_3O_{10}$. Schaak *et al.*[25] recently reported the partial intercalation of *n*-dodecylamine into $H_2CaNaTa_3O_{10}$ in heptane, and to the best of our knowledge this is the only report on the intercalation behavior of the protonated forms derived from the Ruddlesden-Popper phases *via* the acid-base mechanism.

Aurivillius phases ($Bi_2A_{n-1}B_nO_{3n+3}$), another series of layered perovskites, consist of perovskite-like slabs and bismuth-oxide sheets.[26-29] We have reported that acid treatment of the Aurivillius phases resulted in the formation of the protonated forms of layered perovskites; so far, two conversions, from $Bi_2ANaNb_3O_{12}$ into $H_{1.8}[A_{0.8}Bi_{0.2}NaNb_3O_{10}]$ (A=Sr, Ca)[30-32] and from $Bi_2SrTa_2O_9$ into $H_{1.8}[Sr_{0.8}Bi_{0.2}Ta_2O_7]$ (HST),[33] have been reported. The compositions of these

protonated forms are close to those of the Ruddlesden-Popper phases, but the layer charge decreases slightly from -2 per $[A_{n-1}B_nO_{3n+1}]$ to -1.8 per $[A_{n-1}B_nO_{3n+1}]$ because of a cation disorder (Sr, Ca ⟷ Bi). We have shown that $H_{1.8}[Sr_{0.8}Bi_{0.2}NaNb_3O_{10}]$ can accommodate *n*-butylamine and *n*-octylamine in the interlayer space *via* the acid-base mechanism.[30,32] The amounts of intercalated *n*-alkylamines, however, were about 1.0 per $[Sr_{0.8}Bi_{0.2}NaNb_3O_{10}]$; only approximately half of protons reacted with *n*-alkylamines.

We report here the intercalation behavior of *n*-alkylamines into $H_{1.8}[Sr_{0.8}Bi_{0.2}Ta_2O_7]$ (HST). We propose the structural model of the resulting intercalation compounds based on the amounts of intercalated *n*-alkylamines and discuss the reason for the intercalation of limited amounts of *n*-alkylamines. To the best of our knowledge, this is the first systematic study of intercalation behavior of protonated forms of layered perovskites $H_x[A_{n-1}B_nO_{3n+1}]$ with $x>1$.

Experimental

Intercalation of *n*-alkylamines. The preparation procedures for HST were described elsewhere.[33] As reactants *n*-alkylamines, *n*-butylamine (C4A), *n*-octylamine (C8A), *n*-dodecylamine (C12A), *n*-octadecylamine (C18A), and pyridine (Py) were utilizd. About 0.5 g of HST was dispersed in 30 mL of an *n*-alkylamine (or pyridine)-tetrahydrofuran (THF) mixture (1:1 as volume) and refluxed for 7 d. After centrifugation, the crude product was washed with THF and air-dried.

Analyses. The X-ray diffraction (XRD) patterns of the products were obtained with MacScience M03XHF[22] with Mn filtered Fe K_α radiation. Elemental analysis was performed as an internal service at the Waseda University Material Characterization Center. The infra-red (IR) spectra of the products were recorded on a Perkin-Elmer Spectrum One spectrometer with the KBr-disk technique.

Results and Discussion

Figure 1 shows the XRD patterns of HST and its reaction products with *n*-alkylamines (hereafter expressed as C*m*A-HST, where *m* represents the number of carbon atoms in *n*-alkylamines). After the reactions, the (00*l*) peaks of HST disappear, and new sets of peaks that can be ascribed to (00*l*) reflections appear. The *d* value calculated from the low-angle peak position for the reaction products with *n*-alkylamines increases with an increase in the number of carbon atoms in the *n*-alkyl chain; 2.12 (C4A-HST), 2.88 (C8A-HST), 3.99 (C12A-HST), and 5.22 [C18A-HST; calculated from the second order value (2.61 nm)] nm. On the contrary, the (100) and (110) peaks of HST are observed at the same position. Thus *n*-alkylamines are successfully intercalated into HST without any structural change in the perovskite-like slabs.

Figure 1

The reaction of HST with pyridine does not result in any change in the XRD pattern, indicating no intercalation reaction (Fig. 1b). Since pyridine is a much weaker base (pK_b=8.82) than the *n*-alkylamines used (pK_b=3.35-3.40), the basicity of pyridine is not large enough for intercalation; the protons in HST are thus weakly acidic.

Figure 2 demonstrates the IR spectra of C12A-HST and C18A-HST. Both of the spectra exhibit four major bands in the CH stretching region. It is well known that the positions of the anti-symmetric stretching band (~2920 cm^{-1}) and the symmetric stretching band (~2850 cm^{-1}) of CH_2 groups (abbreviated $\nu_{as(CH2)}$ and $\nu_{s(CH2)}$, respectively) are sensitive to chain conformation; these two bands shift to lower wavenumbers as disorder (kink and gaush) is introduced into the *n*-alkyl chains.[34,35] Actually, these band positions have been utilized to the conformational analysis of the *n*-alkyl chains of alkylammonium ions in the interlayer space of montmorillonite.[36] In the IR spectrum of C12A-HST, the $\nu_{as(CH2)}$ band and the $\nu_{s(CH2)}$ band are observed at 2918 and 2849 cm^{-1}, respectively, and these band positions correspond to an all-trans

conformation.[36] The IR spectrum of C18A-HST also exhibits these two bands at the same wavenumbers, indicating that the *n*-alkyl chains possess the all-trans conformation in C18A-HST.

Figure 2

The relationship between the basal spacing (d_b) and the number of carbon atoms in the *n*-alkyl chains (n_C) is demonstrated in Figure 3. A linear relationship is clearly observed, as expressed with d_b=0.23n_C + 1.18. Since IR analysis of C12A-HST and C18A-HST indicates that the *n*-alkyl chains in these intercalation compounds essentially exhibit the all-trans conformation, the linear relationship observed in Figure 3 strongly suggests similar conformations for the *n*-alkyl chains in C4A-HST and C8A-HST. The mean increment of the basal spacing ($\Delta d_b/\Delta n_C$) is 0.23 nm. This value corresponds to a tilted bilayer arrangement of the *n*-alkyl chains in the interlayer space of HST. The tilt angle of the *n*-alkyl chains with respect to the surface of the perovskite-like slabs (*ab* plane) is calculated to be 65°.

Figure 3

The amounts of intercalated *n*-alkylamines are listed in Table 1. Though 1.8 H^+ per $[Sr_{0.8}Bi_{0.2}Ta_2O_7]$ are available for the acid-base reaction, only 0.9-1.0 mol of *n*-alkylamines per $[Sr_{0.8}Bi_{0.2}Ta_2O_7]$ is intercalated. It should be noted that a similar observation was reported for another protonated form derived from an Aurivillius phase, $H_{1.8}[Sr_{0.8}Bi_{0.2}NaNb_3O_{10}]$.

Table 1

The present results can be further compared with the intercalation behavior of *n*-alkylamines into the Dion-Jacobson phases, $H[A_{n-1}B_nO_{3n+1}]$; the surface geometry of the Dion-Jacobson phases is essentially identical to that of HST, but the proton concentration on the surface is lower, ideally 1.0 mol per $[A_{n-1}B_nO_{3n+1}]$. In the studies of triple-layered compounds, $H[Ca_2Nb_3O_{10}]$[19] and $H[CaLaNb_2TiO_{10}]$,[21] a few bilayer arrangements of the *n*-alkyl chains with different tilt angles were observed

for each layered perovskite, and some intercalation compounds exhibited two basal spacings corresponding to different arrangements. In the present study, on the contrary, only one arrangement was detected. Among these reported arrangements, a similar tilt angle was observed for $H[Ca_2Nb_3O_{10}]$ (expressed as d_b=0.2249n_C + 1.7129 nm for C12A-C18A).[19] As a double-layered compound, an intercalation compound of $H[LaNb_2O_7]$ with C8A was reported with a basal spacing of 3.038(5) nm,[15] which is slightly larger than that of C8A-HST (2.88 nm). It should be noted that the reported amounts of *n*-alkylamines in fully-intercalated compounds were essentially 1 mol per $[A_{n-1}B_nO_{3n+1}]$; all the protons were involved in the acid-base reactions.[19,21]

These analytical results and the aforementioned comparison indicate that the intercalation behavior of HST and that of the Dion-Jacobson phases are similar. In order to discuss this similarity, a structural model for the interlayer space of C*m*A-HST should be proposed. For the ion-exchangeable layered perovskites (Dion-Jacobson phases and Ruddlesden-Popper phases), however, the structures of intercalation compounds with *n*-alkylamines have not been sufficiently discussed. On the contrary, another series of <100> terminated layered perovskites, the so-called organic inorganic perovskites, $(RNH_3)_2[(CH_3NH_3)_{n-1}M_nX_{3n+1}]$ (where M is divalent metal and X is halogen; note that CH_3NH_3 acts as A-site ions and RNH_3 is present in the interlayer space), have been structurally characterized; the *n*-RNH_3 ions fit into cavities on the <100> surface of the perovskite-like slabs to form hydrogen bonds with halogen atoms.[37] Thus, though the sizes of the cavities in these $[(CH_3NH_3)_{n-1}M_nX_{3n+1}]$ slabs are larger than those in the $[A_{n-1}B_nO_{3n+1}]$ slabs in the ion-exchangeable layered perovskites, we assume similar configurations of reacted *n*-alkylamines in the following discussion.

Figure 4 demonstrates a proposed structural model along the *ab* plane for the C*m*A-HST intercalation compounds. In the Ruddlesden-Popper phases, the amount of protons is equal to the number of cavities, and a comparable amount of protons is

present in HST (corresponds to ~90% of the number of cavities). On the other hand, the amount of protons corresponds to only half the number of cavities in the Dion-Jacobson phases. (It should be noted that these relationships do not depend on the thickness of the perovskite-like slabs, as indicated by the general formula $H_x[A_{n-1}B_nO_{3n+1}]$.) The diameter of *n*-alkylamines with the all-trans *n*-alkyl chain is estimated from the cross-section (0.186 nm)[38] to be 0.486 nm, and the distance between the nearest neighboring cavities (center to center) corresponds approximately to a_p (*a* parameter of cubic perovskite oxide, about 0.39 nm) for all the ion-exchangeable layered perovskites. Thus, as shown in Figure 4, if one cavity is occupied, the nearest neighboring cavities are not available for another guest species. The second-nearest cavities are separated by ~0.52 nm ($\sqrt{2} \times a_p$), and this distance is sufficient to accommodate two *n*-alkyl chains. In the protonated forms derived from the Dion-Jacobson phases, on the contrary, reacted *n*-alkylamines are expected to occupy every other cavity. Thus, the distance between the nearest occupied cavities is ~0.52 nm. These structural considerations provide a reasonable interpretation for HST behavior, which is similar to that of the Dion-Jacobson phases. The above discussion is also consistent with the presence of 2 mol of RNH_3 ions per $[A_{n-1}B_nX_{3n+1}]$ in the organic inorganic perovskites, since the nearest neighboring cavities are separated by ~0.5 nm, which is sufficient to accommodate two *n*-alkyl chains.[37] Since the interlayer surface geometry of HST is essentially identical with that of $H_{1.8}[Sr_{0.8}Bi_{0.2}NaNb_3O_{10}]$, the intercalation of limited amounts of C4A and C8A (0.9-1.0 mol per $[Sr_{0.8}Bi_{0.2}NaNb_3O_{10}]$) can be interpreted in a similar fashion.

Figure 4

Conclusions

We have demonstrated that $H_{1.8}[Sr_{0.8}Bi_{0.2}Ta_2O_7]$ (HST) can accommodate *n*-alkylamines ($C_mH_{m+1}NH_2$; *m*=4, 8, 12, 18) to form intercalation compounds *via* the

acid-base mechanism. Pyridine, which is a weak base, cannot be intercalated into HST, indicating that the protons attached to TaO_6 octahedra in HST are weakly acidic. The four *n*-alkylamines examined exhibit only one type of orientation in the interlayer space of HST: a bilayer arrangement of the *n*-alkyl chains with a tilt angle of 65°. The amounts of intercalated *n*-alkylamines are 0.9-1.0 mol per $[Sr_{0.8}Bi_{0.2}Ta_2O_7]$, though 1.8 mol can be maximally intercalated on the basis of the proton content. The interlayer surface geometry of the $[Sr_{0.8}Bi_{0.2}Ta_2O_7]$ slabs clearly explains the limited intercalation behavior by assuming the presence of reacted *n*-alkylamines in the cavities on the surface of the perovskite-like slabs; the *n*-alkylamines are too bulky to fit every cavity, and the presence of the *n*-alkylamines is spatially possible only in every other cavity.

Acknowledgment. The authors gratefully thank Prof. Kazuyuki Kuroda, Department of Applied Chemistry, Waseda University, for his valuable suggestions. This work was supported financially in part by the Grant-in-Aid for Scientific Research (No. 10555221) from the Ministry of Education, Science, Sports, and Culture, Japan.

References

1) Jacobson, A. J. *Intercalation Reactions of Layered Compounds*; Cheetham, A. K. and Day, P., Ed.; Clarendon Press: Oxford, 1992, pp 182.
2) O'Hare, D. *Inorganic Intercalation Compounds*; 2nd edition ed.; Bruce, D. W. and O'Hare, D., Ed.; John Wiley & Sons: Chichester, 1996, pp 171.
3) Theng, B. K. G. ; Adam Hilger: London, 1974, pp 243.
4) Lagaly, G. *Solid State Ionics* **1986**, *22*, 43.
5) Clément, P.; Marchand, R. *C. R. Acad. Sci. Paris, Ser. II* **1983**, *296*, 1161.
6) Rebbah, H.; Borel, M. M.; Raveau, B. *Mater. Res. Bull.* **1980**, *15*, 317.
7) Kikkawa, S.; Koizumi, M. *Mater. Res. Bull.* **1980**, *15*, 533.
8) Nedjar, R.; Borel, M. M.; Raveau, B. *Z. Anorg. Allg. Chem.* **1986**, *540/541*, 198.

9) Dion, M.; Ganne, M.; Tournoux, M. *Mater. Res. Bull.* **1981**, *16*, 1429.

10) Jacobson, A. J.; Johnson, J. W.; Lewandowski, J. T. *Inorg. Chem.* **1985**, *24*, 3727.

11) Ruddlesden, S. N.; Popper, P. *Acta Crystallogr.* **1957**, *10*, 538.

12) Ruddlesden, S. N.; Popper, P. *Acta Crystallogr.* **1958**, *11*, 54.

13) Jacobson, A. J.; Lewandowski, J. T.; Johnson, J. W. *J. Less-Common Met.* **1986**, *116*, 137.

14) Gopalakrishnan, J.; Bhat, V. *Inorg. Chem.* **1987**, *26*, 4299.

15) Gopalakrishnan, J.; Bhat, V.; Raveau, B. *Mater. Res. Bull.* **1987**, *22*, 413.

16) Richard, M.; Brohan, L.; Tournoux, M. *J. Solid State Chem.* **1994**, *112*, 345.

17) Byeon, S.-H.; Yoon, J.-J.; Lee, S.-O. *J. Solid State Chem.* **1996**, *127*, 119.

18) Schaak, R. E.; Mallouk, T. E. *J. Solid State Chem.* **2000**, *155*, 46.

19) Jacobson, A. J.; Johnson, J. W.; Lewandowski, J. T. *Mater. Res. Bull.* **1987**, *22*, 45.

20) Mohan-Ram, R. A.; Clearfield, A. *J. Solid State Chem.* **1991**, *94*, 45.

21) Gopalakrishnan, J.; Uma, S.; Bhat, V. *Chem. Mater.* **1993**, *5*, 132.

22) Uma, S.; Raju, A. R.; Gopalakrishnan, J. *J. Mater. Chem.* **1993**, *3*, 709.

23) Nakato, T.; Nakade, M.; Kuroda, K.; Kato, C. *Studies Surf. Sci. Catal.* **1994**, *90*, 285.

24) Zhong, Z.; Ding, W.; Hou, W.; Chen, Y.; Chen, X.; Zhu, Y.; Min, N. *Chem. Mater.* **2001**, *13*, 538.

25) Schaak, R. E.; Mallouk, T. E. *Chem. Mater.* **2000**, *12*, 3427.

26) Frit, B.; Mercurio, J. P. *J. Alloys Compd.* **1992**, *188*, 27.

27) Aurivillius, B. *Ark. Kemi.* **1949**, *1*, 463.

28) Aurivillius, B. *Ark. Kemi.* **1950**, *2*, 519.

29) Aurivillius, B. *Ark. Kemi.* **1952**, *5*, 39.

30) Sugimoto, W.; Shirata, M.; Sugahara, Y.; Kuroda, K. *J. Am. Chem. Soc.* **1999**, *121*,

11601.

31) Shirata, M.; Tsunoda, Y.; Sugimoto, W.; Sugahara, Y. *Mat. Res. Soc. Symp. Proc.* **2001**, *658*, GG6.24.1.

32) Sugimoto, W.; Shirata, M.; Kuroda, K.; Sugahara, Y. *Chem. Mater.* , submitted.

33) Tsunoda, Y.; Shirata, M.; Sugimoto, W.; Liu, Z.; Terasaki, O.; Kuroda, K.; Sugahara, Y. *Inorg. Chem.* **2001**, *40*, 5768.

34) Snyder, R. G.; Strauss, H. L.; Elliger, C. A. *J. Phys. Chem.* **1982**, *86*, 5145.

35) MacPhail, R. A.; Strauss, H. L.; Snyder, R. G.; Elliger, C. A. *J. Phys. Chem.* **1984**, *88*, 334.

36) Vaia, R. A.; Teukolsky, R. K.; Giannelis, E. P. *Chem. Mater.* **1994**, *6*, 1017.

37) Mitzi, D. B. *Prog. Inorg. Chem.* **1999**, *48*, 1.

38) Goñi, A.; Rius, J.; Insausti, M.; Lezama, L. M.; Pizarro, J. L.; Arriortua, M. I.; Rojo, T. *Chem. Mater.* **1996**, *8*, 1052.

Figure Captions

Figure 1 XRD patterns of (a) $H_{1.8}[Sr_{0.8}Bi_{0.2}Ta_2O_7]$ (HST), (b) Py-HST, (c) C4A-HST, (d) C8A-HST, (e) C12A-HST, and (f) C18A-HST.

Figure 2 IR spectra of (a) C12A-HST and (b) C18A-HST.

Figure 3 Plot of basal spacing (d_b) versus the number of carbon atoms in the alkyl chain (n_C) for the *n*-alkylamine-HST intercalation compounds.

Figure 4 Idealized structural model along the *ab* plane. Large circle indicates cross-section of *n*-alkylamine.

Table 1 *N*-alkylamine Contents of the C*m*A-HST intercalation Compounds.

Amine	C / mass %	*N*-alkylamine Content / mol per $[Sr_{0.8}Bi_{0.2}Ta_2O_7]$
C4A	6.62	0.9
C8A	11.8	0.9
C12A	17.6	0.9
C18A	24.7	1.0

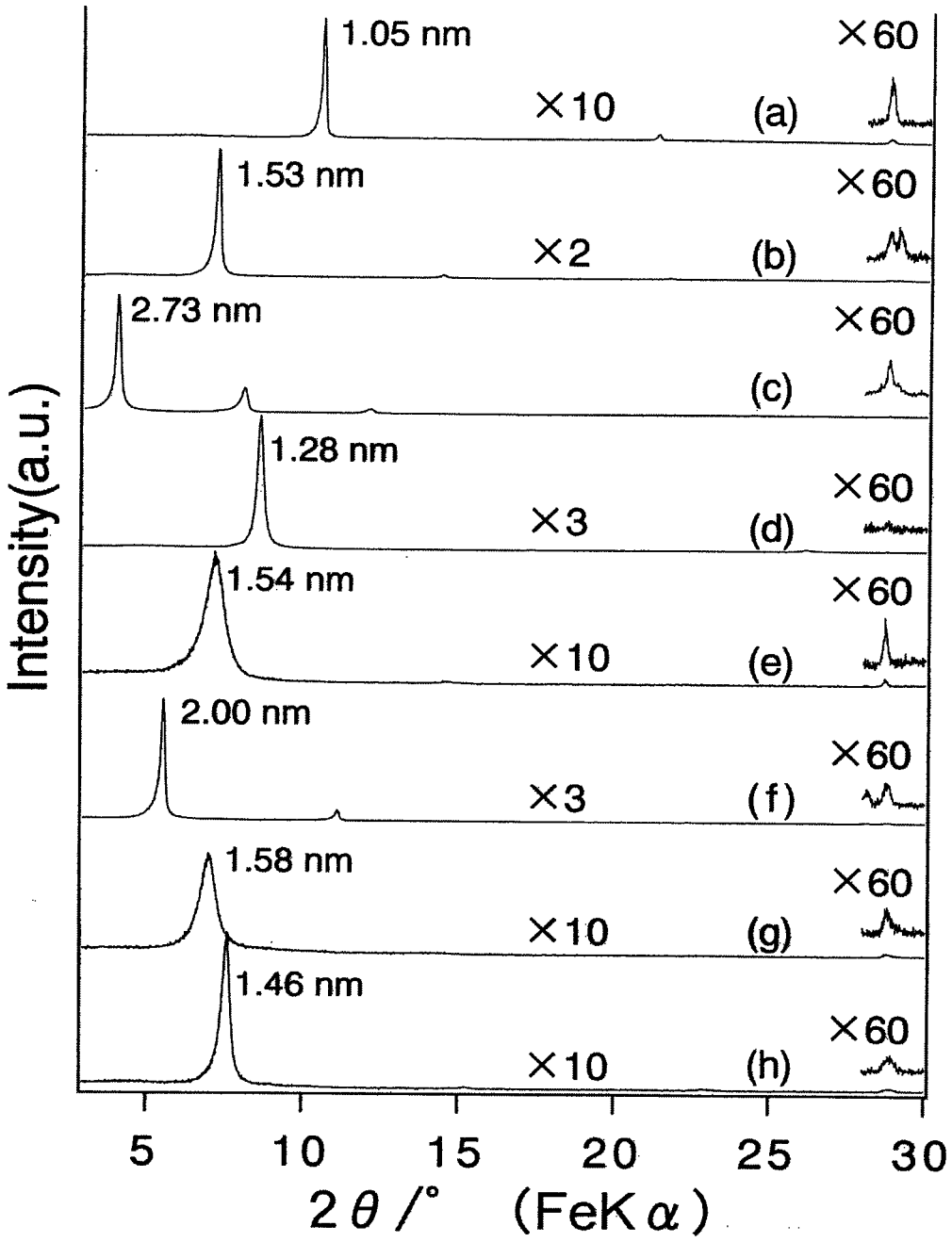

Figure 1. XRD patterns of (a) $HLaNb_2O_7$ (anhydrous HLN), (b) n-propoxyl derivative of HLN (n-propoxyl-HLN), (c) n-propoxyl derivative of HLN after the treatment with n-decanol (n-decoxyl-HLN), (d) n-decoxyl-HLN hydrolyzed with 3 M KOH, (e) n-decoxyl-HLN treated with sec-propanol, (f) n-decoxyl-HLN treated with tert-butanol, (g) n-decoxyl-HLN treated with ethylene glycol (EG), and (h) (g) heated at 200 °C.

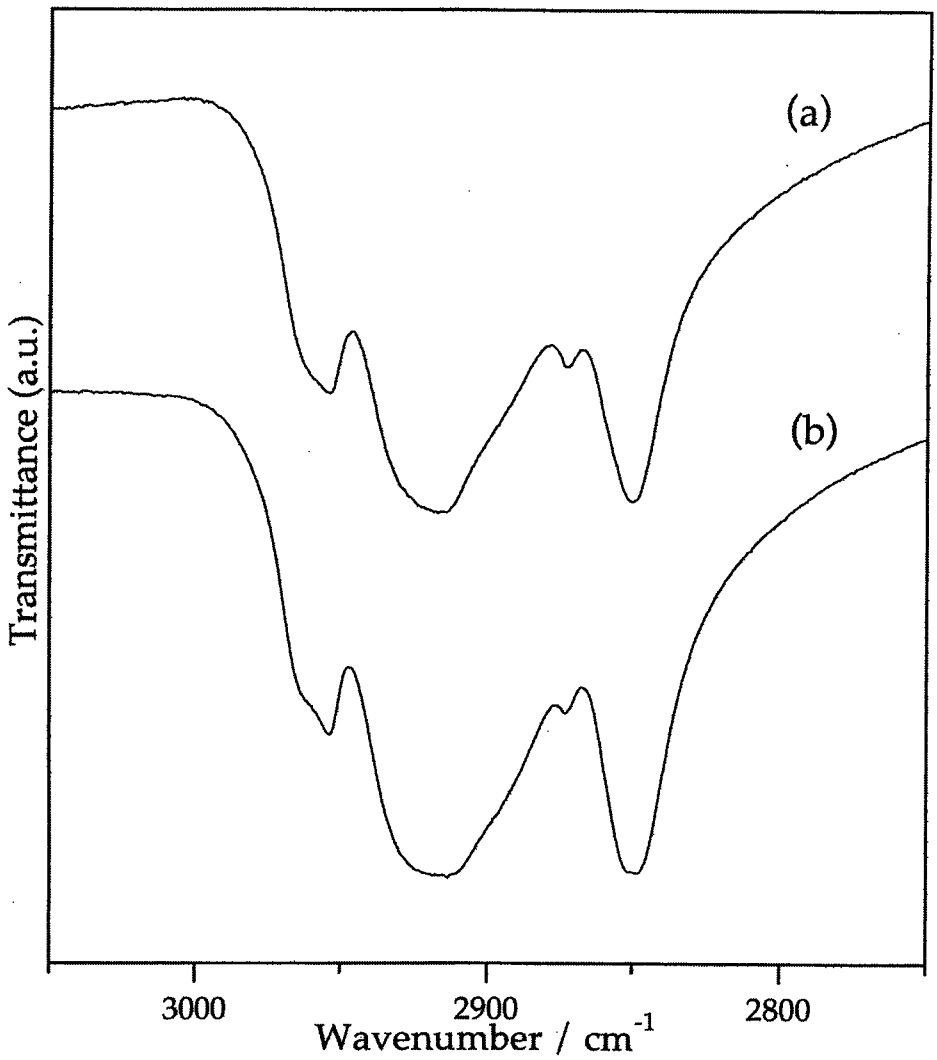

Figure 2 IR spectra of (a) C12A-HST and (b) C18A-HST.

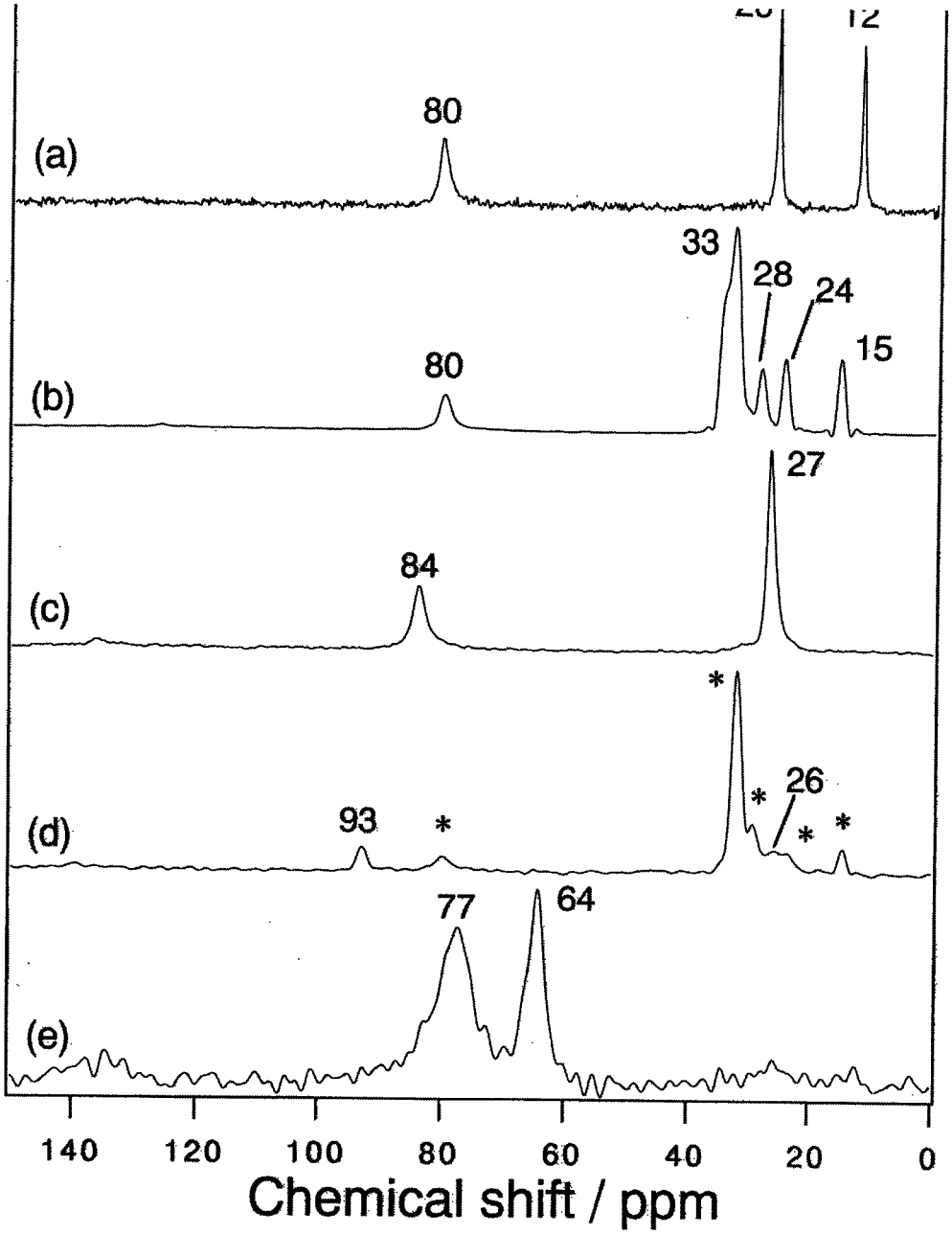

Figure 3. Solid-state ^{13}C CP/MAS NMR spectra of (a) n-propoxyl derivative of HLN (n-propoxyl-HLN), (b) n-propoxyl derivative of HLN after the treatment with n-decanol (n-decoxyl-HLN), (c) n-decoxyl-HLN treated with sec-propanol, (d) n-decoxyl-HLN treated with tert-butanol, and (e) n-decoxyl-HLN treated with ethylene glycol (EG).

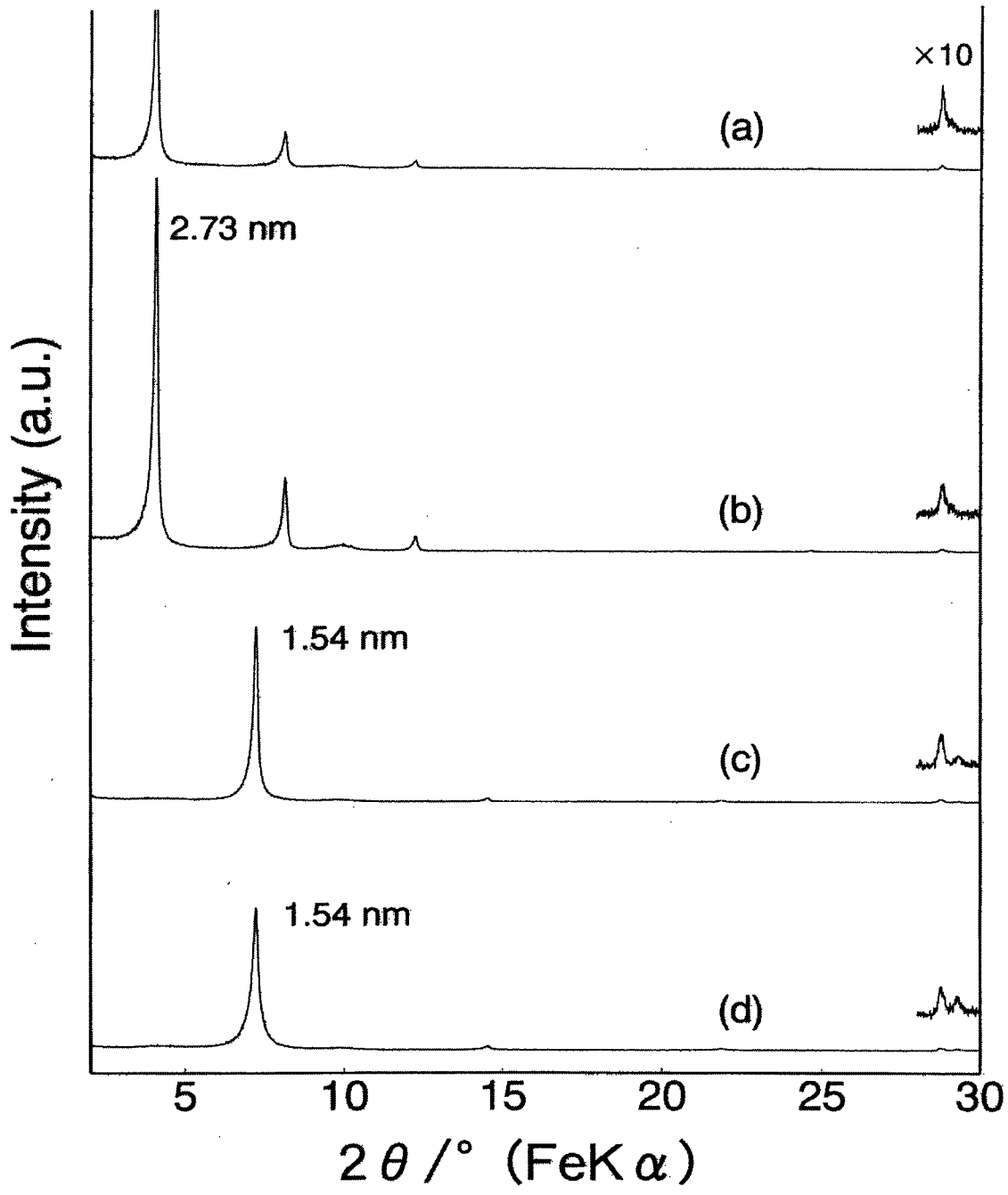

Figure 4. XRD patterns of (a) n-propoxyl-HLN after the treatment with n-decanol containing 3 mass % of distilled water for 1 d,
(b) n-propoxyl-HLN after the treatment with n-decanol containing 3 mass % of distilled water for 7 d,
(c) n-propoxyl-HLN after the treatment with distilled n-decanol for 1 d,
(d) n-propoxyl-HLN after the treatment with distilled n-decanol for 7 d.

olid State Chemistry 148, 508–512 (1999)
ssc.1999.8488, available online at http://www.idealibrary.com on IDEAL®

Synthesis and Structures of Reduced Niobates with Four 'erovskite-like Layers and Their Semiconducting Properties

W. Sugimoto,*,[1] H. Ohkawa,* M. Naito,* Y. Sugahara,*,[2] and K. Kuroda*,†

rtment of Applied Chemistry, School of Science and Engineering, Waseda University, Ohkubo-3, Shinjuku-ku, Tokyo 169-8555, Japan; and ımi Memorial Laboratory for Materials Science and Technology, Waseda University, Nishiwaseda-2, Shinjuku-ku, Tokyo 169-0051, Japan

Received March 29, 1999; in revised form July 27, 1999; accepted August 27, 1999

ı were successfully doped into $RbCa_2NaNb_4O_{13}$ by the n of Sr^{2+} for Na^+, yielding electroconducting niobates ered structure consisting of four perovskite-like layers. se products of polycrystalline $RbCa_2Na_{1-x}Sr_xNb_4O_{13}$ nd 0.4) were synthesized by the solid-state reaction Nb_3O_{10}, $Sr_5Nb_4O_{15}$, Nb_2O_5, and Nb metal. The ions were indexed based on a tetragonal structure, ling to the end-member $RbCa_2NaNb_4O_{13}$. With se in the amount of strontium substitution, an expan- *c*-axis was observed while the *a*-axis was essentially The products showed semiconducting properties.

rds: **niobate; solid-state reaction; layered perovskite; idation state; Rietveld analysis; electrical conduction.**

1. INTRODUCTION

class of transition metal oxides possess struc- sisting of two-dimensionally stacked perovskite- $A_{n+1}B_nO_{3n+1}$ (1), $Bi_2A_{n-1}B_nO_{3n+3}$ (2), and O_{3n+1} are well-known examples (3, 4). These are ideal for relating the thickness of the perov- slabs n with the properties. For example, the the electrical properties of $(La, Sr)_{n+1}Mn_nO_{3n+1}$ 3, and ∞) (5), $Sr_{n+1}V_nO_{3n+1}$ ($n = 1$, 2, and ∞) $_{n+1}Ni_nO_{3n+1}$ ($n = 1$, 2, 3, and ∞) (8), and $_{0.05})_{n+1}Ti_nO_{3n+1-\delta}$ ($n = 1$ and 2) (9) has been based on the difference in the thickness of the -like slabs.

y, the incorporation of conducting electrons bates with a layered-perovskite structure, Nb_nO_{3n+1}], has drawn attention. The structure of Nb_nO_{3n+1}] consists of n perovskite-like layers with a monovalent cation M occupying the interlayer space. The reduced niobates for the $n = 2$ and 3 compounds have been synthesized by chemical or electrochemical intercalation of excess ions (H^+, Li^+, and Rb^+) into the interlayer (9–17) and by cation substitution by solid-state reaction (18, 19). Most of the early studies have emphasized the structural characterization of the reduced products.

The electrical properties of carrier-doped $n = 2$ and 3 members have been reported recently. We have reported the synthesis and electrical properties of the $n = 3$ member $KCa_{2-x}Ln_xNb_3O_{10}$ (Ln = La, Ce, Nd, Sm, and Gd) (18, 19). The observed ($\log \rho$) $\propto T$ dependence was interpreted based on a model assuming tunneling conduction through vibrating barriers, and the structure–property relation was established (18, 19). Recently, it has been reported that the $n = 3$ member $Li_xKCa_2Nb_3O_{10}$ shows a superconducting transition below 6 K (15–17), whereas the $n = 2$ member $Li_xKLaNb_2O_7$ shows no superconducting transition down to 0.5 K (15). This suggests that the thickness of the perovskite-like slabs influences the superconducting properties in $M[A_{n-1}Nb_nO_{3n+1}]$.

The synthesis and structural characterization of the $n = 4$ member, $RbCa_2NaNb_4O_{13}$, have been reported (4, 20). The schematic structure of $RbCa_2NaNb_4O_{13}$ is shown in Fig. 1. In light of the variation in the electrical properties as a function of n in the two-dimensional perovskites reported so far, the electrical properties of higher n members of $M[A_{n-1}Nb_nO_{3n+1}]$ are of interest. Here, we report the doping of carriers into the $n = 4$ member of the layered perovskite $RbCa_2NaNb_4O_{13}$ by the substitution of Sr^{2+} for Na^+ and their structures and electrical properties.

2. EXPERIMENTAL

$RbCa_2Nb_3O_{10}$, $Sr_5Nb_4O_{15}$, and $NaNbO_3$ were prepared by the solid-state reactions of appropriate amounts of Rb_2CO_3, $CaCO_3$, $SrCO_3$, Na_2CO_3, and Nb_2O_5 under ambient atmosphere. A 50% excess amount of Rb_2CO_3 was used in the case of $RbCa_2Nb_3O_{10}$. The product was washed

address: Department of Fine Materials Engineering, Faculty of ıce and Technology, Shinshu University, 3-15-1 Tokida, Ueda pan.
n correspondence should be addressed. E-mail: ys6546@mn.

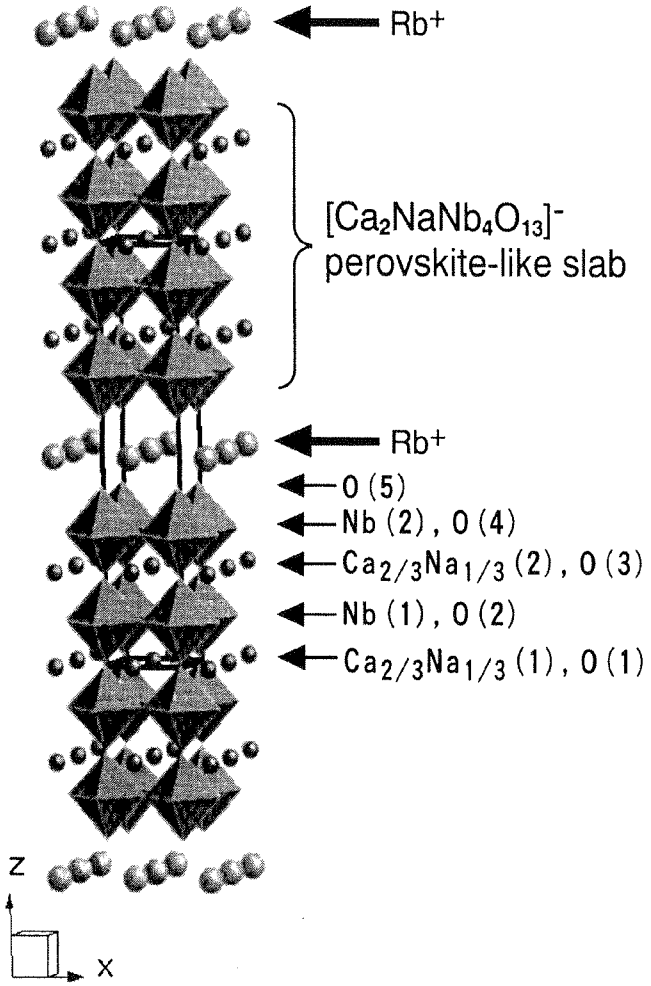

FIG. 1. Schematic crystal structure of $RbCa_2NaNb_4O_{13}$.

ith deionized water after completion of the reaction. X-ray ffraction (XRD) (Mac Science MXP^3 diffractometer with onochromated Cu$K\alpha$ radiation) of the above oxides in-cated single-phase formation, and inductively coupled asma emission spectroscopy (ICP) (Nippon Jarrell Ash, :AP575 Markll) showed that the cation ratios were consis-nt with the nominal ones.

Polycrystalline samples with nominal compositions of $bCa_2Na_{1-x}Sr_xNb_4O_{13}$ ($x = 0.2$, 0.4, and 0.5) were syn-esized from $RbCa_2Nb_3O_{10}$, $NaNbO_3$, $Sr_5Nb_4O_{15}$, and b according to the following equation:

$$)Ca_2Nb_3O_{10} + (1-x)NaNbO_3 + (0.2x)Sr_5Nb_4O_{15} + (0.2x)Nb \rightarrow RbCa_2Na_{1-x}Sr_xNb_4O_{13}. \quad [1]$$

l of the starting oxides were dried for at least 1 day at 0°C before use. The end-member $RbCa_2NaNb_4O_{13}$ was nthesized by the solid-state reactions of $RbCa_2Nb_3O_{10}$ d $NaNbO_3$ at 1200°C for 3 h in air (20). After thorough inding, the reagents were pressed and placed in an umina boat surrounded by powders having the same composition to prevent contamination. The reactor was evacuated to $\sim 8.5 \times 10^{-3}$ Pa before argon pu and Ti powder was placed in the reactor tube as an ox getter to minimize oxidation during the synthesis. Th agents were fired at 1200°C for several hours, with inte tent grinding after every 3 h of firing. The firing sequ was repeated twice.

The morphology of the products was studied a scanning electron microscope (SEM) (Hitachi, S-2 Crystalline phases were identified by XRD. Structural p meters were determined by the Rietveld analysis pro RIETAN (21, 22). The cation ratios were determined by analysis. For the ICP measurements, the samples wer composed in a mixture of HF, HCl, and HNO_3 by he at 200°C for at least 3 h. Resistivity data were collected 80 to 280 K using a standard dc four-probe method.

3. RESULTS AND DISCUSSION

Table 1 summarizes the compositional analysis resul the products obtained as single phases. The cation r were in agreement with the nominal composition for Thus, the discussion herein is based on the assumption the substitution of Sr^{2+} for Na^+ produces an equiv amount of Nb^{4+} during the synthesis.

The XRD patterns of the products are shown in Fi Preferred orientation was observed along the [00l] p consistent with the plate-like morphology of the sam observed in the scanning electron micrographs. The X

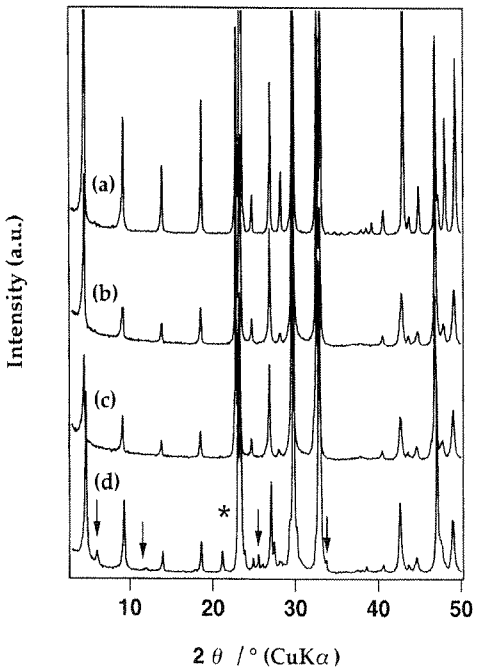

FIG. 2. XRD patterns of $RbCa_2Na_{1-x}Sr_xNb_4O_{13}$ with (a) x (b) $x = 0.2$, (c) $x = 0.4$, and (d) $x = 0.5$. Arrows in (d) represent peaks d the $n = 3$ compound. The peak with an asterisk in (d) is an uniden peak.

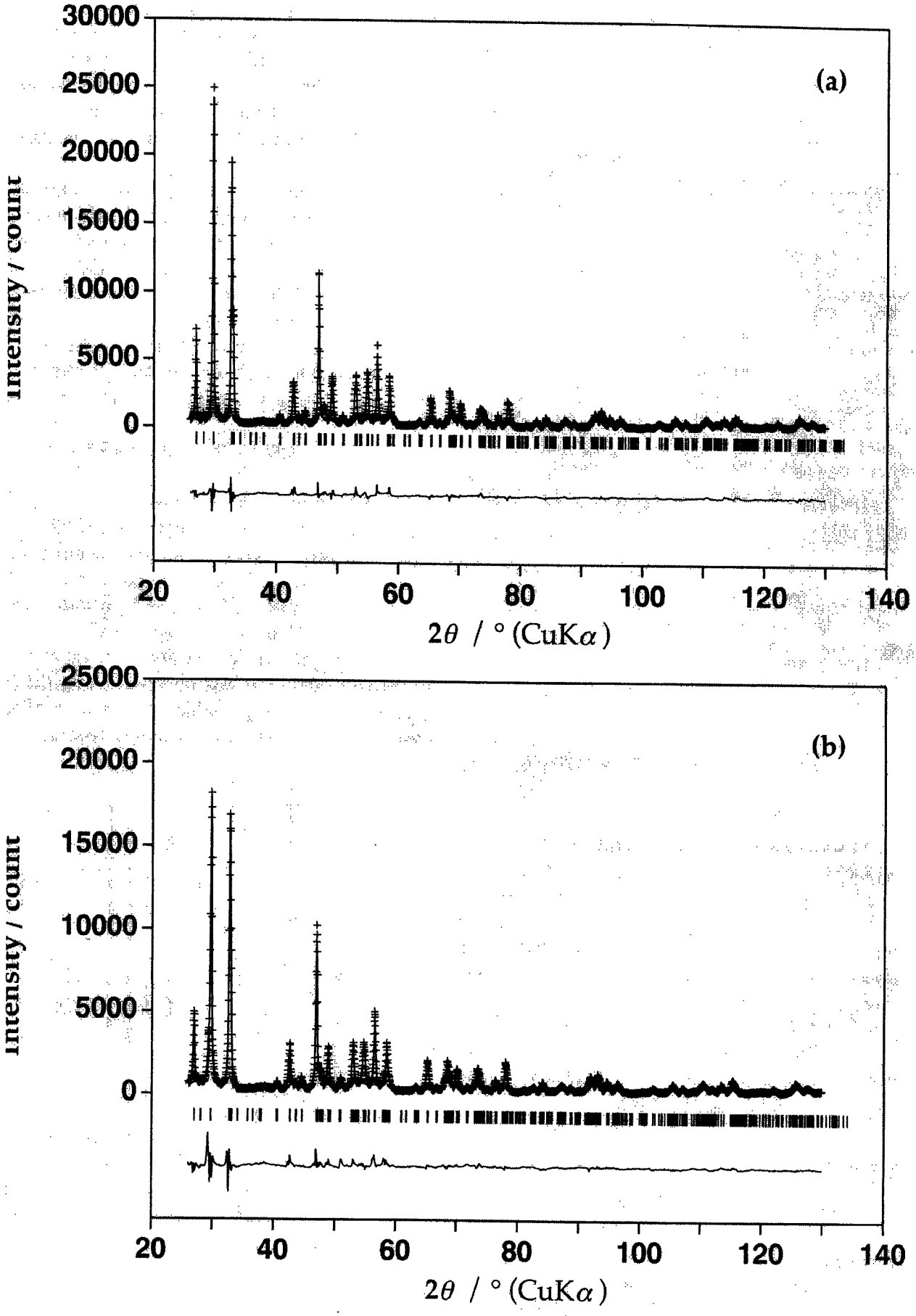

RD pattern fittings for (a) $RbCa_2Na_{0.8}Sr_{0.2}Nb_4O_{13}$ and (b) $RbCa_2Na_{0.6}Sr_{0.4}Nb_4O_{13}$. The observed (crosses) and calculated (solid li hown in the top traces. The vertical lines in the middle represent the positions of the possible Bragg reflections. The lower curves are t ween the observed and calculated intensities

TABLE 1
Composition of the Products

Composition[a,b]
$Rb_{1.00}Ca_{2.06}Na_{1.06}Nb_4O_{13}$
$Rb_{1.00}Ca_{2.00}Na_{0.80}Sr_{0.21}Nb_4O_{13}$
$Rb_{1.04}Ca_{2.07}Na_{0.61}Sr_{0.40}Nb_4O_{13}$

[a] Compositions were normalized by setting the amount of niobium to 4.
[b] Amount of oxygen was set to 13.

ıttern for $x = 0$ was indexed based on a primitive-tetragıal cell, in agreement with a previous report (20). Singleıase $RbCa_2Na_{1-x}Sr_xNb_4O_{13}$ was obtained for $x = 0.2$ ıd 0.4 with repeated firings. No extra reflections for = 0.2 and 0.4 were evident in the XRD patterns when mpared to that of $x = 0$, and all the diffraction peaks were dexed based on a primitive-tetragonal cell. When $x = 0.5$, unidentified peak at $2\theta = 21.16°$ and weak diffraction aks due to $RbCa_2Nb_3O_{10}$ were observed besides the tended phase. A single phase for $x = 0.5$ could not be ıtained even with repeated firings or firing at higher temrature. Thus, the solubility limit is between $x = 0.4$ and 5 under the present synthetic conditions.

The structure of the $x = 0$ compound was refined by etveld analysis assuming a random distribution of Ca and a at the A site (20). The crystallographic data correspond to those of a previous report (20). Since the indexing of e XRD patterns for $x = 0.2$ and 0.4 indicated the preservation of the symmetry with substitution. Rietveld analysis these compounds was conducted with the same space oup as that for $x = 0$. A random distribution of the A-site tions (Ca, Na, and Sr) was also assumed. The outputs om the Rietveld refinement are shown in Fig. 3, and the ystallographic data are given in Table 2. The a-axis was

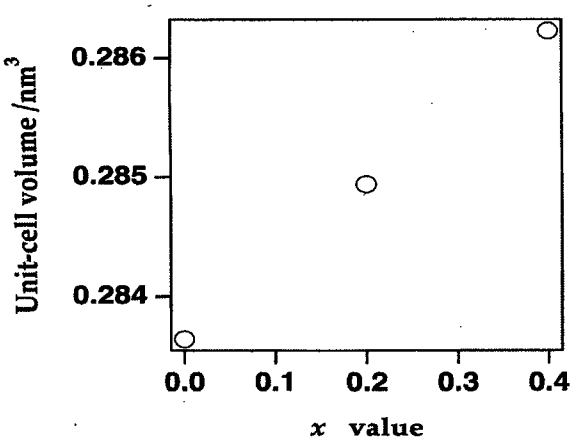

FIG. 4. Evolution of the unit-cell volume as a function of x.

TABLE 2
Crystallographic data for $RbCa_2NaNb_4O_{13}$, $RbCa_2Na_{0.8}Sr$ Nb_4O_{13}, and $RbCa_2Na_{0.6}Sr_{0.4}Nb_4O_{13}$[a]

Sample	Atom	Position	x	y	z	B (nn
$RbCa_2NaNb_4O_{13}$	Rb	1*d*	0.5	0.5	0.5	0.028(
	A(1)[b]	1*c*	0.5	0.5	0	0.010(
$a = 0.38727(1)$ nm	*A*(2)[b]	2*h*	0.5	0.5	0.2240(7)	0.010
$c = 1.89116(6)$ nm	Nb(1)	2*g*	0	0	0.1057(2)	0.002
	Nb(2)	2*g*	0	0	0.3293(2)	0.002
$R_{wp} = 0.1299$	O(1)	1*a*	0	0	0	0.036(
$R_p = 0.0969$	O(2)	4*i*	0	0.5	0.101(1)	0.036
$R_e = 0.0340$	O(3)	2*g*	0	0	0.205(2)	0.036
$R_I = 0.0349$	O(4)	4*i*	0	0	0.309(1)	0.036
$R_F = 0.0217$	O(5)	2*g*	0	0	0.420(2)	0.036
$RbCa_2Na_{0.8}Sr_{0.2}Nb_4O_{13}$	Rb	1*d*	0.5	0.5	0.5	0.048(
	A(1)[b]	1*c*	0.5	0.5	0	0.012(
$a = 0.38716(1)$ nm	*A*(2)[b]	2*h*	0.5	0.5	0.2248(7)	0.010
$c = 1.90092(8)$ nm	Nb(1)	2*g*	0	0	0.1054(3)	0.003(
	Nb(2)	2*g*	0	0	0.3289(3)	0.003(
$R_{wp} = 0.0990$	O(1)	1*a*	0	0	0	0.037(
$R_p = 0.0769$	O(2)	4*i*	0	0.5	0.104(2)	0.037
$R_e = 0.0355$	O(3)	2*g*	0	0	0.214(2)	0.037
$R_I = 0.0339$	O(4)	4*i*	0	0	0.308(1)	0.037
$R_F = 0.0221$	O(5)	2*g*	0	0	0.416(2)	0.037
$RbCa_2Na_{0.6}Sr_{0.4}Nb_4O_{13}$	Rb	1*d*	0.5	0.5	0.5	0.044(
	A(1)[b]	1*c*	0.5	0.5	0	0.008(
$a = 0.38704(3)$ nm	*A*(2)[b]	2*h*	0.5	0.5	0.2236(9)	0.008
$c = 1.9107(1)$ nm	Nb(1)	2*g*	0	0	0.1056(5)	0.006(
	Nb(2)	2*g*	0	0	0.3285(4)	0.006
$R_{wp} = 0.1216$	O(1)	1*a*	0	0	0	0.034(
$R_p = 0.0881$	O(2)	4*i*	0	0.5	0.101(3)	0.034
$R_e = 0.0359$	O(3)	2*g*	0	0	0.215(3)	0.034
$R_I = 0.0426$	O(4)	4*i*	0	0	0.309(2)	0.034
$R_F = 0.0243$	O(5)	2*g*	0	0	0.421(3)	0.034

[a] Space group *P4/mmm*; No. 123. 2θ step size = 0.04, total number of re tions = ca. 400, number of profile points = 2601. Number in parentheses rep ents estimated standard deviation. Values without standard deviation v constrained. The occupation factor was set to unity for all positions.
[b] The cation ratios in *A*(1) and *A*(2) were confined to Ca:Na = 2/3:1/3 $RbCa_2NaNb_4O_{13}$, Ca:Na:Sr = 2/3:4/15:1/15 for $RbCa_2Na_{0.8}$ $Sr_{0.2}Nb_4$ and Ca:Na:Sr = 2/3:3/15:2/15 for $RbCa_2Na_{0.6}Sr_{0.4}Nb_4$ O_{13}.
[c] The istropic atomic displacement parameters for the same cation spe were constrained to be equal.

essentially unchanged, while the c-axis increased linea resulting in an overall increase in the unit-cell volu (Fig. 4). The increase is attributed to the larger ionic ra of Sr^{2+} (0.144 nm) and Nb^{4+} (0.068 nm) compared Na^+ (0.139 nm) and Nb^{5+} (0.064 nm) (23).

Calculation of the bond distances showed that the Nb bond extending toward the interlayer had the shortest c tance (Nb(2)–O(5) = 0.177(6) nm). The longest Nb–O bo was Nb(2)–O(3) = 0.216(7) nm. The inner two perovski like slabs are closer to an ideal octahedron than the ou ones, as was the case for $x = 0$ (20). No drastic change in

SYNTHESIS OF $Na_{1-x}Ln_xNbO_3$ (Ln=La, Nd, Sm, Gd) AND THEIR STRUCTURES AND ELECTRICAL PROPERTIES

Wataru Sugimoto,* Masahiro Naito,* Yoshiyuki Sugahara,* and Kazuyuki Kuroda*, **
* Department of Applied Chemistry, School of Science and Engineering, Waseda University, Ohkubo-3, Shinjuku-ku, Tokyo 169-8555 JAPAN
** Kagami Memorial Laboratory for Materials Science and Technology, Waseda University, Nishiwaseda-2, Shinjuku-ku, Tokyo 169-0051 JAPAN

ABSTRACT

Polycrystalline samples of $Na_{1-x}Ln_xNbO_3$ (Ln=La, Nd, Sm, Gd) were synthesized by solid-state reactions. Reduced niobates were obtained as single-phase perovskites for x=0.05 and 0.1 when Ln=La and Nd and x=0.05 when Ln=Sm. The Gd-substituted samples could not be prepared under the synthetic conditions studied. Compositional analysis of the products revealed a slight amount of sodium loss during synthesis. The structural parameters obtained from Rietveld analysis revealed an increase in unit-cell volume. All of the obtained samples showed semiconducting behavior. Similar semiconducting behavior was observed for the same x value, suggesting the weak influence of the different Ln species to the electrical properties.

INTRODUCTION

Transition-metal based oxides possessing perovskite and perovskite-related structures have attracted attention owing to interesting properties ranging from insulating, semiconducting, metallic to superconducting [1-3]. A few electroconducting niobates with perovskite structure possessing $4d^0$ - $4d^1$ electrons have been synthesized [4-11]. Sr_xNbO_3 and Ba_xNbO_3 (*c.a.* $4d^1$) exhibit metallic behavior [4-8]. Unique semiconducting behavior has been reported for lightly-doped niobates, $Na_{1-x}Sr_xNbO_3$ [9] and $La_{1.05}Nb_3O_9$ [11]. A $\log \rho \propto T$ relationship was observed in a wide temperature range (80–300 K) for $Na_{1-x}Sr_xNbO_3$, and this behavior was interpreted based on the tunneling conduction through vibrating barrier model [9]. The resistance of $La_{1.05}Nb_3O_9$ exhibited a 'bell-like' temperature dependence [11]. We reported earlier that electroconducting niobates $A'_{1-x}A''_xNbO_3$ can be synthesized not only by heterovalent substitution of the monovalent alkali metal ions with a divalent ion ($A''=Sr^{2+}$), but also by the substitution of the monovalent alkali metal ions with a trivalent ion ($A''=La^{3+}$) [12]. The existence of a wide variety of lanthanoids with slightly different ionic radii presents an opportunity to vary the structure of the solid solutions and study the effect on the electrical properties systematically. In fact, the variation in the electrical/magnetic properties of the orthorhombic $RTiO_3$ (lanthanoid and Y) as a function of R has been examined, and the correlation between the structure and the properties has been discussed [13].

We report here the synthesis and properties of $Na_{1-x}Ln_xNbO_3$ (Ln=La, Nd, Sm, Gd),

emphasizing on the variation in the structure and electrical properties with the various Ln species.

EXPERIMENTAL

Polycrystalline samples with nominal compositions of $Na_{1-x}Ln_xNbO_3$ (Ln=La, Nd, Sm, Gd; $0 \le x \le 0.2$) were synthesized from pelletized mixtures of appropriate amounts of $NaNbO_3$, Ln_2O_3, Nb_2O_5, and Nb metal. $NaNbO_3$ was obtained by the solid-state reaction of stoichiometric amounts of Na_2CO_3 and Nb_2O_5 under an ambient atmosphere. The pelletized samples were fired for up to 50 h at 1200°C (with intermediate grinding every 10 h) under Ar atmosphere.

Inductively coupled plasma emission spectroscopy (ICP) (Nippon Jarrel Ash ICAP575Mark II) was used to determine the cation ratios of the products. Crystalline phases were identified using a Mac Science MXP^3 diffractometer (monochromated Cu Kα radiation). Crystallographic data were obtained by the Rietveld analysis program RIETAN [14,15]. Resistivity data were collected from 5 to 280 K using a standard dc four-probe method.

RESULTS

All of the XRD reflections for Ln=La, Nd (x = 0.05 and 0.10) and Sm (x = 0.05) could be indexed based on an orthorhombic cell, consistent with the parent compound. $LnNbO_4$ was observed as the impurity phase for higher x values. When Ln=Gd, a single phase could not be obtained even for x=0.05. The XRD patterns of the single-phase compounds are shown in Fig. 1. The solubility limit decreased in the order La≅Nd>Sm, which is consistent with the order of the decrease in the ionic radius of Ln (Table I). A similar tendency was reported for $R_{1+x}Nb_3O_9$ (R=La, Ce, Nd) [11].

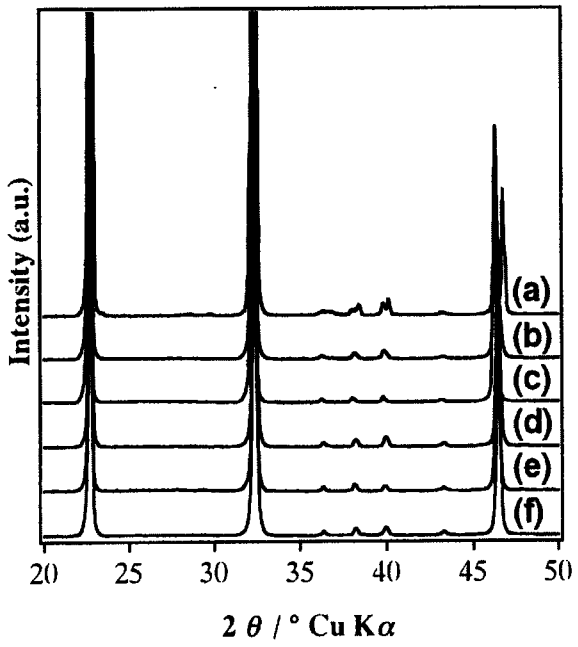

Fig.1 The XRD patterns for the products of nominal composition (a) $NaNbO_3$, (b) $Na_{0.95}La_{0.05}NbO_3$, (c) $Na_{0.90}La_{0.10}NbO_3$, (d) $Na_{0.95}Nd_{0.05}NbO_3$, (e) $Na_{0.90}Nd_{0.10}NbO_3$, (f) $Na_{0.95}Sm_{0.05}NbO_3$.

Table I The ionic radius of the ions (ref. 16)

ion	ionic radius / nm	
	12 coordinated	9 coordinated
Na^+	0.139	0.124
La^{3+}	0.136	0.122
Nd^{3+}	0.127	0.1163
Sm^{3+}	0.124	0.1132
Gd^{3+}	-	0.1107

The ICP results are summarized in Table II. The Ln/Nb ratios in all of the samples were consistent with the nominal compositions within experimental error. The Na/Nb ratios were slightly lower than the nominal values, indicating a slight loss of Na during synthesis.

Table II The composition of the single-phase samples

Ln	x value	composition[(a)]	formal Nb valence[(b)]
-	0	$Na_{1.00}NbO_3$	5
La	0.05	$Na_{0.90}La_{0.06}NbO_3$	4.92
	0.10	$Na_{0.81}La_{0.11}NbO_3$	4.86
Nd	0.05	$Na_{0.92}Nd_{0.06}NbO_3$	4.90
	0.10	$Na_{0.82}Nd_{0.12}NbO_3$	4.82
Sm	0.05	$Na_{0.91}Sm_{0.06}NbO_3$	4.91

(a) The compositions were normalized by setting the values of niobium and oxygen to nominal ones.
(b) The formal Nb valences were calculated based on the ICP results and assuming nominal niobium and oxygen contents.

The same space group as the parent compound, $NaNbO_3$ (Pbcm) [17], was adopted for the Rietveld analysis, as no clear change in the symmetry of the cell was observed. The obtained lattice parameters are summarized in Table III. The *a*/*b* axis ratios for the solid solutions approach to unity with the increase in x, indicating that the structure approaches to a tetragonal symmetry.

Table III The lattice parameters for $Na_{1-x}Ln_xNbO_3$

Ln	x	unit-cell parameter / nm			*a* / *c*
		a	*b*	*c*	
-	0	0.55067(2)	0.55690(2)	1.55143(6)	0.989
La	0.05	0.55268(4)	0.55514(5)	1.5626(1)	0.996
	0.10	0.5545(1)	0.5549(1)	1.5657(1)	0.999
Nd	0.05	0.55213(3)	0.55390(4)	1.5609(1)	0.997
	0.10	0.5532(1)	0.5534(1)	1.5631(2)	1.000
Sm	0.05	0.55155(4)	0.55363(1)	1.5602(1)	0.996

Numbers in parenthesis represent estimated standard deviation.

The unit-cell volume increased monotonously with an increase in x for all Ln, as shown in Fig. 2. The increase is attributed to the increase in the ionic radius of reduced niobium ($Nb^{5+} \rightarrow Nb^{4+}$; 0.064→0.068 nm)) [16], as the ionic radii of Ln are smaller than that of Na (Table I). Moreover, the unit-cell volume decreased in the order La > Nd > Sm, which corresponds to the decrease in the ionic radius of Ln (Table I).

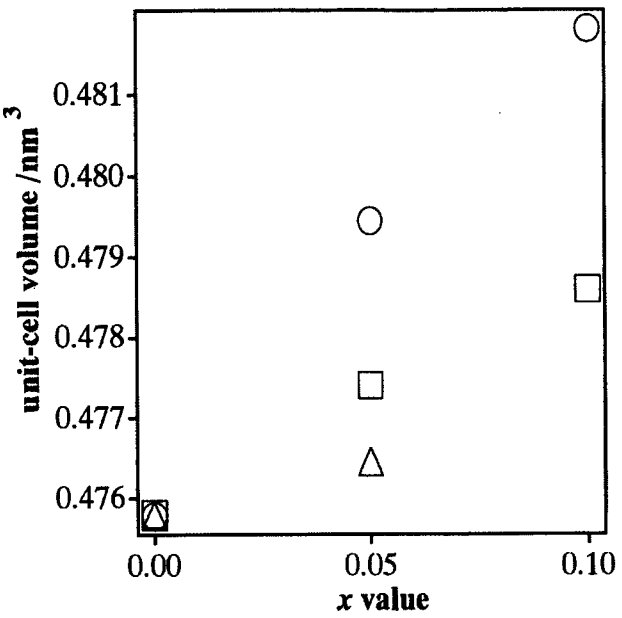

Fig.2 The variation in unit-cell volume as a function of the x value in $Na_{1-x}Ln_xNbO_3$ with Ln=La (circles), Nd (squares), and Sm (triangles).

All of the Ln-substituted compounds showed semiconducting behavior in the temperature range of $5 < T < 280$ [K]. The normalized resistivity for x=0.05 and 0.10 is shown in Fig. 3. The x=0.10 samples exhibited a slightly weaker temperature dependence compared with the x=0.05 samples. Based on the one-electron energy diagram for ReO_3 by Goodenough [1], it is assumed that the π^* conduction band is formed by the overlapping of $4d$ (t_{2g}) and O $2p$ orbitals in $Na_{1-x}Ln_xNbO_3$. A similar one-energy diagram has been proposed for $Na_{1-x}Sr_xNbO_3$ [9] and Eu_xNbO_3 [18]. The localized electrons are expected to occupy states below the π^* conduction band, and localize near Ln^{3+}, due to the charge difference between Na^+ and Ln^{3+}. Also, the random distribution of Na^+ and Ln^{3+}, as well as the presence of cation vacancies, may lead to Anderson localization.

The resistivity behavior could not be sufficiently explained by the thermally-activated hopping conduction ($\log \rho \propto T^{-1}$), variable-range hopping conduction ($\log \rho \propto T^{-0.25}$), or tunneling conduction through vibrating barrier ($\log \rho \propto T$), as a linear relation could not be obtained in a wide range of temperatures for any of these plots. However, as the general shape of the resistivity curve was similar to the lightly doped samples of $Na_{1-x}Sr_xNbO_3$ (x=0.10 and 0.15) [9], the resistivity behavior observed in $Na_{1-x}Ln_xNbO_3$ may be characteristic behavior of lightly-doped

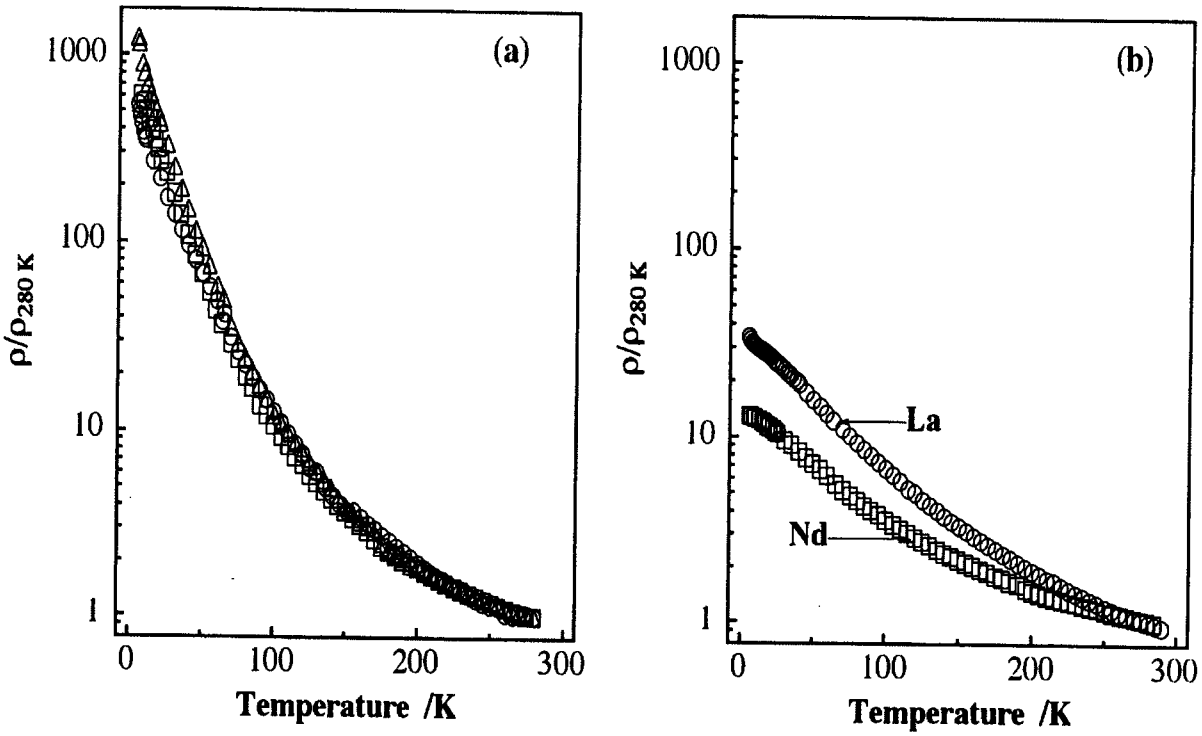

Fig.3 The temperature dependence of normalized resistivity for (a) x = 0.05 and (b) x = 0.10 with Ln=La (circles), Nd (squares), and Sm (triangles).

niobates with distorted perovskite structures. Note that the formal valence of the samples prepared in this study (Table II, $Nb^{4.92+}$ - $Nb^{4.82+}$) are comparable to those of $Na_{1-x}Sr_xNbO_3$ (x=0.10 and 0.15) [9].

No apparent influence on the Ln species to the electrical properties was observed, even though a monotonous change in the structure was observed with the different Ln. This suggests that the semiconducting behavior in lightly-doped $NaNbO_3$ is influenced mainly by the carrier concentration, and the effect by the structural parameters is weak. It is noted that a similar weak dependency of the Ln species to the electrical properties was observed in reduced niobates with a layered-perovskite structure [19].

CONCLUSIONS

Single-phase samples of polycrystalline $Na_{1-x}La_xNbO_3$ (x=0.05, 0.10), $Na_{1-x}Nd_xNbO_3$ (x=0.05, 0.10) and $Na_{1-x}Sm_xNbO_3$ (x=0.05) were obtained by the solid-state reactions under inert atmosphere. The *a/b* axis ratios obtained from Rietveld analysis approached to unity with the increase in x, indicating that the structure of $Na_{1-x}Ln_xNbO_3$ is approaching to a tetragonal structure. An increase in the unit-cell volume with the increase in x was observed for all of the single-phase samples obtained, which was attributed to the larger ionic radius of Nb^{4+}. All of the samples showed semiconducting properties. No clear influence of the Ln species on the semiconducting behavior was observed, despite the variation of their structures.

ACKNOWLEDGMENTS

One of the authors (YS) thanks Advanced Research Center for Science and Engineering, Waseda University for the financial support as Individual Research. This work was financially supported in part by the Grant-in-Aid for JSPS Fellows (No. 5727) from the Ministry of Education, Science, Sports, and Culture.

REFERENCES

1. J.B. Goodenough, Prog. Solid State Chem., **5**, 145 (1972).

2. P.A. Cox, *Transition Metal Oxides*, Clarendon Press, Oxford, 1992.

3. C.N.R. Rao and B. Raveau, *Transition Metal Oxides*, VCH, 1995.

4. D. Ridgley and R. Ward, J. Am. Ceram. Soc., **77**, 6132 (1955).

5. B. Hessen, S.A. Sunshine, T. Siegrist and R. Jimenez, Mater. Res. Bull., **26**, 85 (1991).

6. K. Isawa, J. Sugiyama, K. Matsuura, A. Nozaki and H. Yamauchi, Phys. Rev. B, **47**, 2849 (1993).

7. R.R. Kreiser and R. Ward, J. Solid State Chem., **1**, 368 (1970).

8. M.T. Casais, J.A. Alonso, I. Rasines and M.A. Hidalgo, Mater. Res. Bull., **30**, 201 (1995).

9. B. Ellis, J. Doumerc, P. Dordor, M. Pouchard and P. Hagenmuller, Solid State Commun., **51**, 913 (1984).

10. E.M. Kopnin, S.Ya. Istomin, O.G. D'yachenko, E.V. Antipov, P. Bordet, J.J. Capponi, C. Chaillout, M. Marezio, S.de Brion, and B. Souletie, Mater. Res. Bull., **30**, 1379 (1995).

11. A.M. Abakumov, R.V. Shpanchenko and E.V. Antipoc, Mater. Res. Bull., **30**, 97 (1995).

12. W. Sugimoto, T. Tahara, Y. Sugahara and K. Kuroda, in *Solid State Chemistry of Inorganic Materials*, edited by A. Jacobson, P. Davies, T. Vanderah and C. Torardi (Mater. Res. Soc. Proc. **453**, Boston, MA 1997), p. 361-366.

13. For example; (a) D.A. Maclean, H.-K. Ng and J.E. Greedan, J. Solid State Chem., **30**, 35 (1979); (b) J.E. Greedan, J. Less-Common Metals, **111**, 335 (1985); (c) D.A. Crandles, T. Timusk, J.D. Garret and J.E. Greedan, Physica C, **201**, 407 (1992).

14. F. Izumi, in *The Rietveld Method*, edited by R.A. Young, (Oxford University Press, Oxford 1993), p. 236-253.

15. Y.I. Kim and F. Izumi, J. Ceram. Soc. Jpn. **102**, 401 (1994).

16. R.D. Shannon, Acta Cryst., **A32**, 751 (1976).

17. A.C. Sakowski-Cowley, K. Lukaszewicz and H. Megaw, Acta. Cryst., **B25**, 851 (1969).

18. K. Ishikawa, G. Adachi and J. Shiokawa, Bull. Chem. Soc. Jpn., **55**, 3317 (1982).

19. D. Hamada, W. Sugimoto, Y. Sugahara and K. Kuroda, J. Ceram. Soc. Jpn, **105**, 284 (1997).

May 1999

ELSEVIER

Materials Letters 39 (1999) 184–187

MATERIALS LETTERS

www.elsevier.com/locate/matlet

Synthesis of reduced layered titanoniobates $KTi_{1-x}Nb_{1+x}O_5$

Wataru Sugimoto [a], Naritoshi Hirota [a], Ken Mimuro [a], Yoshiyuki Sugahara [a,*], Kazuyuki Kuroda [a,b]

[a] *Department of Applied Chemistry, School of Science and Engineering, Waseda University, Ohkubo-3, Shinjuku-ku, Tokyo 169-8555, Japan*

[b] *Kagami Memorial Laboratory for Materials Science and Technology, Waseda University, Nishiwaseda-2, Shinjuku-ku, Tokyo 169-0051, Japan*

Received 15 October 1998; accepted 11 December 1998

Abstract

Polycrystalline samples of $KTi_{1-x}Nb_{1+x}O_5$ ($x = 0.1$, 0.2, 0.3) were synthesized by solid-state reactions. The synthesized compounds were blue-colored, suggesting reduced oxidation states. Single phase $KTi_{1-x}Nb_{1+x}O_5$ was obtained for $0 \leq x < 0.2$, suggesting that the solubility limit is between $x = 0.2$ and 0.3. The reduced oxides exhibited semiconducting behavior.

Keywords: Titanoniobate; Reduced oxidation state; Semiconducting behavior

1. Introduction

Reduced niobates with layered-perovskite structures show electrical properties ranging from semiconducting, metallic, and even superconducting [1–5]. As sufficient dt_{2g}–$p\pi$ orbital overlap is crucial for electrical conduction, it is important to take into consideration the connectivity of the octahedra. In the case of the layered-perovskite structures, corner-sharing octahedra spread over two directions. On the other hand, many structures consisting of corner-sharing octahedra in one direction and edge-sharing octahedra in another direction are known [6,7]. Potassium molybdenum oxide, K_xMoO_3 is one of these oxides, and exhibits high conductivity [8–10].

There are a variety of titanates, niobates, and titanoniobates possessing corner-sharing octahedra in only one direction, e.g., $Na_2Ti_3O_7$, $KTiNbO_5$, KNb_3O_8 [6]. The schematic structure of $KTiNbO_5$ is shown in Fig. 1 as an example, showing the different connectivities of the octahedra. These oxides may be good candidates for studying the structure/electrical property relation in low-dimensional structures, as the octahedra connectivity is similar to that of K_xMoO_3. However, the synthesis of these oxides possessing reduced oxidation states have not been reported so far. Based on the successful report of a homologous system $K_{1-x}Ti_{1-x}Nb_{1+x}O_5$ (d^0 state) [11,12], the preparation of the solid solution $KTi_{1-x}Nb_{1+x}O_5$ (d^0–$d^{0.5}$ state) is thought to be possible. We report here on the syntheses of reduced titanoniobates which possess a layered structure different from the layered-perovskite structures.

2. Experimental

$KTiNbO_5$ was synthesized by the solid-state reaction of stoichiometric amounts of K_2CO_3, TiO_2 and

* Corresponding author

00167-577X/99/$ - see front matter
PII: S0167-577X(99)00003-8

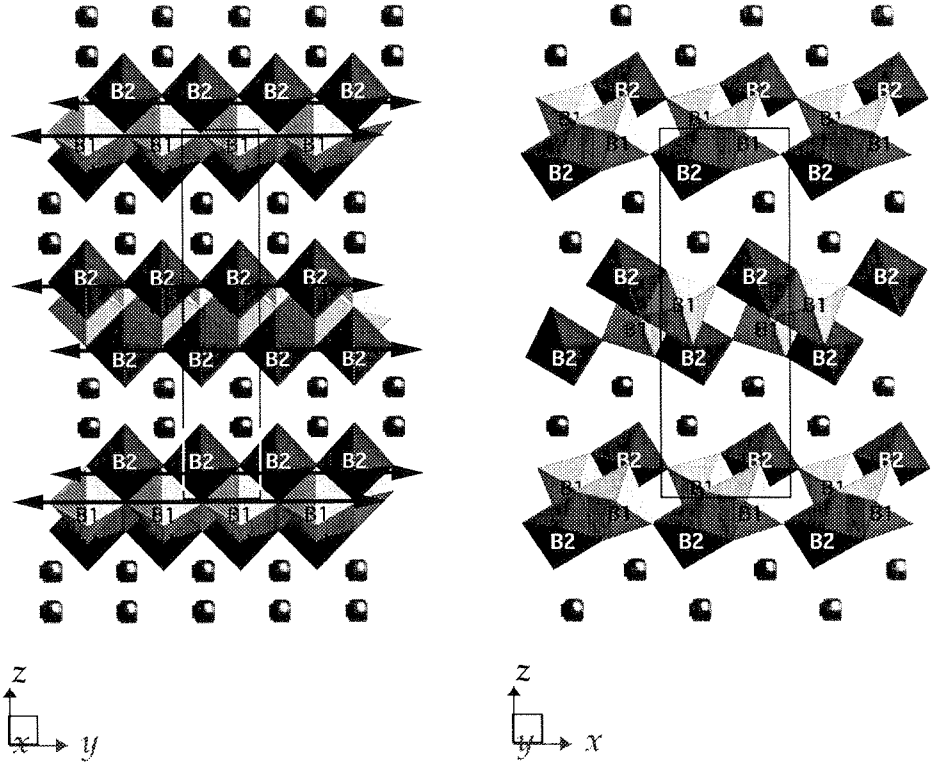

Fig. 1. Schematic structure of $KTiNbO_5$. The arrows indicate the corner-sharing octahedra along the *y*-axis. The light- and dark-shaded octahedra represent the octahedra with the B_1 and B_2 atom at the central position, respectively. The circles represent K ions.

Nb_2O_5 under an ambient atmosphere at 1100°C for 10 h [11]. $KNbO_3$ was synthesized by the solid-state reaction of stoichiometric amounts of K_2CO_3 and Nb_2O_5 under an ambient atmosphere at 1000°C for 1 h. Polycrystalline samples with nominal compositions of $KTi_{1-x}Nb_{1+x}O_5$ ($0 \leq x \leq 0.3$) were synthesized from pelletized mixtures of appropriate amounts of $KTiNbO_5$, $KNbO_3$, Nb_2O_5 and Nb metal. The syntheses were performed under Ar atmosphere in order to prevent oxidation. The pelletized mixtures were fired under Ar atmosphere for 10 h at 1000°C followed by firing at 1100°C for 20 h. The samples were ground and pelletized after every 10-h firing to ensure homogeneity.

Crystalline phases were identified using a Mac Science MXP^3 diffractometer (monochromated Cu Kα radiation). Crystallographic data were obtained by the Rietveld analysis program RIETAN [12,13]. Inductively coupled plasma emission spectroscopy (ICP) (Nippon Jarrel Ash ICAP575Mark II) was used to determine the cation ratios of the products. For the ICP measurements, samples were decomposed in a mixture of HF, H_2SO_4 and HNO_3 by heating at 200°C for at least 2 h. The solution was then measured up with a mixed solution of HNO_3, $(NH_4)_2C_2O_4$ and distilled H_2O. Electron-spin resonance (ESR) spectra were recorded with a JEOL RE2XG spectrometer at room temperature. Standard dc four-probe method was used to collect resistivity data.

3. Results and discussion

The compositional analysis showed that the cation ratios were consistent with the nominal ones for all compositions. Thus, the discussion hereon will be based on the assumption that the formal *d*-electron state was preserved during synthesis. The presence of reduced oxidation states was also confirmed by

the color change (light blue to dark blue with the increase in x) and the appearance of paramagnetic signals in the ESR spectrum for $x = 0.2$. We could not determine which transition metal was reduced from the ESR spectrum. The samples were stored in an evacuated desiccator since the samples gradually lost their color when kept in air.

The XRD patterns for $x = 0$–0.3 are shown in Fig. 2. The XRD measurements were carried out under ambient atmosphere as the degradation of the sample during the course of measurement was negligible. For $x = 0.2$, the XRD patterns were indexed based on an orthorhombic symmetry, consistent with the end-member $KTiNbO_5$. On the other hand, a few peaks besides the intended phase were present in the XRD pattern for $x = 0.3$. A single phase for $x = 0.3$ could not be obtained even with repeated firing. Therefore, the solubility limit for $KTi_{1-x}Nb_{1+x}O_5$ is between $x = 0.2$ and 0.3 under the present synthetic conditions. This solubility limit is comparable to the solubility limit reported for $K_{1-x}Ti_{1-x}Nb_{1+x}O_5$ by Takeda et al. [12].

As the XRD patterns suggested the formation of a solid solution for $x = 0.2$, the same space group as the parent compound, $KTiNbO_5$ (Pnma) [14], was adopted for Rietveld analysis. The obtained lattice parameters are shown in Table 1. The lattice parameters for $KTiNbO_5$ were consistent with earlier studies [11,14]. The monotonous variation of the lattice parameters as a function of x verifies the formation of a solid solution for $0 \leq x \leq 0.2$. The distribution of the transition metals over the sites B_1 and B_2 was studied by allowing the occupation factors of Ti and Nb to vary in the Rietveld refinement. The Ti fraction of occupancy in sites B_1 (τ_1) and B_2 (τ_2) are given in Table 1. A preferential distribution of the Ti ions at the B_1 site and Nb ions at the B_2 site was

Table 1
Crystallographic parameters for $KTi_{1-x}Nb_{1+x}O_5$

x	Lattice parameter (nm)			Ti fraction of occupancy	
	a	b	c	τ_1	τ_2
0	0.64433(1)	0.379674(1)	1.83967(3)	0.80(1)	0.20(1)
0.1	0.64615(7)	0.37945(4)	1.8572(2)	0.71(1)	0.19(1)
0.2	0.64787(4)	0.37978(2)	1.86809(9)	0.68(2)	0.12(2)

Number in parenthesis represent estimated standard deviation. τ_1 and τ_2 represent the Ti fraction of occupancy in sites B_1 and B_2.

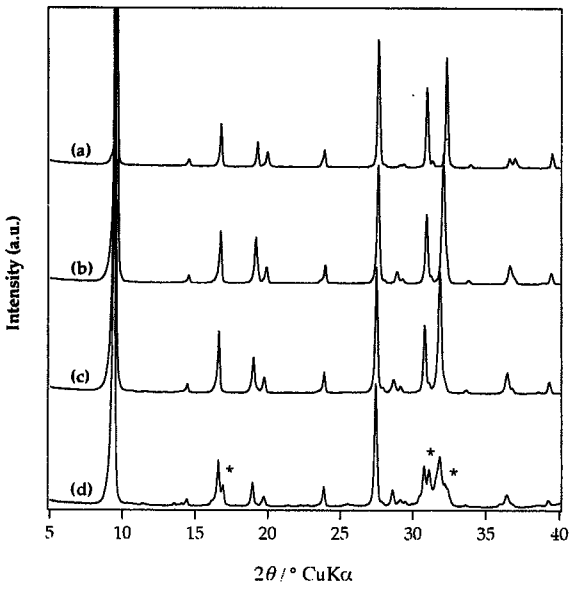

Fig. 2. The XRD patterns for $KTi_{1-x}Nb_{1+x}O_5$ with $x =$ (a) 0, (b) 0.1, (c) 0.2 and (d) 0.3. Asterisks represent unidentified peaks.

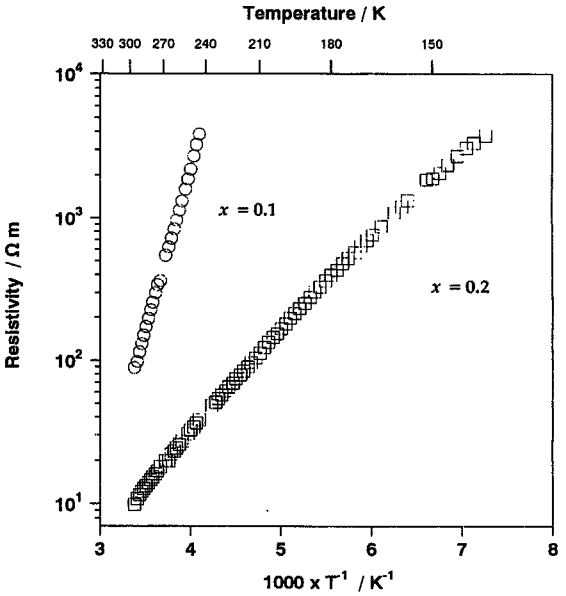

Fig. 3. The temperature dependence of resistivity for $KTi_{1-x}Nb_{1+x}O_5$ with $x = 0.1$ (circles) and 0.2 (squares).

observed for all x. Similar results were reported for $KTiNbO_5$ and $K_{0.85}Ti_{0.85}Nb_{1.25}O_5$ (d^0 state compounds) [11]. It was suggested that the smaller Ti^{4+} ion preferably occupies the B_1 site as it is more repelled from its five-neighboring octahedra compared to three for the B_2 site [11]. Since the structure of the compounds synthesized in this study is analogous to $KTiNbO_5$, the crystallographic environment of the octahedra are unaffected. Therefore it is reasonable that the Ti^{4+} ions mainly occupy the B_1 site as the ionic radius is smaller than Ti^{3+}, Nb^{5+} and Nb^{4+} [12].

The temperature dependencies of the resistivity for $x = 0.1$ and 0.2 are shown in Fig. 3. Data above 10 K Ωm could not be collected as it exceeded our apparatus limits. Both the samples of $x = 0.1$ and 0.2 showed semiconducting behavior. The resistivity behavior agreed with the log ρ–T^{-1} law, indicating that the electrical properties are dominated by the thermally activated hopping electrons. The activation energy for hopping calculated from the slope of the log ρ–T^{-1} plot was 0.4 and 0.1 eV for $x = 0.1$ and 0.2, respectively.

In summary, reduced oxidation states were introduced into a low-dimensional structure possessing corner-sharing octahedra in only one direction. Single-phase samples of titanoniobates possessing reduced oxidation states, $KTi_{1-x}Nb_{1+x}O_5$ ($x = 0.1$ and 0.2), were obtained by the solid-state reaction under an inert atmosphere. The reduced compounds possessed the same structure as $KTiNbO_5$. The monotonous change in the lattice parameters suggested the formation of a solid solution for $0 \leq x \leq 0.2$. The resistivity of the samples showed semiconducting behavior.

Acknowledgements

One of the authors (YS) thanks Advanced Research Center for Science and Engineering, Waseda University for the financial support as Individual Research. This work was financially supported in part by the Grant-in-Aid for JSPS Fellows (No. 5727) from the Ministry of Education, Science, Sports, and Culture.

References

[1] M.R. Palacín, M. Lira, J.L. Garcia, M.T. Caldés, N. Casañ-Pastor, A. Fuertes, P. Gómez-Romero, Mater. Res. Bull. 31 (1996) 217.
[2] D. Hamada, M. Machida, Y. Sugahara, K. Kuroda, J. Mater. Chem. 6 (1996) 69.
[3] D. Hamada, W. Sugimoto, Y. Sugahara, K. Kuroda, J. Ceram. Soc. Jpn. 105 (1997) 284.
[4] Y. Takano, S. Takayanagi, S. Ogawa, T. Yamadaya, N. Môri, Solid State Commun. 103 (1997) 215.
[5] H. Fukuoka, T. Isami, S. Yamanaka, Chem. Lett. (1997) 703.
[6] C.N.R. Rao, B. Raveau, Transition Metal Oxides, VCH Publishers, 1995, p. 103.
[7] A.F. Wells, Structural Inorganic Chemistry, Oxford Univ. Press, 1984, p. 218.
[8] A. Wold, W. Kunnmann, R.J. Arnott, A. Ferretti, Inorg. Chem. 3 (1964) 545.
[9] J. Graham, A.D. Wadsley, Acta. Crystallogr. 20 (1966) 93.
[10] M. Ghedira, J. Chenavas, M. Marezio, J. Marcus, J. Solid State Chem. 57 (1985) 300.
[11] H. Rebbah, G. Desgardin, B. Raveau, J. Solid State Chem. 31 (1980) 321.
[12] Y. Takeda, R. Kanno, S. Kawatsu, O. Yamamoto, J. Mater. Sci. Lett. 5 (1986) 73.
[13] F. Izumi, The Rietveld Method, Oxford Univ. Press, 1993, p. 236.
[14] A.D. Wadsley, Acta Crystallogr. 17 (1964) 623.

メトキシ修飾した層状ペロブスカイト $HLaNb_2O_7$ における光化学的還元

Introduction

遷移金属元素は価数を比較的容易に制御することができ、価数変化によって特有の色を呈すことが知られている。遷移金属元素を含む化合物の中には光エネルギーによって可逆的な色の変化を示すものもある。

Fujishima らは Nb_2O_5 をエタノール蒸気中で紫外光照射することで、低酸化 Nb に起因する青色の着色が観測されることを報告している[1]。この反応は、エタノールが還元剤として作用し、低酸化 Nb が生成したために起こると考えられている。このような Nb_2O_5 の光着色は表面吸着したアルコールによる光還元反応と見なすことができる。

イオン交換性層状ペロブスカイトの一種である $M[A_{n-1}Nb_nO_{3n+1}]$ はペロブスカイト層 $[A_{n-1}Nb_nO_{3n+1}]$ が層間カチオン M を介して積み重なり、層構造を形成する[2~5]。この層間カチオンは様々なアルカリ金属（H^+、Li^+、Na^+、K^+、Rb^+、Ce^+）でイオン交換が可能であり、中でも層間カチオンがプロトンの場合は、興味深い性質を示す。例えば、光触媒として層状ペロブスカイトを用いる場合は、層間で電荷移動が効率的に行われ、従来の光触媒として用いられている TiO_2 よりも優れた触媒能を示すことが知られている[6]。また、H 型層状ペロブスカイトは、層間に様々な有機分子を取り込み、無機-有機複合体を形成することができる[7~11]。特にメタノールとの反応では、層間でメトキシ基を形成すると報告されている[12]。そのためメタノールとの反応によって得られる生成物への光照射は、先の光触媒能と同様に電荷移動が効率的に行われ、Nb_2O_5 とは異なった光還元反応が期待できる。

低酸化 Nb 酸化物は、導電性を示し、その電気的・磁気的性質は多様性に富んでいる。低酸化 Nb の生成にはキャリアードープが不可欠であり、これまでに様々な方法でキャリアードープが試みられてきた。2 層構造（n=2）である $MLaNb_2O_7$ においては、化学的、電気化学的還元、水素還元などによるキャリアードープが報告されている[13、14]。また、Hamada らは 3 層構造の A サイト元素を希土類元素で置換した $KCa_{2-x}La_xNb_2O_{10}$（RE=La、Ce、Nd、Sm、Gd）の合成およびその電気的性質について調査し、置換量の増加に伴って導電性も向上すると報告している[15、16]。また最近、$KLaNb_2O_7$、$KCa_2Nb_3O_{10}$ を n-ブチルリチウム、n-ヘキサン溶液に浸すことによって、層間へのトポタクティックな Li のインターカレーション反応が起こり、Li 量の増加に伴って絶縁体から金属、さらに $KCa_2Nb_3O_{10}$ においては超伝導体へ変化するという興味深い物性も報告されている[17~19]。このように層状ペロブスカイトにおけるキャリアードープは物性変化を伴い、新規機能性材料としての可能性を秘めている。

そこで本研究では新たなキャリアードープの方法として、層状ペロブスカイトとメタノールとの反応によって得られる生成物の光化学的還元を調査することを目的とする。今回用いる層状ペロブスカイトは、Sato ら[20]によって詳細に構造解析がなされている $HLaNb_2O_7$ とする。

Experimental Section

試薬

$RbLaNb_2O_7$の合成の原料として、Rb_2CO_3（添川理化学）、La_2O_3（フルウチ化学）、Nb_2O_5（和光試薬）を用いた。なお、La_2O_3は炭酸化、水酸化を防ぐため、1100℃、1時間以上仮焼を行った。

アルコールはメタノール；CH_3OH（和光純薬、特級）を用いた。

$HLaNb_2O_7$の合成

$RbLaNb_2O_7$は既報に従い、Rb_2CO_3、La_2O_3、Nb_2O_5の混合物（Rb_2CO_3は焼成中の揮発を考慮して30%過剰）を、1100℃、48時間（24時間ごとに粉砕）空気中で焼成し、未反応分のRbを大過剰の水で洗浄した後、120℃で乾燥することで得た。生成物はXRD分析より全てのピークは斜方晶として帰属でき、Reatvelt解析からも単一相であることを確認した（格子定数；a=5.4499(2)、b=21.9997(9)、c=5.499(2)、空間群；Imma）。またICP発光分析からそれぞれの元素比は組成比通りであった。

得られた$RbLaNb_2O_7$を6M-硝酸水溶液中で60℃、72時間撹拌し（24時間ごとに硝酸水溶液を交換）、その後、遠心分離、洗浄、乾燥することでプロトン交換体を得た。乾燥条件は、無水和物（$HLaNb_2O_7$）は120℃乾燥、水和物（$HLaNb_2O_7 \cdot xH_2O$）は風乾とした。プロトン交換体$HLaNb_2O_7$の生成はXRD分析、ICP発光分析により確認した。XRD分析より$HLaNb_2O_7$は正方晶に帰属され、a=0.389nm、c=1.05nmとなり、既報の値とほぼ一致した。また、ICP発光分析より、酸処理によってRbが100%溶出していることを確認した。水和物におけるTG分析から、含水量は3.6mol／$HLaNb_2O_7$であり、既報の値（3.4）とほぼ一致した。

$HLaNb_2O_7$とメタノールとの反応

$HLaNb_2O_7 \cdot xH_2O$をメタノール水溶液中（10mass/%H_2O）で室温、7日間撹拌し、遠心分離、乾燥（室温）する事により試料を得た。得られた試料はXRD分析の結果、基本面間隔の増大が見られた。TG-DTA分析より、300℃以上で発熱を伴った重量減少が観測されメタノールが層間で強い結合を形成していることがわかった。また、赤外吸収スペクトル（Perkin-Elmer FTIR-1640、KBr法）から、既報と同様なスペクトルが得られた。以上よりメタノールは層間でメトキシ基を形成していることを確認した。

光化学反応

光源には500W水銀ランプ（Ushio USH-500SC）を用いた。XRD分析用の試料版（0.2mm）に試料を詰め、光源の筒先から100mmの位置に置き、空気中で5分間光照射した試料について、積分球を用いて紫外可視吸収スペクトル（Shimazu UV3100PC）を測定した。

光照射によって生成した低酸化ニオブ化合物の磁化率は、SQUID（Quantum Design MPMS7）を用いて測定した。均一に光が当たるように、試料を蒸留済みヘキサンに分散さ

せ、Ar 封入し、マグネティックスターラーで撹拌しながら光源の筒先から 100mm の位置に置き光照射した（5、10 時間）。その後、溶媒除去、減圧乾燥、ペレット成型（2mm×4mm×1.5mm）した試料を測定に用いた。

光照射時間の変化に伴う抵抗変化は 2 端子法で測定した。試料をペレット成型（2mm×4mm×1.5mm）した後、3mm の間隔で端子を銀ペーストで接着し、乾燥後 Ar フローし、一定のサイクルで光照射の ON- OFF を繰り返し、デジタルマルチメーターで抵抗値を観測した。その光照射の際、OFF 後、酸素フローによって酸化させ白色に戻してから次のサイクルを行った。

Results and Discussion

光化学的還元

アルコールとの反応により得られた生成物に光照射したところ、光照射後すぐに濃青色に着色した。Fig.1 に光照射後の紫外可視拡散反射スペクトルを示す。光照射後のスペクトルに見られる 500～800nm にかけての吸収は、8N- HCl 中での Nb^{+4}（$[NbOCl_4]^{2-}$ or $[NbO]^{2+}$）スペクトル [21] に類似の吸収である。これより、光照射後の試料の青色着色は光還元によって生成した低酸化 Nb によるものと考えられる。

光照射によって着色した試料における磁気的性質を SQUID 磁束計を用いて測定した。磁化率の温度依存性を Fig.2 に示す。磁化率は、Curie- Weiss 的挙動を示し、$KLaNb_2O_7$ への Li のインターカレーション反応のような金属転移は見られなかった。

また、定性的ではあるが光照射に伴う抵抗値の変化を観察した。Fig. 3 に光照射時間と抵抗値の変化を示す。光照射時間の増加に伴って、抵抗は急激に減少した。光照射時間が 10 分以上になると抵抗値は飽和する傾向にあり、それ以上光照射時間を延ばしても、抵抗値はほとんど変わらなかった。これより低酸化 Nb はある一定量以上は生成しないものと思われる。

光化学還元メカニズムの検討

光化学還元反応のメカニズムについて検討する。Fig. 3 の光照射サイクルと抵抗値の変化からこの反応は可逆反応ののように思われる。しかし、このサイクルを繰り返し行うと、青色着色を示さなくなる。このように、青色着色を示さなくなるまで太陽光により反応を進行させた（3 週間窓際に放置）試料を劣化試料とする。この劣化試料は、青色着色を示さないため、層間の有機基が光照射によって変化していると思われる。

Fig. 4 に各試料の IR スペクトルを示す。既報より 1130cm^{-1}付近の鋭いピークは層間のメトキシ基に帰属されると考えられているが、劣化試料ではこのピークは消滅した。

また、TG-DTA 分析より、劣化試料では、メトキシ基の燃焼による発熱を伴った重量減少は観測されず、300℃付近からの重量減少量は 2.20%であった。これは、多少の有機の残存を考慮すると $HLaNb_2O_7$ のプロトンの脱離による重量減少量 1.81%とほぼ一致する

（Fig. 5）。

また、劣化前後の試料の XRD パターンを Fig. 6 に示す。劣化試料の基本面間隔は、$HLaNb_2O_7$ の基本面間隔とほぼ等しくなり、メトキシ基の脱離に伴って層間隔が減少していることが分かった。

また、既報において、層状ペロブスカイトの無機骨格について Raman 分析より知見が得られると報告されていることから、Raman 分析を行った。得られた Raman スペクトルを Fig. 7 に示す。メトキシ基に起因するピークは、劣化試料では消滅していることが分かる。また 940～1000cm^{-1} 付近のピークは、層間に向いた短い Nb-O 結合によるものであり、このピークは各試料において若干異なっている（Fig. 8）。既報によると、Nb-O の結合次数の変化によりピークはシフトし、高端数側へのシフトは結合次数の増加、低波数側へのシフト結合次数の減少によるものとされている。$HLaNb_2O_7$ と比較すると、メトキシ基の形成に伴いこのピークが 984、968cm^{-1}に分裂している。これはメトキシ修飾により Nb-O に 2 種類の異なる環境が存在していることを意味しており、これは層間に向いた短い Nb-O の修飾サイトのうち半分しか、メトキシ修飾されないという Takahashi らの結果と一致する。プロトンがそのまま存在しているサイトはメトキシ化による層間隔の増加に伴って、O-H 基の相互作用が弱くなり、Nb-O 結合は二重結合に似た高い結合次数を持つようになり、ピークは高端数側にシフトする。また、メトキシ化されたサイトは Nb-O-C 結合の形成により、Nb-O の結合次数が減少し、ピークが低波数側にシフトする。劣化試料では、さらに、984、968cm^{-1} のピークは減少し、974、955cm^{-1} へと変化している。974cm^{-1} は $HLaNb_2O_7$ と同じであり、メトキシ基の脱離による層間隔の減少に伴い、O-H 基の相互作用が $HLaNb_2O_7$ と同程度になったためと思われる。そして、955cm^{-1} のピークはより低い結合次数、すなわち長い Nb-O 結合の存在を示唆している。これは光照射による層間のメトキシ基の脱離によって酸素欠損が生じたことにより、向かい側の Nb-O 結合が長くなったためと考えられる。

これまでに報告されているアルコールの光分解反応では、アルコールはアルデヒド、二酸化炭素に酸化されるとしている[1、22、23]。そこで、光照射により発生する気体の GC 分析を行ったところ、わずかではあるが、CO_2 の生成が確認された。これより、層間のメトキシ基は何らかの中間体を経て CO_2 まで酸化されていることが示唆される。しかし、ホルムアルデヒドや、メタノールなど、CO_2 以外の確認ができず、詳細なメカニズムは確定できなかった。

Summary

メトキシ修飾した $HLaNb_2O_7$ において光照射によって低酸化 Nb に起因する青色着色を確認した。光照射時間の増加に伴って、電気抵抗値は減少した。光照射後の試料の磁化率は Curie-Weiss 的挙動を示し、金属への転移は観測されなかった。また、光照射により発生する気体から CO_2 の生成が確認された。これより、層間のメトキシ基は何らかの中間体を経て CO_2 まで酸化されていることが示唆される。

References

1)J. N. Yao, B.H. Loo, K.Hashimoto, A. Fujishima, *Ber. Bunsenges. Phys. Chem.*, **96**, 699, (1992).

2) M. Dion, M.Ganne, M.Tournoux, *Rev. Chim. Miner.*, **23**, 61, (1986).

3) M. Dion, M.Ganne, M.Tournoux, *Mater. Res. Bull.*, **16**, 1429, (1981).

4) M. A. Subramanian, J. Gopalakrishnan, A.W. Sleight, *Mater. Res. Bull.*, **23**, 837, (1988).

5) J.Gopalakrishnan, V. Bhat, *Mater. Res. Bull.*, **22**, 413, (1987).

6) 田中　彰, 堂免　一成, *セラミックス*, **31**, 426, (1996).

7) A. J. Jacobson, J. W. Johnson, J. T. Lewandowski, *Mater. Res. Bull.*, **22**, 45, (1987).

8) A. J. Jacobson, J. W. Johnson, J. T. Lewandowski, *Inorg. Chem.*, **24**, 3729, (1985).

9) J.Gopalakrishnan, S. Uma, V. Bhat, *Chem. Mater.*, **5**, 132, (1993).

10) S. Uma, J.Gopalakrishnan, *J. Solid State Chem.*, **102**, 332, (1993).

11) S. Uma, A. R. Raju, J.Gopalakrishnan, *J. Mater. Chem.*, **3**, 709, (1993).

12)S. Takahashi, T. Nakato, S. Hayashi, Y.Sugahara, K.Kuroda, *Inorg. Chem.*, **34**, 5065, (1995).

13) P.Gomez- Romero, M. R. Palacin, N.Casan, A. Fuertes, *Solid State Ionics*, **63- 55**, 424, (1993).

14) M. R. Palacin, M.Lira, J. L. Garcia, M. T. Caldes, N. Casan- Pastor, A. Fuertes, P. Gomez-Romeo, *Mater. Res. Bull.*, **32**, 217, (1996).

15) D. Hamada, M. Machida, Y. Sugahara, K.Kuroda, *J. Mater. Chem.*, **6**, 69, (1996).

16) D. Hamada, W. Sugimoto, Y. Sugahara, K.Kuroda, *J. Ceram. Soc. Jpn.*, **105**, 284, (1997).

17) Y. Takano, S. Takayanagi, S.Ogawa, T. Yamadaya, N. Mori, *Solid State Commun.*, **103**, 215, (1997).

18) Y. Takano, H. Taketomi, H. Tsurumi, T. Yamadaya, N. Mori, *Physica B*, **68-70**, 237, (1997).

19) H. Fukuoka, T.Isami, S. Yamanaka, *Chem. Lett.*, 703, (1997).

20) M. Sato, J. Abo, T. Jin, M. Ohta, *J. Alloys Compd.*, **192**, 81, (1993).

21) V. D. Cozzi, S.Vivarelli, *Anorg. Allg. Chem.*, **279**, 166, (1955).

22) E. M. McCarron,　　, R. H. Staley, A. W. Sleight, *Inorg. Chem.*, **23**, 1043, (1984).

23) S. Yamagata, R. Baba, A. Fujishima, *Bull. Chem. Soc. Jpn.*, **62**, 1004, (1989).

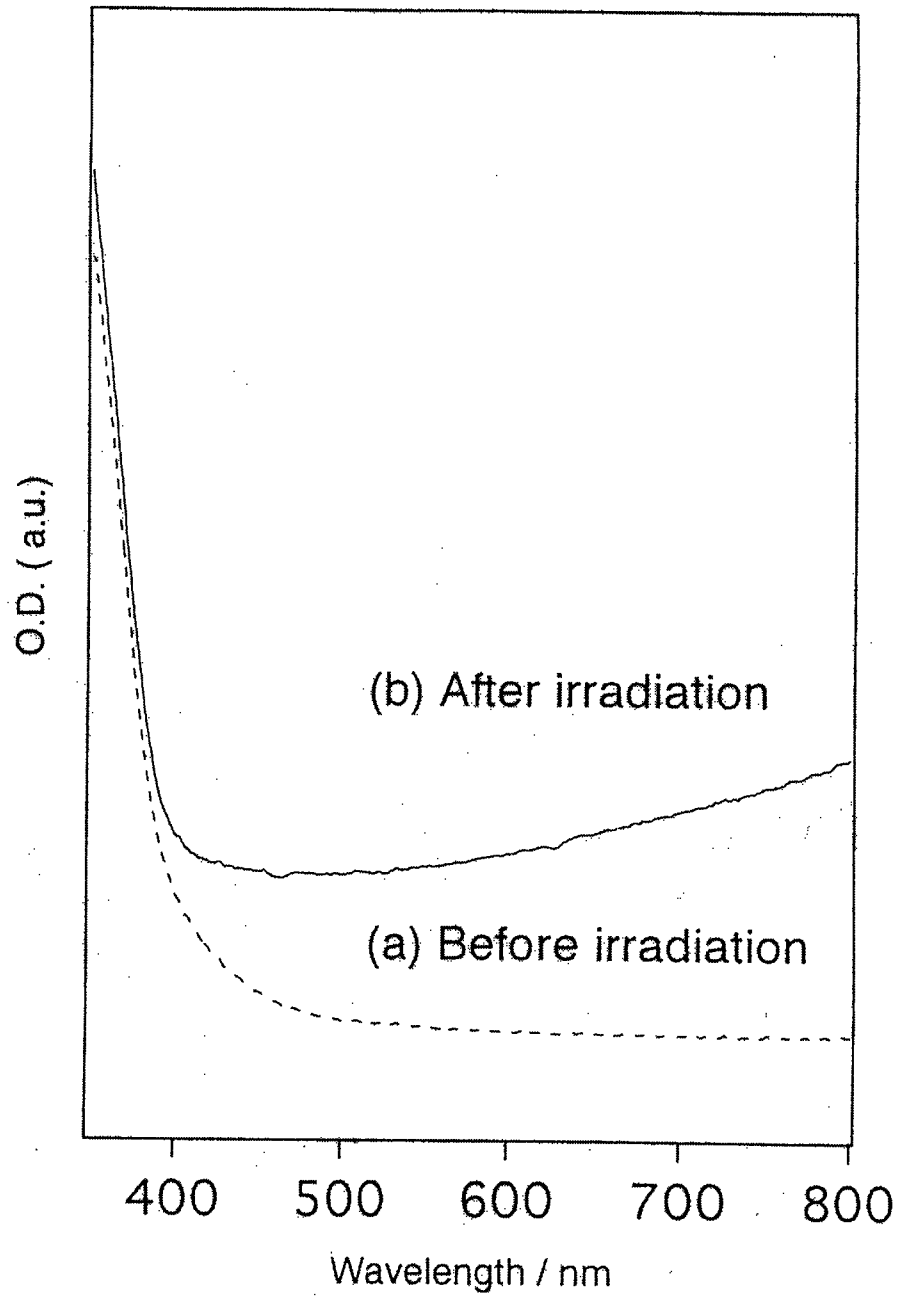

Figure 1. Absorption spectrum of $HLaNb_2O_7$-MeOH (a) before and (b) after irradiation for 5 minutes (Ar flow).

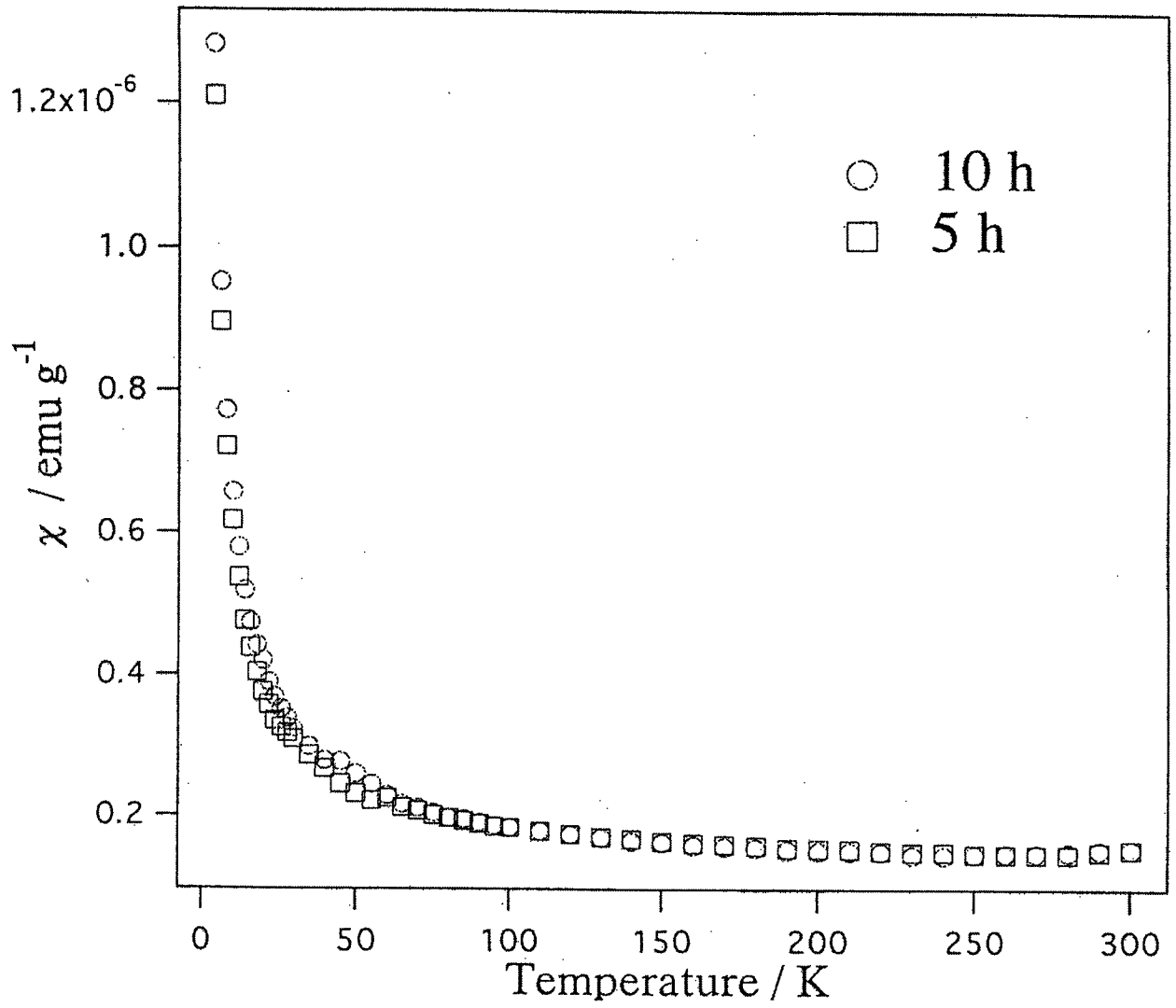

Figure 2. Magnetic susceptibility of photoreduced $HLaNb_2O_7$-MeOH (photoirradiated for 5 and 10 hours).

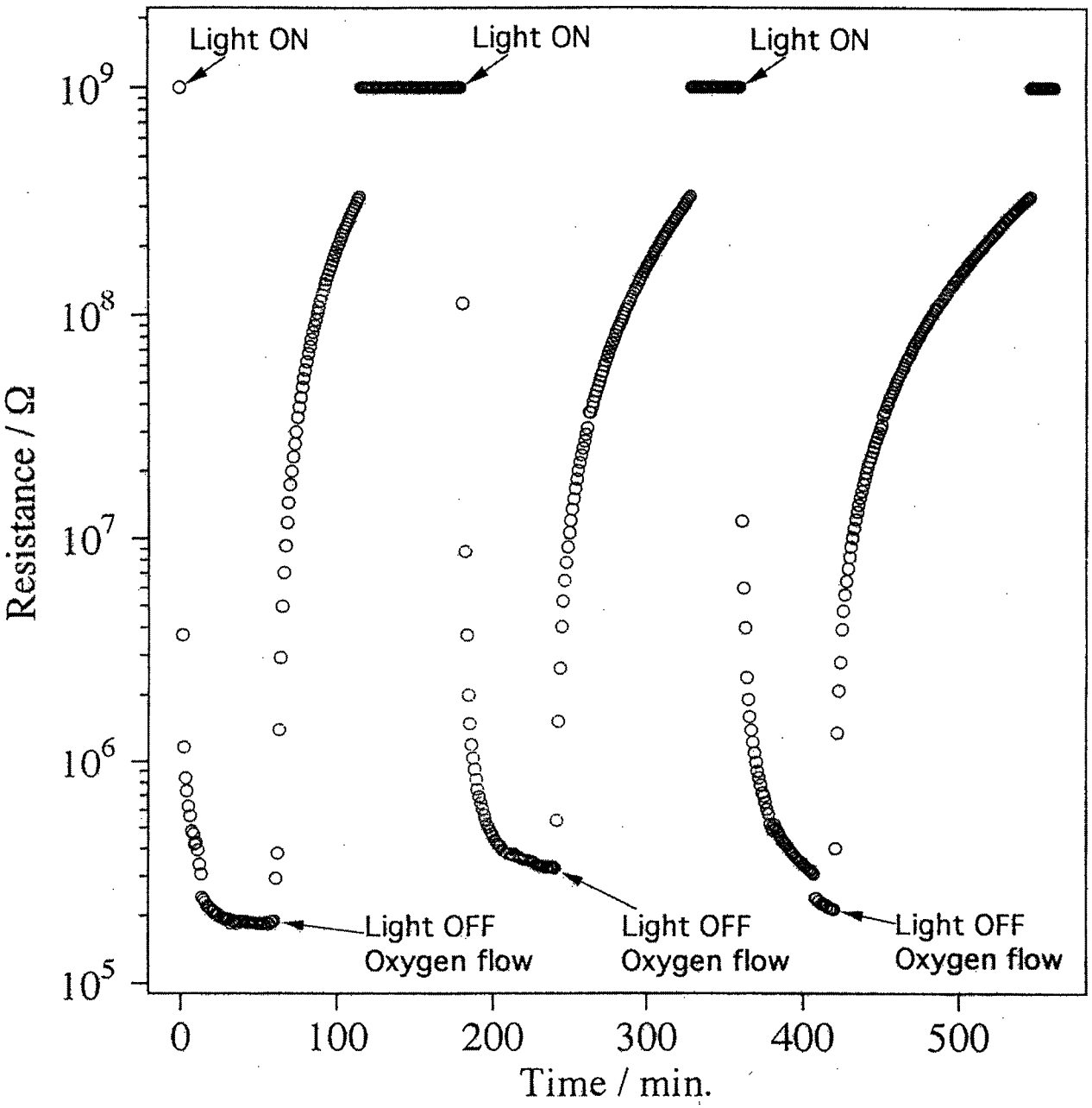

Figure 3. Time dependence of resistance of $HLaNb_2O_7$-MeOH for a cycle of photoirradiation.

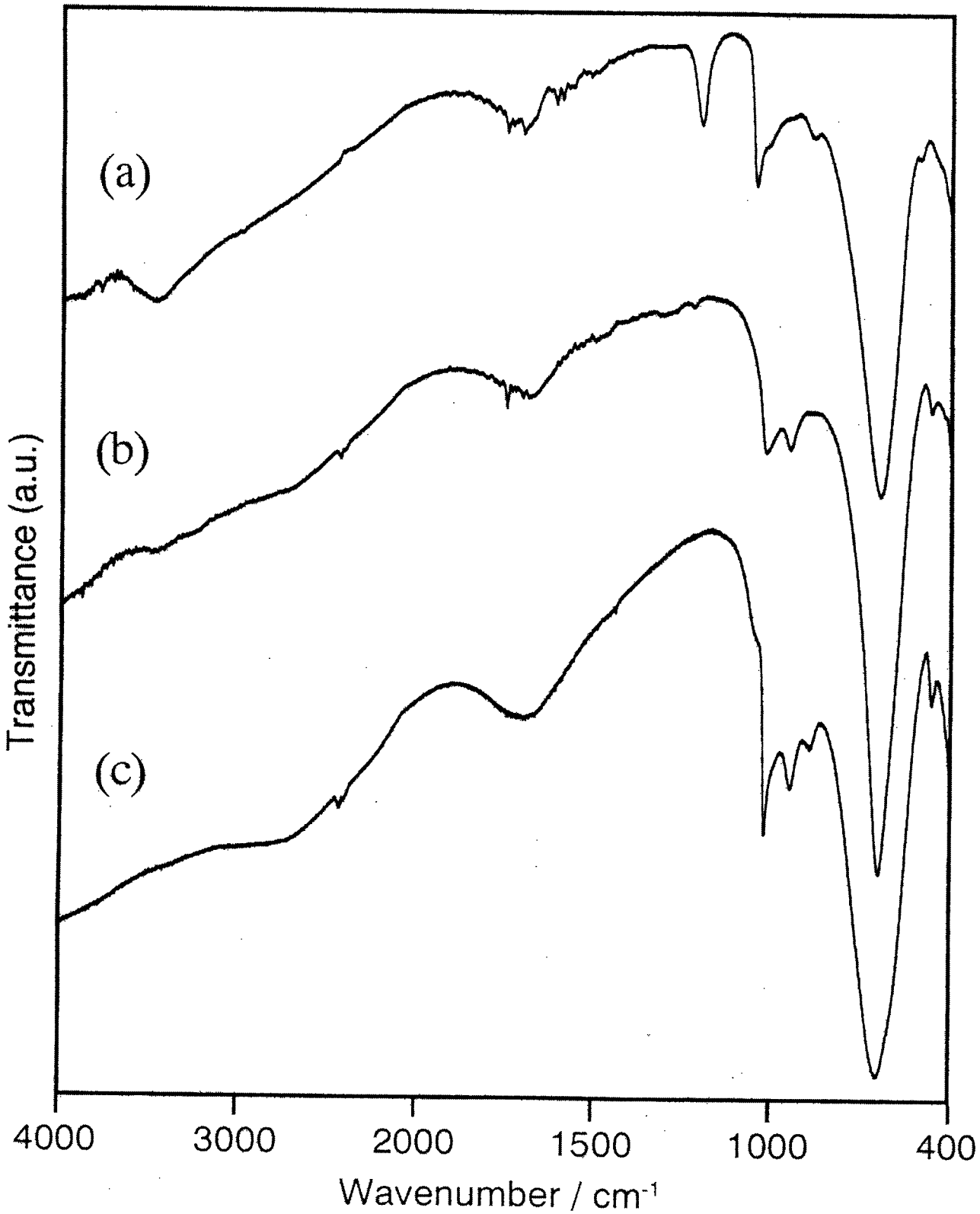

Figure 4. IR spectra of (a) $HLaNb_2O_7$-MeOH as prepared, (b) $HLaNb_2O_7$-MeOH exposed to sun for 3weeks and (c) $HLaNb_2O_7$.

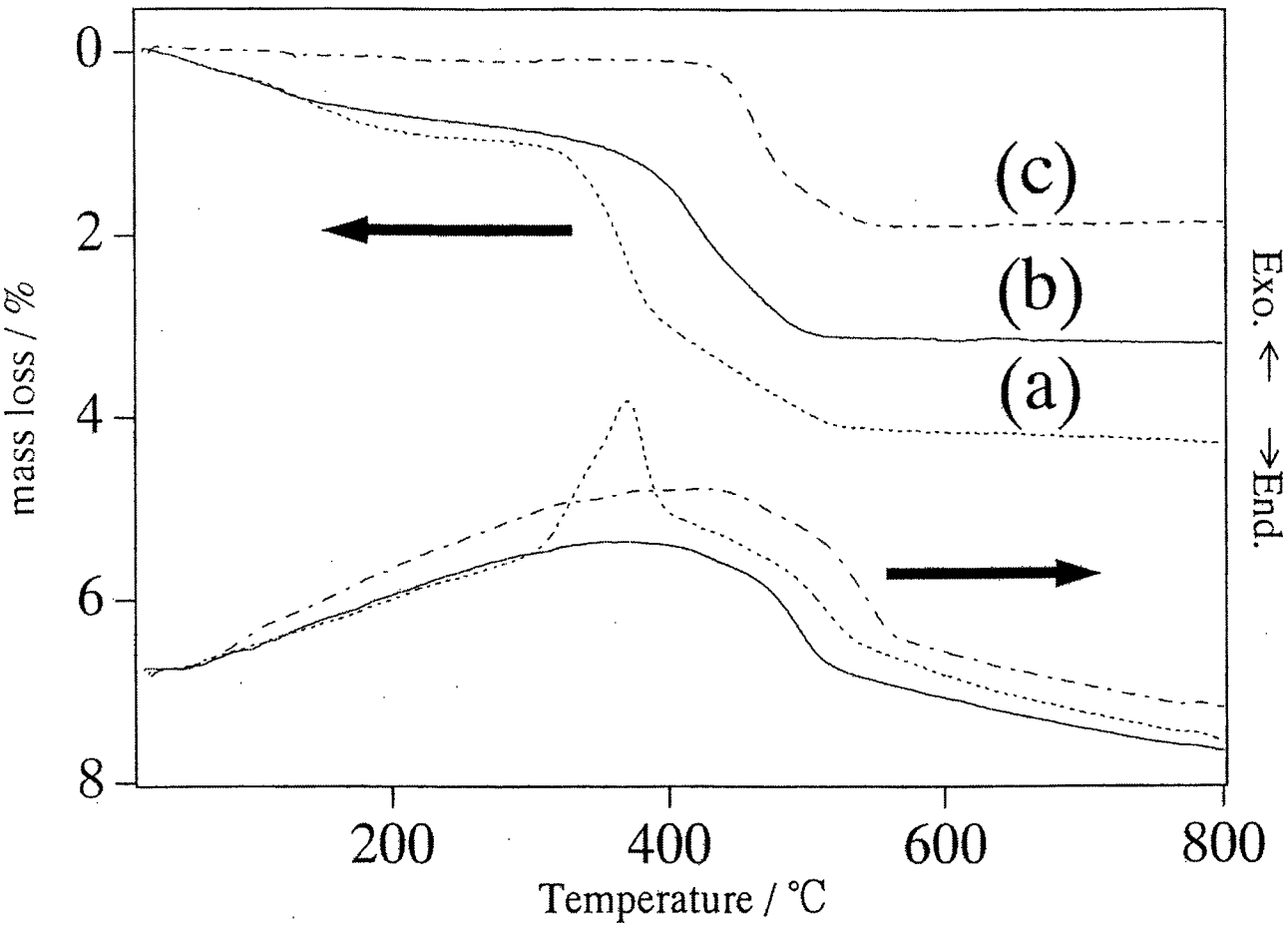

Figure 5. TG-DTA curve of (a) $HLaNb_2O_7$-MeOH, (b) $HLaNb_2O_7$-MeOH exposed to sun for 3 weeks and (c) $HLaNb_2O_7$ exposed to sun for 3 weeks.

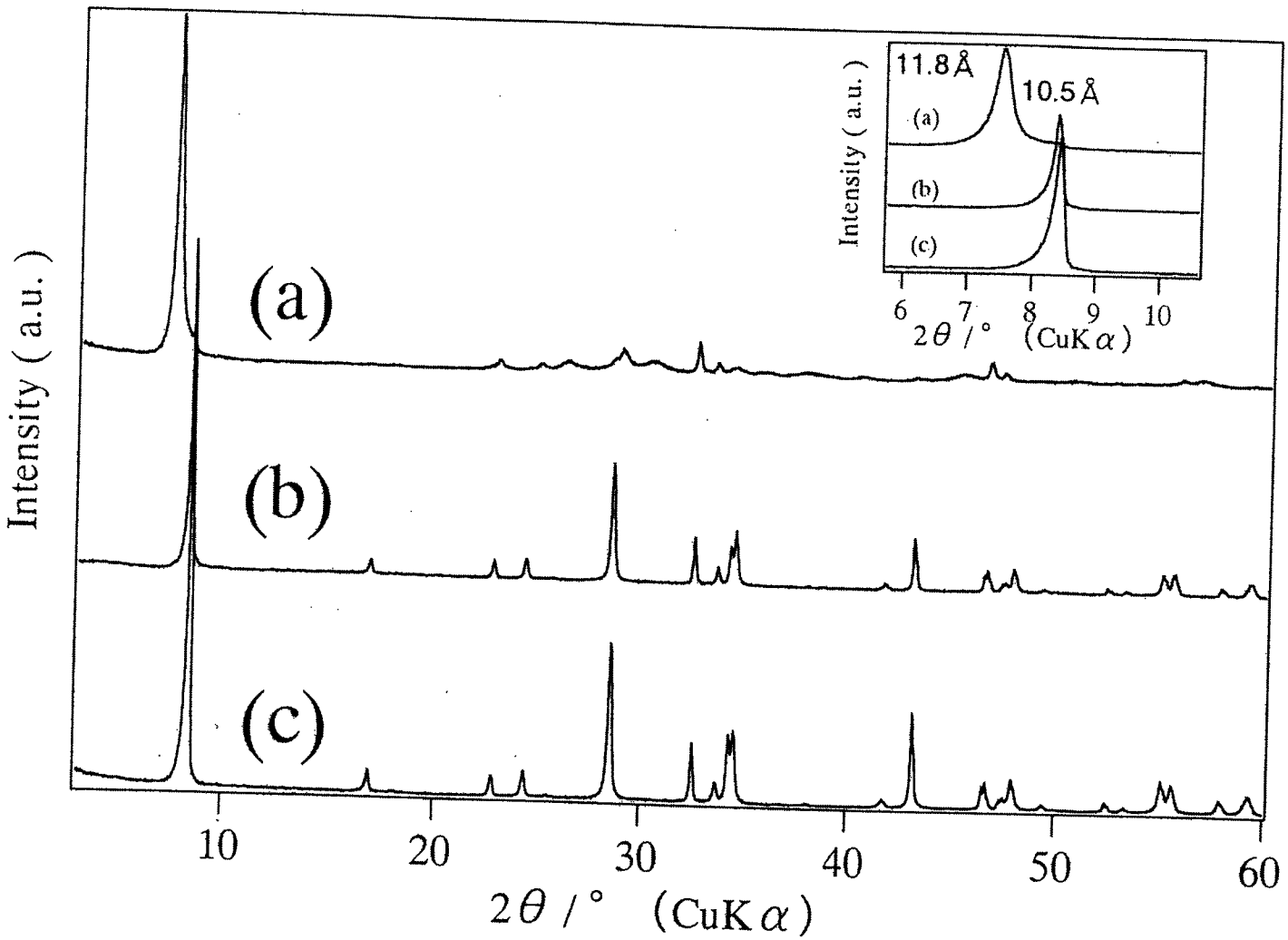

Figure 6. XRD patterns of (a) $HLaNb_2O_7$-MeOH as prepared (room temperature dried sample), (b) $HLaNb_2O_7$-MeOH exposed to sun for 3weeks (120°C dried sample) and (c) $HLaNb_2O_7$ (120°C dried sample).

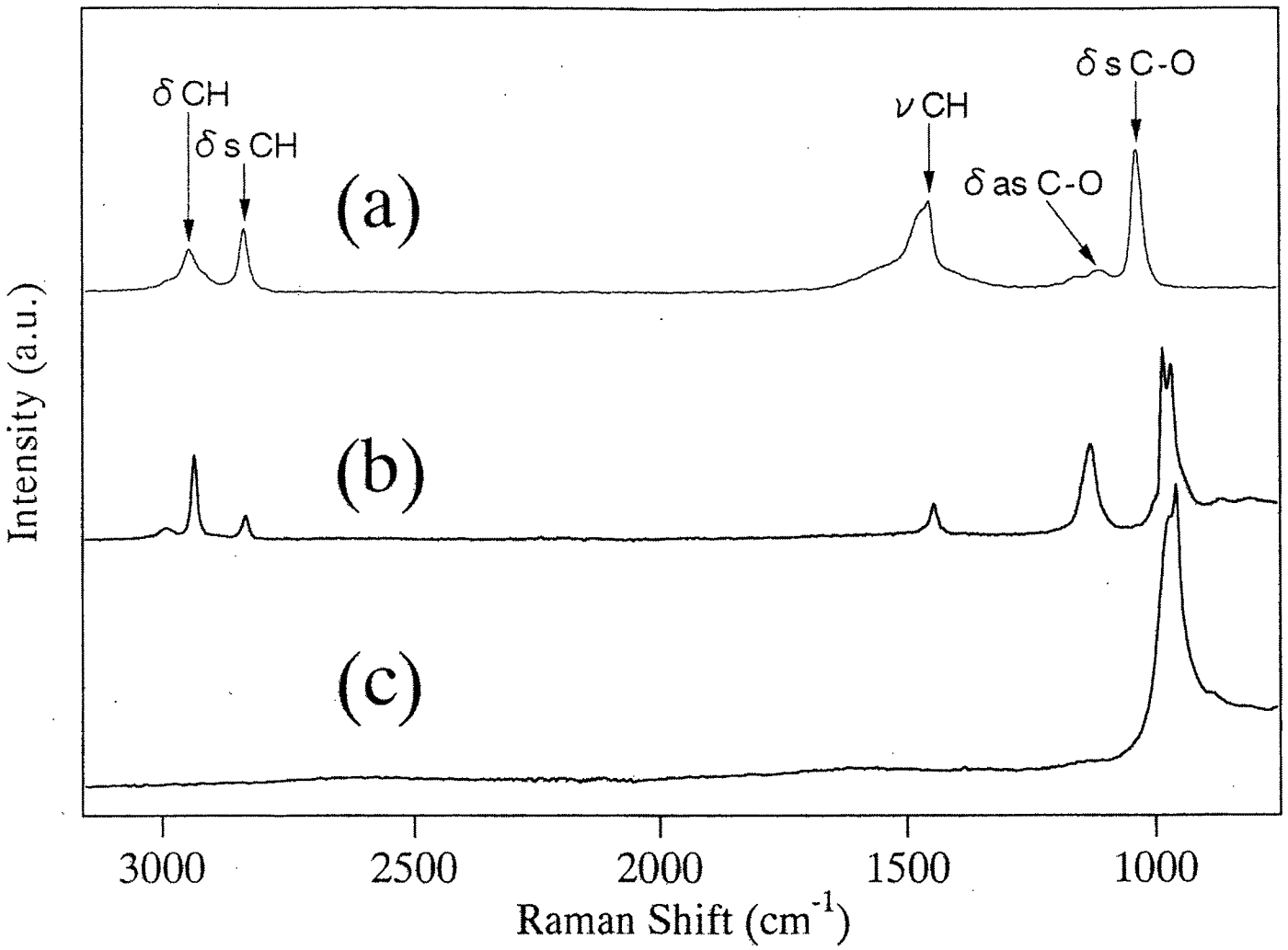

Figure 7. Raman spectra of (a) neat methanol (b) $HLaNb_2O_7$-MeOH as prepared (c) $HLaNb_2O_7$-MeOH exposed to sun for 3weeks.

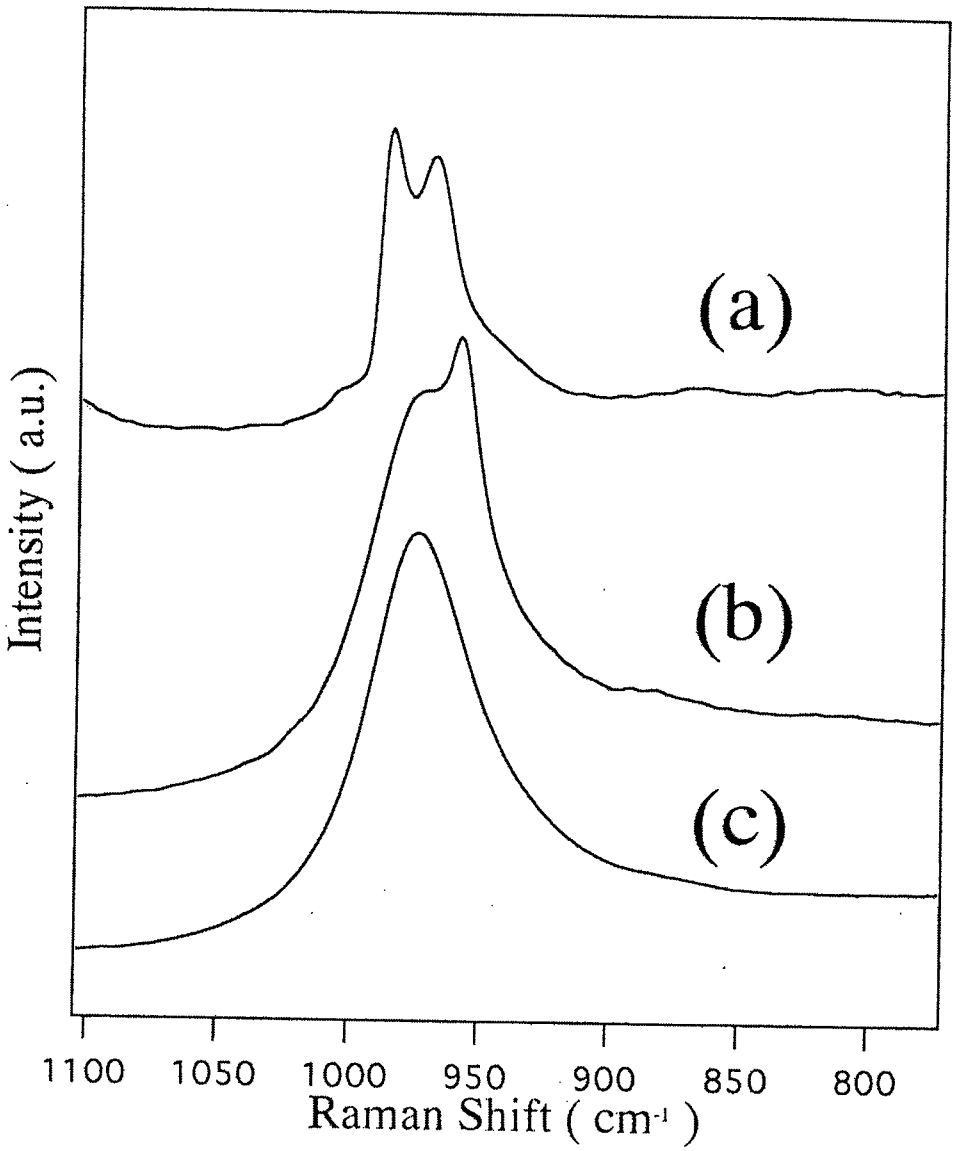

Figure 8. Raman spectra of the $HLaNb_2O_7$ layered oxide compound : (a) $HLaNb_2O_7$-MeOH as prepared ; (b) $HLaNb_2O_7$-MeOH exposed to sun for 3weeks ; (c) $HLaNb_2O_7$.